frontiers | Research Topics

Impact of radiotherapy and radiosurgery on neuro-oncology

Edited by
Alfredo Conti and Maciej Harat

Published in
Frontiers in Oncology

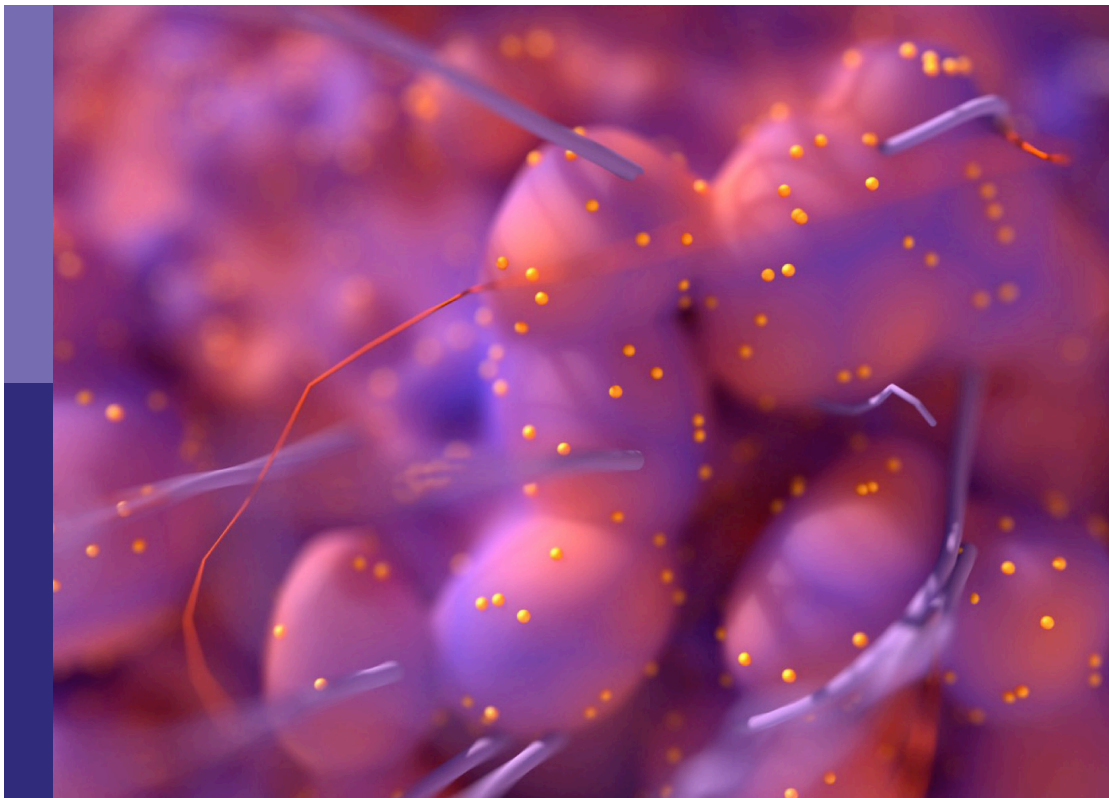

ISSN 1664-8714
ISBN 978-2-88976-858-5
DOI 10.3389/978-2-88976-858-5

About Frontiers

Frontiers is more than just an open access publisher of scholarly articles: it is a pioneering approach to the world of academia, radically improving the way scholarly research is managed. The grand vision of Frontiers is a world where all people have an equal opportunity to seek, share and generate knowledge. Frontiers provides immediate and permanent online open access to all its publications, but this alone is not enough to realize our grand goals.

Frontiers journal series

The Frontiers journal series is a multi-tier and interdisciplinary set of open-access, online journals, promising a paradigm shift from the current review, selection and dissemination processes in academic publishing. All Frontiers journals are driven by researchers for researchers; therefore, they constitute a service to the scholarly community. At the same time, the *Frontiers journal series* operates on a revolutionary invention, the tiered publishing system, initially addressing specific communities of scholars, and gradually climbing up to broader public understanding, thus serving the interests of the lay society, too.

Dedication to quality

Each Frontiers article is a landmark of the highest quality, thanks to genuinely collaborative interactions between authors and review editors, who include some of the world's best academicians. Research must be certified by peers before entering a stream of knowledge that may eventually reach the public - and shape society; therefore, Frontiers only applies the most rigorous and unbiased reviews. Frontiers revolutionizes research publishing by freely delivering the most outstanding research, evaluated with no bias from both the academic and social point of view. By applying the most advanced information technologies, Frontiers is catapulting scholarly publishing into a new generation.

What are Frontiers Research Topics?

Frontiers Research Topics are very popular trademarks of the *Frontiers journals series*: they are collections of at least ten articles, all centered on a particular subject. With their unique mix of varied contributions from Original Research to Review Articles, Frontiers Research Topics unify the most influential researchers, the latest key findings and historical advances in a hot research area.

Find out more on how to host your own Frontiers Research Topic or contribute to one as an author by contacting the Frontiers editorial office: frontiersin.org/about/contact

Impact of radiotherapy and radiosurgery on neuro-oncology

Topic editors

Alfredo Conti — University of Bologna, Italy

Maciej Harat — Franciszek Lukaszczyk Oncology Centre, Poland

Citation

Conti, A., Harat, M., eds. (2023). *Impact of radiotherapy and radiosurgery on neuro-oncology*. Lausanne: Frontiers Media SA. doi: 10.3389/978-2-88976-858-5

Table of contents

frontiers | Frontiers in Oncology

TYPE Editorial
PUBLISHED 26 July 2022
DOI 10.3389/fonc.2022.978709

OPEN ACCESS

EDITED AND REVIEWED BY
David D. Eisenstat,
Royal Children's Hospital, Australia

*CORRESPONDENCE
Alfredo Conti
alfredo.conti2@unibo.it

SPECIALTY SECTION
This article was submitted to Neuro-Oncology and Neurosurgical Oncology, a section of the journal Frontiers in Oncology

RECEIVED 26 June 2022
ACCEPTED 05 July 2022
PUBLISHED 26 July 2022

CITATION
Conti A (2022) Editorial: Impact of radiotherapy and radiosurgery on neuro-oncology.
Front. Oncol. 12:978709.
doi: 10.3389/fonc.2022.978709

Editorial: Impact of radiotherapy and radiosurgery on neuro-oncology

Alfredo Conti*

Neurosurgery, IRCCS Istituto delle Scienze Neurologiche di Bologna, Italy, Dipartimento di Scienze Biomediche e NeuroMotorie (DIBINEM), Alma Mater Studiorum University of Bologna, Bologna, Italy

KEYWORDS

radiotherapy, radiosurgery, brain tumors, radiomics, lower grade gliomas

Editorial on the Research Topic
Impact of Radiotherapy and Radiosurgery on Neuro-Oncology

Radiotherapy is one of the main pillars of neuro-oncology. Used universally in all malignant neoplasms affecting the central nervous system, it is increasingly adopted as an alternative to surgical treatment in numerous malignant and benign lesions including brain metastases (BM), meningiomas, vestibular schwannomas, pituitary adenomas or paragangliomas. The clinical settings in which a radiotherapy treatment is indispensable are, in fact, innumerable and at least in three different scenarios: as a preoperative (or neoadjuvant) treatment, as a postoperative (or adjuvant) treatment, and as a rescue therapy. Furthermore, in many circumstances, radiation therapy is used as a primary or upfront treatment as an alternative to surgical management. This broadening of the indications in the use of ionizing radiation in neuro-oncology has been made possible by the astonishing technological evolution that has been witnessed in the last two decades together with the availability of clinical results that have definitively demonstrated the efficacy of radiation treatments, also allowing a progressive refinement of the techniques and methods of treatment. The technological leap obtained by modern radiotherapy allowed a significant increase treatment of efficacy while simultaneously reducing toxicity. To list just a few of them: 3D treatment planning, the extension of the principles of stereotaxis with the possibility of delivering treatments with very efficient dose gradients providing excellent normal tissue sparing, and the evolution of image-guidance. Furthermore, the use of single and multiple fraction radiosurgery to treat brain lesions has gained momentum over the last few years, and turns out to be now more promising than ever (1–3).

If much has been done with great success and with the transition of radiotherapy treatments for neuro-oncology from simple palliation to a fundamental treatment with prospects for healing the disease, many other aspects remain open. Nonetheless, we are in a historical phase in which many opportunities to improve the efficacy of radiotherapy treatments are within reach, above all through both a further improvement of irradiation techniques and a better understanding of the biomolecular characteristics of tumors, of

the genetic factors associated with the response to ionizing radiation, and the use of increasingly advanced neuro-imaging modalities that make it possible to identify tumor areas with specific biological characteristics differently responding to treatment. These innovations represent a challenge, which we should investigate in order to ensure that all professionals involved in the care of brain cancer are exposed to cutting-edge developments, in order to keep delivering the best possible treatments.

With this in mind, we have decided to propose this Research Topic of Frontiers in Oncology having as topic the impact of radiotherapy and radiosurgery on neuro-oncology. Among several submissions, we selected 9 high quality contributions providing cutting-edge research in the field, exploring major aspects of radiotherapy for neuro-oncology. Particularly, in this Research Topic, we included one study on frameless robotic radiosurgery reporting one of the largest series on the treatment of residual, recurrent, or metastatic intracranial hemangiopericytomas (solitary fibrous tumor) using Cyberknife. Huang et al. reported data of 28 of these rare tumors, with a control rate of 78.5%, that is higher than the mean of the previous studies. A second study on radiosurgery was authored by Li et al. who analyzed the outcome of gamma knife radiosurgery (GKRS) in an outstanding number (369) of nonfunctioning pituitary adenomas (NFPA) reporting progression free survivals of 100%, 98%, 97%, 86% and 77% at 1, 3, 5, 10, and 15 years, respectively. The authors also identified predictors of tumor control including parasellar invasion and tumor margin dose (<12 Gy).

Two studies provide cutting-edge research in the field of biomolecular characterization of brain tumors applied to radiosensitivity. Li et al. analyzed expression of long non-coding RNAs (lncRNA) to predict the radiotherapy response of lower-grade gliomas. These RNA species belong to a class of non-coding RNA with a length of not more than 200 nucleotides and usually lack coding potential. Several studies have confirmed that lncRNA expression is associated with tumor initiation, progression, and treatment. lncRNAs can modulate tumor radiosensitivity by functioning as competitive endogenous RNA (ceRNA). In this study, for the first time, authors systematically investigated the mechanism of ceRNA regulation in the radiosensitivity of LGG based on RNA-seq data and database predictions. In the second study, Du et al. developed a radiosensitivity prediction model based on hypoxia genes for LGG by using weighted correlation network analysis (WGCNA) and least absolute shrinkage and selection operator (Lasso). 12 genes (AGK, ETV4, PARD6A, PTP4A2, RIOK3, SIGMAR1, SLC34A2, SMURF1, STK33, TCEAL1, TFPI, and UROS) were included in the model. A radiosensitivity-related risk score model was established based on the overall rate of The Cancer Genome Atlas (TCGA) dataset in patients who received radiotherapy.

The development of prediction nomograms based on radiomics analysis was proposed in other two studies. Zhou et al. developed and validated an individualized prognostic nomogram by integrating physiological, volumetric, clinical chemistry, and molecular biological surrogates for predicting survival in patients with brain metastases after stereotactic radiosurgery. The nomogram demonstrated precise risk-stratifications to guide personalized treatment for brain metastases. Zhai et al. developed and validated a radiomics nomogram based on the multiparametric MRI imaging. The radiomics nomogram demonstrated a favorable predictive accuracy of meningioma consistency before surgery, which showing the potential of clinical application. Finally, three studies propose some hot-topics in radiotherapy field (4, 5), including new techniques in fractionated photon and proton radiotherapy.

Ahn et al. describe a series of 123 patients who underwent hippocampal-avoidance whole-brain radiation therapy (HA-WBRT) and analyzed the risk of BM in the hippocampal areas using multi-variable logistic regression, classification and regression tree (CART) analyses, and gradient boosting method (GBM).

Eichkorn et al. report results in terms of effectiveness and toxicity of fractionated proton beam radiotherapy for treatment of cranial nerve schwannomas unsuitable for photon stereotactic radiosurgery. Treatment resulted in a promising 100% local control with cranial nerve functional protection rate of 80%.

Arpa et al. propose an innovative approach to improve the efficacy of hypofractionated stereotactic radiotherapy (HSRT) after hyperbaric oxygen therapy (HBO) for the treatment of recurrent high-grade glioma (rHGG) and herein report the results of an ad interim analysis. Results are promising and could represent an alternative, with low toxicity, to systemic therapies.

In conclusion, we are proud of the results obtained with this Research Topic which provides an innovative look at many of the fundamental themes of radiotherapy in the neuro-oncology field. The proposed studies are all state-of-the-art and realistically represent a foundation for future research on the topic.

Author contributions

The author confirms being the sole contributor of this work and has approved it for publication.

Conflict of interest

The author declares that the research was conducted in the absence of any commercial or financial relationships that could be construed as a potential conflict of interest.

Publisher's note

References

1. Conti A, Acker G, Kluge A, Loebel F, Kreimeier A, Budach V, et al. The role of minimally invasive treatment modalities. *Front Oncol* (2019) 9:915. doi: 10.3389/fonc.2019.00915

2. Conti A, Pontoriero A, Salamone I, Siragusa C, Midili F, La Torre D, et al. Protecting venous structures during radiosurgery for parasagittal meningiomas. *Neurosurg Focus* (2009) 27(5):E11. doi: 10.3171/2009.8.FOCUS09-157

3. De Maria L, Terzi di Bergamo L, Conti A, Hayashi K, Pinzi V, Murai T, et al. CyberKnife for recurrent malignant gliomas: A systematic review and meta-analysis. *Front Oncol* (2021) 11:652646. doi: 10.3389/fonc.2021.652646

4. Lambrecht M, Eekers DBP, Alapetite C, Burnet NG, Calugaru V, Coremans IEM, et al. Radiation dose constraints for organs at risk in neuro-oncology; the European particle therapy network consensus. *Radiother Oncol* (2018) 128 (1):26–36. doi: 10.1016/j.radonc.2018.05.001. work package 1 of the taskforce "European Particle Therapy Network" of ESTRO.

5. Fernández E, Morillo V, Salvador M, Santafé A, Beato I, Rodríguez M, et al. Hyperbaric oxygen and radiation therapy: A review. *Clin Transl Oncol* (2021) 23 (6):1047–53. doi: 10.1007/s12094-020-02513-5

frontiers in Oncology

ORIGINAL RESEARCH
published: 03 March 2021
doi: 10.3389/fonc.2021.577054

Treatment of Residual, Recurrent, or Metastatic Intracranial Hemangiopericytomas With Stereotactic Radiotherapy Using CyberKnife

Lichao Huang[1,2], Jingmin Bai[3], Yanyang Zhang[1], Zhiqiang Cui[1], Zhizhong Zhang[1], Jiwei Li[3], Jinyuan Wang[3], Xinguang Yu[1], Zhipei Ling[1], Baolin Qu[3] and Longsheng Pan[1]**

[1] Department of Neurosurgery, The First Medical Center of PLA General Hospital, Beijing, China, [2] Department of Neurosurgery, The Hospital of 81st Group Army PLA, Zhangjiakou, China, [3] Department of Radiation Oncology, The First Medical Center of PLA General Hospital, Beijing, China

Purpose: Hemangiopericytomas are aggressive tumors known for their recurrence. The purpose of this study was to evaluate the management of residual, recurrent, and metastatic intracranial hemangiopericytomas using CyberKnife (CK) stereotactic radiotherapy (SRT).

Materials and Methods: Data were collected from 15 patients (28 tumors; eight men and seven women; 32–58 years) with residual, recurrent, or metastatic intracranial hemangiopericytomas, who were treated with stereotactic radiotherapy using CyberKnife between January 2014 and August 2019. All patients had previously been treated with surgical resection. Initial tumor volumes ranged from 0.84 to 67.2 cm^3, with a mean volume of 13.06 cm^3. The mean marginal and maximum radiosurgical doses to the tumors were 21.1 and 28.76 Gy, respectively. The mean follow-up time for tumors was 34.5 months, ranging from 13 to 77 months.

Results: 15 patients were alive after treatment; the mean post-diagnosis survival at censoring was 45.6 months (range 13–77 months). The volumes of the 28 tumors in the 15 followed patients were calculated after treatment. Postoperative magnetic resonance imaging revealed a mean tumor volume of 6.72 cm^3 and a range of 0–67.2 cm^3, with the volumes being significantly lower than pretreatment values. Follow-up imaging studies demonstrated tumor disappearance in seven (25%) of 28 tumors, reduction in 14 (50%), stability in one (3.57%), and recurrence in six (21.4%). Total tumor control was achieved in 22 (78.5%) of 28 tumors. The tumor grade and fraction time were not significantly associated with progression-free survival. Intracranial metastasis occurred in three patients, and extraneural metastasis in one patient.

Conclusions: On the basis of the current results, stereotactic radiotherapy using CyberKnife is an effective and safe option for residual, recurrent, and metastatic intracranial hemangiopericytomas. Long-term close clinical and imaging follow-up is also necessary.

Keywords: stereotactic radiotherapy, CyberKnife, hemangiopericytomas, tumor control, management

OPEN ACCESS

Edited by:
Abdullah Faruk Zorlu, Hacettepe University, Turkey

Reviewed by:
Selcuk Peker, Koç University, Turkey
Ugur Selek, Koç University, Turkey

***Correspondence:**
Longsheng Pan
panls301@163.com
Baolin Qu
qubl6212@sina.com

Specialty section:
This article was submitted to Neuro-Oncology and Neurosurgical Oncology, a section of the journal Frontiers in Oncology

Received: *28 June 2020*
Accepted: *07 January 2021*
Published: *03 March 2021*

Citation:
Huang L, Bai J, Zhang Y, Cui Z, Zhang Z, Li J, Wang J, Yu X, Ling Z, Qu B and Pan L (2021) Treatment of Residual, Recurrent, or Metastatic Intracranial Hemangiopericytomas With Stereotactic Radiotherapy Using CyberKnife. Front. Oncol. 11:577054. doi: 10.3389/fonc.2021.577054

INTRODUCTION

Hemangiopericytomas (HPCs) are rare tumors that exhibit a high incidence of local recurrence and distant metastasis, even after gross-total resection (1). Central nervous systems HPCs are uncommon, accounting for only 0.4% of all primary intracranial tumors and 2.4% of meningeal tumors (2). Central nervous system (CNS) HPC usually occurs in adults with an average diagnostic age between 40 and 50 years (3). The World Health Organization(WHO) guidelines combine solitary fibrous tumors and HPC into the single entry solitary fibrous tumor(SFT)/HPC, which was classified into three variants in 2016: grades I, II, and III (4). An analysis of surveillance, epidemiology, and end results in 655 patients and a review of CNS (199) and extra-CNS HPCs (456) showed 5- and 10-year overall survival rates of 80 and 54%, respectively. Patients with extracranial HPCs had worse outcomes, with 5- and 10-year overall survival rates of 58 and 44%, respectively (3).

HPCs frequently show involvement of adjacent dural sinuses and the skull base, which can make gross-total resection a challenging, and at times, unrealistic goal. In almost all cases, the initial treatment of larger intracranial HPCs is resection, with surgical excision remaining the gold standard treatment. The local control, progression-free survival, and overall survival rates of patients receiving radiotherapy seem to be higher than those who do not receive radiotherapy (5–7), but the efficacy of adjuvant radiotherapy is still under study. The optimal management of recurrent or residual intracranial HPCs presents a challenge. The roles of Gamma Knife Radiosurgery (GKRS) and CK SRT in the treatment of HPC have been previously described, with tumor control rates ranging from 46 to 100% (2). However, the published reports describing the use of CK SRT in the treatment of HPCs are limited. Furthermore, the optimal dose for successful local control of HPCs without adverse effects remains unclear. In this study, we evaluated the safety and efficacy of SRT using the CK system in 15 patients with residual, recurrent, and metastatic intracranial HPCs.

MATERIALS AND METHODS

Patient Population

This study enrolled 15 patients with HPCs who were treated in our institute between January 2014 and August 2019. Written informed consent was obtained from each participant prior to study inclusion, and the study was approved by the local ethics committee of our institute (No. S2018-119-01). The patient inclusion criteria were: (1) all patients received craniotomy and had histopathologically confirmed diagnoses; (2) all patients received magnetic resonance imaging (MRI), including T1-weighted, T2-weighted, contrast-enhanced T1-weighted and FLAIR sequences; (3) all HPCs were documented as residual, metastatic, or recurrent lesions. Clinical data including sex, age, diagnosis, baseline neurological symptoms, and lesion location were collected. In addition, information on the prescription dose, planning target volume, and concurrent therapy was also obtained.

CK Technique

Before treatment, all patients underwent planning CT (Siemens, Forchheim, Germany) and 3.0T MRI (Siemens, Erlangan, Germany) with slice thickness of 1 mm. Rigid fusion registration was performed between the MRI T1-weighted contrast-enhance sequences and CT scans using MIM Maestro 6.5.4 image processing software (MIM Software Inc., Cleveland, Ohio, USA). The gross tumor volume (GTV) was determined from the fused image, and the planning target volume (PTV) was defined a region extending 1.5 mm outside the gross tumor volume. The treatment plans varied according to the size of the treated tumor, its location in relation to critical structures, and the history of prior radiation. All 28 tumors in the 15 patients were treated with SRT using CK system (Accuray Inc., Sunnyvale, CA).

Follow-Up Evaluation

All patients were interviewed and clinically evaluated to update their clinical and personal data. Follow-up brain MRI was acquired from all 15 patients 3 months after CK, and then regularly at 3- to 6-month intervals. At each follow-up, tumor volumes were determined from the brain MRI using the coniglobus formula: $V = 1/6\pi \times a$ (diameter length) $\times$ b (diameter width) $\times$ m (slice thickness) $\times$ c (slice number). The follow-up time ranged from 13 to 77 months, with a mean of 34.5 months. The tumor volume response was classified in the following manner: 'disappeared' (100% decrease in tumor volume), 'reduction' (25–99% decrease in tumor volume), 'stable' (≤25% decrease or 25% increase in tumor volume), and 'recurrence' (>25% increase).

Statistical Analysis

Statistical analysis was performed using SPSS version 22.0 (SPSS Inc., Chicago, IL, USA). Overall survival and progression-free survival were calculated using Kaplan–Meier plots. Univariate analysis was performed on the Kaplan–Meier curves using the log-rank test. Statistical significance was set at $p < 0.05$.

RESULTS

Imaging Outcomes

The 15 patients consisted of eight men (53.4%) and seven women (46.6%), with a median age of 43 years (range 32–58 years) at the time of initial CK therapy (**Table 1**). All patients were previously treated with surgical resection and had histopathologically confirmed diagnoses. Eight patients had a WHO classification of grade II, two of grades II–III, and five of grade III. One patient had undergone four craniotomies before CK, two patients had undergone three, two patients had undergone two, and 10 patients had undergone one. Four patients had undergone GK treatment after surgical resection, and all had infield recurrence.

Abbreviations: HPCs, hemangiopericytomas; CK, CyberKnife; GK, Gamma Knife; MRI, Magnetic Resonance Imaging; SRT, Stereotactic Radiotherapy; GKRS, Gamma Knife Radiosurgery.

TABLE 1 | Patient characteristics.

Number of patients	Gender	Age at onset (years)	Clinical presentation	Number of craniotomy before CK	Radiation therapy before CK (time, dose)	Grade	Time to CK post-surgery (month)	Number of CK treatments	Site
1	F	58	Headache, walking unsteadily	3	GKRS (1, 15Gy)	III	96	5	Left anterior skull base, temporal lobe, and the fourth ventricle
2	M	49	Headache	1	None	II	1	1	Left parietal and parasagittal
3	M	38	Asymptomatic	1	None	II–III	5	5	Tentorium cerebelli, confluence of sinuses
4	M	38	Headache	1	None	III	8	4	Tentorium cerebelli
5	M	32	Visual impairment	2	GKRS (1, 14.5Gy)	III	2	2	Cavernous sinus, orbital apex
6	F	37	Headache	3	None	II	2	2	Anterior skull base
7	M	43	Asymptomatic	4	GKRS (2, 15Gy, 13Gy)	III	1	1	Right cerebellum
8	F	49	Asymptomatic	2	GKRS (2, 15Gy, 15Gy)	II	19	1	Right parietal and parasagittal
9	M	48	Hemiplegia, alalia	1	None	II	41	1	Right tentorium cerebelli
10	F	46	Asymptomatic	1	None	III	1	1	Left parietal
11	M	34	Headache	1	None	II	1	2	Confluence of sinuses
12	F	42	Headache	1	None	II	2	1	Right parietal
13	F	46	Asymptomatic	1	None	II	36	1	Left cerebellum
14	M	42	Visual impairment	1	None	II	1	1	Sellar region
15	F	46	Asymptomatic	1	None	II–III	2	1	Right parietal

M, male; F, female; CK, CyberKnife; GKRS, Gamma Knife Radiosurgery.

The mean time from surgery to CK treatment was 14.5 months (range 1–96 months). The patients' main symptoms included headache (n = 6), visual impairment (n = 2), and hemiplegia and alalia (n = 1), with six being asymptomatic (**Table 1**). All intracranial HPCs were documented as residual (8), recurrent (9), and/or metastatic (4). Two patients underwent five CK SRT treatments, one patient underwent four treatments, four patients underwent two treatments, and eight patients underwent one treatment. The most recent CK treatments in patients 1, 3, 8 were covered by a follow-up period of less than 12 months at the time of censoring and are not included in the statistical analysis. For the total of 28 tumors in 15 patients, the mean tumor volume was 13.06 cm^3 (range 0.84–67.2 cm^3). The 28 tumors were located in a myriad of locations, including the temporal lobe (n = 2), anterior skull base (n = 3), fourth ventricle (n = 1), parietal and parasagittal region (n = 5), tentorium cerebelli (n = 10), cerebellum(n = 2), confluence of the sinuses (n = 2), cavernous sinus (n = 1), sellar region (n = 1), and orbital apex (n = 1, **Supplementary Table 2**). Among the 28 tumors, four tumors were treated twice and were regarded as recurrent. One patient accepted anti-angiogenesis therapies after metastasis, according to the professional advice of an oncologist.

Twenty-four tumors required treatment in three fractions, one tumor required two fractions, and three tumors required a single session. The mean marginal dose to the tumors was 21.1 Gy (range 14–27 Gy) for the initial CK SRT, and the mean maximum, mean, and minimum radiosurgical doses were 28.86 Gy (range 20–33.75 Gy), 25.53 Gy (range 17.08–30.83 Gy) and 15.74 Gy (range 4.02–26.52 Gy), respectively. The mean isodose line was 73.03% (range 70–80%, **Supplementary Table 2**). In the three fraction treatments, the mean marginal dose was 21.65 Gy (range 18–27 Gy), and the mean maximum, mean, and minimum radiosurgical doses were 29.39 Gy (25.71–33.75 Gy), 25.06 Gy (21.87–30.83 Gy), and 15.72 Gy (4.02–26.52 Gy), respectively. In the two fraction treatment, the marginal dose was 22 Gy, and the maximum, mean, and minimum radiosurgical doses were 31.42, 28.2, and 20.49 Gy, respectively. In the process of one fraction treatments, the mean marginal dose was 16.6 Gy(range 14–20 Gy), the maximum, mean, and minimum radiosurgical doses were 23.8 Gy (20–28.57 Gy), 20.3 Gy (17.08–24.55 Gy), and 14.3 Gy (11.54–19.63 Gy).

For the all surviving 15 patients, the mean post-diagnosis survival at censoring was 45.6 months (range 13–77). But the number of events required for the survival analysis has not been reached, so no formal statistical comparison has been performed. The follow-up time ranged from 13 to 77 months, with a mean of 34.5 months. Postoperative MRI revealed tumor volumes ranging from 0 to 67.2 cm^3, with a mean value of 6.72 cm^3, volumes that were significantly lower than on pretreatment MRI. The follow-up imaging studies demonstrated that seven of 28 (25%) tumors had disappeared at a mean of 30.14 months (range 3–48 months) after CK, 14 (50%) had reduced, one (3.57%) was stable, and six (21.4%) had recurred after reduction at mean of 33.1 months (range 15–55 months) after CK therapy. Tumor recurrence was founded at a time interval of 3 or 6 months

following the reduction. Total tumor control was achieved in 22 (78.5%) of 28 tumors, with the actuarial local control rate of 28 tumors at 1-year being 100% (**Figure 1**). No correlation between treatment dose, tumor volume, and tumor response was apparent in these patients. Total tumor control was achieved in 13 of 17 (76.4%) tumors in the high-grade group and nine of 11 (81.8%) tumors in the low-grade group. The progression-free survival curves in **Figure 2** no statistically significant difference between patients with high-grade tumors and low-grade tumors ($p = 0.754$). In the radiosurgery and hypofractionated groups, total tumor control was achieved in two of three (75%) tumors, and 20 of 25 tumors (80%), respectively. The progression-free survival curves showed no statistically significant differences between radiosurgery and hypofractionated stereotactic radiosurgery ($p = 0.529$; **Figure 3**). Intracranial metastasis occurred in three patients and extraneural metastasis in one patient. Six tumors (one low-grade tumor and five high-grade tumors) showed recurrence after undergoing a reduction in volume. No complications occurred after treatment in any patient in this series. **Figures 4** and **5** show tumor numbers 18 and 20 before and after CK therapy. **Supplementary Table 2** summarizes the patient characteristics and radiotherapy parameters of the treatment plans.

Clinical Outcomes

Clinical symptoms were followed in all 15 patients. Of those with adequate follow up data, six patients reported resolution of headaches, and eight indicated no change in symptoms, while no patients described worsening of the initial clinical presentation. All cranial nerve deficits present at initial presentation remained, with no improvement or worsening.

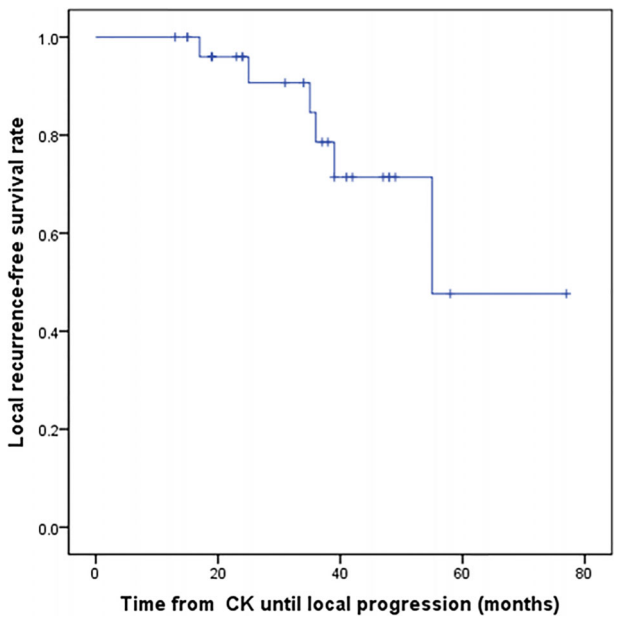

FIGURE 1 | Kaplan–Meier progression-free survival curves after CK treatment for all patients.

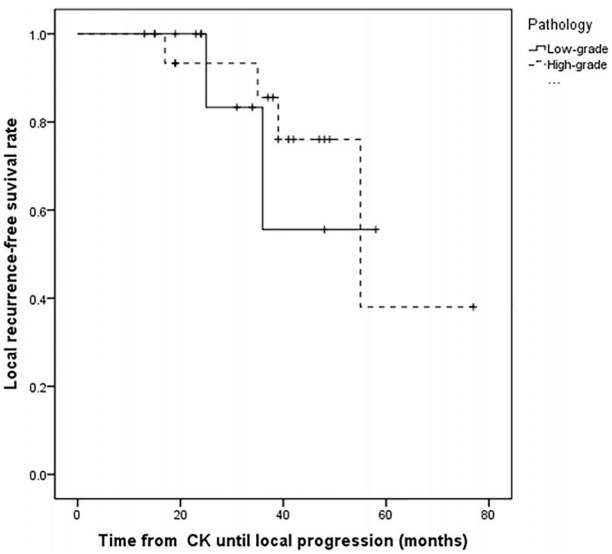

FIGURE 2 | Kaplan–Meier progression-free survival curves for different pathology. There was no statistically significant difference between patients with high-grade tumors and low-grade tumors (P = 0.754).

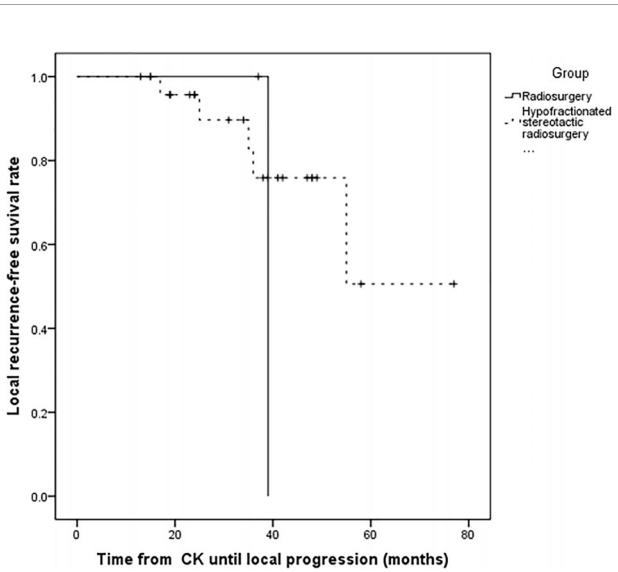

FIGURE 3 | Kaplan–Meier progression-free survival curves for different fraction time. There was no statistically significant difference between radiosurgery and hypofractionated stereotactic radiosurgery (P = 0.529).

DISCUSSION

HPC's are derived from fibro-histiocytic precursor cells, the pericytes of Zimmerman (10). HPCs resemble meningiomas both clinically and radiographically, but are known for their aggressiveness, high recurrence rates, and propensity for extracranial metastasis (11). Therefore, HPCs differ from

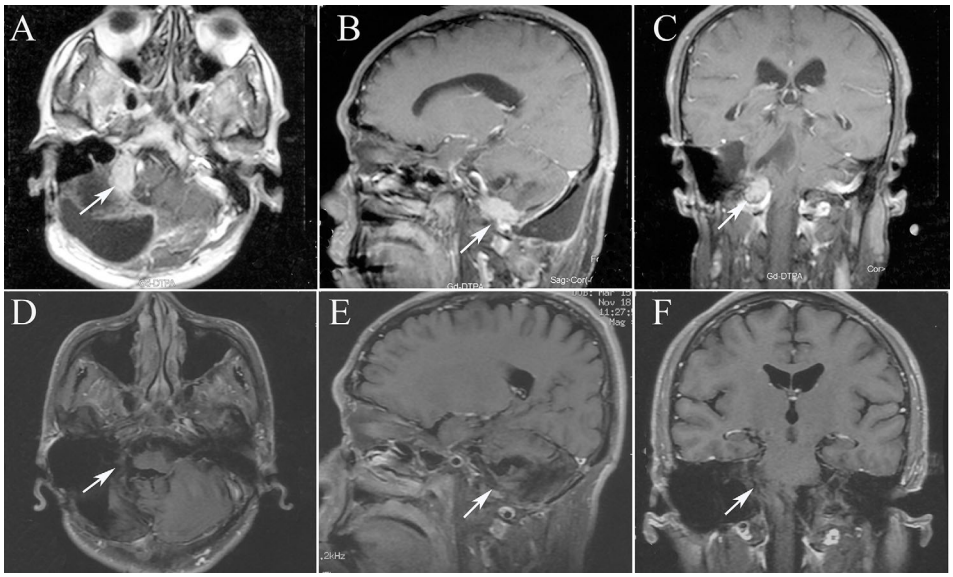

FIGURE 4 | The MRI images of patient 7, tumor 16. **(A)** Axial T1-weighted contrast-enhanced image showing residual enhancement and a pretreatment tumor volume of 11.33 cm^3 (tumor 16); **(B)** Sagittal T1-weighted contrast-enhanced image; **(C)** Coronal T1-weighted contrast-enhanced image; **(D)** Axial T1-weighted contrast-enhanced image after 13 months, the tumor disappeared. **(E)** Sagittal T1-weighted contrast-enhanced image after 13 months; **(F)** Coronal T1-weighted contrast-enhanced image after 13 months.

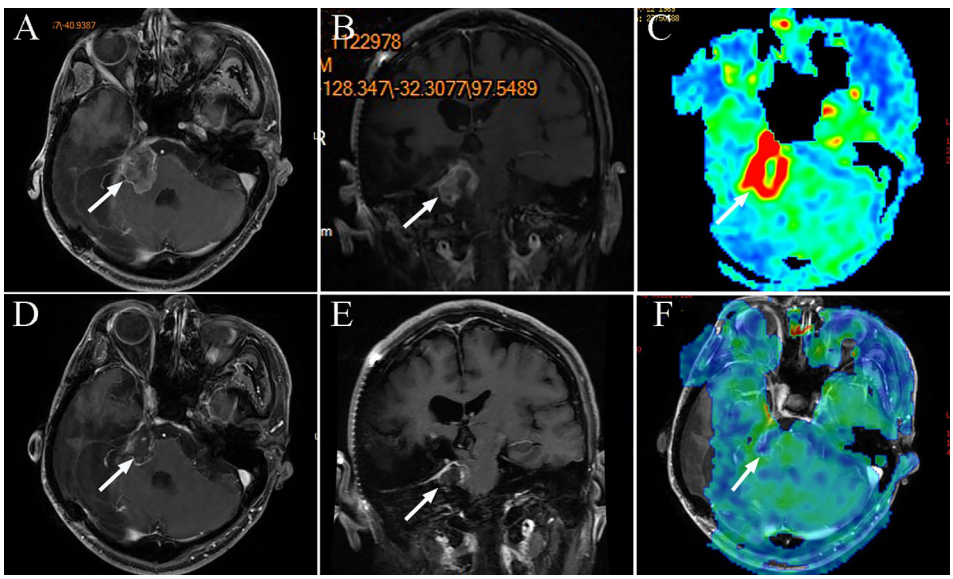

FIGURE 5 | The MRI images of patient 9, tumor 20. **(A)** Axial T1-weighted contrast-enhanced image showing residual enhancement and a pretreatment tumor volume of 13.41 cm^3 (tumor 20); **(B)** Coronal T1-weighted contrast-enhanced image; **(C)** Axial three dimensional arterial spin labeling (3D-ASL) image showing high perfusion; **(D)** Axial T1-weighted contrast-enhanced image after 12 months, the tumor reduced. **(E)** Coronal T1-weighted contrast-enhanced image after 12 months; **(F)** Axial 3DASL image showing low perfusion after 12 months.

meningiomas and require systemic management and long-term follow-up. The efficacy of radiotherapy and chemotherapy for recurrent intracranial HPCs remains unclear because of the scarcity and deficiencies of the available clinical data (8, 12). The optimal CK SRT dose for successful local control of HPCs without adverse effects also remains unclear.

Resection provides the benefits of histological confirmation and reduces mass effects, and is usually the primary treatment for

HPC. In previous studies, gross-total resection (GTR) was significantly associated with longer progression-free survival and overall survival. In a systematic review of 523 patients with CNS HPCs (13), the mean survival in patients undergoing surgery with complete resection was 157.97 months. In contrast, patients with an incomplete resection had a mean survival of 110.75 months, which was observed to be related to a higher incidence of mortality. Although gross-total resection can be challenging as the tumor frequently infiltrates the sinuses and is highly vascular, it should still be the primary treatment goal in patients with HPC. Patients with tumors of the posterior fossa had a shorter survival time (median 10.75 *vs.* 15.6 years) than those with tumors located elsewhere (14). Another challenge with surgical resection alone is the high rate of recurrence after resection; a study by Sheehan et al. reported a local recurrence rate of 88% for surgery alone (9). In our study, 14 of 28 tumors (50%) were recurrences after complete resection and before CK treatment, and the median time to CK from resection was 2 months (range 1–96). Multiple resections are not an attractive option for such patients, and they present considerable surgical risk and trauma. Stereotactic radiosurgery (SRS) combines the efficacy of resection with a lower rate of radiotherapy-induced morbidity (11), and may be much more suitable for this highly-vascular tumors (15).

Many studies have demonstrated the important role of adjuvant radiotherapy following surgical resection for intracranial HPC. In the most recent systematic review of 523 patients with HPC, adjuvant radiation led to a longer median survival of 123 months in comparison with the 93 months in patients who did not receive it, ($p < 0.0001$) (13). In another study by Sheehan et al, the local recurrence rate was reported as 88% with surgery alone, which compared with 12.5% with surgery and adjuvant radiotherapy (9). An external beam radiation dose >50 Gy was suggested to give the greatest benefit in previous series (16, 17), but it was not effective in preventing metastasis (7).

Compared with conventional radiotherapy, radiosurgery can achieve a steep dose gradient that minimizes the radiation delivered to surrounding areas (1). Gamma Knife Radiosurgery (GKRS) has become a well-established treatment option for various intracranial tumors and it can administer an accurately-focused high dose of radiation in a single session. In 1993, Coffey et al. published the first preliminary SRS report on HPCs treated using GKS (Elekta Instruments, Tucker, Georgia). The overall tumor control rate was 81.8% after a median follow-up of 14.8 months. Veeravagu et al. summarized 11 published studies on stereotactic radiosurgery covering a total of 137 patients with 241 recurrent and residual HPC tumors treated between 1987 and 2010. They found a mean tumor control rate of 81.3% after a mean follow-up period of 37.2 months, with a mean prescription margin dose of 16.2 Gy (11).

Table 2 summarizes 16 published studies (including this present series) on the use of stereotactic radiotherapy for recurrent and residual HPCs. Between the years of 1987 and 2019, a total of 294 patients with 529 lesions were treated with stereotactic radiotherapy and were reported in the literature. For these lesions, the mean prescription dose to the tumor margin was 16.7 Gy, the mean follow-up period was 39.9 months, and the mean tumor control rate was 75.2% (1, 2, 5, 6, 9, 10, 12, 14, 17–23). Our series covered 15 patients with 28 tumors, and at a mean margin dose of 21.2 Gy, the control rate was 78.5% after 34.5 months of follow-up, a control rate that is higher than the mean of the previous studies. Higher prescription doses seem to translate to increased tumor control rates. The average total tumor control rates of GKRS series (14) and CK series (3) over the sixteen published studies are 74.7 and 78.4%, respectively. Postoperative SRT seems to provide an effective and safe adjuvant management option for patients with residual, recurrent and metastatic intracranial HPCs. However, determination of the best stereotactic radiotherapy option requires more results from large, multi-center series.

The CK system is one available device for stereotactic radiotherapy. The system offers both single- and multi-session SRT options. The two previously published studies on patients with HPC treated using CK SRT were both from Stanford. The first series was conducted by Chang and Sakamoto in 2003 (5) and demonstrated tumor control in 75% of the HPCs treated during a mean follow-up time of 44 months. Although the mean radiosurgery dose to the tumor margin was higher (20.5 Gy) than that from GKRS in another series (16.2 Gy), there were no radiosurgery related complications and very ideal tumor control rates. In the second series, the tumor margin dose was slightly higher (21.5 Gy) than in the first series (20.5 Gy). The rates of tumor reduction, stability, recurrence, and total tumor control were 54.5, 27.3, 18.2, and 81.8%, respectively. The tumor margin dose in our series was 21.2 Gy, and the rates of tumor reduction, stability, recurrence, and total tumor control were 75, 3.5, 21.4, and 78.5%, respectively. Although the rate of tumor control was similar to the previous two series, the follow-up time in our study was not long enough. A satisfactory result in our study was the disappearance of seven tumors over the relatively short follow-up time, although the longer-term outcomes require further observation. In the six tumors that recurred after CK therapy, and the marginal doses were 27, 16, 22.5, 19.5, 22.5, and 22.5 Gy, and the grades were III, II–III, III, II, II, and II, respectively. There is no obvious correlation between the marginal dose and the grade. Sun et al. considered that a high margin dose appeared to achieve a reduction in the rate of local recurrence (19). Therefore, a higher prescription dose needs to be tried gradually for HPCs. Moreover, we found that four of 15 patients in the current series whose tumor arose at the deep of the brain had a poor prognosis.

Previous studies reported that the most common sites of extraneural metastases were the lungs, bones, liver, intra-abdominal and subcutaneous tissues, breast, pleura, and thyroid (13). Galanis et al. noted that bones and liver were the most common metastatic sites (82 and 41% of extraneural recurrences, respectively) in their series (17). Incidences of extracranial metastasis of 13, 33, and 64% at 5, 10, and 15 years have been reported, and their occurrence significantly shortens survival (17). The mean time to extraneural metastasis shows substantial variance, ranging from several months to many years (25), even from initial diagnosis (11). One of our patients currently alive

TABLE 2 | Literature review of previous studies that reported control rates in patients treated for hemangiopericytoma with SRT.

Authors	Institution	Study period	Number of patients/Lesions	Volume (ml), mean (range)	Type of radiotherapy	Number of fractions	Prescription dose (Gy), mean (range)	Follow-up (months), mean (range)	Tumor control at last follow-up (%)	Intracranial metastasis, n (%)	Extraneural metastasis, n (%)	Extraneural metastasis site
Coffey et al. (9)	Mayo Clinic	1990–1992	5/11	8.53(0.40–24.25)	GK	1	15.5(12–18)	14.8(10–17)	81.8	2(40)	1(20)	Liver, spinal
Galanis et al. (17)	Mayo Clinic	1976–1996	10/20(Includes five patients from Coffey et al.)	–	GK	1	(12–18)	–(6-36)	100	–	–	–
Payne et al. (18)	U of Virginiac	1991–1999	10/12	7.6(0.3–33.6)	GK	1	14(2.8–25)	24.8(3–56)	75	2(20)	0	–
Sheehan et al. (14)	U of Pittsburgh	1987–2001	14/15	8.8(0.3–26.6)	GK	1	15(11–20)	31.3(5–76)	80	2(14.5)	2(14.5)	Spinal, rib, lung
Chang et al. (5)	Stanford	1992–2002	8/8	–	LINAC,CK	1	20.5(16–24)	44(8–77)	75	0	1 (12.5)	Temporalis muscle
Ecker et al (11)	Mayo Clinic	1980–2000	15/45(Includes five patients from Coffey et al)	7.8(0.4–58.3)	GK	1	16 (12–21)	45.6 (–)	93	4(don't mention the site)(27)	0	
Kano et al. (6)	U of Pittsburgh	1989–2006	20/29	4.5(0.07–34.3)	GK	1	15(10–20)	37.9(–)	72.4	3(15)	3+2 both intracranial and extraneural (25)	Lung, liver, rib, neck, vertebral body
Sun et al. (19)	Beijing Neu. Ins	1994–2006	22/58	5.4(0.4–31.2)	GK	1	13.5(10–20)	26(5–90)	89.7	7(31.8)	3(13.6)	Orbit, bone, liver, lungs, pleura, subcutis
Iwai et al. (20)	Osaka City Hosp	–	5/6	11(4.5–18.8)	GK	1	13.7(12–16)	34(10–48)	66.7	1(20)	1(20)	Lung
Olson et al. (1)	U of Virginia	1989–2008	21/28	4.6(0.3–18.7)	GK	1	17(2.8–22)	69(2–138)	46.4	3(14)	4(19)	Liver, lung, kidney, bone, bowel, external auditory canal
Veeravagu et al. (10)	Stanford	2002–2009	12(Spine 3)/22(Spine 9)	9.16(0.03–56.7)	CK	1-5	21.2(16–30)	37(10–73)	81.8	–	–	–
Tsugawa et al. (21)	Nagoya Kyoritsu Hospital	2004–2010	7/10	5.2(0.3–23.9)	GK	1	17.5(10–20)	52.1 (13–71)	69.7	2(28.5)	1(14.2)	–
Copeland et al. (22)	Mayo Clinic	1990–2010	22/64	3.3 (0.1–58.3)	GK	1	15(12–21)	31(1–155)	59	9(40.9)	–	–
Kim et al. (23)	Kosin University Gospel Hospital	2002–2014	18/40	1.2 (0.4–7.4)	GK	1	20.5(13–30)	71.8 (3.3–153.3)	80	8 (44.4)	7 (38.9)	Liver, spine, lung, kidney, bone, pancreas
Cohen-Inbar (2)	Multicenter	1988–2014	90/133	4.9(0.2–42.4)	GK	1	15(2.8–24)	59 (6–183)	54.8	25(27.8)	22(24.4)	Liver, lung, kidney, bone, bowel, and external auditory canal
Present study	PLA General Hospital	2014–2019	15/28	13.06(0.84–67.2)	CK	1-3	21.1(14–27)	34.5(1–77)	78.5	3(20)	1(6.6)	Liver, spine

SRT, stereotactic radiotherapy; GK, Gamma Knife; CK, CyberKnife.

with liver and bone metastases 6 years after diagnosis, with the patient having developed. Two intracranial metastases at 2 and 3 years after diagnosis. The rate of intracranial metastases in the 22 patients of Sun's series was 31.8% (n = 7), whereas the rate of extracranial metastases was 13.6% (n = 3). In our study, the intracranial metastasis rate was 20% (n = 3) and the extracranial metastasis rate 6.6% (n = 1). The variability in these results is related to the unpredictable nature of HPCs. Other CK SRT series made paid little mention to intracranial or extraneural metastases. Because HPCs are highly aggressive, the initial tumor volume can be regenerated, even if it is reduced or has disappeared after previous treatment (10); in our series, six tumors (1, 9, 11, 14, 19 and 22) showed such a changing course. Stereotactic radiotherapy is a focal localized treatment modality, and the possibility of repeatable treatment is an advantage, but it may also be ineffective in preventing metastasis. Hence, CNS HPC requires long-term follow-up and surveillance for recurrence and metastasis. The appropriate interval is uncertain, but 3 or 6 months might be considered reasonable.

Until now, the use of chemotherapy for treating CNS HPCs has been very disappointing, although chemotherapy may be helpful in the specific case of recurrence after radiotherapy (8). However the efficacies of new therapies for extracranial HPCs, including anti-angiogenesis therapies, are currently being evaluated (26), and these treatments may also be useful for intracranial HPCs. In our series, one patient (number 4) accepted anti-angiogenesis therapies (pazopanib hydrochloride) after liver and bone metastases were found. Partial embolization of the liver metastases was also performed at the same time. We found that the metastatic tumors shrank after 6 months. Programmed cell death ligand-1 (PD-L1) is frequently expressed in intracranial SFT/HPCs, and diffuse or intense PD-L1 expression might be associated with the early occurrence of extracranial metastasis (27). A combination of SRS and targeted drugs may improve the local control rate and extend survival time, but multicenter prospective large-sample clinical trials are needed to confirm this.

The main limitations of our study are the retrospective design, the small number of patients, and the relatively short follow-up. Although no severe complications occurred after a mean follow-up period of 34.5 months, the follow-up periods were insufficient. We also failed to identify the relationship between dose and volume change. Obviously, much longer, follow-up and a larger population will be required to establish the long-term efficacy of CK-based SRT for HPC. Therefore, we must be cautious with our conclusions, because these findings are preliminary. Although a longer follow-up period and a larger population are necessary to confirm these early results, this analysis documenting our preliminary experience of CK-based SRT for intracranial HPCs is very encouraging.

CONCLUSIONS

On the basis of the current results, fractioned radiotherapy using CyberKnife is an effective and safe option for the management of intracranial HPCs after surgical resection. Our patients experienced total tumor control rates similar to those described in previous studies. Therefore, SRT using CK can be considered an important adjuvant radiation treatment for residual, recurrent, and metastatic intracranial HPCs.

DATA AVAILABILITY STATEMENT

The original contributions presented in the study are included in the article/**Supplementary Material**. Further inquiries can be directed to the corresponding authors.

ETHICS STATEMENT

The studies involving human participants were reviewed and approved by Institutional Review Board in PLA General Hospital. The patients/participants provided their written informed consent to participate in this study. Written informed consent was obtained from the individual(s) for the publication of any potentially identifiable images or data included in this article.

AUTHOR CONTRIBUTIONS

LH prepared for the writing of manuscript preparation. YZ performed the data analyses. JB prepared for MRI data analysis. ZC performed literature research. ZZ performed clinical studies. JL performed statistics of treatment plan parameters. JW performed statistical analysis. XY proposed amendments to the manuscript. ZL corrected the manuscript. BQ helped perform the analysis with constructive discussions. LP designed the experiment. All authors contributed to the article and approved the submitted version.

SUPPLEMENTARY MATERIAL

The Supplementary Material for this article can be found online at: https://www.frontiersin.org/articles/10.3389/fonc.2021.577054/full#supplementary-material

REFERENCES

1. Olson C, Yen CP, Schlesinger D, Sheehan J. Radiosurgery for intracranial hemangiopericytomas: outcomes after initial and repeat Gamma Knife surgery. *J Neurosurg* (2010) 112(1):133–9. doi: 10.3171/2009.3.JNS0923
2. Cohen-Inbar O, Lee CC, Mousavi SH, Kano H, Mathieu D, Meola A, et al. Stereotactic radiosurgery for intracranial hemangiopericytomas: a multicenter study. *J Neurosurg* (2017) 126(3):744–54. doi: 10.3171/2016.1.JNS152860
3. Hall WA, Ali AN, Gullett N, Crocker I, Landry JC, Shu HK, et al. Comparing central nervous system (CNS) and extra-CNS hemangiopericytomas in the Surveillance, Epidemiology, and End Results program: analysis of 655 patients and review of current literature. *Cancer* (2012) 118(21):5331–8. doi: 10.1002/cncr.27511
4. Gupta A, Dwivedi T. A Simplified Overview of World Health Organization Classification Update of Central Nervous System Tumors 2016. *J Neurosci Rural Pract* (2017) 8(4):629–41. doi: 10.4103/jnrp.jnrp_168_17

5. Chang SD, Sakamoto GT. The role of radiosurgery for hemangiopericytomas. *Neurosurg Focus* (2003) 14(5):e14. doi: 10.3171/foc.2003.14.5.15
6. Kano H, Niranjan A, Kondziolka D, Flickinger JC, Lunsford LD. Adjuvant stereotactic radiosurgery after resection of intracranial hemangiopericytomas. *Int J Radiat Oncol Biol Phys* (2008) 72(5):1333–9. doi: 10.1016/j.ijrobp.2008.03.024
7. Schiariti M, Goetz P, El-Maghraby H, Tailor J, Kitchen N. Hemangiopericytoma: long-term outcome revisited. Clinical article. *J Neurosurg* (2011) 114(3):747–55. doi: 10.3171/2010.6.JNS091660
8. Chamberlain MC, Glantz MJ. Sequential salvage chemotherapy for recurrent intracranial hemangiopericytoma. *Neurosurgery* (2008) 63(4):720–6. author reply 726-7. doi: 10.1227/01.NEU.0000325494.69836.51
9. Coffey RJ, Cascino TL, Shaw EG. Radiosurgical treatment of recurrent hemangiopericytomas of the meninges: preliminary results. *J Neurosurg* (1993) 78(6):903–8. doi: 10.3171/jns.1993.78.6.0903
10. Veeravagu A, Jiang B, Patil CG, Lee M, Soltys SG, Gibbs IC, et al. CyberKnife stereotactic radiosurgery for recurrent, metastatic, and residual hemangiopericytomas. *J Hematol Oncol* (2011) 4:26. doi: 10.1186/1756-8722-4-26
11. Ecker RD, Marsh WR, Pollock BE, Kurtkaya-Yapicier O, McClelland R, Scheithauer BW, et al. Hemangiopericytoma in the central nervous system: treatment, pathological features, and long-term follow up in 38 patients. *J Neurosurg* (2003) 98(6):1182–7. doi: 10.3171/jns.2003.98.6.1182
12. Laviv Y, Thomas A, Kasper EM. Hypervascular Lesions of the Cerebellopontine Angle: The Relevance of Angiography as a Diagnostic and Therapeutic Tool and the Role of Stereotactic Radiosurgery in Management. *A Compr Review World Neurosurg* (2017) 100:100–17. doi: 10.1016/j.wneu.2016.12.091
13. Ghose A, Guha G, Kundu R, Tew J, Chaudhary R. CNS Hemangiopericytoma: A Systematic Review of 523 Patients. *Am J Clin Oncol* (2017) 40(3):223–7. doi: 10.1097/COC.0000000000000146
14. Sheehan J, Kondziolka D, Flickinger J, Lunsford LD. Radiosurgery for treatment of recurrent intracranial hemangiopericytomas. *Neurosurgery* (2002) 51(4):905–10. discussion 910-1. doi: 10.1227/00006123-200210000-00008
15. Rutkowski MJ, Sughrue ME, Kane AJ, Aranda D, Mills SA, Barani IJ, et al. Predictors of mortality following treatment of intracranial hemangiopericytoma. *J Neurosurg* (2010) 113(2):333–9. doi: 10.3171/2010.3.JNS091882
16. Bastin KT, Mehta MP. Meningeal hemangiopericytoma: defining the role for radiation therapy. *J Neurooncol* (1992) 14(3):277–87. doi: 10.1007/BF00172604
17. Galanis E, Buckner JC, Scheithauer BW, Kimmel DW, Schomberg PJ, Piepgras DG, et al. Management of recurrent meningeal hemangiopericytoma. *Cancer* (1998) 82(10):1915–20. doi: 10.1002/(SICI)1097-0142(19980515)82:10<1915::AID-CNCR15>3.0.CO;2-W
18. Payne BR, Prasad D, Steiner M, Steiner L. Gamma surgery for hemangiopericytomas. *Acta Neurochir (Wien)* (2000) 142(5):527–36. discussion 536-7. doi: 10.1007/s007010050465
19. Sun S, Liu A, Wang C. Gamma knife radiosurgery for recurrent and residual meningeal hemangiopericytomas. *Stereotact Funct Neurosurg* (2009) 87(2):114–9. doi: 10.1159/000202978
20. Iwai Y, Yamanaka K. Gamma knife radiosurgery for other primary intra-axial tumors. *Prog Neurol Surg* (2009) 22:129–41. doi: 10.1159/000163395
21. Tsugawa T, Mori Y, Kobayashi T, Hashizume C, Shibamoto Y, Wakabayashi T. Gamma knife stereotactic radiosurgery for intracranial hemangiopericytoma. *J Radiosurg SBRT* (2014) 3(1):29–35.
22. Copeland WR, Link MJ, Stafford SL, Pollock BE. Single-fraction stereotactic radiosurgery of meningeal hemangiopericytomas. *J Neurooncol* (2014) 120(1):95–102. doi: 10.1007/s11060-014-1521-3
23. Kim BS, Kong DS, Seol HJ, Nam DH, Lee JI. Gamma knife radiosurgery for residual or recurrent intracranial hemangiopericytomas. *J Clin Neurosci* (2017) 35:35–41. doi: 10.1016/j.jocn.2016.10.002
24. Dufour H, Métellus P, Fuentes S, Murracciole X, Régis J, Figarella-Branger D, et al. Meningeal hemangiopericytoma: a retrospective study of 21 patients with special review of postoperative external radiotherapy. *Neurosurgery* (2001) 48(4):756–62. discussion 762-3. doi: 10.1227/00006123-200104000-00011
25. Kim JH, Jung HW, Kim YS, Kim CJ, Hwang SK, Paek SH, et al. Meningeal hemangiopericytomas: long-term outcome and biological behavior. *Surg Neurol* (2003) 59(1):47–53. discussion 53-4. doi: 10.1016/S0090-3019(02)00917-5
26. Park MS, Araujo DM. New insights into the hemangiopericytoma/solitary fibrous tumor spectrum of tumors. *Curr Opin Oncol* (2009) 21(4):327–31. doi: 10.1097/CCO.0b013e32832c9532
27. Kamamoto D, Ohara K, Kitamura Y, Yoshida K, Kawakami Y, Sasaki H. Association between programmed cell death ligand-1 expression and extracranial metastasis in intracranial solitary fibrous tumor/hemangiopericytoma. *J Neurooncol* (2018) 139(2):251–9. doi: 10.1007/s11060-018-2876-7

Conflict of Interest: The authors declare that the research was conducted in the absence of any commercial or financial relationships that could be construed as a potential conflict of interest.

frontiers in Oncology

ORIGINAL RESEARCH
published: 05 March 2021
doi: 10.3389/fonc.2021.627428

Characteristic of Tumor Regrowth After Gamma Knife Radiosurgery and Outcomes of Repeat Gamma Knife Radiosurgery in Nonfunctioning Pituitary Adenomas

Yanli Li[1†], Lisha Wu[2†], Tingting Quan[3†], Junyi Fu[4†], Linhui Cao[5], Xi Li[6], Shunyao Liang[7], Minyi Huang[7], Yinhui Deng[7] and Jinxiu Yu[7]*

[1] Department of Endocrinology, The Second Affiliated Hospital of Guangzhou Medical University, Guangzhou, China, [2] Department of Medical Oncology, Sun Yat-sen Memorial Hospital, Sun Yat-sen University, Guangzhou, China, [3] Department of Radiology, Sun Yat-sen University Cancer Center, State Key Laboratory of Oncology in South China, Collaborative Innovation Center for Cancer Medicine, Guangzhou, China, [4] Department of Neurology, The Second Affiliated Hospital of Guangzhou Medical University, Guangzhou, China, [5] Department of Traditional Chinese Medicine, Sun Yat-sen Memorial Hospital, Sun Yat-sen University, Guangzhou, China, [6] Department of Radiology, The Second Affiliated Hospital of Guangzhou Medical University, Guangzhou, China, [7] Department of Radiotherapy, The Second Affiliated Hospital of Guangzhou Medical University, Guangzhou, China

Objective: This study aimed to report the characteristic of tumor regrowth after gamma knife radiosurgery (GKRS) and outcomes of repeat GKRS in nonfunctioning pituitary adenomas (NFPAs).

Design and Methods: This retrospective study consisted of 369 NFPA patients treated with GKRS. The median age was 45.2 (range, 7.2–84.0) years. The median tumor volume was 3.5 (range, 0.1–44.3) cm^3.

Results: Twenty-four patients (6.5%) were confirmed as regrowth after GKRS. The regrowth-free survivals were 100%, 98%, 97%, 86% and 77% at 1, 3, 5, 10 and 15 year, respectively. In multivariate analysis, parasellar invasion and margin dose (<12 Gy) were associated with tumor regrowth (hazard ratio [HR] = 3.125, 95% confidence interval [CI] = 1.318–7.410, p = 0.010 and HR = 3.359, 95% CI = 1.347–8.379, p = 0.009, respectively). The median time of regrowth was 86.1 (range, 23.2–236.0) months. Previous surgery was associated with tumor regrowth out of field (p = 0.033). Twelve patients underwent repeat GKRS, including regrowth in (n = 8) and out of field (n = 4). Tumor shrunk in seven patients (58.3%), remained stable in one (8.3%) and regrowth in four (33.3%) with a median repeat GKRS margin dose of 12 (range, 10.0–14.0) Gy. The actuarial tumor control rates were 100%, 90%, 90%, 68%, and 68% at 1, 3, 5, 10, and 15 years after repeat GKRS, respectively.

Conclusions: Parasellar invasion and tumor margin dose (<12 Gy) were independent risk factors for tumor regrowth after GKRS. Repeat GKRS might be effective on tumor control for selected patients. For regrowth in field due to relatively insufficient radiation dose,

OPEN ACCESS

Edited by:
Maciej Harat, Franciszek Lukaszczyk Oncology Centre, Poland

Reviewed by:
Christoph Straube, Technical University of Munich, Germany
Constantin Tuleasca, Centre Hospitalier Universitaire Vaudois (CHUV), Switzerland

***Correspondence:**
Jinxiu Yu
josse_yu@foxmail.com

†These authors have contributed equally to this work

Specialty section:
This article was submitted to Neuro-Oncology and Neurosurgical Oncology, a section of the journal Frontiers in Oncology

Received: *09 November 2020*
Accepted: *21 January 2021*
Published: *05 March 2021*

Citation:
Li Y, Wu L, Quan T, Fu J, Cao L, Li X, Liang S, Huang M, Deng Y and Yu J (2021) Characteristic of Tumor Regrowth After Gamma Knife Radiosurgery and Outcomes of Repeat Gamma Knife Radiosurgery in Nonfunctioning Pituitary Adenomas. Front. Oncol. 11:627428. doi: 10.3389/fonc.2021.627428

repeat GKRS might offer satisfactory tumor control. For regrowth out of field, preventing regrowth out of field was the key management. Sufficient target coverage and close follow-up might be helpful.

Keywords: gamma knife, radiosurgery, regrowth, pituitary adenoma, aggressive, nonfunctioning

INTRODUCTION

Nonfunctioning pituitary adenomas (NFPAs) represent about 30% (1) of pituitary tumors. The managements of NFPAs include surgical resection, radiotherapy, medical treatment, and observation. Surgical resection is firstly recommended as the primary treatment of symptomatic patients with NFPA (2). Radiotherapy is recommended for residual or recurrent NFPAs (3). When patients are not candidate to surgical resection because of significant comorbidities, an advanced age or cavernous sinus invasion, radiotherapy may be used as primary management (4). Gamma Knife radiosurgery (GKRS) which has advantages of a highly precise, better dose conformity and focused delivery of radiation in a single session, is one of the best radiation technique and essential part in the treatment of pituitary tumors. As previous publications reported (4–12), GKRS has been proved to offer a high tumor control rate of 83–95% and a low new-onset hypopituitarism rate of 9–32% for pituitary adenomas. Treatment failure after GKRS for NFPAs consists of progressive cystic enlargement, tumor apoplexy and tumor regrowth (4). Tumor regrowth is the most common type of treatment failure in GKRS for NFPAs. Most publications reported tumor recurrence in 0–9.6% of treated patients with NFPA after GKRS (11, 13–18). However, there are few studies reporting the characteristics of tumor regrowth after GKRS and outcomes of repeat GKRS. Since 1993, the Second Affiliated Hospital of Guangzhou Medical University has more than 26 years' experience in using Gamma Knife (Elekta, Stockholm, Sweden) for NFPAs. To report the characteristics of tumor regrowth and outcomes of repeat GKRS for NFPA patients with tumor regrowth after GKRS, we performed a single-center study.

METHODS

Patient Population

Between 1993 and 2016, there were 2557 patients with pituitary adenomas treated with GKRS at the Second Affiliated Hospital of Guangzhou Medical University. Most of patients were lost to follow up because of coming from a long distance. Finally, there were only 751 pituitary adenoma patients had clinical and sufficient follow-up (>12 months) information at our hospital. Of the 751 patients, 369 NFPA patients were enrolled in this study. The patients were diagnosed by surgical pathology or MRI findings. There was no evidence of hormonal hypersecretion in these patients. This retrospective study was approved by the institutional committee of the Second Affiliated Hospital of Guangzhou Medical University.

Clinical and Radiological Evaluations

All of patients were routinely followed up with MRI of the sellar and clinical evaluations. No matter when it was possible, patients took follow-up examination at our hospital. If not, clinical information, MRI and laboratory tests were sent and reviewed at our center. The follow-up evaluations were collected and reviewed by the treating radiologists and clinicians.

Tumor dimensions were got from MR imaging by manual. The tumor dimensional indices were measured and recorded in three orthogonal planes: transverse (TR), anteroposterior (AP), and craniocaudal (CC). The tumor volumes were estimated using the formula: $V = (\pi \times [TR \times AP \times CC])/6$ (19). Considering the irregular shape of some tumors, tumor volume measurement was only a rough estimate of the actual volume. Tumor progression was defined as tumor enlargement at least 20% in tumor volume. Tumor shrinkage was defined as at least a 20% shrinkage in tumor volume. Stable tumor was defined as tumor volume change within 20%. Tumor regrowth was defined as new lesion detected on follow-up MRI or regrowth on residual tumor. Tumor regrowth on adjacent or within the prescribed isodose was considered as regrowth in field (**Figure 1**). Tumor regrowth outside the prescribed isodose was considered as regrowth out of field (**Figure 2**). The Knosp grade 3 or 4 was considered as parasellar invasion. The tumor close to optic structure (<2 mm) was considered as suprasellar extension.

Gamma Knife Radiosurgery Technique

The procedure was performed using Leksell Gamma Knife. Model B Leksell Gamma Knife Unit was used until April 2014 and was then replaced by Perfexion Unit (Elekta Instrument, Inc.). Stereotactic Leksell frame placement was performed under local anesthetic. Following frame placement, thin-slice stereotactic MR imaging with the administration of intravenous contrast material was performed through the sellar. The maximal dose to the optic pathway was ≤10 Gy. Small collimators of 4 and 8 mm were mainly used to get better conformality.

Statistical Analysis

The normal distribution of continuous variables was checked by Kolmogorov–Smirnov test. The mean (± SEM) was used to describe continuous variables with normal distribution. The median and interquartile ranges (IQR) was used to describe variables not normally distributed. F test was used for homogeneity of variance in continuous variables. Independent-sample t test was used to compare means of continuous variables with normal distribution. When continuous variables were not normally distributed, Wilcoxon rank sum test was used. Chi-square test and Fisher exact test were used for statistical analysis of categorical variables. Log-rank test statistics and a step forward

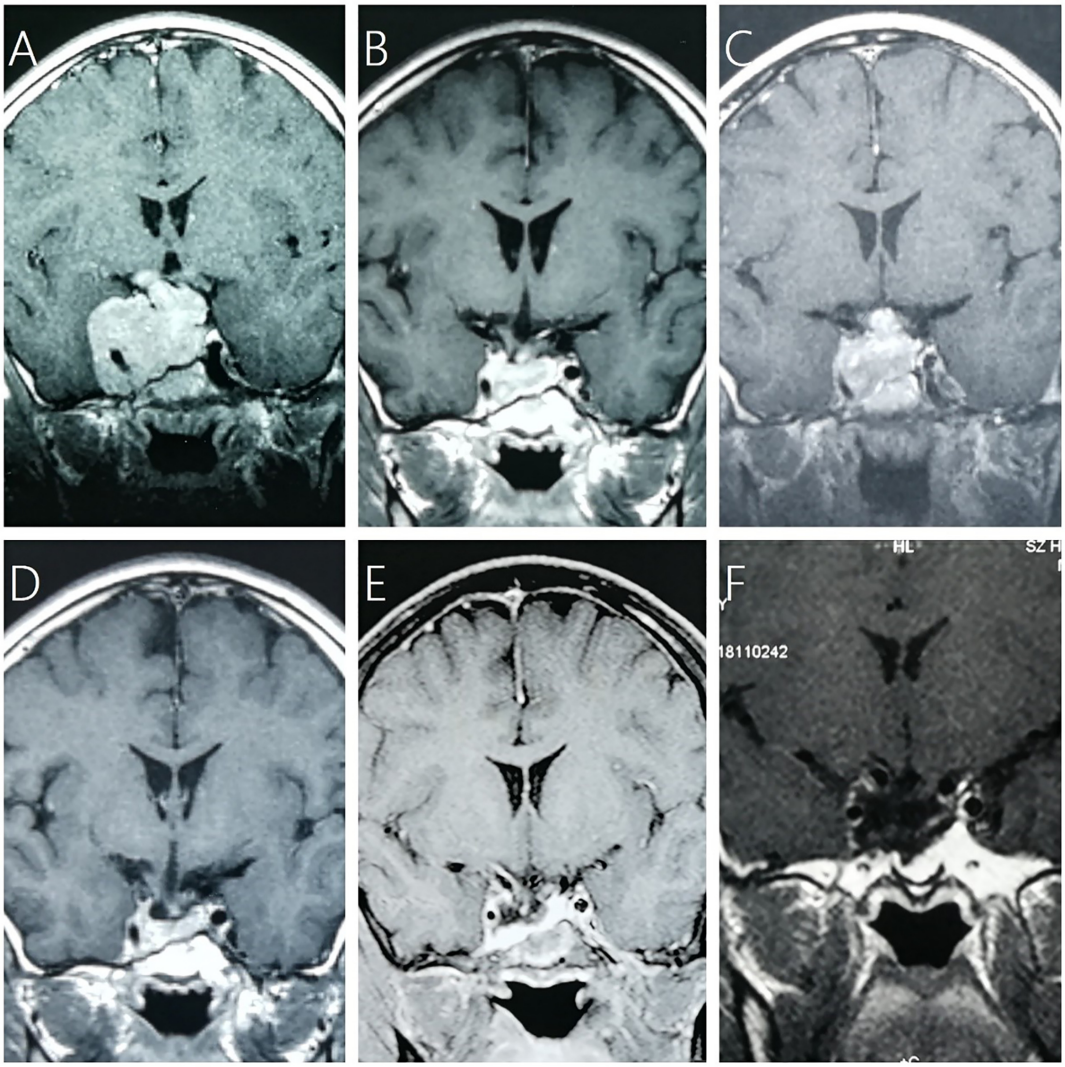

FIGURE 1 | A 13-year-old boy with NFPA (max diameter of 7.6 cm) received adjuvant GKRS (10 Gy/35%) after subtotal resection and repeat GKRS (12 Gy/35%) for tumor regrowth at 36.5 months after prior GKRS. **(A)** contrast-enhanced coronal T1-weighted magnetic resonance imaging (MRI) scans showed residual giant NFPA after surgical resection. **(B)** MRI showed tumor shrinkage at 24.6 months after GKRS. **(C)** MRI showed tumor regrowth at 37.9 months after prior GKRS. **(D)** MRI showed tumor shrinkage at 10.1 months after repeat GKRS. **(E)** MRI showed tumor shrinkage at 68.8 months after repeat GKRS. **(F)** MRI showed tumor shrinkage at 205.0 months after repeat GKRS.

likelihood ratio method of Cox proportional hazard models were used for univariate and multivariate analysis, respectively. Kaplan-Meier curves were plotted for regrowth-free survival. Probability values < 0.05 were defined as statistically significant. For statistical analysis, IBM's SPSS (version 26.0) was used.

RESULTS

Patient Characteristics

There were 369 NFPA patients in this study. The population consisted of 185 male (50.1%) and 184 female (49.9%) patients with a median age of 45.2 (range, 7.2–84.0) years. The median follow-up was 60.8 (range, 12.8–283.0) months. The median tumor volume was 3.5 (range, 0.1–44.3) cm^3. There were four patients (1.1%) underwent radiation before GKRS. There were 173 patients (46.9%) treated with adjuvant GKRS after surgery. There were 162 patients (43.9%) with suprasellar extension and 138 patients (34.8%) with parasellar invasion. The median tumor margin dose was 13.3 (range, 8.0–22.0) Gy at a median prescription isodose 40% (range, 25–71%). The median maximum dose was 33.3 (range, 14.0–66.7) Gy (**Table 1**).

Risk Factors Associated With Tumor Regrowth

Of the 369 NFPA patients who underwent GKRS, 24 patients (6.5%) confirmed as tumor regrowth. The regrowth-free

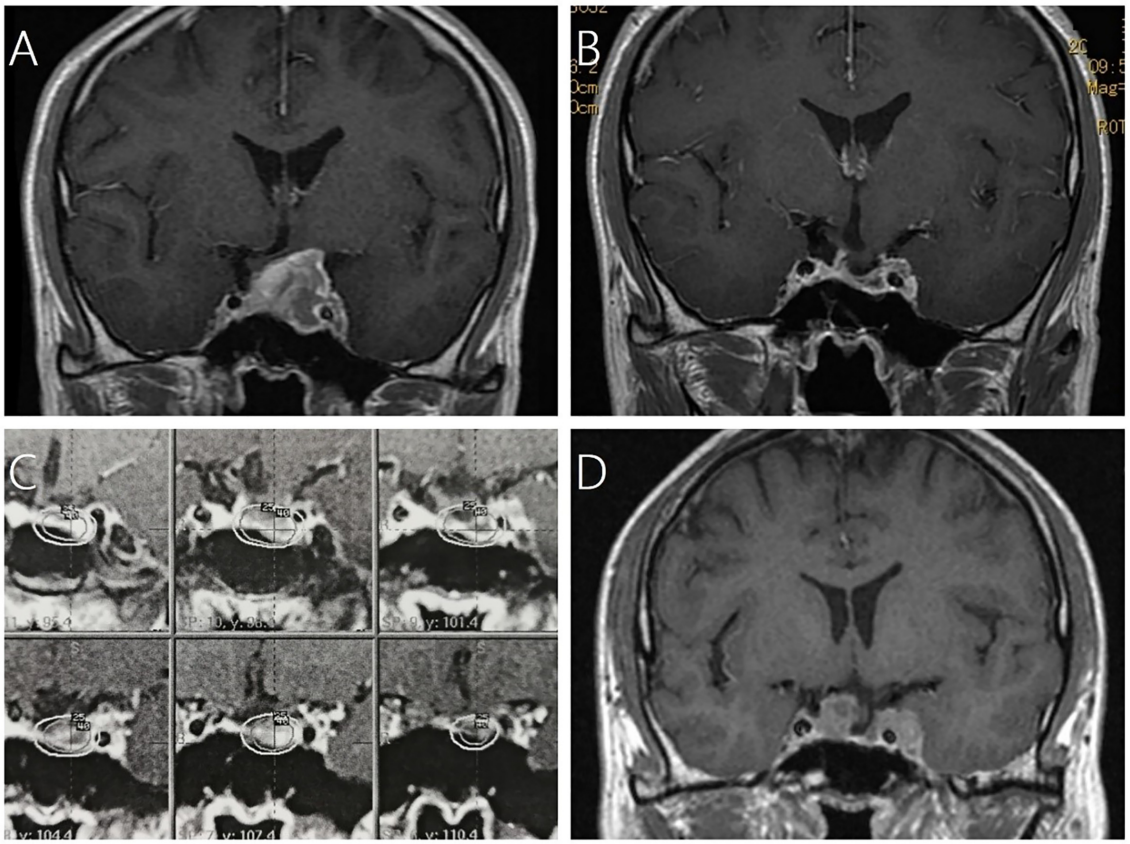

FIGURE 2 | A 43-year-old male patient with residual NFPA after surgical resection received GKRS and developed tumor regrowth out of field at 71 months after GKRS. **(A)** contrast-enhanced coronal T1-weighted magnetic resonance imaging (MRI) scans showed pituitary adenoma. **(B)** MRI showed subtotal resection for pituitary adenoma after 3.5 months. **(C)** Dose distribution of adjuvant GKRS after surgical resection. **(D)** MRI showed tumor regrowth was either in the sellar as well as in the cavernous sinus out of field.

survivals were 100%, 98%, 97%, 86% and 77% at 1, 3, 5, 10, and 15 year, respectively (**Figure 3**). In univariate analysis, risk factors associated with tumor regrowth included prior surgical resection ($p = 0.034$), parasellar invasion ($p \leq 0.001$) (**Figure 4**), tumor margin dose (<12 Gy) ($p \leq 0.001$) (**Figure 5**), and tumor volume (≥5 cm^3) ($p = 0.003$). In multivariate analysis, only parasellar invasion and tumor margin dose (<12 Gy) were significantly related with tumor regrowth (hazard ratio [HR] = 3.125, 95% confidence interval [CI] = 1.318–7.410, p = 0.010 and HR = 3.359, 95% CI = 1.347–8.379, P = 0.009, respectively) (**Table 2**).

Characteristics of Tumor Regrowth

Of the 24 patients with tumor regrowth after GKRS, there were 13 male (54.2%) and 11 female (45.8%) patients with a mean age of 40.7 (median, 49.2, range, 16.4–70.2) years. The mean follow-up was 144.1 (median, 134.1, range, 22.5–260.8) months. There were 15 (62.5%) and 9 patients (37.5%) with tumor regrowth in and out of field, respectively. There were 14 patients (58.3%) underwent surgical resection previously. The mean tumor volume at prior GKRS was 13.1 (median, 9.8, range, 0.9–34.8) cm^3. There were 22 patients (91.7%) with suprasellar extension and 17 patients (70.8%) with parasellar invasion. The mean prior GKRS margin dose was 10.0 (median, 10.0, range, 9.0–17.0) Gy. The mean prior GKRS maximum dose was 33.1 (median, 33.2, range, 25.0–40.0) Gy. The mean time of regrowth was 91.8

TABLE 1 | Baseline clinical characteristics of 369 patients with nonfunctioning pituitary adenomas and GKRS parameters.

Characteristic	value
Male/Female, n (%)	185/184 (50.1/49.9)
Median age, (range), years	45.2 (7.2–84.0)
Median FU length, (range), months	60.8 (12.8–283.0)
Median tumor volume at GKRS, (range), cm^3	3.5 (0.1–44.3)
Previous radiotherapy, n (%)	4 (1.1)
Prior surgical resection, n (%)	173 (46.9)
Parasellar invasion, n (%)	138 (34.8)
Suprasellar extension, n (%)	162 (43.9)
GKRS parameters	
Median tumor margin radiation dose, (range), Gy	13.3 (8.0–22.0)
Median maximum radiation dose, (range), Gy	33.0 (14.0–66.7)
Median prescription isodose, (range), %	40.0 (25.0–71.0)

FU, follow up; GKRS, gamma knife radiosurgery.

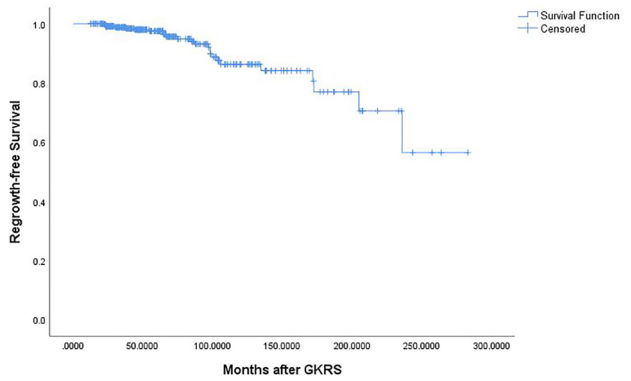

FIGURE 3 | Kaplan–Meier curve of tumor regrowth-free survival.

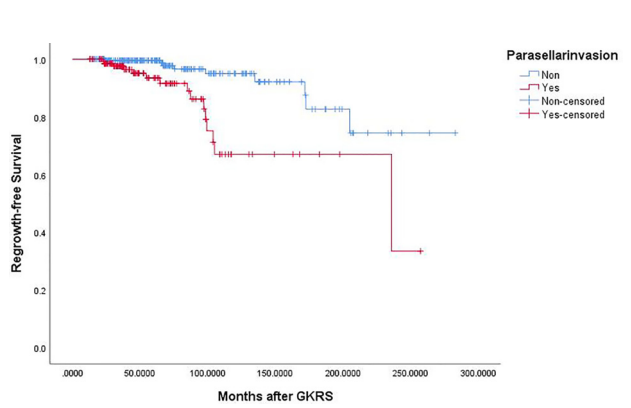

FIGURE 4 | Kaplan–Meier curve of tumor regrowth-free survival of parasellar invasion (p = 0.000).

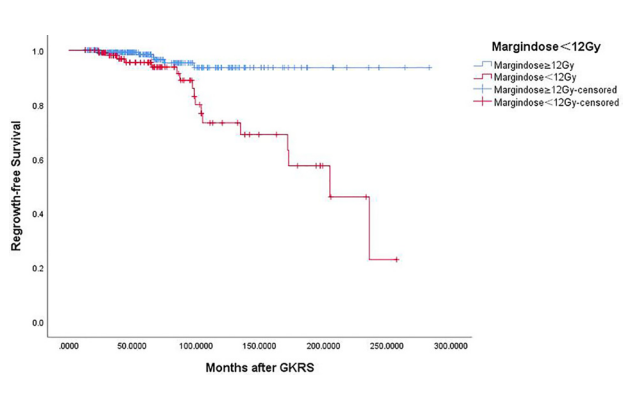

FIGURE 5 | Kaplan–Meier curve of tumor regrowth-free survival of tumor margin dose ≥12 Gy vs. <12 Gy. Tumor margin dose <12 Gy showed a lower tumor regrowth-free survival rate (p = 0.000).

TABLE 2 | Results of univariate and multivariate analyses for tumor regrowth after GKRS.

Variables	Tumor regrowth			
	Univariate, *p*	Multivariate, *p*	HR	95% CI
Age (≥55 years)	0.847	NA	NA	NA
Sex (male VS female)	0.649	NA	NA	NA
Prior surgical resection	0.034*	0.169	NA	NA
Parasellar invasion	≤0.001*	0.010*	3.125	1.318–7.410
Suprasellar invasion	0.096	0.194	NA	NA
Tumor margin dose (<12 Gy)	≤0.001*	0.009*	3.359	1.347–8.379
Tumor volume (≥5 cm^3)	0.003*	0.920	NA	NA

GKRS, gamma knife radiosurgery; CI, confidential interval; HR, hazards ratio; NA, not available.
**Statistically significant (P < 0.05).*

(median, 86.1, range, 23.2–236.0) months. The characteristics of the 24 patients, grouped according to the type of tumor regrowth, were summarized in **Table 3**. There were more patients who previously underwent surgery developed tumor regrowth out of field (p = 0.033). the proportion of gender, parasellar invasion, suprasellar extension, age, margin dose, maximum dose, tumor volume, and time of regrowth, were similar in the two groups (**Table 3**).

Further Treatment and Outcomes of Repeat GKRS

Among the 24 patients, 16 patients (66.7%) underwent repeat GKRS alone, 2 patients (8.3%) underwent surgery, 2 patients (8.3%) underwent surgery and repeat GKRS, 2 patients (8.3%) were under observation, 2 patients were lost to follow up. There was no other medical treatment except hormone supplement in these patients.

There were 18 patients underwent repeat GKRS. Six patients were lost to follow up. Finally, only 12 patients underwent repeat GKRS alone had follow-up MRI. The data was showed in **Table 4**. The patient population consisted of six male (50%) and 6 females (50%) patients with a median age of 46.7 (range, 16.4–70.2) years. There were 8 (66.7%) and 4 patients (33.3%) with tumor regrowth in and out of field, respectively. There were 8 patients (66.7%) with parasellar invasion. The median previous GKRS margin dose was 10.0 (range, 9.0–15.5) Gy. The median previous GKRS maximal dose was 33.2 (range, 25.0–36.0) Gy. The median tumor volume at repeat GKRS was 9.8 (range, 0.6–66.8) cm^3. The median repeat margin dose and maximum dose was 12 (range, 10.0–14.0) Gy and 33.2 (range, 28–40) Gy, respectively. Finally, with a median imaging follow-up of 84.8 (range,11.4–205.0) months after repeat GKRS, tumor shrunk in 7 patients (58.3%), remained stable in 1 patient (8.3%) and tumor regrowth in 4 patients (33.3%). The actuarial tumor control rates were 100%, 90%, 90%, 68%, and 68% at 1, 3, 5, 10, and 15 years after repeat GKRS, respectively (**Figure 6**). Among the eight patients with tumor control, there were two patients with short imaging follow-up of 11.4 and 14.1 months, respectively, which might overestimate tumor control rate in this study. For the patient with tumor shrinkage at imaging follow-up of 11.4 months, we had follow-up by telephone at 216.9 months after

TABLE 3 | Characteristics of 24 NFPA patients grouped according to the type of tumor regrowth after GKRS.

Characteristic	Regrowth in field (n = 15)	Regrowth out of field (n = 9)	All patients (n = 24)	P value
Female sex, n (%)	7 (46.7)	4 (44.4)	11 (45.8)	1.000
Mean age at prior GKRS (years)	41.1 ± 3.8	39.9 ± 3.9	40.7 ± 2.7	0.833
Parasellar invasion, n (%)	9 (60)	8 (88.9)	17 (70.8)	0.191
Suprasellar extension, n (%)	13 (86.7)	9 (100)	22 (91.7)	0.511
Previous surgical resection, n (%)	6 (40)	8 (88.9)	14 (58.3)	0.033*
Prior GKRS margin dose, median (IQR), (Gy)	10.0 (9.0–12.0)	11.0 (10.0–12.8)	10.0 (9.9–12.6)	0.528
Mean prior GKRS maximum dose (Gy)	33.3 ± 1.0	33.4 ± 0.6	33.1 ± 0.6	0.723
Time of regrowth, median (IQR), (months)	85.0 (64.8–134.8)	97.0 (23.5–102.2)	86.1 (46.8–104.8)	0.325
Mean tumor volume at prior GKRS, median (IQR), (cm^3)	9.4 (5.8–15.7)	13.6 (4.6–27.9)	9.8 (5.3–20.1)	0.421

Data are expressed as number, mean ± SEM, median and IQR, or percentage.
GKRS, gamma knife radiosurgery; IQR interquartile range.
**Statistically significant (P < 0.05).*

TABLE 4 | Imaging outcomes of repeat GKRS for 12 NFPA patients with tumor regrowth after GKRS.

Sex/Age	Type of regrowth	Previous GKRS dose	Repeat GKRS dose	Imaging outcome	FU after repeat GKRS (months)
Male/31.4	Out of field	10.0 Gy at 30%	14.4 Gy at 40%	Regrowth (out of field)	71.4
Female/49.1	In field	15.1 Gy at 50%	10.0 Gy at 25%	Shrinkage	11.4
Female/55.9	In field	9.0 Gy at 36%	11.7 Gy at 35%	Regrowth (out of field)	193.8
Female/48.1	In field	10.0 Gy at 30%	13.0 Gy at 40%	Shrinkage	89.9
Male/16.4	In field	10.0 Gy at 35%	12.0 Gy at 40%	Shrinkage	205.0
Male/53.6	In field	11.6 Gy at 35%	11.7 Gy at 35%	Shrinkage	156.9
Female/70.2	In field	10.0 Gy at 30%	14.0 Gy at 50%	Shrinkage	38.2
Female/31.9	In field	9.9 Gy at 30%	11.8 Gy at 33%	Shrinkage	109.3
Female/49.7	Out of field	10.0 Gy at 30%	10.5 Gy at 35%	Stable	14.1
Male/43.1	Out of field	11.0 Gy at 35%	12.0 Gy at 40%	Regrowth (out of field)	15.3
Male/22.3	In field	12.0 Gy at 35%	13.2 Gy at 40%	Regrowth (in field)	79.6
Male/45.4	Out of field	14.4 Gy at 40%	14.0 Gy at 40%	Shrinkage	120.0

FU, follow up; GKRS, gamma knife radiosurgery; TV, tumor volume.

repeat GKRS, the patient had a good quality of life and nothing to complain, including headache, visual impairment, and cranial nerve impairment. Another patient with a large tumor volume of 66.8 cm^3 remained stable at 14.1 months was lost to follow-up. Among the four patients with tumor regrowth after repeat GKRS, three patients presented with tumor regrowth out of field. In these three patients, all of the tumors within the repeat GKRS radiation field were shrinkage, one patient received 3rd GKRS for tumor regrowth in cavernous sinus, one patient was under observation, and another patient was lost to follow-up. It was indicated that these patients were heavily infiltrating NFPA and should be cautious of tumor regrowth out of field. Another patient with tumor regrowth in field previously presented tumor regrowth in field again after repeat GKRS and was advised to receive surgical resection. It was indicated that the tumor might be resistant to radiation. After repeat GKRS, one patient who presented with tumor regrowth in the cavernous sinus occurred new oculomotor neuropathy, another patient whose optic chiasm was compressed by tumor regrowth in the suprasellar region occurred new or worsened visual impairment.

Risk factors such as age, sex, parasellar invasion, suprasellar extension, prior surgery, repeat GKRS margin dose, maximal repeat GKRS radiation dose, type of regrowth, and time of regrowth were analyzed. No factors were significantly associated with progression. The small number of cases limited statistical power.

DISCUSSION

Our study was a single-center series reporting the characteristic of tumor regrowth after GKRS and outcomes of repeat GKRS in NFPA patients. In the current study, 24 patients (6.5%) were confirmed as regrowth after GKRS. The regrowth-free survivals

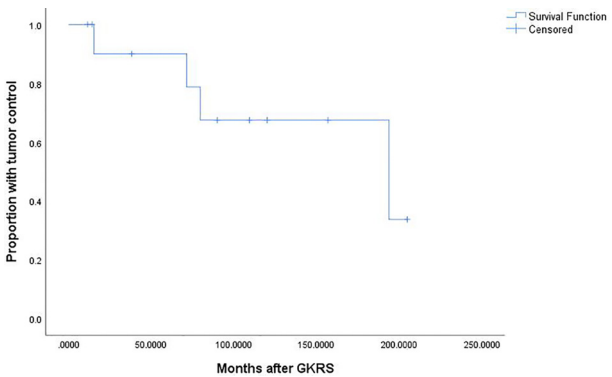

FIGURE 6 | Kaplan-Meier curve of tumor control for the 12 patients who undergoing repeat GKRS. The actuarial tumor control rates were 100%, 90%, 90%, 68%, and 68% at 1, 3, 5, 10, and 15 years after repeat GKRS, respectively.

were 100%, 98%, 97%, 86% and 77% at 1, 3, 5, 10, and 15 years, respectively. The median time of regrowth was 86.1 (range, 23.2–236.0) months. In multivariate analysis, only parasellar invasion and tumor margin dose (<12 Gy) were significantly associated with tumor regrowth. Twelve patients underwent repeat GKRS, including regrowth in (n = 8) and out of field (n = 4). Tumor shrunk in seven patients (58.3%), remained stable in one (8.3%) and regrowth in four (33.3%) with a median repeat GKRS margin dose of 12 (range, 10.0–14.0) Gy. The actuarial tumor control rates were 100%, 90%, 90%, 68%, and 68% at 1, 3, 5, 10 and 15 years after repeat GKRS, respectively.

In previous studies, 0–9.6% of NFPA patients occurred tumor recurrence after GKRS (11, 13–18). In a large study of 543 patients with pituitary adenomas by Losa et al. (18), there were more patients with NFPA than functioning pituitary adenomas had a tumor recurrence (9.6% VS 4.8%). In the 272 NFPA patients, there were 26 patients (9.6%) developed tumor recurrence, which was higher than our study. In the NFPA group, there were no risk factors associated with tumor recurrence. Sheehan et al. (9) reported a pooled analysis of data from nine center in North America, 31 of 469 NFPA patients (6.6%) developed tumor regrowth after a shorter median follow-up of 36 months. Tumor volume at GKRS was the only risk factor associated with tumor recurrence. Sun et al. (5) also reported parasellar invasion was risk factor associated with tumor control in the treatment of GKRS for postsurgical NFPAs. Radiosurgery with single doses of ≥12 Gy is recommended for greater local tumor control rate of ≥90% in a systematic review and evidence-based guideline (3). In our study, a large tumor volume and tumor close to optic nerve were the reasons of a relative low tumor margin dose to tumor. Therefore, these patients were prone to regrow due to a relative low dose. For the tumors with large volume or close to optic nerve, multisession GKRS or fractioned stereotactic radiation therapy might have advantage for tumor control comparing with single session GKRS. Tomotherapy, Cyberknife or linear accelerator were not available in our hospital. Leksell Gamma Knife Unit B was replaced by Perfexion Unit until 2014. These may be disadvantage for treatment of tumors with large volume.

In current study, with a median imaging follow-up of 84.8 (range,11.4–205.0) months after repeat GKRS for 12 patients with regrowth, tumor shrunk in seven patients (58.3%), remained stable in one patient (8.3%), and tumor regrowth in four patients (33.3%). The actuarial tumor control rates were 100%, 90%, 90%, 68%, and 68% at 1, 3, 5, 10, and 15 years after repeat GKRS, respectively. In the study of Losa et al. (18), 16 of 26 NFPA patients received GKRS as further therapy, and 15 of them had final outcomes. With median follow-up of 68 (range, 14–167) months in these patients, tumor improving in 1 patient (6.7%), remained stable in 13 patients (86.7%), only 1 patient (6.7%) with tumor progression. The actuarial tumor control rates were 93 and 93% at 5 and 10 years, respectively, which were higher than our study. However, the proportion of tumor improving was much lower than our study. Besides, the only patient with tumor improving received GKRS and temozolomide. Did the tumor shrinkage was due to GKRS or temozolomide or both of them? What's more, the definition of tumor improving and stable were not available in the literature.

In this study, we defined two clearly distinct patterns of tumor regrowth after GKRS: tumor regrowth in and out of previous radiation field. The tumor regrowth in field was more frequent than out of field (66.7 VS 33.3%) in our study. In the study of Losa et al. (18), of the 26 patients, there were 18 patients (69.2%) developed recurrence out of field, which was higher than our study. We found previous surgery was significantly associated with tumor regrowth out of field (p = 0.033). In the study of Losa et al. (18), 91.5% of NFPA patients had previous surgery. However, because of significant comorbidities, an advanced age, preoperative functional status and cavernous sinus invasion, only 14 patients (58.3%) had previous surgery in our study. A higher proportion of surgery contributed to a higher proportion of recurrence out of field. The underlying pathogenesis might be different in the two kind of tumor regrowth, which might have influence on prognostic and therapeutic outcomes. Tumor regrowth out of field usually represented insufficient target coverage because of the tumor infiltrating into surrounding structures or difficulty of differentiating postsurgical changes from residual tumor. Therefore, the tumor target contouring should be performed on presurgical and postsurgical MRI, in order to avoid missing the small residual tumor. Thus, the tumor regrowth out of field seemed to be a low correlation with radiation resistance. In the four patients presented tumor regrowth after repeat GKRS, three of them who were regrowth out of field still showed well response to repeat GKRS radiation field. In the study of Losa et al. (18), most patients with "out of field" recurrence also responded well to GKRS and had stable disease at last follow-up. Preventing tumor regrowth out of field was the key management. Sufficient target coverage and close MRI follow-up might be helpful. Nevertheless, the reasons of tumor regrowth in field might consist of radiation resistance and relatively insufficient radiation dose. If the tumors were resistant to radiation, it might present with aggressive behavior and limit the treatment options. If the tumors regrowth in field were due to relatively insufficient radiation dose, then a high radiation dose might be helpful to control tumor regrowth. In the eight patients with tumor regrowth in field in our study, seven patients received a higher repeat GKRS margin dose than previous dose, two patients (25%) developed regrowth again, including regrowth in field (n = 1) and out of field (n = 1). The patient regrowth in field after repeat GKRS should be considered more resistant to radiation than other patients.

The 2018 European Society of Endocrinology Clinical Practice Guidelines for the management of aggressive pituitary tumors and carcinomas suggested aggressive pituitary adenomas should be considered in patients with a radiologically invasive tumor and unusually rapid tumor growth rate, or clinically relevant tumor growth despite optimal standard therapies (surgery, radiotherapy and conventional medical treatments) (20). Of the 12 patients receiving repeat GKRS in our study, only 8 patients (66.7%) were radiologically cavernous sinus

invasion. Another patient without cavernous sinus invasion was considered refractory to radiation. Most of cases had characteristics of aggressive behavior. There was no standard therapy for aggressive pituitary adenomas. There had been a low-level evidence for temozolomide in small case series (21–26). Recently, an international survey of clinical practice (27) recommended temozolomide as first line chemotherapeutic treatment of aggressive pituitary tumors or pituitary carcinomas. As previous reported, 69% (28) of patients could obtain complete response, partial response or stable disease. The success rate of clear tumor volume reduction (complete response or partial response) was 42% (28). There was rare data about radiotherapy for aggressive pituitary adenomas. In the international survey of clinical practice (27), there were 10 patients underwent radiotherapy as second and third line treatments. Six patients (60%) developed progression. The effect was limited. Our study reported a better tumor control rate. Perhaps, it was due to the heterogenous of the tumors between the studies. For aggressive pituitary tumors, patients should be treated by multidisciplinary team consisting of a neurosurgeon, radiation oncologist, radiologist, endocrinologist and pathologist.

In this study, there were several limitations should be noticed. Firstly, this was a single-center retrospective study with small sample size and thereby reflected selection and treatment biases, as well as limiting statistical power. Secondly, some patients did not receive surgical resection before GKRS, the pathological information was not available, which might indicate aggressive behavior in these patients. Thirdly, tumor volume measurement in this study was only a rough estimate of the actual volume because of the irregular shape of some pituitary tumors. Fourthly, because many patients came from a long distance from nationwide, endocrine tests were usually took in local hospital for their convenience. Therefore, endocrine evaluations before and after GKRS were incomplete in this study.

In this study, parasellar invasion and tumor margin dose (<12 Gy) were independent risk factors for tumor regrowth after GKRS. Tumor regrowth may occur several years after GKRS, long-term regular follow-up is necessary. Tumor regrowth in and out of field may possess different mechanisms and affect prognosis. Repeat GKRS might be effective on tumor control for selected patients. For the pattern of regrowth in field due to relatively insufficient radiation dose, repeat GKRS may still offer satisfactory tumor control rate. For tumor regrowth out of field, preventing tumor regrowth out of field was the key management. Sufficient target coverage and close MRI follow-up might be helpful. All in all, for better management of aggressive pituitary tumors, it should be conducted by a multidisciplinary team consisting of a neurosurgeon, radiation oncologist, radiologist, endocrinologist and pathologist.

DATA AVAILABILITY STATEMENT

The original contributions presented in the study are included in the article/supplementary material. Further inquiries can be directed to the corresponding author.

ETHICS STATEMENT

The studies involving human participants were reviewed and approved by the institutional committee of the Second Affiliated Hospital of Guangzhou Medical University. The patients/participants provided their written informed consent to participate in this study.

AUTHOR CONTRIBUTIONS

Research idea and study design: JF, YL, TQ, and LW. Data acquisition: JF, YL, LW, LC, YD, JY, XL, TQ, SL, and MH. Statistical analysis: LW, YL, and JF. Manuscript drafting: YL, TQ, and LW. Supervision: JY. All authors contributed to the article and approved the submitted version.

FUNDING

This work was supported by National Key Research and Development Project (grants number: 2017YFC0113700); National Natural Science Foundation of China (grants number: 81800682; grant number: 81902928); the Medical and Health Project of Guangzhou (grants number: 20201A011079).

REFERENCES

1. Hoybye C, Rahn T. Adjuvant Gamma Knife radiosurgery in non-functioning pituitary adenomas; low risk of long-term complications in selected patients. *Pituitary* (2009) 12(3):211–6. doi: 10.1007/s11102-008-0163-x
2. Lucas JW, Bodach ME, Tumialan LM, Oyesiku NM, Patil CG, Litvack Z, et al. Congress of Neurological Surgeons Systematic Review and Evidence-Based Guideline on Primary Management of Patients With Nonfunctioning Pituitary Adenomas. *Neurosurgery* (2016) 79(4):E533–5. doi: 10.1227/neu.0000000000001389
3. Sheehan J, Lee CC, Bodach ME, Tumialan LM, Oyesiku NM, Patil CG, et al. Congress of Neurological Surgeons Systematic Review and Evidence-Based Guideline for the Management of Patients With Residual or Recurrent Nonfunctioning Pituitary Adenomas. *Neurosurgery* (2016) 79(4):E539–40. doi: 10.1227/neu.0000000000001385
4. Yu J, Li Y, Quan T, Li X, Peng C, Zeng J, et al. Initial Gamma Knife radiosurgery for nonfunctioning pituitary adenomas: results from a 26-year experience. *Endocrine* (2020) 68(2):399–410. doi: 10.1007/s12020-020-02260-1
5. Sun S, Liu A, Zhang Y. Long-Term Follow-Up Studies of Gamma Knife Radiosurgery for Postsurgical Nonfunctioning Pituitary Adenomas. *World Neurosurg* (2019). doi: 10.1016/j.wneu.2019.01.009
6. Bir SC, Murray RD, Ambekar S, Bollam P, Nanda A. Clinical and Radiologic Outcome of Gamma Knife Radiosurgery on Nonfunctioning Pituitary Adenomas. *J Neurol Surg Part B Skull Base* (2015) 76(5):351–7. doi: 10.1055/s-0035-1549309
7. Starke RM, Williams BJ, Jane JA Jr, Sheehan JP. Gamma Knife surgery for patients with nonfunctioning pituitary macroadenomas: predictors of tumor control, neurological deficits, and hypopituitarism. *J Neurosurg* (2012) 117(1):129–35. doi: 10.3171/2012.4.Jns112250

8. Losa M, Valle M, Mortini P, Franzin A, da Passano CF, Cenzato M, et al. Gamma knife surgery for treatment of residual nonfunctioning pituitary adenomas after surgical debulking. *J Neurosurg* (2004) 100(3):438–44. doi: 10.3171/jns.2004.100.3.0438
9. Sheehan JP, Starke RM, Mathieu D, Young B, Sneed PK, Chiang VL, et al. Gamma Knife radiosurgery for the management of nonfunctioning pituitary adenomas: a multicenter study. *J Neurosurg* (2013) 119(2):446–56. doi: 10.3171/2013.3.JNS12766
10. Zibar Tomsic K, Dusek T, Kraljevic I, Heinrich Z, Solak M, Vucinovic A, et al. Hypopituitarism after gamma knife radiosurgery for pituitary adenoma. *Endocr Res* (2017) 42(4):318–24. doi: 10.1080/07435800.2017.1323913
11. Pollock BE, Cochran J, Natt N, Brown PD, Erickson D, Link MJ, et al. Gamma knife radiosurgery for patients with nonfunctioning pituitary adenomas: results from a 15-year experience. *Int J Radiat Oncol Biol Phys* (2008) 70 (5):1325–9. doi: 10.1016/j.ijrobp.2007.08.018
12. Deng Y, Li Y, Li X, Wu L, Quan T, Peng C, et al. Long-term results of Gamma Knife Radiosurgery for Postsurgical residual or recurrent nonfunctioning Pituitary Adenomas. *Int J Med Sci* (2020) 17(11):1532–40. doi: 10.7150/ijms.47168
13. Mingione V, Yen CP, Vance ML, Steiner M, Sheehan J, Laws ER, et al. Gamma surgery in the treatment of nonsecretory pituitary macroadenoma. *J Neurosurg* (2006) 104(6):876–83. doi: 10.3171/jns.2006.104.6.876
14. Wowra B, Stummer W. Efficacy of gamma knife radiosurgery for nonfunctioning pituitary adenomas: a quantitative follow up with magnetic resonance imaging-based volumetric analysis. *J Neurosurg* (2002) 97(5 Suppl):429–32. doi: 10.3171/jns.2002.97.supplement
15. Petrovich Z, Yu C, Giannotta SL, Zee CS, Apuzzo ML. Gamma knife radiosurgery for pituitary adenoma: early results. *Neurosurgery* (2003) 53 (1):51–9; discussion 9-61. doi: 10.1227/01.neu.0000068702.00330.47
16. Kobayashi T. Long-term results of stereotactic gamma knife radiosurgery for pituitary adenomas. Specific strategies for different types of adenoma. *Prog Neurol Surg* (2009) 22:77–95. doi: 10.1159/000163384
17. Liscak R, Vladyka V, Marek J, Simonova G, Vymazal J. Gamma knife radiosurgery for endocrine-inactive pituitary adenomas. *Acta Neurochir* (2007) 149(10):999–1006; discussion. doi: 10.1007/s00701-007-1253-7
18. Losa M, Spatola G, Albano L, Gandolfi A, Del Vecchio A, Bolognesi A, et al. Frequency, pattern, and outcome of recurrences after gamma knife radiosurgery for pituitary adenomas. *Endocrine* (2017) 56(3):595–602. doi: 10.1007/s12020-016-1081-8
19. Mak HK, Lai SW, Qian W, Xu S, Tong E, Vance ML, et al. Effective time window in reducing pituitary adenoma size by gamma knife radiosurgery. *Pituitary* (2015) 18(4):509–17. doi: 10.1007/s11102-014-0603-8
20. Raverot G, Burman P, McCormack A, Heaney A, Petersenn S, Popovic V, et al. European Society of Endocrinology Clinical Practice Guidelines for the management of aggressive pituitary tumours and carcinomas. *Eur J Endocrinol* (2018) 178(1):G1–G24. doi: 10.1530/EJE-17-0796
21. Lim S, Shahinian H, Maya MM, Yong W, Heaney AP. Temozolomide: a novel treatment for pituitary carcinoma. *Lancet Oncol* (2006) 7(6):518–20. doi: 10.1016/S1470-2045(06)70728-8
22. Fadul CE, Kominsky AL, Meyer LP, Kingman LS, Kinlaw WB, Rhodes CH, et al. Long-term response of pituitary carcinoma to temozolomide. Report of two cases. *J Neurosurg* (2006) 105(4):621–6. doi: 10.3171/jns.2006.105.4.621
23. Bruno OD, Juarez-Allen L, Christiansen SB, Manavela M, Danilowicz K, Vigovich C, et al. Temozolomide Therapy for Aggressive Pituitary Tumors: Results in a Small Series of Patients from Argentina. *Int J Endocrinol* (2015) 2015:587893. doi: 10.1155/2015/587893
24. Raverot G, Sturm N, de Fraipont F, Muller M, Salenave S, Caron P, et al. Temozolomide treatment in aggressive pituitary tumors and pituitary carcinomas: a French multicenter experience. *J Clin Endocrinol Metab* (2010) 95(10):4592–9. doi: 10.1210/jc.2010-0644
25. Losa M, Bogazzi F, Cannavo S, Ceccato F, Curto L, De Marinis L, et al. Temozolomide therapy in patients with aggressive pituitary adenomas or carcinomas. *J Neuro Oncol* (2016) 126(3):519–25. doi: 10.1007/s11060-015-1991-y
26. Lasolle H, Cortet C, Castinetti F, Cloix L, Caron P, Delemer B, et al. Temozolomide treatment can improve overall survival in aggressive pituitary tumors and pituitary carcinomas. *Eur J Endocrinol* (2017) 176 (6):769–77. doi: 10.1530/EJE-16-0979
27. McCormack A, Dekkers OM, Petersenn S, Popovic V, Trouillas J, Raverot G, et al. Treatment of aggressive pituitary tumours and carcinomas: results of a European Society of Endocrinology (ESE) survey 2016. *Eur J Endocrinol* (2018) 178(3):265–76. doi: 10.1530/EJE-17-0933
28. Whitelaw BC. How and when to use temozolomide to treat aggressive pituitary tumours. *Endocr Relat Cancer* (2019) 26(9):R545–52. doi: 10.1530/ERC-19-0083

Conflict of Interest: The authors declare that the research was conducted in the absence of any commercial or financial relationships that could be construed as a potential conflict of interest.

frontiers in Oncology

ORIGINAL RESEARCH
published: 09 March 2021
doi: 10.3389/fonc.2021.622880

Developing a lncRNA Signature to Predict the Radiotherapy Response of Lower-Grade Gliomas Using Co-expression and ceRNA Network Analysis

Zhongyang Li[1], Shang Cai[2,3], Huijun Li[4,5], Jincheng Gu[4,5], Ye Tian[2,3], Jianping Cao[1,6], Dong Yu[1] and Zaixiang Tang[4,5]**

[1] School of Radiation Medicine and Protection, Soochow University Medical College (SUMC), Suzhou, China, [2] Department of Radiotherapy and Oncology, The Second Affiliated Hospital of Soochow University, Suzhou, China, [3] Institute of Radiotherapy and Oncology, Soochow University, Suzhou, China, [4] Department of Biostatistics, School of Public Health, Medical College of Soochow University, Suzhou, China, [5] Jiangsu Provincial Key Laboratory of Geriatrics Prevention and Translational Medicine, School of Public Health, Soochow University Medical College, Suzhou, China, [6] School of Radiation Medicine and Protection and Collaborative Innovation Center of Radiation Medicine of Jiangsu Higher Education Institutions, Soochow University, Suzhou, China

OPEN ACCESS

Edited by:
Haotian Zhao,
New York Institute of Technology, United States

Reviewed by:
Ibrahim Abdelrahim Qaddoumi, St. Jude Children's Research Hospital, United States
Desi Shang, Harbin Medical University, China

***Correspondence:**
Zaixiang Tang
tangzx@suda.edu.cn
Dong Yu
yudong@suda.edu.cn

Specialty section:
This article was submitted to Neuro-Oncology and Neurosurgical Oncology, a section of the journal Frontiers in Oncology

Received: *10 November 2020*
Accepted: *15 January 2021*
Published: *09 March 2021*

Citation:
Li Z, Cai S, Li H, Gu J, Tian Y, Cao J, Yu D and Tang Z (2021) Developing a lncRNA Signature to Predict the Radiotherapy Response of Lower-Grade Gliomas Using Co-expression and ceRNA Network Analysis. Front. Oncol. 11:622880. doi: 10.3389/fonc.2021.622880

Background: Lower-grade glioma (LGG) is a type of central nervous system tumor that includes WHO grade II and grade III gliomas. Despite developments in medical science and technology and the availability of several treatment options, the management of LGG warrants further research. Surgical treatment for LGG treatment poses a challenge owing to its often inaccessible locations in the brain. Although radiation therapy (RT) is the most important approach in this condition and offers more advantages compared to surgery and chemotherapy, it is associated with certain limitations. Responses can vary from individual to individual based on genetic differences. The relationship between non-coding RNA and the response to radiation therapy, especially at the molecular level, is still undefined.

Methods: In this study, using The Cancer Genome Atlas dataset and bioinformatics, the gene co-expression network that is involved in the response to radiation therapy in lower-grade gliomas was determined, and the ceRNA network of radiotherapy response was constructed based on three databases of RNA interaction. Next, survival analysis was performed for hub genes in the co-expression network, and the high-efficiency biomarkers that could predict the prognosis of patients with LGG undergoing radiotherapy was identified.

Results: We found that some modules in the co-expression network were related to the radiotherapy responses in patients with LGG. Based on the genes in those modules and the three databases, we constructed a ceRNA network for the regulation of radiotherapy responses in LGG. We identified the hub genes and found that the long non-coding RNA, DRAIC, is a potential molecular biomarker to predict the prognosis of radiotherapy in LGG.

Keywords: The Cancer Genome Atlas, low-grade glioma, bioinformatics, long non-coding RNA, radiosensitivity

INTRODUCTION

Gliomas are the most prevalent malignant primary brain tumors accounting for 81% of all malignant brain tumors (1). The World Health Organization (WHO) has classified gliomas into four grades; WHO grade II and III gliomas are not as malignant as WHO grade IV glioblastoma (GBM). Therefore, WHO grade II and grade III gliomas are defined as lower-grade gliomas (LGG) by The Cancer Genome Atlas (TCGA). Lower-grade gliomas include astrocytomas, oligodendrogliomas, and oligoastrocytomas (2).

Standard treatment of LGG includes surgery, chemotherapy, and radiation therapy. Because lower-grade gliomas occur primarily in the functional areas of the brain and tend to grow aggressively with diffuse infiltration, the suitability of surgery is often controversial. Chemotherapy with temozolomide has some limitations (such as hematological toxicity and myelosuppression (3, 4)). Radiation therapy has significant advantages in the treatment of LGG. Almost all patients with LGG receive radiation therapy during their treatment (5).

Although radiotherapy is associated with several advantages in the treatment of LGG, there exists the problem of heterogeneity in the efficacy of radiotherapy. Patients who receive radiation therapy show varying responses; some show better short-term responses and overall survival compared to others (6). Moreover, side effects such as cognitive abnormality and seizure due to the brain damage caused by ionizing radiation have been observed in some patients (7, 8). With progress in precision medicine, the study of biomarkers for use in radiation therapy and the molecular mechanisms regulating the sensitivity of radiation therapy have gradually become the focus of research in radiation oncology in recent times.

Long non-coding RNAs (lncRNA) belong to a class of non-coding RNA with a length of not more than 200 nucleotides and usually lack coding potential. Several studies have confirmed that lncRNA expression is associated with tumor initiation, progression, and treatment (9–13). Some lncRNAs have also been implicated in the regulation of tumor radiosensitivity. For example, lncRNA CYTOR sponges miR-195 to regulate the radiosensitivity of non-small cell lung cancer (NSCLC) (14). And lncRNA GAS5 can interact with miR-21 and enhance radiosensitivity in NSCLC (15) whereas lncRNA ANRIL enhances the radiosensitivity of nasopharyngeal carcinoma *via* miR-125a (16). Collectively, these studies reveal that lncRNAs can modulate tumor radiosensitivity by functioning as competitive endogenous RNA (ceRNA).

The mechanism of ceRNA is a hypothesis that some RNAs, such as lncRNA, act as a molecular sponge and compete with mRNA for binding to miRNA *via* the miRNA response element (MRE) (17). Although increasing research on ceRNA reveals its role in the progression of many diseases and the treatment responses (18, 19), few studies pertaining to the radiosensitivity of LGG currently focus on the regulatory function of their non-coding RNAs or the mechanism of ceRNAs. Therefore, additional systematic studies on the mechanisms of the regulation of radiosensitivity in LGG are needed.

In this study, we used weighted correlation network analysis (WGCNA) to screen the most relevant modules in the co-expression network and construct a ceRNA network. WGCNA is a systems biology method used to detect the co-expression of gene modules (20, 21) and genes in the same module having a similar expression mode. This technique has been widely used in biological research. Our study provides clues to determine the mechanism of post-transcriptional regulation in LGG radiosensitivity using transcriptome level data. Through analysis of the expression level of hub genes in the co-expression network, we found a lncRNA as a potential biomarker that can be used to predict the prognosis of patients with LGG undergoing radiotherapy.

DATA SOURCES AND METHODS

Data Sources

Gene expression data and clinical follow-up data from patients with LGG were downloaded from The Cancer Genome Atlas (TCGA). TCGA is the world's largest oncogene database, providing a large number of gene expression data, mutation data, epigenetic data, clinical data, and survival data of different tumors.

The expression levels in the RNA-seq data are normalized by TCGA. We directly used the data standardized by Fragments Per Kilobase per Million (FPKM) provided by TCGA as the expression level of the gene.

We categorized patients into radiosensitive and radioresistant groups based on the short-term response of their primary tumor to radiotherapy. Patients who showed complete remission after radiotherapy were considered radiosensitive whereas those exhibiting disease progression after radiotherapy were considered resistant to radiotherapy. For survival analysis, our inclusion criteria for patients were follow-up survival time greater than 30 days and those who had received radiation therapy.

The lncRNA and mRNA expression data were extracted from RNA-seq expression data of TCGA-LGG according to the GENCODE (https://www.gencodegenes.org/) annotations database V34.

To validate our findings of the biomarkers related to TCGA-LGG radiosensitivity, we performed overall survival validation using two independent datasets of Chinese Glioma Genome Atlas (CGGA, http://www.cgga.org.cn). The expression of the two CGGA datasets was sequence matched using STAR (22) and transcripts were quantified using RSEM (23). The two CGGA datasets included 325 (24, 25) and 693 patients with glioma (26, 27), respectively.

In both CGGA datasets, patients were screened based on criteria, such as glioma grade WHO II and III, whether or not they received radiation therapy, and survival follow-up longer than 30 days.

The clinical data of patients from TCGA and CGGA are uploaded as supplementary material.

WGCNA Co-expression Analysis

Co-expression network analysis was conducted using the "WGCNA" package in R 4.0 software. Genes with a low amplitude of change and low expression are generally not considered to play a critical biological role in the regulation of

organismal function and in improving the computational efficiency of WGCNA. The filter standard of miRNA is a median absolute deviation (MAD) higher than 0.01. MAD is a robust statistic used to describe the dissociation between samples. For lncRNA and mRNA, the top 5000 lncRNA and mRNA with high MAD were selected. Hierarchical clustering analysis was conducted to remove the outliers.

We performed a co-expression network analysis on lncRNA, mRNA, and miRNA expression levels. First, the value of the powers (beta) was estimated using the "pickSoftThreshold" function in the WGCNA package. The R-squared criterion was set to 0.9. Pearson correlation coefficients were calculated using the expression data to generate a correlation matrix, which was converted to a weighted adjacency matrix based on the power. Lastly, a topological overlap matrix (TOM) was generated to describe the connection between genes. Genes with high co-expression were then grouped into same modules based on the TOM. The merge cut-off threshold was set to 0.2, which meant that modules with a similarity higher than 0.8 were merged into one module.

Module-Radiosensitivity Relationship

Principal component analysis (PCA) of the modules in the co-expression network of lncRNA, mRNA, and miRNA was performed. The first principal component (Eigengene) represented the gene expression level within the module and was used for Pearson correlation analysis for radiosensitivity. The modules with the strongest correlation and p-value < 0.05 were considered to play a key role in radiosensitivity.

ceRNA Network Construction and Visualization

We predicted these genes using three RNA interaction databases, including lncBase (http://carolina.imis.athena-innovation.gr/diana_tools/web/index.php?r=lncbasev2%2Findex-predicted), miRDB (http://mirdb.org/), and mirTarbase (http://mirtarbase.cuhk.edu.cn/php/index.php). The lncBase was used to predict the interaction of lncRNA with miRNA, whereas miRDB and mirTarbase were used to predict the interaction of miRNA with mRNA. The threshold for the miTGscore in the lncBase was set to 0.9. Interaction pairs with an miTGscore above 0.9 were considered reliable and were included in the construction of the ceRNA network. The target mRNAs of miRNAs were predicted using miRDB and mirTarbase, and the sum aggregate of these two databases was considered as the target of miRNA. The R package "ggalluvial" (28) was used for the visualization of the ceRNA network.

Gene Ontology and Pathway Enrichment Analysis

Gene ontology (GO) and Kyoto Encyclopedia of Genes and Genomes (KEGG) enrichment analysis of target genes in the ceRNA network were implemented using the R package "clusterprofiler" (29). GO enrichment analysis included three ontologies, namely, biological process (BP), molecular function (MF), and cellular component (CC). The p-value of GO and KEGG enrichment analysis was adjusted using the Benjamini-Hochberg method. The R package "GOplot" (30) was used to visualize the GO enrichment data.

Selection of Hub Genes

To further screen biomarkers, RNA within the three modules were identified as hub genes. Hub genes are considered to be genes with high connectivity within the module that play a key pivotal role in regulation and are, therefore, more meaningful as biomarkers. Gene significance (GS) and module membership (MM) were calculated for each gene. The selection criteria for hub genes were set to GS > 0.2 and MM > 0.8.

Survival Analysis

To identify the relationship between the expression level of these hub genes and patient prognosis after radiotherapy, all patients who had received radiotherapy and had valid survival data were selected for survival analysis. Patients were divided into high and low groups based on the expression level of each gene. Kaplan-Meier curves and log-rank test were used for survival analysis to calculate the effect of the expression of each gene on the prognosis of patients with LGG who had received radiotherapy. Survival analysis and visualization were performed using the "survival" (31) and "survminer" R package. The p-value was adjusted using the false discovery rate.

RESULTS

Processing of Data

This study included 49 patients with LGG (**Table 1**), among whom 30 had gliomas that showed complete response after radiotherapy and 19 showed radiographic progressive disease. The RNA-seq expression data of all patients were available, but because the miRNA-seq data of one of the patients in the complete response group was missing, only 48 patients were included for the miRNA co-expression network analysis.

TABLE 1 | Patient characteristics (n=49).

	Progressive disease group	Complete Response group
Total	19 (100%)	30 (100%)
Age		
>40	11 (57.90%)	20 (66.67%)
≦40	8 (42.10%)	10 (33.33%)
Grade		
II	7 (36.84%)	6 (25.00%)
III	12 (63.16%)	24 (75.00%)
Gender		
Male	11 (57.90%)	12 (40.00%)
Female	8 (42.10%)	18 (60.00%)
IDH1		
Mutation	5 (26.32%)	6 (20.00%)
Wild	3 (15.79%)	4 (13.33%)
NA	11 (57.89%)	20 (66.67%)
RT dose		
≥5400cGy	17 (89.47%)	29 (96.67%)
<5400cGy	2 (10.53%)	1 (3.33%)

A total of 19,600 mRNA and 14,085 lncRNA were identified using GENCODE annotation database v34. The MAD of genes were calculated. There were a total of 2142 miRNAs in the miRNA expression data, of which 792 had MADs greater than 0.01. The top 5000 lncRNA and mRNA with larger MAD were extracted for further analyses.

WGCNA Analysis

The mRNA expression data of one of the patients in the complete response group was identified as an outlier in hierarchical clustering analysis and was removed. Beta value is key to build a high-efficiency co-expression network to find the most relevant module in WGCNA analysis. The power value was calculated using the function "pickSoftThreshold." The minimum R-squared value was set to 0.9 (**Figure 1**). The beta value of lncRNA for the construction of the co-expression network was set to 4, whereas it was set to 9 and 8 for mRNA and miRNA, respectively.

A total of 29 modules were identified from the lncRNA co-expression network. Seventeen mRNA modules from the mRNA co-expression network and 8 miRNA modules from miRNA co-expression network are shown in **Figure 2**. In the module-trait correlation analysis, the lncRNA module, MEred, the mRNA module, MEgreen, and the miRNA module, MEred, are the modules that are most correlated to the radiotherapy response of patients (**Figure 3**). The genes in these three modules are highly related to radiotherapy response in LGG.

ceRNA Network Analysis

Using the Lncbase database, 3142 lncRNA-miRNA interaction pairs were predicted by lncRNA in MEred. Among those, 32 lncRNA-miRNA interaction pairs were related to 21miRNA in module MEgreen. MiRDB and mirTarBase were used to predict the target mRNAs of the 21miRNAs. There were 21 and 53 interaction pairs between miRNA and mRNA found in the miRDB and miRTarBase, respectively. The miRNA-mRNA predictions were combined and 19 lncRNAs, 20 miRNAs, and 61 mRNAs were included in the ceRNA network (**Figure 4**).

GO and KEGG Pathway Enrichment Analysis

A total of 56 GO terms were identified from 61 target mRNAs. The target mRNAs in ceRNA were primary associated with GO terms such as translational inhibition, negative regulation of ubiquitin-dependent protein catabolic process, and positive regulation of translation (**Figure 5**). The most significant

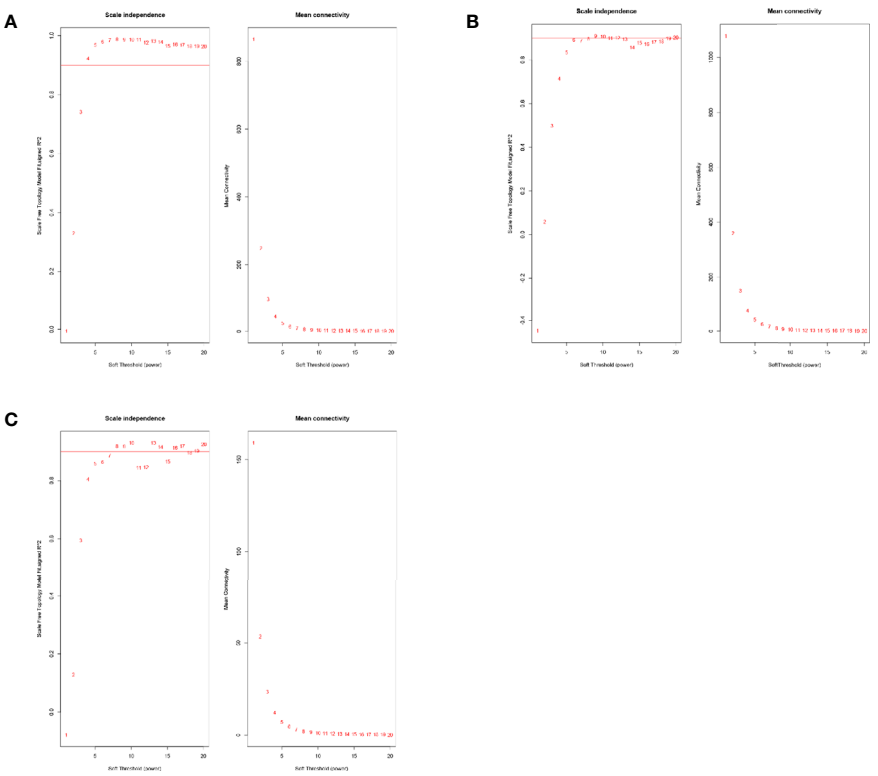

FIGURE 1 | **(A)** The power value selection of lncRNA co-expression networks. **(B)** The power value selection of mRNA co-expression networks. **(C)** The power value selection of miRNA co-expression networks.

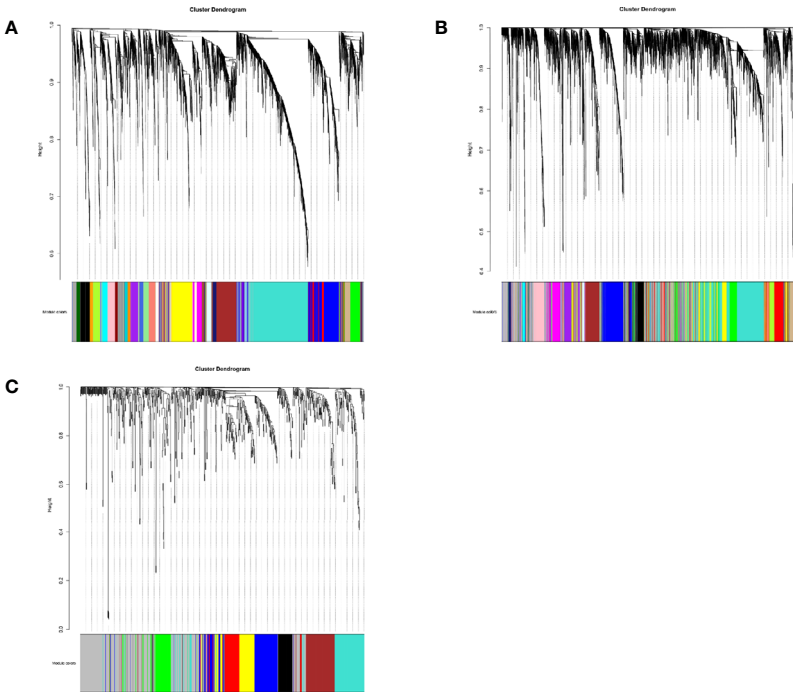

FIGURE 2 | **(A)** The cluster dendrogram of lncRNA co-expression network. **(B)** The cluster dendrogram of mRNA co-expression network. **(C)** The cluster dendrogram of miRNA co-expression network.

KEGG pathway that the target mRNA was associated with was the ribosome pathway (**Figure 6**).

Hub Gene Selection and Survival Analysis

After the calculation of GS and MM, 13 lncRNAs, 28 miRNAs, and 74 mRNAs were selected as hub genes. Results from the survival analysis (**Table 2**) indicated that DRAIC was the most significant lncRNA affecting the overall survival (OS) of patients who had received radiotherapy. The group with high lncRNA DRAIC expression showed a significantly better overall survival than that with low lncRNA DRAIC expression ($p < 0.0001$) (**Figure 7**).

We also noticed that the group with high lncRNA DRAIC expression level exhibited better progression-free survival than that with the low expression level of lncRNA DRAIC ($p < 0.0001$) (**Figure 8**).

Two CGGA datasets were used as independent datasets to validate the relationship between the expression level of lncRNA DRAIC and the OS of patients with LGG. From the CGGA325 dataset, we extracted the data of 137 patients with WHO grade II and III tumors with survival follow-up greater than 30 days who had received radiation therapy. We also extracted the data of 308 patients from the CGGA693 dataset based on similar criteria.

The OS data of patients with high DRAIC expression obtained from the CGGA325 dataset was significantly better than those of patients in the low expression group ($p<0.0001$) (**Figure 9**). Although the long-term survival of patients was not significantly better in the DRAIC high expression group, the OS and five-year survival were significantly better than that in the DRAIC low expression group in the CGGA693 dataset ($p=0.0013$) (**Figure 10**).

Chi-square test was used to evaluate the relationship between DRAIC expression and levels of the traditional biomarkers in the CGGA datasets. We found that the expression level of lncRNA DRAIC was highly correlated with IDH mutation and 1p/19q codeletion. In both CGGA datasets, the DRAIC high expression group had more 1p/19q codeletion and IDH1 mutations compared to those in the low expression group. However, lncRNA DRAIC expression was not related to MGMT methylation (**Tables 3** and **4**).

DISCUSSION

The response of patients who receive radiotherapy for tumors varies widely. Radiotherapy induces several effects including double-strand breaks (DSB) in the DNA, DNA damage repair, and the generation of oxygen radicals by the ionizing radiation (32, 33). The sensitivity of individuals to radiotherapy varies widely and depends on several factors. Each patient responds differently and the nature of the response to radiotherapy is highly dependent on the genetic makeup (34, 35). Radiotherapy sensitivity has been one of the most important

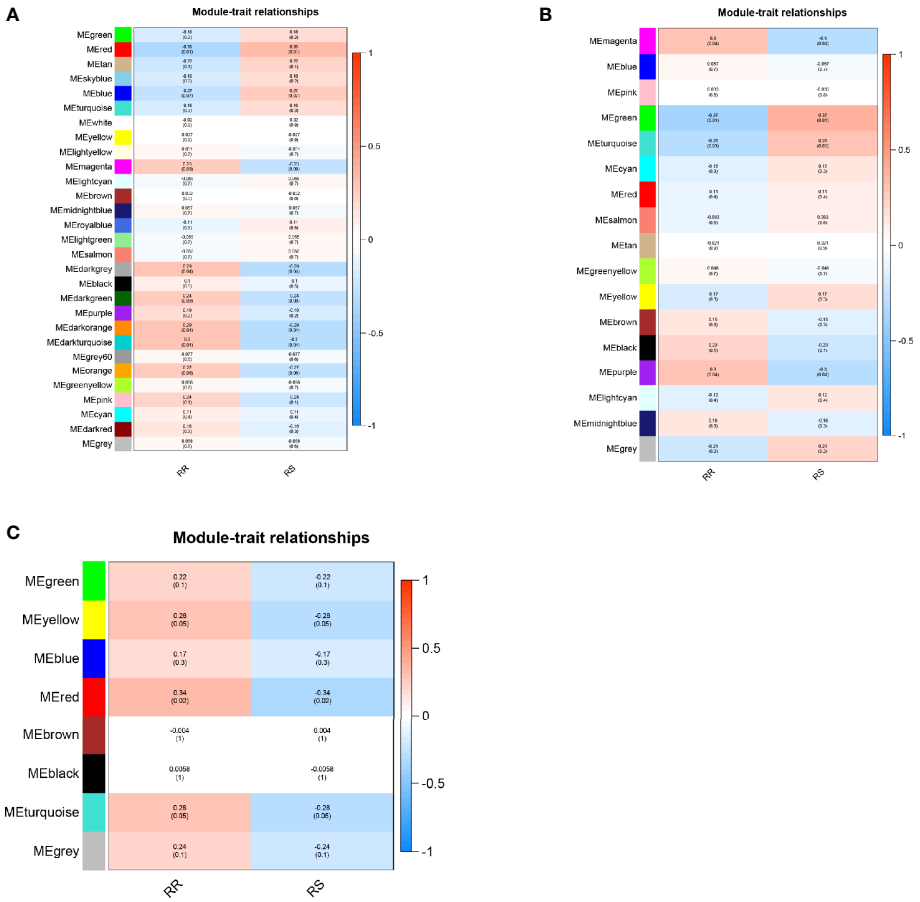

FIGURE 3 | **(A)** Module-trait relationship of lncRNA co-expression network. **(B)** Module-trait relationship of mRNA co-expression network. **(C)** Module-trait relationship of miRNA co-expression network.

topics of research in radiation oncology for a long time. However, few studies have focused on the regulation of radiosensitivity at the post-transcriptional level. Molecular biomarkers, such as IDH1 and IDH2 mutation (36–39) and 1p19q codeletion (40, 41), have been used to predict the prognoses of patients with LGG. The molecular mechanism involved in the regulation of radiation response in patients with LGGs is still undefined and, to date, there is no effective or reliable biomarker that can be used to determine the prognosis of patients undergoing radiotherapy.

In this study, for the first time, we systematically investigated the mechanism of ceRNA regulation in the radiosensitivity of LGG based on RNA-seq data and database predictions. Consequently, a lncRNA was identified as a biomarker that could be effective in predicting the prognosis of patients after radiotherapy.

After obtaining data from TCGA-LGG, we categorized patients into different groups based on their short-term response of their primary tumor to radiotherapy. Although the TCGA-LGG project did not provide details of surgical resection, we believe that for low-grade gliomas, even if maximum resection is performed (e.g., gross total resection), some microscopic lesions may still be present. These residual microscopic lesions may still have the potential for local recurrence and distal metastasis. This is one of the reasons why lower-grade gliomas are treated using radiotherapy after surgery. However, patients may still present differently after postoperative radiotherapy, and some patients may develop local recurrence and distant metastases (42). Therefore, TCGA takes into consideration not only the imaging performance of the lesion before and after radiotherapy but also new tumor events when assessing the response to radiotherapy. Complete response is defined as the disappearance of all target lesions after receiving radiotherapy without the formation of new lesions for at least 4 weeks. Also, by reviewing the survival and follow-up data of patients in the CR group, we found that the majority of patients in the CR group had no new tumor events during their long-term follow-up. Therefore, we believe that TCGA is accurate in assessing the recovery of patients and the efficacy of the treatment modality, and our practice of using

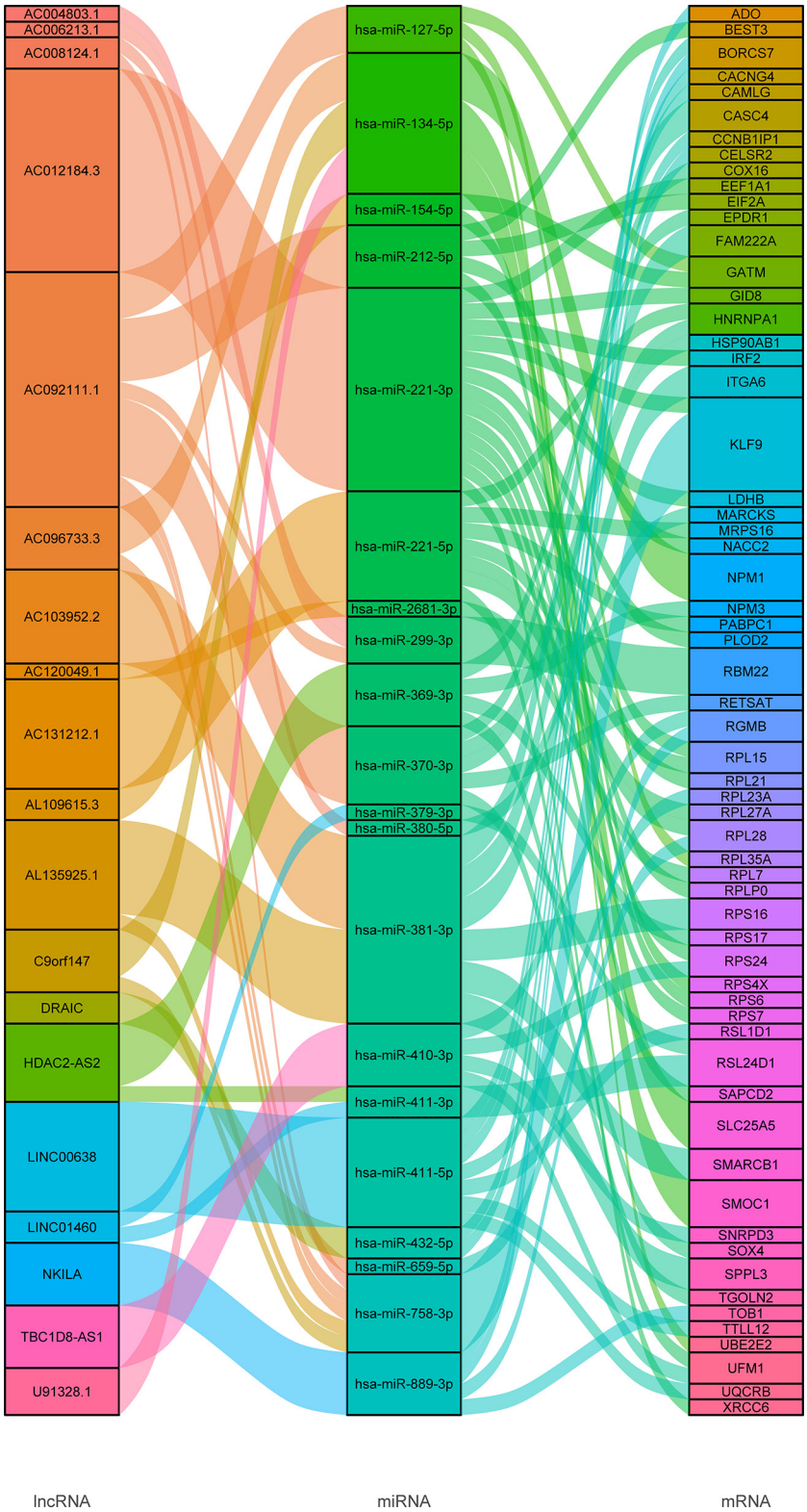

FIGURE 4 | Sankey diagram of ceRNA network.

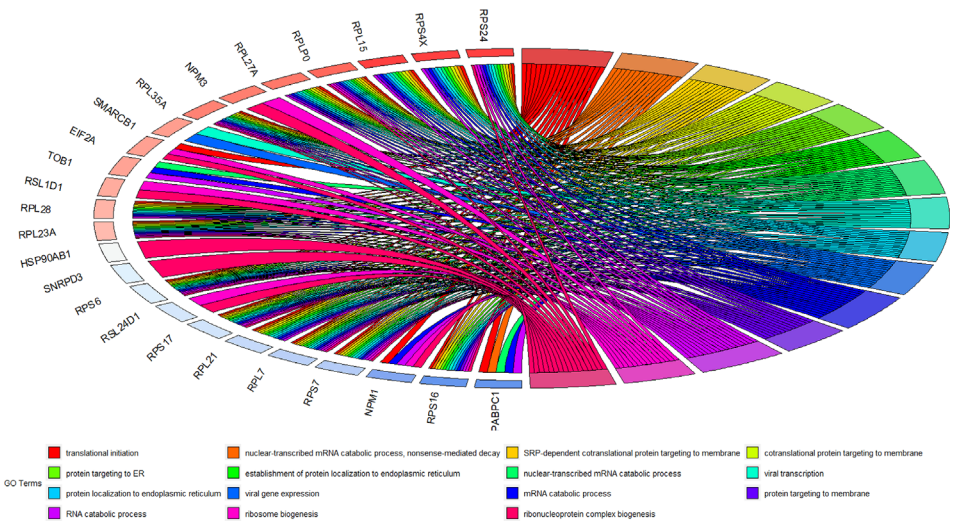

FIGURE 5 | GO terms of 61 target mRNAs in ceRNA network.

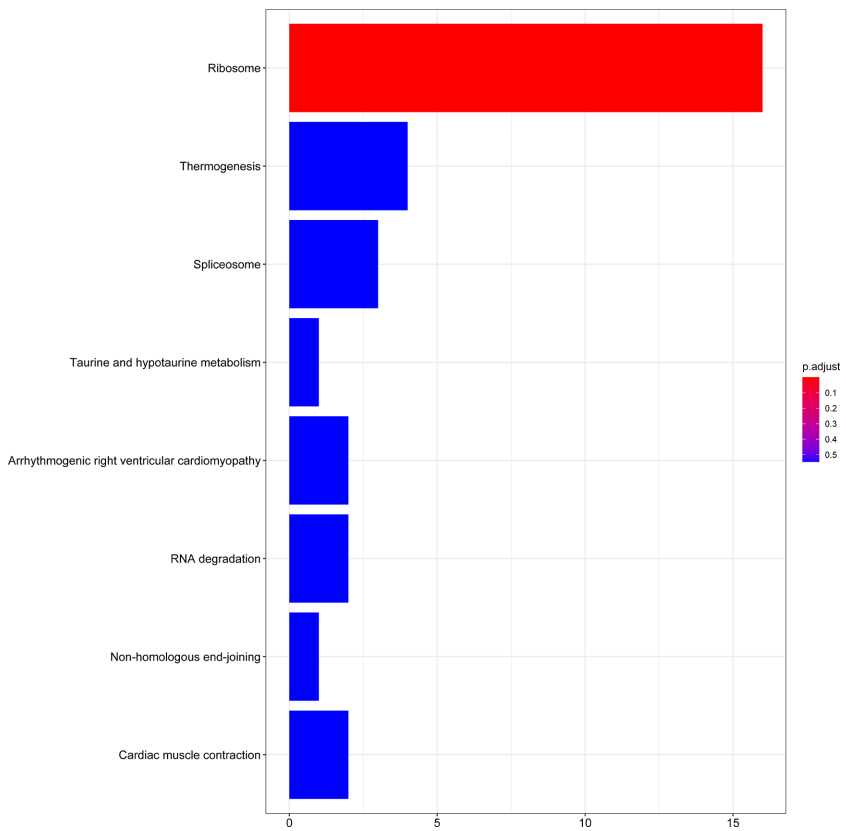

FIGURE 6 | KEGG enrichment analysis of 61 target mRNAs.

TABLE 2 | Survival analysis results of hub lncRNAs.

Ensembl ID	Gene Symbol	p-value
ENSG00000203497	PDCD4-AS1	0.023584
ENSG00000229980	TOB1-AS1	0.033365
ENSG00000239415	AP001469.3	0.000122
ENSG00000245750	DRAIC	1.24E-07
ENSG00000253669	GASAL1	0.019953
ENSG00000260830	AL135744.1	0.033365
ENSG00000261777	AC012184.3	0.404931
ENSG00000262362	AC004233.1	0.010548
ENSG00000270403	AP001554.1	0.019953
ENSG00000272079	AC004233.2	0.019953
ENSG00000274367	AC004233.3	0.050642
ENSG00000277182	AC006449.5	0.010548
ENSG00000278012	AL031658.2	0.000122

the short-term response to radiotherapy in TCGA to group patients is reasonable.

Normally, the RNA-seq studies involve gene analyses to identify genes related to the trait. All gene expression levels are analyzed using differential gene expression analysis and the differentially expressed genes (DEGs) are selected based on a foldchange threshold. However, the foldchange threshold is not the ideal choice in biology research as there is no significant difference in the function of a gene with expression levels a little higher or lower than the foldchange threshold. Therefore, in this study, we chose WGCNA analysis to discover the important genes that are involved in the radiosensitivity in LGG. The WGCNA algorithm avoids the problem of threshold by using a soft threshold. In WGCNA analysis, the correlation coefficient of all genes is taken as the power of n, the coefficient distribution conforms to the scale-free network, and the genes are classified into different modules based on the mode of expression. Genes in the same module exhibit highly similar expression. The distribution pattern of nodes in the scale-free network corresponds to the mode of action of genes and has a biological significance, which is the advantage of using the WGCNA algorithm.

Using WGCNA analysis, we observed that the most relevant modules of lncRNA and mRNA were positively correlated with radiosensitivity and the most relevant module of miRNA was negatively correlated with radiosensitivity. These findings were consistent with the competitive binding mechanism of ceRNA. In the gene function enrichment analysis, we noticed that most of the functions of the target mRNAs in the ceRNA network were highly concentrated in the ribosomal pathway. Currently, the role of ribosomes in the response of tumor cells to ionizing radiation has not been elucidated in the field of gene research pertaining to radiosensitivity.

We noticed that lncRNA DRAIC had the most significant effect in predicting the prognosis of patients after receiving radiotherapy; lncRNA DRAIC has been shown to inhibit the progression of prostate cancer by interacting with IκB kinase (IKK) and inhibiting NF-κB activity (43). Activation of NF-κB is

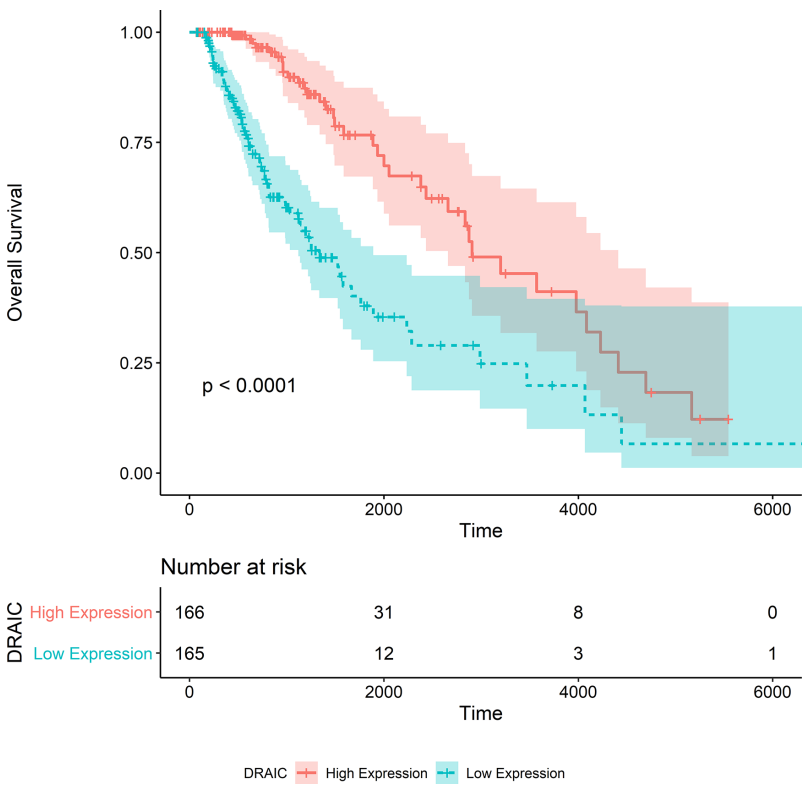

FIGURE 7 | Kaplan-Merier survival curve of overall survival in the TCGA-LGG dataset.

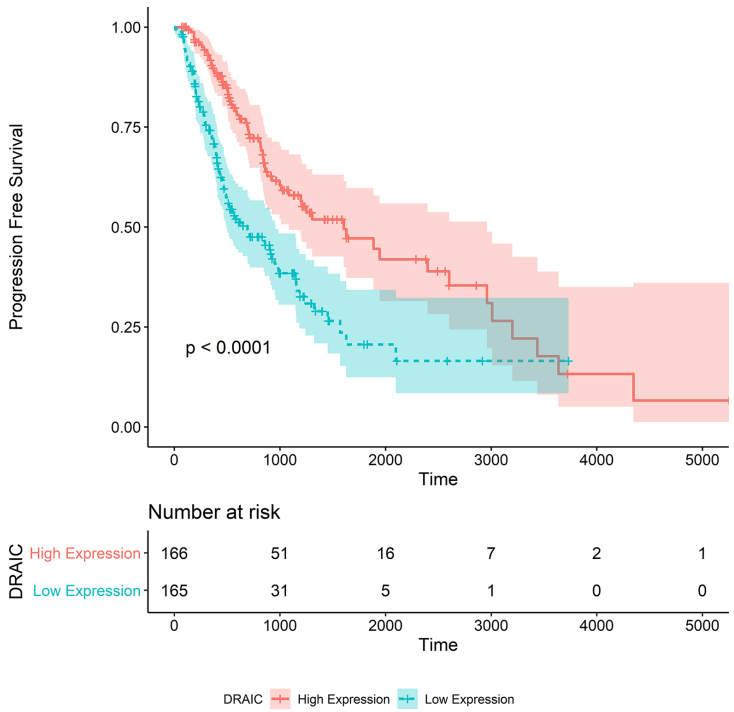

FIGURE 8 | Kaplan-Meier survival curve of progression free survival in the TCGA-LGG dataset.

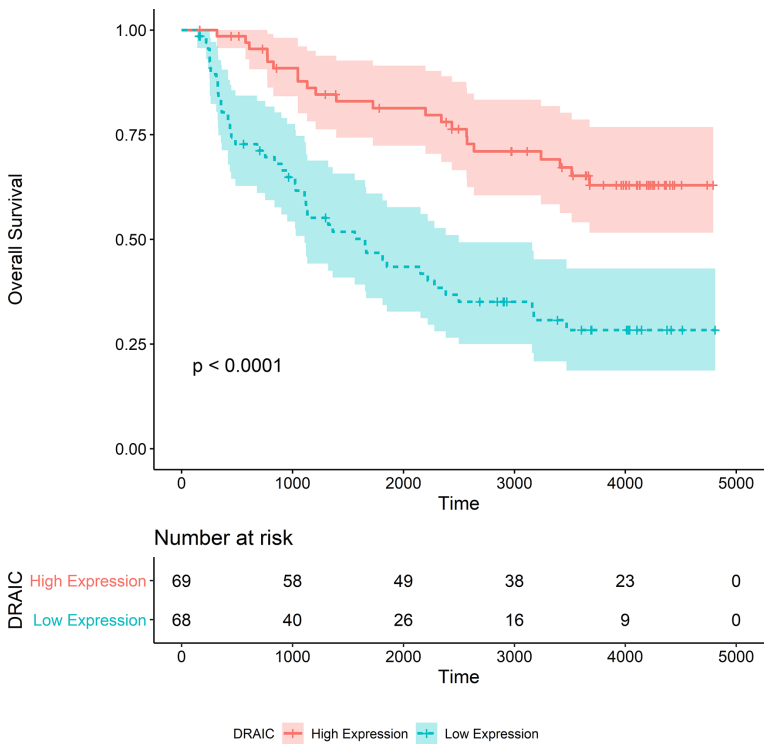

FIGURE 9 | Kaplan-Merier survival curve of overall survival in the CGGA325 dataset.

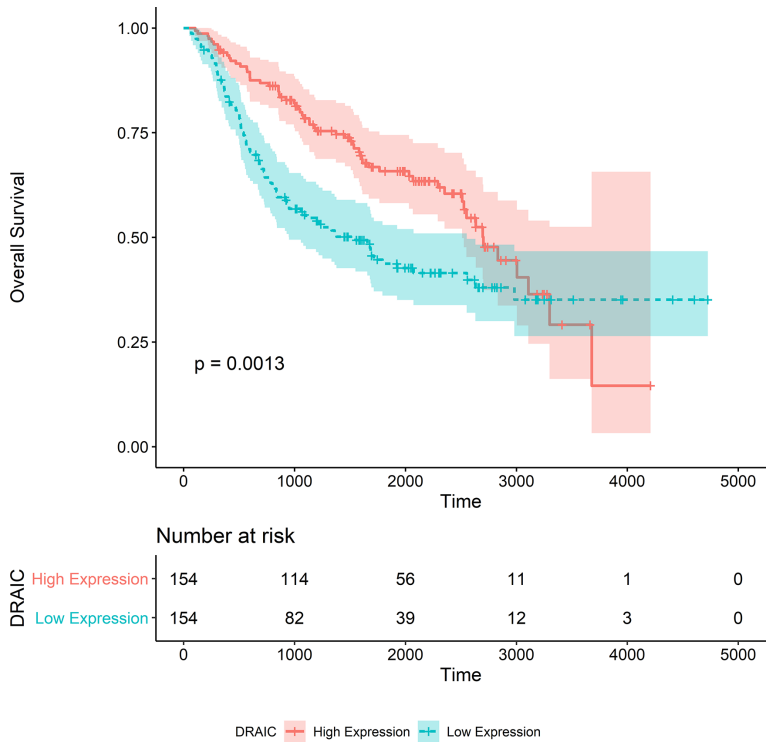

FIGURE 10 | Kaplan-Merier survival curve of overall survival in the CGGA693 dataset.

TABLE 3 | Relationship between lncRNA DRAIC expression and 1p/19q, IDH mutation, and MGMT methylation in CGGA325 dataset.

CGGA325 dataset	High DRAIC expression group (n=69)	Low DRAIC expression group (n=68)	p-value
1p/19q			<0.0001
Codel	40	10	
Non-codel	28	58	
IDH			<0.0001
Mutant	65	37	
Wildtype	4	31	
MGMT			0.7483
Methylated	37	32	
Unmethylated	27	28	

TABLE 4 | Relationship between lncRNA DRAIC expression and 1p/19q, IDH mutation, and MGMT methylation in CGGA693 dataset.

CGGA693 dataset	High DRAIC expression group (n=154)	Low DRAIC expression Group (n=154)	p-value
1p/19q			<0.0001
Codel	67	23	
Non-codel	68	122	
IDH			<0.0001
Mutant	132	86	
Wildtype	13	50	
MGMT			0.1311
Methylated	79	69	
Unmethylated	40	54	

associated with the radiosensitivity of gliomas (44–46). DRAIC might be the key lncRNA involved in the radiosensitivity regulation of LGG. Studies report that DRAIC can be a biomarker to predict prognosis in many malignancies (47). However, there is no direct evidence to confirm the involvement of lncRNA DRAIC in the regulation of radiosensitivity in LGG; therefore, further studies are warranted.

To further strengthen the conclusions based on the data obtained from TCGA dataset, we performed independent validation of the OS in patients who underwent radiotherapy. To this effect, we used two CGGA datasets to validate DRAIC as a biomarker of the response to radiotherapy. The conclusions obtained based on both CGGA datasets were similar to those derived from TCGA, which indicated that patients in the high DRAIC expression group would achieve better OS after radiation therapy compared to those in the low-expression group. Furthermore, we noticed that in the CGGA datasets, IDH mutation and 1p/19q codeletion status were highly correlated with lncRNA DRAIC expression. Previous studies have shown that IDH mutation and 1p/19q codeletion are related to the radiosensitivity of gliomas (48–50). IDH mutation and 1p/19q codeletion increase the radiosensitivity of gliomas. These results are in agreement with our findings that lncRNA DRAIC can be used as a potentially suitable biomarker to determine radiosensitivity in patients.

Our study has some limitations. Although the number of patients who were included in this study based on their specific

response to radiotherapy is justified and adequate for WGCNA analysis, additional samples may help increase the confidence levels of our findings. *In vivo* and *in vitro* studies (such as knockdown/knockout of DRAIC and molecular functional tests) can help further corroborate the conclusions of our study. This will be the focus of our subsequent study.

DATA AVAILABILITY STATEMENT

Publicly available datasets were analyzed in this study. These data can be found here: https://portal.gdc.cancer.gov/repository, http://www.cgga.org.cn/download.jsp.

AUTHOR CONTRIBUTIONS

Study conception and design: ZL, ZT, and DY. Real data and analysis: ZL, SC, and JG. Drafting of the manuscript: ZL, SC, JG, YT, and JC. All authors contributed to the article and approved the submitted version.

FUNDING

This work was supported in part by the National Natural Science Foundation of China (81773541), funded from the Priority Academic Program Development of Jiangsu Higher Education Institutions at Soochow University, the State Key Laboratory of Radiation Medicine and Protection (GZK1201919) to ZT; a project by the Second Affiliated Hospital of Soochow University (XKTJ-RC202007), Scientific Research Program for Young Talents of China National Nuclear Corporation (51003), Suzhou Science and Education Project (KJXW2017010), The Natural Science Foundation of Jiangsu Province (BK20180195), the National Natural Science Foundation of China (81902715) to SC; National Natural Science Foundation of China (U1967220 and 81872552) to JC; Jiangsu Provincial Key Project in Research and Development of Advanced Clinical Technique (BL2018657) to YT; and the Natural Science Foundation of Jiangsu Province (BK2016), National Natural Science Foundation of China (11475125), and The Starting Research Fund from the Soochow University (Q412600711) to DY. The funding body did not play any roles in the design of the study and collection, analysis, and interpretation of data and in writing the manuscript.

SUPPLEMENTARY MATERIAL

The Supplementary Material for this article can be found online at: https://www.frontiersin.org/articles/10.3389/fonc.2021.622880/full#supplementary-material

REFERENCES

1. Ostrom QT, Bauchet L, Davis FG, Deltour I, Fisher JL, Langer CE, et al. The epidemiology of glioma in adults: A state of the science review. *Neuro Oncol* (2014) 16(7):896–913. doi: 10.1093/neuonc/nou087
2. Cancer Genome Atlas Research Network, Brat DJ, Verhaak RG, Aldape KD, Yung WK, Salama SR, et al. Comprehensive, Integrative Genomic Analysis of Diffuse Lower- Grade Gliomas The Cancer Genome Atlas Research Network*. *N Engl J Med* (2015) 372(26):2481–98. doi: 10.1056/NEJMoa1402121.Comprehensive
3. Scaringi C, De Sanctis V, Minniti G, Enrici M. Temozolomide-Related Hematologic Toxicity. *Oncol Res Treat* (2013) 36:444–9. doi: 10.1159/000353752
4. Sengupta S, Marrinan J, Frishman C, Sampath P. Impact of Temozolomide on Immune Response during Malignant Glioma Chemotherapy. *Clin Dev Immunol* (2012) 2012:831090. doi: 10.1155/2012/831090
5. Bourne TD, Schiff D. Update on molecular findings, management and outcome in low-grade gliomas. *Nat Rev Neurol* (2010) 6(12):695–701. doi: 10.1038/nrneurol.2010.159
6. Domina EA, Philchenkov A, Dubrovska A. Individual response to ionizing radiation and personalized radiotherapy. *Crit Rev Oncog* (2018) 23:69–92. doi: 10.1615/CritRevOncog.2018026308
7. Douw L, Klein M, Fagel SSAA, van den Heuvel J, Taphoorn MJB, Aaronson NK, et al. Cognitive and radiological effects of radiotherapy in patients with low-grade glioma: long-term follow-up. *Lancet Neurol* (2009) 8(9):810–8. doi: 10.1016/S1474-4422(09)70204-2
8. Rudá R, Magliola U, Bertero L, Trevisan E, Bosa C, Mantovani C, et al. Seizure control following radiotherapy in patients with diffuse gliomas: A retrospective study. *Neuro Oncol* (2013) 15:1739–49. doi: 10.1093/neuonc/not109
9. Cui C, Zhai D, Cai L, Duan Q, Xie L, Yu J. Long noncoding rna heih promotes colorectal cancer tumorigenesis via counteracting mir-939-mediated transcriptional repression of Bcl-Xl. *Cancer Res Treat* (2018) 50(3):992–1008. doi: 10.4143/crt.2017.226
10. He C, Wang X, Luo J, Ma Y, Yang Z. Long Noncoding RNA Maternally Expressed Gene 3 Is Downregulated, and Its Insufficiency Correlates With Poor-Risk Stratification, Worse Treatment Response, as Well as Unfavorable Survival Data in Patients With Acute Myeloid Leukemia. *Technol Cancer Res Treat* (2020) 19(5):1–8. doi: 10.1177/1533033820945815
11. Shen SN, Li K, Liu Y, Yang CL, He CY, Wang HR. Down-regulation of long noncoding RNA PVT1 inhibits esophageal carcinoma cell migration and invasion and promotes cell apoptosis via microRNA-145-mediated inhibition of FSCN1. *Mol Oncol* (2019) 13(12):2554–73. doi: 10.1002/1878-0261.12555
12. Jing H, Qu X, Liu L, Xia H. A novel long noncoding rna (LncRNA), LL22NC03-N64E9.1, promotes the proliferation of lung cancer cells and is a potential prognostic molecular biomarker for lung cancer. *Med Sci Monit* (2018) 24:4317–23. doi: 10.12659/MSM.908359
13. Wang Q, Liu L, Zhang S, Ming Y, Liu S, Cheng K, et al. Long noncoding RNA NEAT1 suppresses hepatocyte proliferation in fulminant hepatic failure through increased recruitment of EZH2 to the LATS2 promoter region and promotion of H3K27me3 methylation. *Exp Mol Med* (2020) 52(3):461–72. doi: 10.1038/s12276-020-0387-z
14. Zhang J, Li W. Long noncoding RNA CYTOR sponges miR-195 to modulate proliferation, migration, invasion and radiosensitivity in nonsmall cell lung cancer cells. *Biosci Rep* (2018) 38(6):1–12. doi: 10.1042/BSR20181599
15. Chen L, Ren P, Zhang Y, Gong B, Yu D, Sun X. Long non-coding RNA GAS5 increases the radiosensitivity of A549 cells through interaction with the miR-21/PTEN/Akt axis. *Oncol Rep* (2020) 43(3):897–907. doi: 10.3892/or.2020.7467
16. Hu X, Jiang H, Jiang X. Downregulation of lncRNA ANRIL inhibits proliferation, induces apoptosis, and enhances radiosensitivity in nasopharyngeal carcinoma cells through regulating miR-125a. *Cancer Biol Ther* (2017) 18(5):331–8. doi: 10.1080/15384047.2017.1310348
17. Salmena L, Poliseno L, Tay Y, Kats L, Pandolfi PP. A ceRNA hypothesis: The rosetta stone of a hidden RNA language? *Cell* (2011) 146:353–8. doi: 10.1016/j.cell.2011.07.014
18. Zheng P, Yin Z, Wu Y, Xu Y, Luo Y, Zhang TC. LncRNA HOTAIR promotes cell migration and invasion by regulating MKL1 via inhibition miR206

expression in HeLa cells. *Cell Commun Signal* (2018) 16(1):1–15. doi: 10.1186/s12964-018-0216-3
19. Wu M, Huang Y, Chen T, Wang W, Yang S, Ye Z, et al. LncRNA MEG3 inhibits the progression of prostate cancer by modulating miR-9-5p/QKI-5 axis. *J Cell Mol Med* (2019) 23(1):29–38. doi: 10.1111/jcmm.13658
20. Langfelder P, Horvath S. Fast R functions for robust correlations and hierarchical clustering. *J Stat Software* (2012) 46(11):1–17. doi: 10.18637/jss.v046.i11
21. Langfelder P, Horvath S. WGCNA: An R package for weighted correlation network analysis. *BMC Bioinf* (2008) 9:559. doi: 10.1186/1471-2105-9-559
22. Dobin A, Davis CA, Schlesinger F, Drenkow J, Zaleski C, Jha S, et al. STAR: Ultrafast universal RNA-seq aligner. *Bioinformatics* (2013) 29(1):15–21. doi: 10.1093/bioinformatics/bts635
23. Li B, Dewey CN. RSEM: Accurate transcript quantification from RNA-seq data with or without a reference genome. *BMC Bioinformatics* (2011) 12:323. doi: 10.1186/1471-2105-12-323
24. Bao Z-S, Chen H-M, Yang M-Y, Zhang C-B, Yu K, Ye W-L, et al. RNA-seq of 272 gliomas revealed a novel, recurrent PTPRZ1-MET fusion transcript in secondary glioblastomas. *Genome Res* (2014) 24:1765–73. doi: 10.1101/gr.165126.113
25. Zhao Z, Meng F, Wang W, Wang Z, Zhang C, Jiang T. Comprehensive RNA-seq transcriptomic profiling in the malignant progression of gliomas. *Sci Data* (2017) 4:170024. doi: 10.1038/sdata.2017.24
26. Wang Y, Qian T, You G, Peng X, Chen C, You Y, et al. Localizing seizure-susceptible brain regions associated with low-grade gliomas using voxel-based lesion-symptom mapping. *Neuro Oncol* (2015) 17:282–8. doi: 10.1093/neuonc/nou130
27. Liu X, Li Y, Qian Z, Sun Z, Xu K, Wang K, et al. A radiomic signature as a non-invasive predictor of progression-free survival in patients with lower-grade gliomas. *NeuroImage Clin* (2018) 20:1070–7. doi: 10.1016/j.nicl.2018.10.014
28. Brunson J. ggalluvial: Layered Grammar for Alluvial Plots. *J Open Source Software* (2020) 5(49):2017. doi: 10.21105/joss.02017
29. Yu G, Wang LG, Han Y, He QY. ClusterProfiler: An R package for comparing biological themes among gene clusters. *Omi A J Integr Biol* (2012) 16(5):284–7. doi: 10.1089/omi.2011.0118
30. Walter W, Sánchez-Cabo F, Ricote M. GOplot: An R package for visually combining expression data with functional analysis. *Bioinformatics* (2015) 31 (17):2912–4. doi: 10.1093/bioinformatics/btv300
31. Therneau TM, Grambsch PM. The Cox Model. In: *Modeling Survival Data: Extending the Cox Model. Statistics for Biology and Health*. New York, NY: Springer (2000). doi: 10.1007/978-1-4757-3294-8_3.
32. Hall EJ, Giaccia AJ. *Radiobiology for the radiologist*. Philadelphia: Wolters Kluwer Health/Lippincott Williams & Wilkins (2012).
33. Santivasi WL, Xia F. Ionizing radiation-induced DNA damage, response, and repair. *Antioxid Redox Signal* (2014) 21(2):251–9. doi: 10.1089/ars.2013.5668
34. Young A, Berry R, Holloway AF, Blackburn NB, Dickinson JL, Skala M, et al. RNA-seq profiling of a radiation resistant and radiation sensitive prostate cancer cell line highlights opposing regulation of DNA repair and targets for radiosensitization. *BMC Cancer* (2014) 14:808. doi: 10.1186/1471-2407-14-808
35. Begg AC. Predicting response to radiotherapy: Evolutions and revolutions. *Int J Radiat Biol* (2009) 85:825–36. doi: 10.1080/09553000903184366
36. Turcan S, Rohle D, Goenka A, Walsh LA, Fang F, Yilmaz E, et al. IDH1 mutation is sufficient to establish the glioma hypermethylator phenotype. *Nature* (2012) 483:479–83. doi: 10.1038/nature10866
37. Sturm D, Witt H, Hovestadt V, Khuong-Quang DA, Jones DTW, Konermann C, et al. Hotspot Mutations in H3F3A and IDH1 Define Distinct Epigenetic and Biological Subgroups of Glioblastoma. *Cancer Cell* (2012) 22:425–37. doi: 10.1016/j.ccr.2012.08.024
38. Lu C, Ward PS, Kapoor GS, Rohle D, Turcan S, Abdel-Wahab O, et al. IDH mutation impairs histone demethylation and results in a block to cell differentiation. *Nature* (2012) 483:474–8. doi: 10.1038/nature10860
39. Bai H, Harmanci AS, Erson-Omay EZ, Li J, Coşkun S, Simon M, et al. Integrated genomic characterization of IDH1-mutant glioma malignant progression. *Nat Genet* (2015) 48:59–66. doi: 10.1038/ng.3457
40. Tang L, Deng L, Bai HX, Sun J, Neale N, Wu J, et al. Reduced expression of DNA repair genes and chemosensitivity in 1p19q codeleted lower-grade gliomas. *J Neurooncol* (2018) 139:563–71. doi: 10.1007/s11060-018-2915-4
41. Huang SP, Chan YC, Huang SY, Lin YF. Overexpression of PSAT1 gene is a favorable prognostic marker in lower-grade gliomas and predicts a favorable outcome in patients with IDH1 mutations and chromosome 1p19q codeletion. *Cancers (Basel)* (2020) 12(1):1–15. doi: 10.3390/cancers12010013
42. Im JH, Hong JB, Kim SH, Choi J, Chang JH, Cho J. Recurrence patterns after maximal surgical resection and postoperative radiotherapy in anaplastic gliomas according to the new 2016 WHO classification. *Sci Rep* (2018) August 2017):1–9. doi: 10.1038/s41598-017-19014-1
43. Saha S, Kiran M, Kuscu C, Chatrath A, Wotton D, Mayo MW, et al. Long noncoding RNA DRAIC inhibits prostate cancer progression by interacting with IKK to inhibit NF-κB activation. *Cancer Res* (2020) 80:950–63. doi: 10.1158/0008-5472.CAN-19-3460
44. You R, Liu Y-P, Lin D-C, Li Q, Yu T, Zou X, et al. Clonal mutations activate the NF-kB pathway to promote recurrence of nasopharyngeal carcinoma. *Cancer Res* (2019) 79:5930–43. doi: 10.1158/0008-5472.CAN-18-3845
45. Bhat KPL, Balasubramaniyan V, Vaillant B, Ezhilarasan R, Hummelink K, Hollingsworth F, et al. Mesenchymal Differentiation Mediated by NF-κB Promotes Radiation Resistance in Glioblastoma. *Cancer Cell* (2013) 24:331–46. doi: 10.1016/j.ccr.2013.08.001
46. Hou Y, Liang H, Rao E, Zheng W, Huang X, Deng L, et al. Non-canonical NF-κB Antagonizes STING Sensor-Mediated DNA Sensing in Radiotherapy. *Immunity* (2018) 49:490–503.e4. doi: 10.1016/j.immuni.2018.07.008
47. Sakurai K, Reon BJ, Anaya J, Dutta A. The lncRNA DRAIC/PCAT29 locus constitutes a tumor-suppressive nexus. *Mol Cancer Res* (2015) 13:828–38. doi: 10.1158/1541-7786.MCR-15-0016-T
48. Molenaar RJ, Botman D, Smits MA, Hira VV, van Lith SA, Stap J, et al. Radioprotection of IDH1-mutated cancer cells by the IDH1-mutant inhibitor AGI-5198. *Cancer Res* (2015) 75:4790–802. doi: 10.1158/0008-5472.CAN-14-3603
49. Wang Y, Wild AT, Turcan S, Wu WH, Sigel C, Klimstra DS, et al. Targeting therapeutic vulnerabilities with PARP inhibition and radiation in IDH-mutant gliomas and cholangiocarcinomas. *Sci Adv* (2020) 6:eaaz3221. doi: 10.1126/sciadv.aaz3221
50. Dittmann LM, Danner A, Gronych J, Wolter M, Stühler K, Grzendowski M, et al. Downregulation of PRDX1 by promoter hypermethylation is frequent in 1p/19q-deleted oligodendroglial tumours and increases radio-and chemosensitivity of Hs683 glioma cells in vitro. *Oncogene* (2012) 31:3409–18. doi: 10.1038/onc.2011.513

Conflict of Interest: The authors declare that the research was conducted in the absence of any commercial or financial relationships that could be construed as a potential conflict of interest.

frontiers in Oncology

ORIGINAL RESEARCH
published: 30 March 2021
doi: 10.3389/fonc.2021.643469

Role of Hyperbaric Oxygenation Plus Hypofractionated Stereotactic Radiotherapy in Recurrent High-Grade Glioma

Donatella Arpa[1], Elisabetta Parisi[1], Giulia Ghigi[1], Annalisa Cortesi[1], Pasquale Longobardi[2], Patrizia Cenni[3], Martina Pieri[1], Luca Tontini[1], Elisa Neri[1], Simona Micheletti[1], Francesca Ghetti[1], Manuela Monti[4], Flavia Foca[4], Anna Tesei[5], Chiara Arienti[5], Anna Sarnelli[6], Giovanni Martinelli[7] and Antonio Romeo[1]*

[1] Radiotherapy Unit, IRCCS Istituto Romagnolo per lo Studio dei Tumori (IRST) "Dino Amadori", Meldola, Italy, [2] Centro Iperbarico, Ravenna, Italy, [3] Neuroradiology Unit, "Santa Maria delle Croci" Hospital, Ravenna, Italy, [4] Unit of Biostatistics and Clinical Trials, IRCCS Istituto Romagnolo per lo Studio dei Tumori (IRST) "Dino Amadori", Meldola, Italy, [5] Biosciences Laboratory, IRCCS Istituto Romagnolo per lo Studio dei Tumori (IRST) "Dino Amadori", Meldola, Italy, [6] Medical Physics Unit, IRCCS Istituto Romagnolo per lo Studio dei Tumori (IRST) "Dino Amadori", Meldola, Italy, [7] Scientific Directorate, IRCCS Istituto Romagnolo per lo Studio dei Tumori (IRST) "Dino Amadori", Meldola, Italy

OPEN ACCESS

Edited by:
Alfredo Conti, University of Bologna, Italy

Reviewed by:
Tu Dan, University of Texas Southwestern Medical Center, United States
Piotr Zielinski, Gdansk University of Physical Education and Sport, Poland

***Correspondence:**
Donatella Arpa
donatella.arpa@irst.emr.it

Specialty section:
This article was submitted to Neuro-Oncology and Neurosurgical Oncology, a section of the journal Frontiers in Oncology

Received: *18 December 2020*
Accepted: *09 March 2021*
Published: *30 March 2021*

Citation:
Arpa D, Parisi E, Ghigi G, Cortesi A, Longobardi P, Cenni P, Pieri M, Tontini L, Neri E, Micheletti S, Ghetti F, Monti M, Foca F, Tesei A, Arienti C, Sarnelli A, Martinelli G and Romeo A (2021) Role of Hyperbaric Oxygenation Plus Hypofractionated Stereotactic Radiotherapy in Recurrent High-Grade Glioma. Front. Oncol. 11:643469. doi: 10.3389/fonc.2021.643469

Background: The presence of hypoxic cells in high-grade glioma (HGG) is one of major reasons for failure of local tumour control with radiotherapy (RT). The use of hyperbaric oxygen therapy (HBO) could help to overcome the problem of oxygen deficiency in poorly oxygenated regions of the tumour. We propose an innovative approach to improve the efficacy of hypofractionated stereotactic radiotherapy (HSRT) after HBO (HBO-RT) for the treatment of recurrent HGG (rHGG) and herein report the results of an *ad interim* analysis.

Methods: We enrolled a preliminary cohort of 9 adult patients (aged >18 years) with a diagnosis of rHGG. HSRT was administered in daily 5-Gy fractions for 3-5 consecutive days a week. Each fraction was delivered up to maximum of 60 minutes after HBO.

Results: Median follow-up from re-irradiation was 11.6 months (range: 3.2-11.6 months). The disease control rate (DCR) 3 months after HBO-RT was 55.5% (5 patients). Median progression-free survival (mPFS) for all patients was 5.2 months (95%CI: 1.34-NE), while 3-month and 6-month PFS was 55.5% (95%CI: 20.4-80.4) and 27.7% (95%CI: 4.4-59.1), respectively. Median overall survival (mOS) of HBO-RT was 10.7 months (95% CI: 7.7-NE). No acute or late neurologic toxicity >grade (G)2 was observed in 88.88% of patients. One patient developed G3 radionecrosis.

Conclusions: HSRT delivered after HBO appears to be effective for the treatment of rHGG, it could represent an alternative, with low toxicity, to systemic therapies for patients who cannot or refuse to undergo such treatments.

Clinical Trial Registration: www.ClinicalTrials.gov, identifier NCT 03411408.

Keywords: recurrent high-grade glioma, hypofractionated stereotactic radiotherapy, hyperbaric oxygenation, TomoTherapy, re-irradiation

INTRODUCTION

High-grade gliomas (HGGs) represent the most malignant and most frequently encountered primary brain tumour in clinical neuro-oncology. Despite improvements in diagnostic and therapeutic strategies, the clinical prognosis for patients with HGG remains poor, with a median overall survival of <16 months. The majority of cases relapse within a year of diagnosis, and almost always at the initial site of disease (1). Life expectancy in this group is even poorer, with a median survival of around 6-11 months (2–6). Developing effective salvage treatments at recurrence is thus urgently needed to prolong overall survival (7). Hypoxia is thought to play a role in tumour development, angiogenesis and growth, and resistance to chemotherapy, antiangiogenic therapy and radiotherapy (RT) in a large number of human cancers (8, 9). Brain tumours, especially highly aggressive GBM with its necrotic tissue, are more likely to be affected by hypoxia. GBM is a highly vascularized tumour with a functionally inefficient microcirculation that may contribute to hypoxia and necrosis within a tumour (10–15). Several studies have reported that the median partial pressure of oxygen (PO2) of high-grade gliomas in patients under anaesthesia was approximately 5-7 mmHg, with a significant proportion of PO2 values <2.5 mmHg (16–19). The radiosensitivity of brain tumours could potentially be increased by performing hyperbaric oxygenation (HBO) before the RT session (20–25).

Recent studies suggest that the PO2 within tumours increases during HBO and is maintained for several minutes after the procedure (17, 26, 27). It is known that the cellular metabolism of malignant glioma is anaerobic, with the tumour exhibiting a lower oxygen consumption rate than normal white matter (28, 29). Thus, in contrast to normal brain tissue, the PO2 within the tumour decreases more slowly after decompression because of low oxygen consumption and poor blood flow to the tumour. It can thus be hypothesized that HBO before RT is capable of increasing the sensitivity of hypoxic tumour cells to treatment without increasing the damage to normal brain tissue (20, 30–32).

We propose an innovative approach to improve the efficacy of HSRT using image-guided helical TomoTherapy after HBO for the treatment of recurrent HGG (rHGG). Herein we report the results of an *ad interim* analysis.

MATERIALS AND METHODS

Patient Eligibility

Adult patients (aged >18 years) with rHGG, as defined by RANO (Response Assessment for Neuro-Oncology) criteria (33), underwent HBO followed by re-irradiation (RE-RT). Main inclusion criteria are shown in **Table 1**. Exclusion criteria were as follows: radiotherapy ≤12 weeks prior to diagnosis of progression if the lesion was in the radiation field; b) cardiopulmonary disease (heart failure, bullous emphysema, pneumothorax, chronic obstructive pulmonary disease with hypercapnia sinusitis); and closed-angle glaucoma with ocular pressure >24 mmHg.

Study Design

This was a pilot study of Hypofractionated Stereotactic Radiotherapy (HSRT) using TomoTherapy. This trial provided 5 Gy/day for 3-5 consecutive days after daily HBO for the treatment of recurrent malignant high-grade glioma(rHGGs). The maximum time from completion of decompression to HRT was 60 min. The primary objective of this study was to evaluate the disease control rate (DCR) of treated patients. DCR was defined as the percentage of patients with rHGG who have achieved complete response, partial response and stable disease 3 months after HBO-RT. Secondary objectives were safety assessment (acute and late toxicity), OS and progression-free survival (PFS).

HBO Therapy

HBO was administrated in a multiplace hyperbaric chamber according to the following schedule: ten min of compression with a fraction of inspired oxygen (*Fi*O2) >90% from 152 to 253 kilopascal, 60 min of *Fi*O2 >90% at 253 kilopascal (three breathing cycles in oxygen of 22 min each, with 2-minute intervals breathing air and 10 min of decompression with a *Fi*O2 >90% from 253 to 152 kilopascal. Following the HBO session, each patient underwent RT.

Abbreviations: AA, anaplastic astrocytoma; AO, anaplastic oligodendroglioma; BED, biologically effective dose; CT, computed tomography; DCE, dynamic contrast-enhanced; DCE, dynamic contrast-enhanced; DCR, disease control rate; DCR, disease control rate; DSC, dynamic susceptibility contrast-enhanced; DSC, dynamic susceptibility contrast-enhanced; DWI, diffusion-weighted imaging; DWI, diffusion-weighted imaging; *Fi*O2, fraction of inspired oxygen; FLAIR, fluid-attenuated inversion recovery imaging; Gd-MRI, axial imaging with gadolinium; HBO, hyperbaric oxygen therapy; HGG, high-grade glioma; HSRT, hypofractionated stereotactic radiotherapy; HSRT, hypofractionated stereotactic radiotherapy; HT, helical TomoTherapy; IMRT, intensity-modulated radiotherapy; KPS, Karnofsky performance status; MMSE, mini-mental state examination; mOS median overall survival; mPFS, median progression-free survival; MRI, magnetic resonance imaging; OAR, organs-at-risk; OS, overall survival; PFS, progression-free survival; PO2, pressure of oxygen; PTV, planning treatment volume; RANO, response assessment for neuro-oncology; RE-RT, re-irradiation; rHGG, recurrent HGG; rHGGs, recurrent malignant high-grade glioma; RT, radiotherapy.

TABLE 1 | Eligibility criteria.

- Male or female, aged >18 years
- Karnofsky Performance Scale (KPS)> 60
- Imaging confirmation of first tumour progression or regrowth as defined by RANO criteria at least 12 weeks after completion of radiotherapy, unless the recurrence is outside the radiation field or has been histologically documented.
- Recurrence after adjuvant treatment (surgery followed by radiotherapy and chemotherapy)
- Adequate bone marrow, liver function and renal function measured by laboratory tests no more than 7 days before start of study treatment.
- Participant is willing and able to give informed consent to take part in the study.
- If female and of child-bearing potential, the patient must have a negative pregnancy test a maximum of 7 days before starting therapy.

RANO, Response Assessment in Neuro-Oncology.

Radiotherapy

Target Volume Definition

Computed tomography (CT) planning (Brilliance Big Bore CT Philips, Crowley, UK) was performed with a 1- to 3-mm slice thickness. Patients were placed in a supine position with arms close to their body and immobilized with a thermoplastic mask. A co-registration of volumetric CT and magnetic resonance imaging (MRI) sequences (1- to 3-mm slice thickness) was performed to define the targets and organs-at-risk (OAR). MRI sequences were performed using a 1.5-T with T1-weighted imaging, contrast-enhanced T1-weighted axial imaging with gadolinium (Gd-MRI), fluid-attenuated inversion recovery imaging (FLAIR), axial T2- weighted imaging, coronal T2-weighted imaging, DWI (diffusion-weighted imaging), dynamic susceptibility contrast-enhanced (DSC) and dynamic contrast-enhanced (DCE) perfusion. The planning treatment volume 1 (PTV1) was defined as the visible tumour on enhanced T1-MRI with a 1-mm margin expansion. In accordance with the neuroradiology team, another treatment volume (PTV FLAIR) was delineated to include the surrounding edema in cases where non-enhanced areas highlighted by increased T2-weighted FLAIR signal were evaluated as disease progression. OARs were identified as healthy brain, optic chiasm, optic nerves and brainstem.

Treatment Planning and Irradiation

In patients in whom PTV FLAIR was delineated, a total dose of 12 and 20 Gy was delivered (99% isodose line covering 99% of the PTV); 15 Gy and 25 Gy were prescribed to the PTV1 in 3-5 daily fractions at the isodose of 67% (**Figure 1**). The treatment dose was chosen on the basis of the Karnofsky Performance Status (KPS) of the patient, the interval between the first and second radiotherapy course, tumour size, and the proximity of critical organs to the targets. All patients underwent image-guided helical TomoTherapy (HT) (TomoTherapy Inc., Madison, WI, USA). The HT system uses image-guided RT in which a CT scan is performed before each treatment, allowing the radiotherapist to verify and adjust the patient's position as needed to ensure that the radiation is directed exactly at the target area.

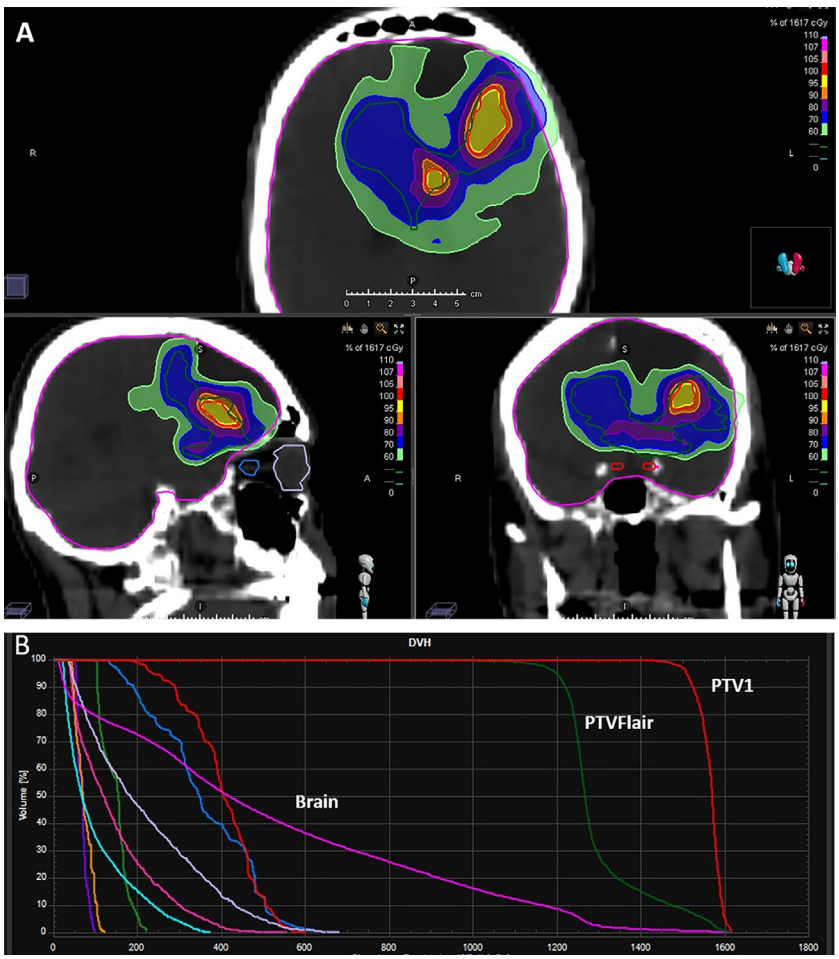

FIGURE 1 | Examples of **(A)** dose distribution and **(B)** typical dose volume histogram (DVH) for a prescription dose of 15 Gy in 3 fractions to PTV1 and 12 Gy in 3 fractions to PTV FLAIR.

Assessment of Response and Toxicity

The assessment of radiological and clinical response was based on MRI sequences obtained before and after HBO-RT according to RANO Criteria. The radiological protocol consisted in MRI T1-weighted imaging, contrast-enhanced T1-weighted axial imaging with gadolinium (Gd-MRI), fluid-attenuated inversion recovery imaging (FLAIR), axial T2- weighted imaging, DWI (diffusion-weighted imaging), dynamic susceptibility contrast-enhanced (DSC) and dynamic contrast-enhanced (DCE) perfusion. Each patient underwent MRI evaluation, neurological examination and Mini-Mental State examination (MMSE) 40 days after the end of RT and every 3 months thereafter for one year. Patients were followed until disease progression or death. All toxicities were recorded and graded according to NCI CTCAE (National Cancer Institute Common Toxicity Criteria for Adverse Events), version 4.3 (34).

Evaluation and Statistical Analysis

Simon's two-stage design was used to estimate sample size (35). In the first stage, nine patients would be accrued. If there were 3 or fewer DCRs in these 9 patients, the study would be stopped. Otherwise, 15 additional patients would be accrued for a total of 24. The null hypothesis would be rejected if 13 or more patients with DCR were observed in 24 patients. This design yielded a type I error rate of 0.05 and power of 80% for a true DCR of 0.62. The percentage of patients who achieved complete response, partial response and stable disease were calculated to evaluate the primary endpoint, and 95% confidence intervals (95%CI) were derived from the exact binominal distribution. For the safety assessment, the number and percentage of treated patients experiencing grades 1-4 adverse events were tabulated. OS and PFS were estimated with the Kaplan-Meier Method (two-sided 95%CI) and the role of potential stratification factors was analysed with the log-rank test.

RESULTS

Patient Characteristics

Nine patients (2 females and 7 males) with rHGG were enrolled in this trial between February 2018 and October 2019. At time of the initial diagnosis, 7 (77.7%) had GBM, one had anaplastic oligodendroglioma (AO) and one had anaplastic astrocytoma (AA). The median age at the time of HBO-RT was 58.8 years (range 35.8-71.7 years). All patients had a Karnofsky Performance status (KPS) of ≥60. The entire cohort received adjuvant primary radiation therapy with concomitant chemotherapy after primary surgery. Eight patients underwent post-operative fractionated RT with a total dose of 60 Gy in 30 fractions and one received adjuvant hypofractionated RT with a total dose of 25 Gy delivered in 5 fractions. The median interval between primary RT and salvage RT was 17.2 months (range 4.3-23.5 months).The site of recurrence included 4 frontal lobe, 2 peritrigonal region, 1 temporal lobe, 1 hippocampus, 1 parietal lobe. The prognostic factor classes established by Carson et al. were applied to all patients (36). Specific patient characteristics are reported in **Table 2** and in **Supplementary Table 1**.

Treatment Delivered

All 9 patients completed RE-RT after HBO without interruption. Five patients underwent HBO-RT treatment over 3 consecutive days and the remaining four over 5 days (**Figure 1**). Details of the RT planning are reported in **Table 3**. The median time between HBO and the radiotherapy fraction was 24 minutes (04-50 minutes).

Outcomes

Median follow-up from RE-RT was 11.6 months (range 3.2-11.6 months). No patient was lost to follow-up. Three months after treatment, 5 patients (55.5%) maintained local disease control, while 4 showed progression and the accrual of the first stage of the two-stage design was completed. Median progression-free survival (mPFS) for all patients was 5.2 months (95%CI: 1.34-NE) (**Figure 2**), while 3-month and 6-month PFS was 55.5% (95%CI: 20.4-80.4) and 27.7% (95%CI: 4.4-59.1), respectively. Upon progression, 2 patients underwent treatment with temozolomide, one with fotemustine and one with PCV (procarbazine, lomustine and vincristine).

Median overall survival (mOS) of HBO-RT was 10.7 months (95% CI: 7.7-NE) (**Figure 3**). At time of this analysis, 5 patients with recurrent GBM (rGBM) had died (disease progression) and 4 were still alive, all living virtually normal daily lives until PD. Of this group, a 60-year-old woman obtained local disease control (3 months after HBO-RT); a 36-year-old man with recurrent GBM developed PD 12 months after completing HBO-RT and underwent treatment with bevacizumab; one

TABLE 2 | Patient characteristics.

	No. (%)
Median age at start of HBO-RT therapy (range)	58.8 (35.8-71.7)
Gender	
Female	2 (22.2)
Male	7 (77.8)
KPS	
65	1 (11.1)
80	2 (22.2)
90	4 (44.5)
100	2 (22.2)
Carson RPA classes	
1	1 (11.11)
2	1(11.11)
4	1 (11.11)
6	5 (55.5)
7	1 (11.11)
Post-operative RT (no. patients)	
2 Gy daily (total dose 60 Gy)	8 (88.88)
5 Gy daily(total dose 25 Gy)	1 (11.12)
Median interval between post-operative radiotherapy and salvage HBO-RT, months [range]	17.2 [4.3-23.5]
Salvage therapy before HBO-RT	
None	9 (100)

HBO, hyperbaric oxygenation; Carson RPA, Carson recursive partitioning analysis; RT, radiotherapy.

TABLE 3 | Treatment details of HRT.

Patient	Site of recurrence	No. fractions	PTV1 (cc)	PTV FLAIR (cc)	Dose prescription to PTV1 (cGy)	Dose prescription to PTV FLAIR (cGy)	D1 (cGy) (PTV1)	D1 (cGy) (PTV FLAIR)
1	Right frontal	3	9.60	133.74	1500	1200	2401	2286
2	Left parietal	5	7.01	–	2500	–	3970	–
3	Left peritrigonal	5	7.26	59.62	2500	2000	3891	3891
4	Left frontal	3	12.40	–	1500	–	2437	–
5	Left temporal	3	23.08	–	1500	–	1556	–
6	Left frontal	3	5.57	94.46	1500	1200	1614	1589
7	Left peritrigonal	5	0.94	34.94	2500	2000	3876	3552
8	Left hippocampus	3	6.51	–	1500	–	2279	
9	Right frontal	5	5.96	50.73	2500	2000	3881	3253

HSRT, Hypofractionated Stereotactic Radiotherapy; PTV, planning target volume; FLAIR, fluid-attenuated inversion recovery; cGy, centigray; D1, dose to 1% of the volume.

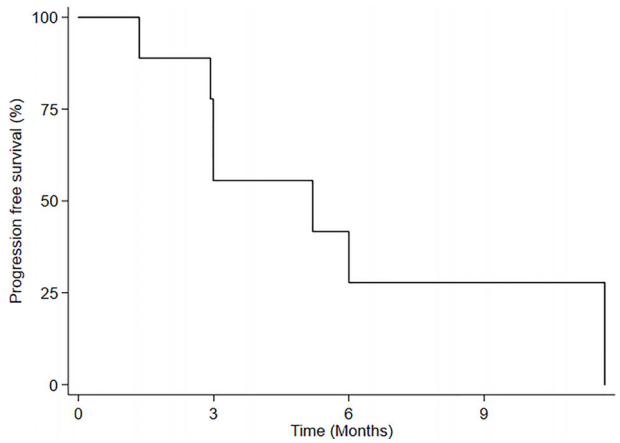

FIGURE 2 | Progression-free survival (PFS) after HBO-RT.

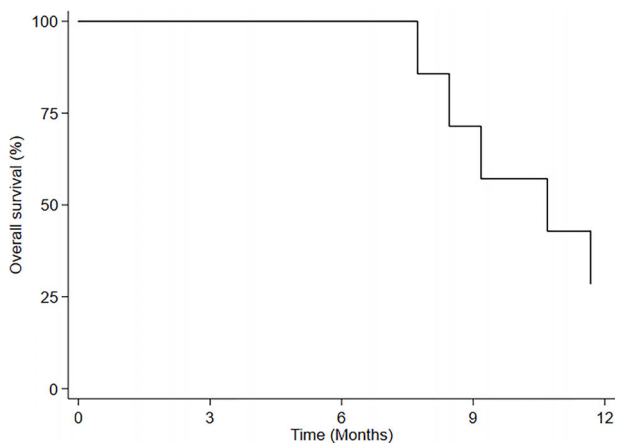

FIGURE 3 | Overall survival (OS) after HBO-RT.

patient with recurrent anaplastic oligodendroglioma progressed after 6 months; and one patient with recurrent AA progressed after 3months. Neurocognitive functions remained stable until PD. MMSE values for each patient were stable until PD.

Toxicity

During HBO, only one patient experienced ear pain, without barotrauma. No patients had convulsive seizures during or after HBO. RE-RT was well tolerated. All patients completed treatment without interruption. During treatment dexamethasone ≥2 mg was administered to all patients. Three months after HBO-RT treatment Three patients continued with 2 mg dexamethasone while two took 4 mg dexamethasone and one 8 mg and three none. No acute or late neurologic toxicity >grade 2 (CTCAE version 4.3) was observed in 8 patients. A 71-year-old man with rGBM showed symptoms and radiological signs of grade 3 radionecrosis. When first diagnosed, the patient had GBM with unmethylated MGMT, negative IDH1 and IDH2, Mib1 10%, and positive GFAP. He underwent re-irradiation 24 months after postoperative RT, with a total dose of 25 Gy in 5 fractions to PTV1 (volume 0.96 cc) and 20 Gy in 5 sessions to PTV FLAIR (volume 34.94 cc). During follow-up, Gd-MRI, DWI, DSC and DCE perfusion MRI revealed a suspicion of radionecrosis and concomitant O-(2-[^{18}F]fluoroethyl-)-L-tyrosine (^{18}F-FET) PET/CT was performed to support the differential diagnosis of PD or treatment-related changes. The scans confirmed the radionecrosis. The patient was treated successfully with corticosteroids and bevacizumab.

DISCUSSION

The survival of patients with HGG depends on local disease control because the majority of patients die of recurrence at close proximity to the site of the primary tumour (37). Life expectancy after relapse is poor, and there is still no standard treatment for recurrent HGG, highlighting the need to develop effective salvage treatments to prolong OS (7). Several studies have suggested that re-irradiation may be a useful option for recurrent HGG, with acceptable toxicity (38). In fact, the availability of high-precision radiotherapy techniques permits retreatment, which is generally performed with single-fraction stereotactic radiosurgery, fractionated stereotactic RT (FSRT) or HSRT alone or in combination with systemic chemotherapy (39). The present paper reports the results of the first phase of a clinical trial, conducted according to a Simon's two-stage design, to evaluate whether re-irradiation of rHGG after HBO can improve the efficacy of RT.

Failure of RT in malignant gliomas is primarily due to the presence of hypoxic, intrinsically radioresistant, cells in the lesion. In the early 1950s, Gray et al. postulated that oxygen deficiency was a main source of radiation resistance (40). The biological effect of ionizing radiation has been reported to be around 3-fold higher when it is delivered under well-oxygenated rather than anoxic conditions (40). Overgaard et al. (41, 42) studied various hypoxic modification techniques, reporting that HBO showed the most pronounced effect and could thus potentially improve RT results. Bennett et al. (43) recently reported that HBO may increase the effectiveness of RT in patients with head and neck cancer, reducing tumour regrowth and improving survival. HBO is based on the administration of 100% oxygen at higher than normal atmospheric pressure. It increases O_2 tissue delivery independently of haemoglobin levels (44). Several authors have reported that the increase in tumour oxygen pressure is preserved for several minutes after HBO exposure. Kinoshita et al. monitored changes in MRI signal intensity after HBO exposure using non-invasive MRI. The authors demonstrated that the signal change related to the oxygen tension in murine squamous cell carcinoma VII (SCCVII) tumours decreased rapidly in the muscle after HBO but slowly in the tumour mass, and was still high 60 minutes after decompression (27). Beppu et al. stereotactically measured pO2 in both peritumoural and intratumoural glioma tissue after HBO, reporting significantly increased pO2 levels that remained stable for up to 15 minutes in both regions (17). Like Kinoshita et al., we estimated a maximum interval of 60 minutes between decompression and HSRT. Koshi et al. suggested that the timing of irradiation is vital to the overall success of RT following HBO exposure. In their study of the retreatment of high-grade gliomas, gamma FSRT was started within 7 minutes of the end of HBOT and lasted a full 80 minutes. In our study, the overall treatment time of TomoTherapy plans was much shorter, around 10 minutes (32). Al-Waili et al. showed that a combination of HBO and RT reduced tumour growth and improved local control, resulting in increased survival (45). Several studies have shown the feasibility of this treatment regimen in primary HGG, suggesting that HBO improves response rates and survival without serious side-effects in patients treated with RT (46–49).

Ogawa et al. treated 57 HGG patients with RT immediately after HBO, reporting a 52% objective response rate (47). Kohshi et al. used radiotherapy after HBO in HGG patients with residual disease, registering a 50% reduction in tumour mass and a median survival of 24 months (48). Yahara et al. evaluated the feasibility and efficacy of RT using an intensity-modulated radiotherapy (IMRT) boost after HBO together with chemotherapy in glioblastoma patients, reporting a median OS of 22 months (49). Only one study has been carried out on recurrent HGG patients treated with FSRT immediately after HBO (32). The authors, Kohshi et al., treated 25 patients with a median total dose of 22 Gy (range 18-27 Gy) in 8 fractions delivered to the tumour margin (32). They confirmed a survival benefit from this treatment, with low toxicity.

In our study, the disease control rate (DCR) 3 months after HBO-RT was 55.5% (5 patients), fulfilling the primary objective of the study and enabling us to open the second phase of recruitment. Median progression-free survival (mPFS) for all patients was 5.2 months (95%CI: 1.34-NE), while 3-month and 6-month PFS was 55.5% (95%CI: 20.4-80.4) and 27.7% (95%CI: 4.4-59.1), respectively. Median overall survival (mOS) of HBO-RT was 10.7 months (95% CI: 7.7-NE). These preliminary results are similar to those of other HSRT re-irradiation studies, i.e. PFS ranged from 4 months to 7.9 months and OS from 7.5 months to 11 months (**Table 4**).

Our pilot study consisted of HSRT after daily HBO for rHGG. The prescription doses delivered to PTV1 were 15 Gy in 3 fractions (5 patients), 25 Gy in 5 fractions (4 patients), and 12 Gy-20Gy to the PTV FLAIR in patient in whom PTV FLAIR was delineated. The equivalent dose in 2 Gy per fraction (EQD2) with alpha/beta 10 of 15 Gy in 3 fractions was 18.75 Gy, with a biologically effective dose (BED_{10}) of 22.50 Gy_{10}. The EQD2 of

TABLE 4 | Studies on HSRT for recurrent high-grade glioma.

Author	No. patients	Median tumour volume	Median total dose (Gy)	Dose per fraction (Gy)	Median no. fractions	Bed_{10}	Associated systemic therapy	Median PFS (m)	Median OS (m)
Vordemark et al. (50)	19	15	30	5	6	48	–	4.9	9.3
Ernst-Stecken et al. (51)	15	22.4	35	7	5	59.50	–	75% at 6 m 53% at 12 m	12
Fokas et al. (52)	53	35	30	3	10	39	–	22% at 12 m	9
Kim et al. (53)	8	69.5	25	5	5	37.50	–	4.6	7.6
Minniti et al. (54)	54	9.7	30	6	5	48	Tmz	6	12.4
Shapiro et al. (55)	24	35.3	30	6	5	48	Beva	7.5	12
Yazici et al. (56)	37	24	30	6	5	48		7.9	10.6
Minniti et al. (57)	54	12.4	25	5	5	37.50	Beva	6	11
							Fote	4	8.3
Navarria et al. (58)	25	35	25	5	5	37.50	Tmz Fotemustine Beva	16	18
Combs et al. (59)	325	54.4	36	2.67	20	42.48	Different regimens	–	7.5 (IV grade) 9.5 (III grade)

Beva, bevacizumab; Fote, fotemustine; TMZ, temozolomide; m, months.

25 Gy in 5 fractions was 31.25 Gy_2, with a BED of 37.50 Gy_{10}. Very different radiotherapy regimens were used in other HSRT re-irradiation studies, with fraction sizes ranging from 3 to 7 Gy and the number of fractions varying from 5 to 10 (**Table 4**) (50–62). Yazici et al. treated 37 patients with recurrent glioblastoma with a median dose of 30 Gy in a median 5 fractions (1-5 fractions) with a median volume of 24 cc (range 2-81). The authors reported a mPFS of 7.9 months and a median OS of 10.6 months (1.1-20 months) (56). The BED_{10} calculated for 30 Gy in 5 fractions was 48 Gy_{10}. Minniti et al. delivered 25 Gy in 5 fractions in association with bevacizumab or fotemustine. Median PFS was 4 months for patients treated with HSRT plus fotemustine, and 6 months for HSRT and bevacizumab, with a median OS of 11 months (57). The BED_{10} calculated for 25 Gy in 5 fractions was 37.50 Gy_{10}.

In a recent multicentre study on re-irradiation of recurrent glioma, Navarria et al. identified a BED_{10} threshold of >43 Gy that influenced survival (60). Although our calculated BED is lower than that of other series, in particular that of 22.50 Gy_{10}, our patients showed similar outcomes to those of other studies. Our ad interim analysis thus suggests a possible advantage of adding HBO to HSRT for the local control of rHGG.

Bennet et al. suggested that the dose per fraction may influence the importance of the benefit derived from hypoxic modification. They concluded that the use of hypofractionation results in a more pronounced modification of hypoxia (43). In our case series, we also used altered fractionation i.e. hypofractionation delivered by image-guided helical TomoTherapy, which enables large tumour volumes to be treated, minimizing the toxicity associated with high dose fractionation.

Our analysis ad interim showed only one case of radionecrosis grade 3 CTCAE.

Although the results from the present study suggest that the use of RT after HBO is a safe and practical procedure, our preliminary findings must obviously be interpreted with caution because of the small number and inhomogeneity of the patients involved. We thus aim to validate the results in the second part of the study in which another 15 patients will be recruited.

In conclusion, HBO-RT could represent an alternative, with low toxicity, to systemic therapies for patients who cannot or refuse to undergo such treatments. One of advantages of HBO-RT is the reduced overall treatment time (3-5 consecutive days). Further randomized studies in primary and recurrent settings are needed to confirm our findings.

DATA AVAILABILITY STATEMENT

The original contributions presented in the study are included in the article/**Supplementary Material**. Further inquiries can be directed to the corresponding author.

ETHICS STATEMENT

The studies involving human participants were reviewed and approved by IRCCS IRST Ethics Committee. The patients/participants provided their written informed consent to participate in this study.

AUTHOR CONTRIBUTIONS

DA, EP, GG, PL, and PC conceived the idea for and designed the study. DA, MP, LT, EN, SM, MM, CA, FG, AC, and AS collected and assembled the study data. DA, EP, GG, PL, AT, and PC analysed and interpreted the data. FF performed the statistical analysis. DA drafted the manuscript. AR and GM revised the manuscript for important intellectual content. All authors contributed to the article and approved the submitted version.

ACKNOWLEDGMENTS

The authors thank Gráinne Tierney for editorial assistance.

SUPPLEMENTARY MATERIAL

The Supplementary Material for this article can be found online at: https://www.frontiersin.org/articles/10.3389/fonc.2021.643469/full#supplementary-material

REFERENCES

1. Stupp R, Hegi ME, Mason WP, van den Bent MJ, Taphoorn MJ, Janzer RC, et al. Effects of radiotherapy with concomitant and adjuvant temozolomide versus radiotherapy alone on survival in glioblastoma in a randomised phase III study: 5-year analysis of the EORTC-NCIC trial. *Lancet Oncol* (2009) 10:459–66. doi: 10.1016/S1470-2045(09)70025-7
2. Niyazi M, Siefert A, Schwarz SB, Ganswindt U, Kreth F-W, Tonn J-C, et al. Therapeutic options for recurrent malignant glioma. *Radiother Oncol* (2011) 98:1–14. doi: 10.1016/j.radonc.2010.11.006
3. Wick W, Gorlia T, Bendszus M, Taphoorn M, Sahm F, Harting I, et al. Lomustine and Bevacizumab in Progressive Glioblastoma. *N Engl J Med* (2017) 377:1954–63. doi: 10.1056/nejmoa1707358
4. Taal W, Oosterkamp HM, Walenkamp AME, Dubbink HJ, Beerepoot LV, Hanse MCJ, et al. Single-agent bevacizumab or lomustine versus a combination of bevacizumab plus lomustine in patients with recurrent glioblastoma (BELOB trial): A randomised controlled phase 2 trial. *Lancet Oncol* (2014) 15:943–53. doi: 10.1016/S1470-2045(14)70314-6
5. Reardon DA, Brandes AA, Omuro A, Mulholland P, Lim M, Wick A, et al. Effect of Nivolumab vs Bevacizumab in Patients with Recurrent Glioblastoma: The CheckMate 143 Phase 3 Randomized Clinical Trial. *JAMA Oncol* (2020) 6:1003–10. doi: 10.1001/jamaoncol.2020.1024
6. Tsien C, Pugh S, Dicker AP, Raizer JJ, Matuszak MM, Lallana E, et al. Randomized Phase II Trial of Re-Irradiation and Concurrent Bevacizumab versus Bevacizumab Alone as Treatment for Recurrent Glioblastoma (NRG Oncology/RTOG 1205): Initial Outcomes and RT Plan Quality

Report. *Int J Radiat Oncol* (2019) 105:S78. doi: 10.1016/j.ijrobp.2019.06.539
7. Seystahl K, Wick W, Weller M. Therapeutic options in recurrent glioblastoma–An update. *Crit Rev Oncol Hematol* (2016) 99:389–408. doi: 10.1016/j.critrevonc.2016.01.018
8. Jensen RL. Hypoxia in the tumorigenesis of gliomas and as a potential target for therapeutic measures. *Neurosurg Focus* (2006) 20:E24. doi: 10.3171/foc.2006.20.4.16
9. Jensen RL. Brain tumor hypoxia: Tumorigenesis, angiogenesis, imaging, pseudoprogression, and as a therapeutic target. *J Neurooncol* (2009) 92:317–35. doi: 10.1007/s11060-009-9827-2
10. Kaynar MY, Sanus GZ, Hnimoglu H, Kacira T, Kemerdere R, Atukeren P, et al. Expression of hypoxia inducible factor-1α in tumors of patients with glioblastoma multiforme and transitional meningioma. *J Clin Neurosci* (2008) 15:1036–42. doi: 10.1016/j.jocn.2007.07.080
11. Fischer I, Gagner J-P, Law M, Newcomb EW, Zagzag D. Angiogenesis in Gliomas: Biology and Molecular Pathophysiology. *Brain Pathol* (2006) 15:297–310. doi: 10.1111/j.1750-3639.2005.tb00115.x
12. Onishi M, Ichikawa T, Kurozumi K, Date I. Angiogenesis and invasion in glioma. *Brain Tumor Pathol* (2011) 28:13–24. doi: 10.1007/s10014-010-0007-z
13. Tate MC, Aghi MK. Biology of Angiogenesis and Invasion in Glioma. *Neurotherapeutics* (2009) 6:447–57. doi: 10.1016/j.nurt.2009.04.001
14. Nakabayashi H, Yawata T, Shimizu K. Anti-invasive and antiangiogenic effects of MMI-166 on malignant glioma cells. *BMC Cancer* (2010) 10:339. doi: 10.1186/1471-2407-10-339
15. Chi A, Norden AD, Wen PY. Inhibition of angiogenesis and invasion in malignant gliomas. *Expert Rev Anticancer Ther* (2007) 7:1537–60. doi: 10.1586/14737140.7.11.1537
16. Lally BE, Rockwell S, Fischer DB, Collingridge DR, Piepmeier JM, Knisely JPS. The interactions of polarographic measurements of oxygen tension and histological grade in human glioma. *Cancer J* (2006) 12:461–6. doi: 10.1097/00130404-200611000-00005
17. Beppu T, Kamada K, Yoshida Y, Arai H, Ogasawara K, Ogawa A. Change of oxygen pressure in glioblastoma tissue under various conditions. *J Neurooncol* (2002) 58:47–52. doi: 10.1023/A:1015832726054
18. Kayama T, Yoshimoto T, Fujimoto S, Sakurai Y. Intratumoral oxygen pressure in malignant brain tumor. *J Neurosurg* (1991) 74:55–9. doi: 10.3171/jns.1991.74.1.0055
19. Collingridge DR, Piepmeier JM, Rockwell S, Knisely JPS. Polarographic measurements of oxygen tension in human glioma and surrounding peritumoural brain tissue. *Radiother Oncol* (1999) 53:127–31. doi: 10.1016/S0167-8140(99)00121-8
20. Kohshi K, Beppu T, Tanaka K, Ogawa K, Inoue O, Kukita I, et al. Potential roles of hyperbaric oxygenation in the treatments of brain tumors. *Undersea Hyperb Med* (2013) 40:351–62.
21. Stępień K, Ostrowski RP, Matyja E. Hyperbaric oxygen as an adjunctive therapy in treatment of malignancies, including brain tumours. *Med Oncol* (2016) 33:101. doi: 10.1007/s12032-016-0814-0
22. Moen I, Stuhr LEB. Hyperbaric oxygen therapy and cancer - A review. *Target Oncol* (2012) 7:233–42. doi: 10.1007/s11523-012-0233-x
23. Bennett MH, Feldmeier J, Hampson NB, Smee R, Milross C. Hyperbaric oxygen therapy for late radiation tissue injury. *Cochrane Database Syst Rev* (2016) 4:CD005005. doi: 10.1002/14651858.CD005005.pub4
24. Bennett MH, Feldmeier J, Smee R, Milross C. Hyperbaric oxygenation for tumour sensitisation to radiotherapy. *Cochrane Database Syst Rev* (2012) 5:CD005005. doi: 10.1002/14651858.CD005005.pub3
25. Huang L, Boling W, Zhang J. Hyperbaric oxygen therapy as adjunctive strategy in treatment of glioblastoma multiforme. *Med Gas Res* (2018) 8:24–8. doi: 10.4103/2045-9912.229600
26. Kunugita N, Kohshi K, Kinoshita Y, Katoh T, Abe H, Tosaki T, et al. Radiotherapy after hyperbaric oxygenation improves radioresponse in experimental tumor models. *Cancer Lett* (2001) 164:149–54. doi: 10.1016/S0304-3835(00)00721-7
27. Kinoshita Y, Kohshi K, Kunugita N, Tosaki T, Yokota A. Preservation of tumour oxygen after hyperbaric oxygenation monitored by magnetic resonance imaging. *Br J Cancer* (2000) 82:88–92. doi: 10.1054/bjoc.1999.0882
28. Wise RJ, Bernardi S, Frackowiak RS, Jones T, Legg NJ, Lenzi GL. Measurement of regional cerebral blood flow, oxygen extraction ratio and oxygen utilization in stroke patients using positron emission tomography. *Exp Brain Res* (1982) Suppl 5:182–86. doi: 10.1007/978-3-642-68507-1_25
29. Tyler JL, Diksic M, Villemure JG, Evans AC, Meyer E, Yamamoto YL, et al. Metabolic and hemodynamic evaluation of gliomas using positron emission tomography. *J Nucl Med* (1987) 28:1123–33.
30. Chen JR, Xu HZ, Ding JB, Qin ZY. Radiotherapy after hyperbaric oxygenation in malignant gliomas. *Curr Med Res Opin* (2015) 31:1977–84. doi: 10.1185/03007995.2015.1082988
31. Ogawa K, Kohshi K, Ishiuchi S, Matsushita M, Yoshimi N, Murayama S. Old but new methods in radiation oncology: Hyperbaric oxygen therapy. *Int J Clin Oncol* (2013) 18:364–70. doi: 10.1007/s10147-013-0537-6
32. Kohshi K, Yamamoto H, Nakahara A, Katoh T, Takagi M. Fractionated stereotactic radiotherapy using gamma unit after hyperbaric oxygenation on recurrent high-grade gliomas. *J Neurooncol* (2007) 82:297–303. doi: 10.1007/s11060-006-9283-1
33. Wen PY, Macdonald DR, Reardon DA, Cloughesy TF, Sorensen AG, Galanis E, et al. Updated response assessment criteria for high-grade gliomas: Response assessment in neuro-oncology working group. *J Clin Oncol* (2010) 28:1963–72. doi: 10.1200/JCO.2009.26.3541
34. Cancer Institute N. *Common Terminology Criteria for Adverse Events (CTCAE) Version 4.0* (2009). Available at: http://www.meddramsso.com (Accessed May 23, 2020).
35. Simon R. Optimal Two-Stage Designs for Phase II Clinical Trials. *Control Clin Trials* (1989) 10:1–10. doi: 10.1016/0197-2456(89)90015-9
36. Carson KA, Grossman SA, Fisher JD, Shaw EG. Prognostic factors for survival in adult patients with recurrent glioma enrolled onto the new approaches to brain tumor therapy CNS Consortium phase I and II clinical trials. *J Clin Oncol* (2007) 25:2601–6. doi: 10.1200/JCO.2006.08.1661
37. Minniti G, Amelio D, Amichetti M, Salvati M, Muni R, Bozzao A, et al. Patterns of failure and comparison of different target volume delineations in patients with glioblastoma treated with conformal radiotherapy plus concomitant and adjuvant temozolomide. *Radiother Oncol* (2010) 97:377–81. doi: 10.1016/j.radonc.2010.08.020
38. Kim H. Appraisal of re-irradiation for the recurrent glioblastoma in the era of MGMT promotor methylation. *Radiat Oncol J* (2019) 37:1–12. doi: 10.3857/roj.2019.00171
39. Shanker M, Chua B, Bettington C, Foote MC, Pinkham MB. Re-irradiation for recurrent high-grade gliomas: A systematic review and analysis of treatment technique with respect to survival and risk of radionecrosis. *Neuro Oncol Pract* (2019) 6:144–55. doi: 10.1093/nop/npy019
40. Gray LH, Conger AD, Ebert M, Hornsey S, Scott OC. The concentration of oxygen dissolved in tissues at the time of irradiation as a factor in radiotherapy. *Br J Radiol* (1953) 26:638–48. doi: 10.1259/0007-1285-26-312-638
41. Overgaard J. Hypoxic modification of radiotherapy in squamous cell carcinoma of the head and neck - A systematic review and meta-analysis. *Radiother Oncol* (2011) 100:22–32. doi: 10.1016/j.radonc.2011.03.004
42. Horsman MR, Overgaard J. The impact of hypoxia and its modification of the outcome of radiotherapy. *J Radiat Res* (2016) 57 Suppl 1:i90–8. doi: 10.1093/jrr/rrw007
43. Bennett MH, Feldmeier J, Smee R, Milross C. Hyperbaric oxygenation for tumour sensitisation to radiotherapy. *Diving Hyperb Med* (2018) 48:116–7. doi: 10.1002/14651858.CD005007.pub4
44. Gill AL, Bell CNA. Hyperbaric oxygen: Its uses, mechanisms of action and outcomes. *QJM - Mon J Assoc Physicians* (2004) 97:385–95. doi: 10.1093/qjmed/hch074
45. Al-Waili NS. Hyperbaric oxygen and malignancies: a potential role in radiotherapy, chemotherapy, tumor surgery and phototherapy. *Med Sci Monit* (2005) 11(9):RA279–89.
46. Beppu T, Kamada K, Nakamura R, Oikawa H, Takeda M, Fukuda T, et al. A phase II study of radiotherapy after hyperbaric oxygenation combined with interferon-beta and nimustine hydrochloride to treat supratentorial malignant gliomas. *J Neurooncol* (2003) 61:161–70. doi: 10.1023/A:1022169107872
47. Ogawa K, Ishiuchi S, Inoue O, Yoshii Y, Saito A, Watanabe T, et al. Phase II trial of radiotherapy after hyperbaric oxygenation with multiagent chemotherapy (procarbazine, nimustine, and vincristine) for high-grade gliomas: Long-term results. *Int J Radiat Oncol Biol Phys* (2012) 82:732–8. doi: 10.1016/j.ijrobp.2010.12.070

48. Kohshi K, Kinoshita Y, Imada H, Kunugita N, Abe H, Terashima H, et al. Effects of radiotherapy after hyperbaric oxygenation on malignant gliomas. *Br J Cancer* (1999) 80:236–41. doi: 10.1038/sj.bjc.6690345
49. Yahara K, Ohguri T, Udono H, Yamamoto J, Tomura K, Onoda T, et al. Radiotherapy using IMRT boosts after hyperbaric oxygen therapy with chemotherapy for glioblastoma. *J Radiat Res* (2017) 58:351–6. doi: 10.1093/jrr/rrw105
50. Vordermark D, Kölbl O, Ruprecht K, Vince GH, Bratengeier K, Flentje M. Hypofractionated stereotactic re-irradiation: Treatment option in recurrent malignant glioma. *BMC Cancer* (2005) 5:1–7. doi: 10.1186/1471-2407-5-55
51. Ernst-Stecken A, Ganslandt O, Lambrecht U, Sauer R, Grabenbauer G. Survival and quality of life after hypofractionated stereotactic radiotherapy for recurrent malignant glioma. *J Neurooncol* (2007) 81:287–94. doi: 10.1007/s11060-006-9231-0
52. Fokas E, Wacker U, Gross MW, Henzel M, Encheva E, Engenhart-Cabillic R. Hypofractionated Stereotactic Reirradiation of Recurrent Glioblastomas. *Strahlentherapie und Onkol* (2009) 185:235–40. doi: 10.1007/s00066-009-1753-x
53. Kim B, Soisson E, Duma C, Chen P, Hafer R, Cox C, et al. Treatment of recurrent high grade gliomas with hypofractionated stereotactic image-guided helical tomotherapy. *Clin Neurol Neurosurg* (2011) 113:509–12. doi: 10.1016/j.clineuro.2011.02.001
54. Minniti G, Scaringi C, De Sanctis V, Lanzetta G, Falco T, Di Stefano D, et al. Hypofractionated stereotactic radiotherapy and continuous low-dose temozolomide in patients with recurrent or progressive malignant gliomas. *J Neurooncol* (2013) 111:187–94. doi: 10.1007/s11060-012-0999-9
55. Shapiro LQ, Beal K, Goenka A, Karimi S, Iwamoto FM, Yamada Y, et al. Patterns of Failure After Concurrent Bevacizumab and Hypofractionated Stereotactic Radiation Therapy for Recurrent High-Grade Glioma. *Int J Radiat Oncol* (2013) 85:636–42. doi: 10.1016/j.ijrobp.2012.05.031
56. Yazici G, Cengiz M, Ozyigit G, Eren G, Yildiz F, Akyol F, et al. Hypofractionated stereotactic reirradiation for recurrent glioblastoma. *J Neurooncol* (2014) 120:117–23. doi: 10.1007/s11060-014-1524-0
57. Minniti G, Agolli L, Falco T, Scaringi C, Lanzetta G, Caporello P, et al. Hypofractionated stereotactic radiotherapy in combination with bevacizumab or fotemustine for patients with progressive malignant gliomas. *J Neurooncol* (2015) 122:559–66. doi: 10.1007/s11060-015-1745-x
58. Navarria P, Ascolese AM, Tomatis S, Reggiori G, Clerici E, et al. Hypofractionated Stereotactic Radiation Therapy in Recurrent High-Grade Glioma: A New Challenge. *Cancer Res Treat* (2016) 48:37–44. doi: 10.4143/crt.2014.259
59. Combs SE, Niyazi M, Adeberg S, Bougatf N, Kaul D, Fleischmann DF, et al. Re-irradiation of recurrent gliomas: pooled analysis and validation of an established prognostic score—report of the Radiation Oncology Group (ROG) of the German Cancer Consortium (DKTK). *Cancer Med* (2018) 7:1742–9. doi: 10.1002/cam4.1425
60. Navarria P, Minniti G, Clerici E, Tomatis S, Pinzi V, Ciammella P, et al. Re-irradiation for recurrent glioma: outcome evaluation, toxicity and prognostic factors assessment. A multicenter study of the Radiation Oncology Italian Association (AIRO). *J Neurooncol* (2019) 142:59–67. doi: 10.1007/s11060-018-03059-x
61. Arpa D, Parisi E, Ghigi G, Savini A, Colangione SP, Tontini L, et al. Re-irradiation of recurrent glioblastoma using helical TomoTherapy with simultaneous integrated boost: preliminary considerations of treatment efficacy. *Sci Rep* (2020) 10:19321. doi: 10.1038/s41598-020-75671-9
62. Chapman CH, Hara JH, Molinaro AM, Clarke JL, Oberheim Bush NA, Taylor JW, et al. Reirradiation of recurrent high-grade glioma and development of prognostic scores for progression and survival. *Neuro Oncol Pract* (2019) 6:364–74. doi: 10.1093/nop/npz017

Conflict of Interest: The authors declare that the research was conducted in the absence of any commercial or financial relationships that could be construed as a potential conflict of interest.

frontiers in Oncology

ORIGINAL RESEARCH
published: 13 May 2021
doi: 10.3389/fonc.2021.659538

Individualized Nomogram for Predicting Survival in Patients with Brain Metastases After Stereotactic Radiosurgery Utilizing Driver Gene Mutations and Volumetric Surrogates

Cheng Zhou[1†], Changguo Shan[1†], Mingyao Lai[1], Zhaoming Zhou[1,2], Junjie Zhen[1], Guanhua Deng[1], Hainan Li[3], Juan Li[1], Chen Ren[4], Jian Wang[4], Ming Lu[5], Liang Zhang[5], Taihua Wu[5], Dan Zhu[5], Feng-Ming (Spring) Kong[6], Longhua Chen[4], Linbo Cai[1] and Lei Wen[1*]*

[1] Department of Oncology, Guangdong Sanjiu Brain Hospital, Guangzhou, China, [2] Department of Radiation Medicine, School of Public Health, Southern Medical University, Guangzhou, China, [3] Department of Pathology, Guangdong Sanjiu Brain Hospital, Guangzhou, China, [4] Department of Radiation Oncology, Nanfang Hospital, Southern Medical University, Guangzhou, China, [5] Department of Neurosurgery, Guangdong Sanjiu Brain Hospital, Guangzhou, China, [6] Department of Clinical Oncology, The University of Hong Kong Shenzhen Hospital, Shenzhen, China

It is well-known that genomic mutational analysis plays a significant role in patients with NSCLC for personalized treatment. Given the increasing use of stereotactic radiosurgery (SRS) for brain metastases (BM), there is an emerging need for more precise assessment of survival outcomes after SRS. Patients with BM and treated by SRS were eligible in this study. The primary endpoint was overall survival (OS). Cox regression models were used to identify independent prognostic factors. A survival predictive nomogram was developed and evaluated by Concordance-index (C-index), area under the curve (AUC), and calibration curve. From January 2016 to December 2019, a total of 356 BM patients were eligible. The median OS was 17.7 months [95% confidence interval (CI) 15.5–19.9] and the actual OS at 1- and 2-years measured 63.2 and 37.6%, respectively. A nomogram for OS was developed by incorporating four independent prognostic factors: Karnofsky Performance Score, cumulative tumor volume, gene mutation status, and serum lactate dehydrogenase. The nomogram was validated in a separate cohort and demonstrated good calibration and good discriminative ability (C-index = 0.780, AUC = 0.784). The prognostic accuracy of the nomogram (0.792) was considerably enhanced when compared with classical prognostic indices, including the Graded Prognostic Assessment (0.708), recursive partitioning analysis (0.587), and the SRS (0.536). Kaplan–Meier curves showed significant differences in OS among the stratified low-, median- and high-risk groups ($P < 0.001$). In conclusion, we developed and validated an

OPEN ACCESS

Edited by:
Jennifer Yu,
Case Western Reserve University, United States

Reviewed by:
Ann-Christin Hau,
Laboratoire National de Santé (LNS), Luxembourg
Yubo Wang,
First Affiliated Hospital of Jilin University, China

***Correspondence:**
Lei Wen
wenlei1998@sina.com
Linbo Cai
cailinbo999@163.com

[†]These authors share first authorship

Specialty section:
This article was submitted to Neuro-Oncology and Neurosurgical Oncology, a section of the journal Frontiers in Oncology

Received: *27 January 2021*
Accepted: *13 April 2021*
Published: *13 May 2021*

Citation:
Zhou C, Shan C, Lai M, Zhou Z, Zhen J, Deng G, Li H, Li J, Ren C, Wang J, Lu M, Zhang L, Wu T, Zhu D, Kong F-M, Chen L, Cai L and Wen L (2021) Individualized Nomogram for Predicting Survival in Patients with Brain Metastases After Stereotactic Radiosurgery Utilizing Driver Gene Mutations and Volumetric Surrogates. Front. Oncol. 11:659538. doi: 10.3389/fonc.2021.659538

individualized prognostic nomogram by integrating physiological, volumetric, clinical chemistry, and molecular biological surrogates. Although this nomogram should be validated by independent external study, it has a potential to facilitate more precise risk-stratifications to guide personalized treatment for BM.

Keywords: brain metastases, stereotactic radiosurgery, nomogram, gene mutation, prediction model

INTRODUCTION

Brain metastases (BM) represent the most common intracranial tumors in adults, which occur up to 10-times more frequently than primary central nervous system tumors. For brain metastases, stereotactic radiosurgery (SRS) offers an excellent minimally invasive ablative treatment option due to its favorable local control efficacy and late onset toxicity (1, 2). Previous reports have indicated that the survival probability for patients after SRS varies with age, Karnofsky Performance Status (KPS), primary cancer site, driver gene mutations, tumor volume, number of metastatic sites, extracranial disease burden, and systemic treatments (3). Nevertheless, the prognosis of BM is rather complex, and the weighted value for a variety of risk factors in the prediction of survival outcomes is largely unknown.

Several well-known prognostic indices are widely utilized for clinical decision-making and outcome research, and include recursive partitioning analysis (RPA), the Score Index for Radiosurgery (SIR), the Basic Score for Brain Metastases (BSBM), and the Graded Prognostic Assessment (GPA) (4–6). These prognostic scoring systems were established by integrating several clinicopathological features such as age, the KPS, the number of metastatic lesions, extracranial metastases, and the control of the primary tumor, and allowed a certain degree of prognostic discrimination. In the era of precision medicine, the identification of driver gene mutations is essential to understand the molecular profiles of tumors and hence provides specific insights for risk assessment as well as tailored treatment (7). Furthermore, volumetric and clinical chemistry parameters might also be associated with prognosis (8, 9). In the light of new knowledge in cancer biology, the incorporation of molecular and physiological tumor characteristics into clinical stratification schemes may further advance the prognostic predictive capacity for brain metastases patients who received SRS.

The nomogram is widely used to predict specific prognosis of cancer patients in the form of numerical probability by quantifying each prognostic factor (10, 11). The present study aimed to identify independent prognostic factors using a large retrospective cohort of patients with brain metastases. Given the important insight from currently available prognostic indices (4–6), we will further develop and validate a multivariable nomogram prediction model by integrating several featured molecular and physiological surrogates. The established prognostic algorithm could thus facilitate personalized surveillance programs and appropriate treatment strategies for this devastating disease following SRS.

METHODS

Patient Population and Data Collection

Between 1 Jan 2016 and 31 December 2019, a total of 594 patients with brain metastases extracted from a prospectively compiled database at our institution were screened. This study was conducted under the Institutional Ethics Committee approved retrospective review, which included a waiver for the requirement of informed consent for participation in the study. Patients were eligible if they: a) had a pathologically proven primary cancer; and b) had undergone SRS for a newly diagnosed BM. The exclusion criteria were: a) tumor combined with leptomeningeal metastases, b) diffuse or countless metastases ineligible for SRS, and c) surgical resection of metastatic lesions before SRS. A total of 356 patients were finally included in the present study. For the nomogram analysis, patients were randomly divided into a training set (n = 230) and a validation set (n = 126) using a random number generator by R software (**Supplementary Figure S1**). Detailed patient characteristics were collected. We evaluated all brain metastatic lesions based on contrast-enhanced MRI. Largest tumor volume was defined as the largest contiguous lesion present on the pre-SRS (T1-weighted postcontrast image). The cumulative tumor volume (CTV) was defined as the sum of tumor volume of all treated BM lesions. For example, a female patient with two metastatic lesions in the brain, the diameter and volume of the two lesions were 4.3 cm and 14.43 cm^3, 1.7 cm and 1.47 cm^3, respectively (**Supplementary Figure S2**). Then diameter of the largest tumor was 4.3 cm, the largest tumor volume was 14.43 cm^3, and CTV was 15.90 cm^3 (14.43 cm^3 plus 1.47 cm^3).

Stereotactic Radiosurgery Treatment

All patients included were treated by single or fractionated SRS (FSRS) *via* the Novalis Tx® system (BrainLAB AG, Feldkirchen, Germany; Varian Medical System, Palo Alto, CA, USA). In brief, patients were treated either by single SRS with the radiation dose of 16–18 Gy, or FSRS in two or three fractions at 8–12 Gy/fraction. For FSRS, fractions were administrated with an interval of 1–3 days. Prophylactic dehydration measures such as mannitol were regularly administrated after SRS unless there were contraindications.

Statistics and Nomogram Development

The endpoint of the present study was overall survival (OS), which was defined as the time from SRS treatment to death from any cause or censored at the date of last follow-up unless otherwise specified. Descriptive statistics for quantitative variables were expressed as means (± standard deviation, SD)

or medians (interquartile range, IQR), and categorical variables were expressed as numbers (percentages). OS was estimated using Kaplan–Meier analysis.

The American Joint Committee on Cancer (AJCC)-proposed checklist was used for guidance in building the prediction model (12). In the training cohort, Cox proportional hazards models were used to identify significant prognostic factors associated with OS. A stepwise variable selection with *P*-values less than 0.15 by univariable analysis was used as the criteria for entry and retention in the multivariable analysis. Hazard ratios (HRs) were presented with their 95% confidence intervals (CIs). Continuous predictors [*i.e.*, tumor size, largest tumor volume (LTV), and CTV] were categorized by optimal cutoffs using the receiver-operating characteristic (ROC) curve method with 1-year OS as the dependent variable and tumor diameter, LTV, and CTV as the independent variables (13). The optimal cutoffs of tumor diameter, LTV, and CTV that maximized sensitivity while minimizing 1-specificity were determined to be 2.0 cm, 2.5 cm^3, and 3.5 cm^3, respectively. The KPS score was calculated as a continuous variable, while age (≥65 *vs* <65) and serum lactate dehydrogenase (LDH) (<200 *vs* 200–300 *vs* >300) as categorical variables in Cox regression analysis. Cox proportional hazards models were utilized to predicting clinical outcomes in the constructed nomogram for 1-year and 2-year OS rates for patients with brain metastases after SRS.

The established nomogram was further analyzed in a validation cohort. Model performance was assessed by the predictive accuracy (discriminating ability) and by the accuracy of point estimates of the survival function (calibration). The value of the Concordance index (C-index) and the area under the curve (AUC) were used to evaluate the discriminative ability of the nomogram (14). A C-index of 0.5 indicates the absence of discrimination, whereas 1.0 indicates perfect separation of patients with different outcomes. Calibration was evaluated using a calibration plot to compare the relationship between the observed outcome frequencies *versus* the predicted outcomes.

For each patient, the total number of points based on the nomogram was calculated and the patients were stratified into three risk groups (high-, medium-, and low-) based on the sum of the points, the 25^{th} and 75^{th} percentiles of the sum of risk scores were used as the cutoff values (15). Kaplan–Meier curves of the three risk group patients were plotted to further assess calibration. The prediction capacity of the established nomogram was also compared with the more well-established GPA, RPA, and SIR models by ROC curves. All analyses were performed using R version 4.0.2 (https://www.rproject.org), SPSS version 26 (IBM, Armonk, NY, USA) and GraphPad Prism 6.0 (San Diego, California, USA). All statistical tests were two sided, and *P*-value <0.05 was considered statistically significant.

RESULTS

Patient Characteristics and Survival

A total of 356 patients who received SRS for 1,481 brain metastases were analyzed. The median follow-up was 12.2 months (range 1.5–34.1 months) for living patients. A summary of the patient demographics and tumor characteristics is shown in **Table 1**. Most patients (268/356, 75.3%) were diagnosed with a primary NSCLC, followed by breast cancer (38/356, 10.7%), digestive system cancer (23/356, 6.5%), and other cancer types (27/356, 7.6%). Among the 268 BM patients with NSCLC, 146 harbored an *EGFR/ALK* mutation and 122 were *EGFR/ALK* wild-type or of unknown gene status. Most patients (72.3%) had multiple BM lesions and the median CTV was 9.5 cm^3 (IQR 2.3–21.5). Single SRS was conducted in 189 patients while FSRS (2–3 fx) in 167 patients. The median biologically effective dose (BED) of radiation was 41.6 Gy (IQR 41.6–50.4) for the α/β value of 10 (16). In the overall cohort, the median OS was 17.7 months (95% CI 15.5–19.9). Actual 1- and 2-year OS rates were 63.2 and 37.6%, respectively.

Univariate and Multivariate Analyses for Overall Survival in the Training Cohort

Univariable and multivariable Cox regression analysis were performed to assess variables associated with the OS in training cohort (**Table 2**). Univariable analysis identified several significant variables for OS: age, KPS score, mutation status, CTV, and serum LDH (**Figure 1**). These five significant variables, together with three marginally significant factors (sex, systematic disease status, and largest tumor volume) were included in the multivariate analysis. According to multivariable analysis, the KPS score (P = 0.049), mutation status (P < 0.001), cumulative tumor volume (P = 0.021), as well as serum LDH (P = 0.001) were independently associated with OS in the training cohort.

Development of a Nomogram for Overall Survival

Based on identified predictive factors from the training cohort, we developed a nomogram to predict the OS of the patients with brain metastases after SRS (**Figure 2**). The nomogram integrated four factors: the KPS score (range 40–90), primary cancer and mutation status (NSCLC mutation or NSCLC wild-type/unknown or non-NSCLC), CTV (<3.5 or ≥3.5 cc) and serum LDH levels (<200 or 200–300 or >300 U/L). Higher total points based on the sum of the assigned number of points for each factor in the nomogram indicated a favorable OS. For example, a patient with a good KPS score (80 points), EGFR-mutant NSCLC, large CTV (5.2 cc) and medium serum LDH levels (270 U/L) would have a total of 205.5 points (80 points for KPS, 100 points for EGFR mutation, 25.5 points for LDH, and 0 points for CTV), for a predicted 1-year and 2-year OS of 63.5 and 50%, respectively.

Nomogram Validation and Evaluation

The established nomogram was validated internally with a separate validation cohort. The C-index of nomogram to predict OS in the training cohort, validation cohort, and overall cohort were 0.792, 0.780, and 0.788, respectively. The AUC of the nomogram for the prediction of 12-month OS was 0.797 for the training cohort (**Figure 3A**), 0.784 for the validation cohort (**Figure 3C**), and 0.792 for the overall cohort.

TABLE 1 | Demographics and clinical characteristics of the study population.

Characteristics	Overall cohort N = 356	Training Cohort (n = 230)	Validation Cohort (n = 126)
Gender, n (%)			
Male	188 (52.8%)	120 (52.2%)	68 (54.0%)
Female	168 (47.2%)	110 (47.8%)	58 (46.0%)
Age (yrs.)			
Median (IQR)	58 (49–65)	58 (49–65)	57 (49–64)
≥65	92 (25.8%)	61 (26.5%)	31 (24.6%)
<65	264 (74.2%)	169 (73.5%)	95 (75.4%)
KPS			
Median (IQR)	80 (70–80)	80 (70–80)	80 (70–90)
≥70	280 (78.7%)	181 (78.7%)	99 (78.6%)
<70	76 (21.3%)	49 (21.3%)	27 (21.4%)
Primary tumor			
NSCLC	268 (75.3%)	170 (73.9%)	98 (77.8%)
Breast cancer	38 (10.7%)	26 (11.3%)	12 (9.5%)
Digestive system cancer	23 (6.5%)	15 (6.5%)	8 (6.3%)
Others	27 (7.6%)	19 (8.3%)	8 (6.3%)
Mutation status			
NSCLC mutant	146 (41.0%)	90 (39.1%)	56 (44.4%)
NSCLC wild type/unknown	122 (34.3%)	79 (34.3%)	43 (34.1%)
N.A. (non-NSCLC)	88 (24.7%)	61 (26.5%)	27 (21.4%)
Systemic disease control			
Controlled	146 (41.0%)	97 (42.2%)	50 (39.7%)
Uncontrolled	210 (59.0%)	134 (58.3%)	76 (60.3%)
Number of BM			
Solitary	97 (27.2%)	65 (28.3%)	32 (25.4%)
Multiple	259 (72.8%)	165 (71.7%)	94 (74.6%)
Distribution of BM			
Supratentorial	166 (46.6%)	108 (47.0%)	58 (46.0%)
Infratentorial	34 (9.6%)	21 (9.1%)	13 (10.3%)
Both	156 (43.8%)	99 (43.0%)	57 (45.2%)
Diameter of largest tumor (cm)			
Median (IQR)	2.7 (1.7–3.9)	2.7 (1.8–3.9)	2.7 (1.7–3.9)
≥2.5	197 (55.3%)	128 (55.7%)	69 (54.8%)
<2.5	159 (44.7%)	102 (44.3%)	57 (45.2%)
Largest tumor volume (cm^3)			
Median (IQR)	6.2 (1.6–15.4)	6.3 (1.7–15.5)	6.1 (1.6–15.3)
≥2.5	241 (67.7%)	156 (67.8%)	85 (67.5%)
<2.5	115 (32.3%)	74 (32.2%)	41 (32.5%)
Cumulative tumor volume (cm^3)			
Median (IQR)	9.5 (2.3–21.5)	9.5 (2.4–21.0)	9.5 (2.3–22.2)
≥3.5	242 (68.0%)	156 (67.8%)	86 (68.3%)
<3.5	114 (32.0%)	74 (32.2%)	40 (31.7%)
SRS/FSRS			
Single SRS	189 (53.1%)	125 (54.3%)	64 (50.8%)
FSRS	167 (46.9%)	105 (45.7%)	62 (49.2%)
BED (Gy)			
Median (IQR)	41.6 (41.6–50.4)	43.2 (41.6–50.4)	41.6 (41.6–50.4)
LDH (U/L)			
Median (IQR)	197 (167–249)	197 (167–247)	201 (167–257)
<200	181 (50.8%)	119 (31.3%)	62 (49.2%)
200–300	122 (34.3%)	77 (22.6%)	45 (35.7%)
>300	53 (14.9%)	34 (9.6%)	19 (15.1%)

KPS, Karnofsky Performance Score; N.A., not applicable; NSCLC, non-small cell lung cancer; BM, brain metastases; IQR, interquartile range; SRS, stereotactic radiosurgery; FSRS, fractionated stereotactic radiosurgery; BED, biologically effective dose; LDH, lactate dehydrogenase.

Furthermore, the calibration plots presented good agreement for the 12-, 18- and 24-month OS in the training and validation cohorts between the nomogram-predicted and actual observed OS rates (**Figures 3B, D**).

The prediction values of this nomogram were compared with more well-established prognostic indices including the GPA, RPA, and SIR models as well as the volumetric variable CTV. In the overall cohort, the AUC of the nomogram (0.792) was higher than that of the GPA (0.708), CTV (0.589), RPA (0.587), and SIR (0.536) models (**Figure 4**). According to nomogram predicted risk scores, patients from the overall cohort were classified into high-risk and low-risk groups. As a result, the

TABLE 2 | Univariate and multivariate analysis for overall survival in BM patients treated by SRS in the training cohort.

Covariate	Univariate analysis		Multivariate analysis	
	HR (95%CI)	***P-value***	**HR (95%CI)**	***P-value***
Gender				
Male	1 [Reference]		1 [Reference]	
Female	0.699 (0.452–1.081)	0.107	0.747 (0.473–1.179)	0.210
Age				
<65	1 [Reference]			
≥65	1.192 (0.732–1.941)	0.480		
KPS	0.975 (0.960–0.991)	0.002	0.981 (0.962–1.000)	0.049
Mutation status				
NSCLC mutant	1 [Reference]		1 [Reference]	
NSCLC wild type/unknown	1.736 (0.993–3.036)	0.053	1.517 (0.813–2.832)	0.078
N.A. (non-NSCLC)	3.058 (1.734–5.393)	<0.001	2.984 (1.627–5.472)	<0.001
Systemic disease status				
Controlled	1 [Reference]		1 [Reference]	
Uncontrolled	1.446 (0.909–2.299)	0.120	1.273 (0.781–2.075)	0.333
Number of BM				
Solitary	1 [Reference]			
Multiple	0.964 (0.586–1.587)	0.887		
Distribution of BM				
Supratentorial	1 [Reference]			
Infratentorial	0.866 (0.401–1.869)	0.714		
Both	0.943 (0.587–1.515)	0.809		
Location of largest tumor				
Supratentorial	1 [Reference]			
Infratentorial	1.108 (0.672–1.828)	0.688		
Diameter of largest tumor (cm)				
<2.5	1 [Reference]		1 [Reference]	
≥2.5	1.650 (0.988–2.755)	0.055	1.714 (0.833–3.530)	0.144
Largest tumor volume (cm^3)				
<2.5	1 [Reference]		1 [Reference]	
≥2.5	1.449 (0.890–2.357)	0.136	1.819 (0.575–5.747)	0.308
Cumulative tumor volume (cm^3)				
<3.5	1 [Reference]		1 [Reference]	
≥3.5	1.758 (1.063–2.907)	0.028	3.369 (1.109–10.232)	0.032
LDH				
<200	1 [Reference]		1 [Reference]	
200–300	2.144 (1.319–3.487)	0.002	1.852 (1.109–3.095)	0.005
>300	3.124 (1.734–5.628)	>0.001	2.640 (1.390–5.011)	0.001
SRS				
Single SRS	1 [Reference]			
FSRS	1.361 (0.883–2.099)	0.163		
BED				
<43.2	1 [Reference]			
≥43.2	0.942 (0.601–1.477)	0.796		

HR, hazard ratio; CI, confidence interval; KPS, Karnofsky Performance Score; N.A., not applicable; NSCLC, non-small cell lung cancer; BM, brain metastases; SRS, stereotactic radiosurgery; FSRS, fractionated stereotactic radiosurgery; BED, biologically effective dose; LDH, lactate dehydrogenase.
Underlined values: the P value of mutation status on OS.

distributions of the death events were predominant in the high-risk group compared to the low-risk group (**Figure 5A**). The Kaplan–Meier survival curve demonstrated a significant difference in OS among low-, median-, and high-risk groups with reference to the total risk score by the 25^{th} and 75^{th} percentiles ($P < 0.001$) (**Figure 5B**).

DISCUSSION

Given the increasingly recognized role of SRS in the treatment of brain metastases, specific scoring criteria integrating a spectrum of volumetric, physiological, clinical chemistry, and molecular biological surrogates for precise assessment of patients following SRS have yet to be established. Notably, the long-term survival of BM patients after SRS was not only associated with features of local BM lesions, but also with the outcome of post-SRS systematic treatment, *i.e.*, molecular characteristics of primary cancer. In the present study, we demonstrated that the cumulative tumor volume, driver gene mutation status, serum LDH, and KPS were significant prognostic factors for brain metastases after SRS. Furthermore, we developed and validated a robust nomogram to predict overall survival in patients with BM treated by SRS. By incorporating these four-independent prognostic clinicopathological parameters, the established nomogram exhibited excellent performance. It was found to have a robust AUC for the prediction of OS and enhanced prediction accuracy compared to classical prognostic indices.

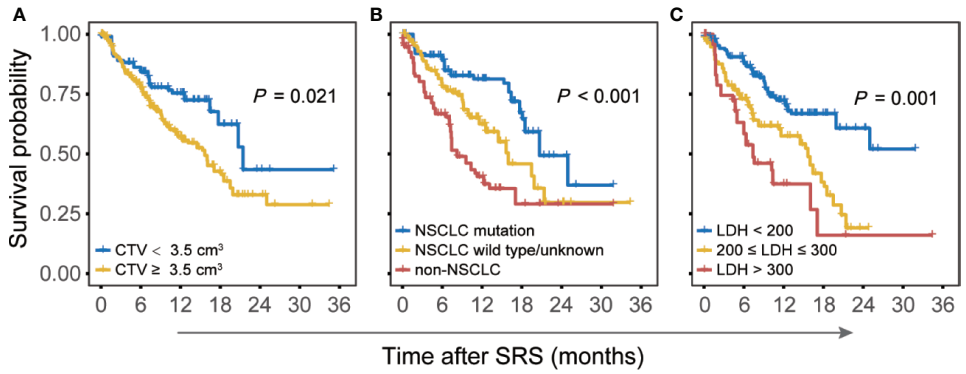

FIGURE 1 | Kaplan–Meier curves for overall survival after stereotactic radiosurgery (SRS) in patients with brain metastases (BM) with reference to **(A)** cumulative tumor volume (CTV), **(B)** primary tumor type (mutation status), and **(C)** serum lactate dehydrogenase (LDH) levels.

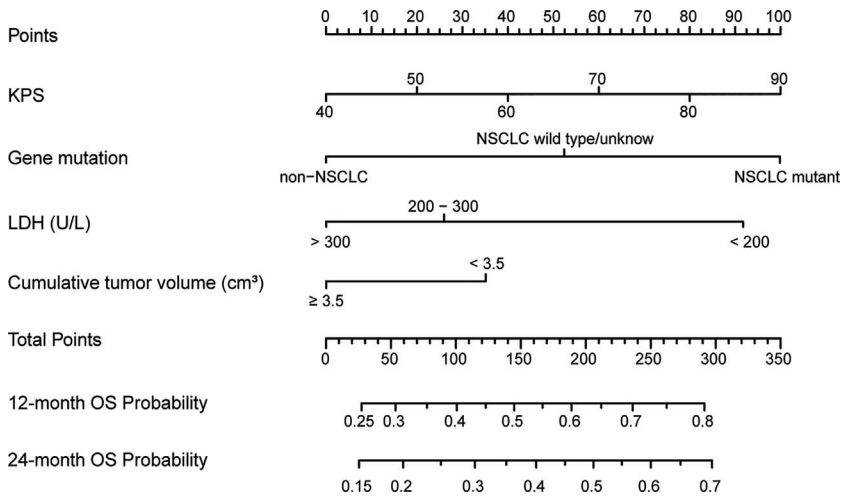

FIGURE 2 | The established nomogram to predict overall survival created based on four independent prognostic factors.

Several well-known prognostic models had been established for BM. Based on analysis from three consecutive Radiation Therapy Oncology Group (RTOG) trials conducted between 1979 and 1993, the RTOG RPA divided patients into three distinct prognostic classes according to four clinical variables: age, KPS, controlled primary tumor, and extracranial metastases (4). Similar to the RPA, the new index, GPA, was developed from five randomized trials in 2008 (17). SIR was also a reliable prognostic score index for patients with BM submitted to SRS (18). A nomogram can calculate individualized estimates of prognosis and have been widely used. Using the nomogram proposed by Tien et al., the probability of survival with first-line paclitaxel and carboplatin with or without bevacizumab in non-squamous NSCLC patients can be estimated (19). Zhang F et al. (20) established an effective nomogram which could be used to identify high-risk patients of brain metastases after resection of primary lung cancer. Diandra NA et al. (21) and Daniel G et al. (22) had developed nomograms to predict distant brain failure and whole brain radiotherapy-free survival for brain metastases after SRS, respectively. To our knowledge, our proposed nomogram is among the first to predict OS for patients with BM following SRS.

Owing to the spatial limitation of the skull, clinical manifestations as well as prognosis is subjective to several volumetric factors such as the number, location, and volume of intracranial metastatic lesions. SIR is a well-established prognostic score specific for brain metastases patients treated by SRS (18). Compared to RPA and GPA, SIR assessment integrated the largest brain lesion volume, which is a critical factor for SRS. Our study comprehensively evaluated the impact of physical characteristics of brain metastases lesions on OS, and included the number of BM metastasis, distribution of metastases, location of the largest tumor, the diameter of the largest tumor, the largest tumor volume and CTV. Although the

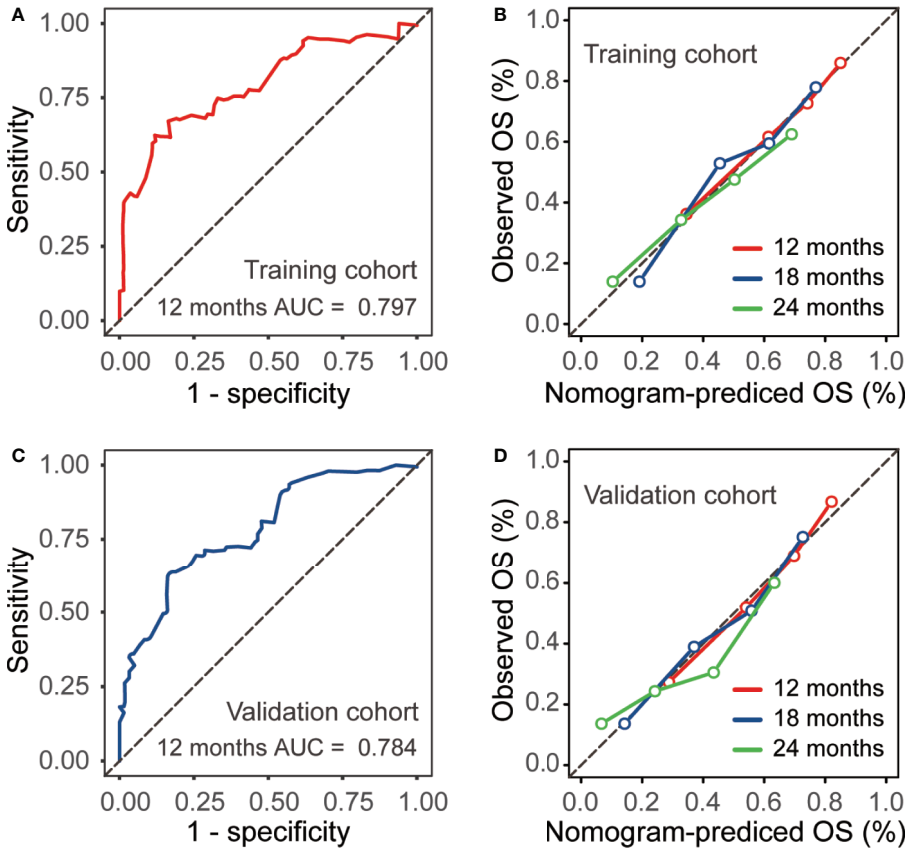

FIGURE 3 | Receiver operating characteristic (ROC) analysis and calibration curves for the training and validation cohort. **(A)** ROC curve for the prediction model in the training cohort. **(B)** Calibration plot comparing nomogram-predicted and observed overall survival in the training cohort. **(C)** ROC for the prediction model in the validation cohort. **(D)** Calibration plot comparing nomogram-predicted and observed overall survival in the validation cohort.

largest tumor volume or number of metastases were widely considered to affect long-term survival of brain metastases after SRS (6, 18), multivariate analysis in the present study revealed CTV played an overwhelming role when using OS as the endpoint. Our results are consistent with the serial studies from Chen et al. (23), whereby cumulative intracranial tumor volume was a superior prognostic factor compared to largest intracranial tumor volume in radiosurgery-treated BM patients. They also found that cumulative intracranial tumor volume could enhance the prognostic value of the lung-specific GPA model based on two independent cohorts (13).

The last decade saw huge progresses in NSCLC treatment by appreciating molecular characterization of the tumor and druggable targets. The therapeutic approaches for NSCLC have therefore changed since the milestone study Iressa Pan-Asia Study (IPASS) was published in 2009 (24). Nevertheless, the classical GPA, RPA, and SIR models were all reported prior to the ready availability of driver genes identification mutational status and development of druggable targets in NSCLC. Recently, several studies have addressed the favorable prognostic role of activating mutation/rearrangement status determination in BM from NSCLC (25, 26). Median OS has almost doubled for *EGFR*/*ALK*+ NSCLC brain metastases patients compared to wild-type patients (26). As a result, Sperduto et al. revised their original disease specific-GPA scale to Lung-molGPA, which improved the prognostic ability over the RTOG RPA and the original disease specific-GPA by incorporating the impact of *EGFR* and *ALK* gene alterations on survival in patients with NSCLC and BM (27). The present study, as well as many others (27–30), have provided clearly supportive data indicating that the mutation status was an independent prognostic factor for patients with BM treated by SRS.

Anomalous energy metabolism represents a common characteristic of cancer (31). LDH, the enzyme responsible for the conversion of pyruvate to lactate during glycolysis, is known as a prognostic marker of cancer (9). Based on prospectively collected serum LDH from 7,895 patients, Wulaningsih et al. (9) demonstrated that high LDH correlated with an increased risk of death from prostate, pulmonary, colorectal, gastro-esophageal, gynecological, and hematological cancers. Our results also indicated a strong inverse association of pre-SRS serum LDH with overall survival. The underlying mechanism of LDH promotes cancer progression might related to its prominent role for basal autophagy and cancer cell proliferation (32). As a

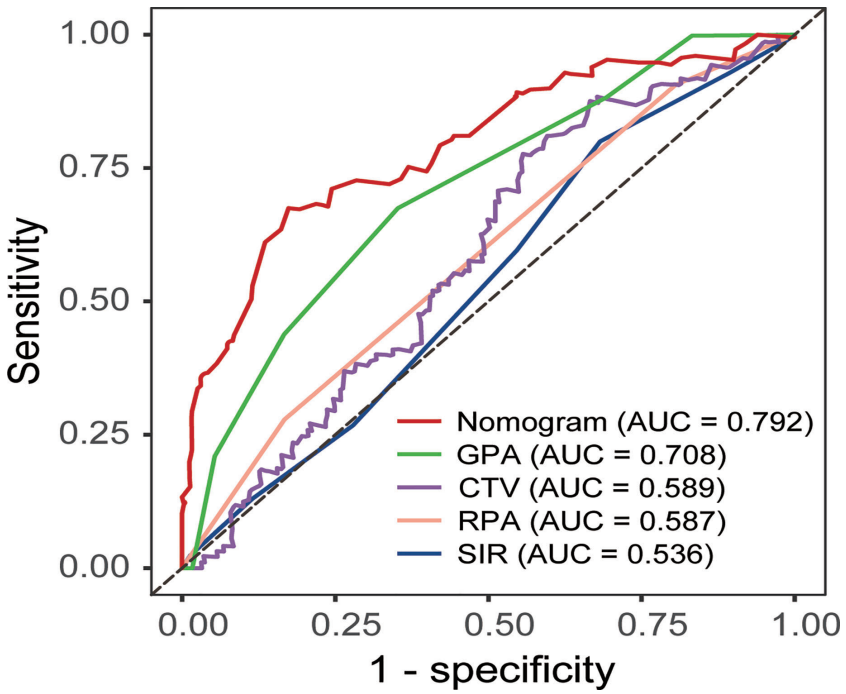

FIGURE 4 | Receiver operating characteristic curve (ROC) comparing the predictive value of the present nomogram, GPA, RPA, SIR models, and cumulative tumor volume (CTV) alone for the prognosis of BM after SRS.

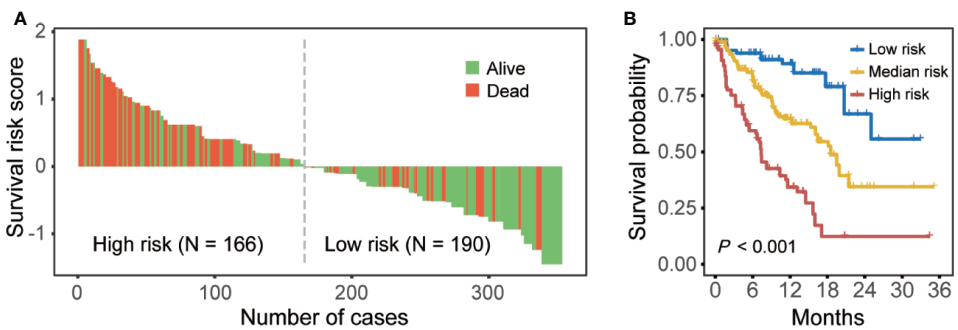

FIGURE 5 | Nomogram-based risk stratifications for BM patients. **(A)** Waterfall plot of risk scores from nomogram prediction. **(B)** Kaplan–Meier curves for overall survival for patients with low-, medium-, and high-risk scores in the overall cohort.

key enzyme involved in cancer metabolism, LDH also allows neoplastic cells to suppress and evade the immune system by altering the tumor microenvironment (33).

Our results did not indicate the presence of a definite correlation between OS and the number of BM or extracranial metastases, which were included in the GPA, RAP, and SIR scores. Regarding the number of metastases, the prospective JLGK 0901 study also suggested that SRS treatment outcomes in patients with five to ten brain metastases were non-inferior to outcomes in patients with two to four brain metastases (1). A case-matched study also found that OS differences between BM numbers of one to four and greater than five was only 0.9 months, which was statistically significant but clinically meaningless (34). We propose that the total volume, rather than the total number of BM is a superior prognostic factor. There was only a slight trend for worse OS for uncontrolled systematic disease ($P = 0.12$) in our cohort. This may be a result of more patients receiving systemic treatments in recent years and the availability of more effective agents, especially for Asian patients who have a higher probability of EGFR mutation (35, 36). Additionally, we did not include patients treated by adjuvant SRS following surgical resection in our cohort because we only

focused on patients who received radical SRS in the present study. The prognostic value of number, diameter, and volume of brain metastases lesions might differ between adjuvant SRS and radical SRS. Thus, this nomogram may not be applicable to BM patients who have received prior surgical resection.

Potential must be appreciated in the present study. First, it was a single institutional retrospective study carrying the caveats of such studies. Although our training cohort-based nomogram was validated internally, an external validation based on multi-institutional data is needed. Secondly, the primary cancer in this cohort included mostly NSCLC patients (268, 73.9%) and a relatively small number of patients with breast cancer (38 patients), digestive system cancer (23 patients), and other cancer types (27 patients). Thus, the applicability of this nomogram for the prognostic evaluation of BM from cancer other than NSCLC should be used with caution.

In conclusion, we developed and validated a robust prognostic nomogram for patients with BM after radical SRS by integrating a panel of independent surrogate markers. In the context of targeted therapy, the established nomogram incorporating molecular biological (driver gene mutations), and radiation biological (total irradiated volume *vs* maximum tumor volume *vs* number of metastatic sites) insights, contributes to a more precise risk assessment and personalized surveillance program. However, the developed nomogram warrants further investigation in external or large-scale multi-center cohorts.

DATA AVAILABILITY STATEMENT

The raw data supporting the conclusions of this article will be made available by the authors, without undue reservation.

ETHICS STATEMENT

The studies involving human participants were reviewed and approved by the Ethics Committee of Guangdong Sanjiu Brain Hospital. Written informed consent for participation was not required for this study in accordance with the national legislation and the institutional requirements.

AUTHOR CONTRIBUTIONS

Conceptualization: CZ, LW, CS, and LC. Methodology: LW, MYL, ZZ, JZ, HL, and JL. Formal analysis and investigation: LW, ZZ, CR, JW, ML, LZ, TW, and DZ. Writing—original draft preparation: LW, CZ, and CS. Writing—review and editing: CZ, GD, F-MK, LHC, and LC. Supervision: LW, CZ, F-MK, LHC, and LC. All authors contributed to the article and approved the submitted version.

FUNDING

This work was supported by the Natural Science Foundation of Guangdong Province (No. 2019A1515011943), China Postdoctoral Science Foundation (No. 2019M662974) and Science and Technology Program of Guangzhou (No. 202002030445, No. 202002030086), and Medical Scientific Research Foundation of Guangdong Province (No. A2020505, No. A2020499, No. B2021203, No. B2021139). The funders had no role in study design, data collection and analysis, decision to publish or preparation of the manuscript.

ACKNOWLEDGMENTS

We thank all members of our study team for their wonderful cooperation.

SUPPLEMENTARY MATERIAL

The Supplementary Material for this article can be found online at: https://www.frontiersin.org/articles/10.3389/fonc.2021.659538/full#supplementary-material

Supplementary Figure 1 | Flow chart of the present study.

Supplementary Figure 2 | An example of volumetric parameters of a female patient with two metastatic lesions in the brain.

Supplementary Figure 3 | Receiver operating characteristic curve (ROC) curve for 1-year survival by cumulative tumor volume with the optimal cutoff point.

REFERENCES

1. Yamamoto M, Serizawa T, Shuto T, Akabane A, Higuchi Y, Kawagishi J, et al. Stereotactic Radiosurgery for Patients With Multiple Brain Metastases (JLGK0901): A Multi-Institutional Prospective Observational Study. *Lancet Oncol* (2014) 15(4):387–95. doi: 10.1016/s1470-2045(14)70061-0
2. Brown PD, Jaeckle K, Ballman KV, Farace E, Cerhan JH, Anderson SK, et al. Effect of Radiosurgery Alone Vs Radiosurgery With Whole Brain Radiation Therapy on Cognitive Function in Patients With 1 to 3 Brain Metastases: A Randomized Clinical Trial. *Jama* (2016) 316(4):401–9. doi: 10.1001/jama.2016.9839
3. Gonda DD, Kim TE, Goetsch SJ, Kawabe T, Watanabe S, Alksne JF, et al. Prognostic Factors for Stereotactic Radiosurgery-Treated Patients With Cerebral Metastasis: Implications on Randomised Control Trial Design and Inter-Institutional Collaboration. *Eur J Cancer (Oxford Engl 1990)* (2014) 50(6):1148–58. doi: 10.1016/j.ejca.2014.01.001
4. Gaspar L, Scott C, Rotman M, Asbell S, Phillips T, Wasserman T, et al. Recursive Partitioning Analysis (RPA) of Prognostic Factors in Three Radiation Therapy Oncology Group (RTOG) Brain Metastases Trials. *Int J Radiat Oncol Biol Phys* (1997) 37(4):745–51. doi: 10.1016/s0360-3016(96)00619-0
5. Lorenzoni J, Devriendt D, Massager N, David P, Ruíz S, Vanderlinden B, et al. Radiosurgery for Treatment of Brain Metastases: Estimation of Patient Eligibility Using Three Stratification Systems. *Int J Radiat Oncol Biol Phys* (2004) 60(1):218–24. doi: 10.1016/j.ijrobp.2004.02.017
6. Yamamoto M, Serizawa T, Sato Y, Kawabe T, Higuchi Y, Nagano O, et al. Validity of Two Recently-Proposed Prognostic Grading Indices for Lung, Gastro-Intestinal, Breast and Renal Cell Cancer Patients With

Radiosurgically-Treated Brain Metastases. *J Neurooncol* (2013) 111(3):327–35. doi: 10.1007/s11060-012-1019-9
7. Lee YT, Tan YJ, Oon CE. Molecular Targeted Therapy: Treating Cancer With Specificity. *Eur J Pharmacol* (2018) 834:188–96. doi: 10.1016/j.ejphar.2018.07.034
8. Donofrio CA, Cavalli A, Gemma M, Riccio L, Donofrio A, Panni P, et al. Cumulative Intracranial Tumour Volume Prognostic Assessment: A New Predicting Score Index for Patients With Brain Metastases Treated by Stereotactic Radiosurgery. *Clin Exp Metastasis* (2020) 37(4):499–508. doi: 10.1007/s10585-020-10037-z
9. Wulaningsih W, Holmberg L, Garmo H, Malmstrom H, Lambe M, Hammar N, et al. Serum Lactate Dehydrogenase and Survival Following Cancer Diagnosis. *Br J Cancer* (2015) 113(9):1389–96. doi: 10.1038/bjc.2015.361
10. Choi SH, Park SW, Seong J. A Nomogram for Predicting Survival of Patients With Locally Advanced Pancreatic Cancer Treated With Chemoradiotherapy. *Radiotherapy Oncol J Eur Soc Ther Radiol Oncol* (2018) 129(2):340–6. doi: 10.1016/j.radonc.2018.08.006
11. Chisholm JC, Marandet J, Rey A, Scopinaro M, de Toledo JS, Merks JH, et al. Prognostic Factors After Relapse in Nonmetastatic Rhabdomyosarcoma: A Nomogram to Better Define Patients Who Can Be Salvaged With Further Therapy. *J Clin Oncol Off J Am Soc Clin Oncol* (2011) 29(10):1319–25. doi: 10.1200/jco.2010.32.1984
12. Kattan MW, Hess KR, Amin MB, Lu Y, Moons KG, Gershenwald JE, et al. American Joint Committee on Cancer Acceptance Criteria for Inclusion of Risk Models for Individualized Prognosis in the Practice of Precision Medicine. *CA: Cancer J Clin* (2016) 66(5):370–4. doi: 10.3322/caac.21339
13. Marcus LP, Marshall D, Hirshman BR, McCutcheon BA, Gonda DD, Koiso T, et al. Cumulative Intracranial Tumor Volume (CITV) Enhances the Prognostic Value of the Lung-Specific Graded Prognostic Assessment (GPA) Model. *Neurosurgery* (2016) 79(2):246–52. doi: 10.1227/neu.0000000000001123
14. Harrell FE,Jr., Lee KL, Mark DB. Multivariable Prognostic Models: Issues in Developing Models, Evaluating Assumptions and Adequacy, and Measuring and Reducing Errors. *Stat Med* (1996) 15(4):361–87. doi: 10.1002/(sici)1097-0258(19960229)15:4<361::aid-sim168>3.0.co;2-4
15. Huang WY, Tsai CL, Que JY, Lo CH, Lin YJ, Dai YH, et al. Development and Validation of a Nomogram for Patients With Nonmetastatic BCLC Stage C Hepatocellular Carcinoma After Stereotactic Body Radiotherapy. *Liver Cancer* (2020) 9(3):326–37. doi: 10.1159/000505693
16. Zhuang QY, Li JL, Lin FF, Lin XJ, Lin H, Wang Y, et al. High Biologically Effective Dose Radiotherapy for Brain Metastases May Improve Survival and Decrease Risk for Local Relapse Among Patients With Small-Cell Lung Cancer: A Propensity-Matching Analysis. *Cancer control J Moffitt Cancer Center* (2020) 27(2):1073274820936287. doi: 10.1177/1073274820936287
17. Sperduto PW, Berkey B, Gaspar LE, Mehta M, Curran W. A New Prognostic Index and Comparison to Three Other Indices for Patients With Brain Metastases: An Analysis of 1,960 Patients in the RTOG Database. *Int J Radiat Oncol Biol Phys* (2008) 70(2):510–4. doi: 10.1016/j.ijrobp.2007.06.074
18. Weltman E, Salvajoli JV, Brandt RA, de Morais Hanriot R, Prisco FE, Cruz JC, et al. Radiosurgery for Brain Metastases: A Score Index for Predicting Prognosis. *Int J Radiat Oncol Biol Phys* (2000) 46(5):1155–61. doi: 10.1016/s0360-3016(99)00549-0
19. Hoang T, Dahlberg SE, Sandler AB, Brahmer JR, Schiller JH, Johnson DH. Prognostic Models to Predict Survival in Non-Small-Cell Lung Cancer Patients Treated With First-Line Paclitaxel and Carboplatin With or Without Bevacizumab. *J Thoracic Oncol Off Publ Int Assoc Study Lung Cancer* (2012) 7(9):1361–8. doi: 10.1097/JTO.0b013e318260e106
20. Zhang F, Zheng W, Ying L, Wu J, Wu S, Ma S, et al. A Nomogram to Predict Brain Metastases of Resected Non-Small Cell Lung Cancer Patients. *Ann Surg Oncol* (2016) 23(9):3033–9. doi: 10.1245/s10434-016-5206-3
21. Ayala-Peacock DN, Attia A, Braunstein SE, Ahluwalia MS, Hepel J, Chung C, et al. Prediction of New Brain Metastases After Radiosurgery: Validation and Analysis of Performance of a Multi-Institutional Nomogram. *J Neurooncol* (2017) 135(2):403–11. doi: 10.1007/s11060-017-2588-4
22. Gorovets D, Ayala-Peacock D, Tybor DJ, Rava P, Ebner D, Cielo D, et al. Multi-Institutional Nomogram Predicting Survival Free From Salvage Whole Brain Radiation After Radiosurgery in Patients With Brain Metastases. *Int J Radiat Oncol Biol Phys* (2017) 97(2):246–53. doi: 10.1016/j.ijrobp.2016.09.043
23. Hirshman BR, Wilson B, Ali MA, Proudfoot JA, Koiso T, Nagano O, et al. Superior Prognostic Value of Cumulative Intracranial Tumor Volume Relative to Largest Intracranial Tumor Volume for Stereotactic Radiosurgery-Treated Brain Metastasis Patients. *Neurosurgery* (2018) 82(4):473–80. doi: 10.1093/neuros/nyx225
24. Mok TS, Wu YL, Thongprasert S, Yang CH, Chu DT, Saijo N, et al. Gefitinib or Carboplatin-Paclitaxel in Pulmonary Adenocarcinoma. *New Engl J Med* (2009) 361(10):947–57. doi: 10.1056/NEJMoa0810699
25. Yuan R, Yamada A, Weber B, Ho C. Radiographic Patterns and Survival of Patients With Early and Late Brain Metastases in EGFR Wild Type and Mutant Non Small Cell Lung Cancer. *J Neurooncol* (2016) 127(3):525–33. doi: 10.1007/s11060-016-2057-5
26. Balasubramanian SK, Sharma M, Venur VA, Schmitt P, Kotecha R, Chao ST, et al. Impact of EGFR Mutation and ALK Rearrangement on the Outcomes of Non-Small Cell Lung Cancer Patients With Brain Metastasis. *Neuro-oncology* (2020) 22(2):267–77. doi: 10.1093/neuonc/noz155
27. Sperduto PW, Yang TJ, Beal K, Pan H, Brown PD, Bangdiwala A, et al. Estimating Survival in Patients With Lung Cancer and Brain Metastases: An Update of the Graded Prognostic Assessment for Lung Cancer Using Molecular Markers (Lung-Molgpa). *JAMA Oncol* (2017) 3(6):827–31. doi: 10.1001/jamaoncol.2016.3834
28. Chen K, Zhang F, Fan Y, Cheng G. Lung-Molgpa Index Predicts Survival Outcomes of Non-Small-Cell Lung Cancer Patients With Synchronous or Metachronous Brain Metastases. *OncoTargets Ther* (2020) 13:8837–44. doi: 10.2147/ott.s255478
29. Sperduto PW, Jiang W, Brown PD, Braunstein S, Sneed P, Wattson DA, et al. Estimating Survival in Melanoma Patients With Brain Metastases: An Update of the Graded Prognostic Assessment for Melanoma Using Molecular Markers (Melanoma-Molgpa). *Int J Radiat Oncol Biol Phys* (2017) 99(4):812–6. doi: 10.1016/j.ijrobp.2017.06.2454
30. Nieder C, Hintz M, Oehlke O, Bilger A, Grosu AL. Validation of the Graded Prognostic Assessment for Lung Cancer With Brain Metastases Using Molecular Markers (Lung-Molgpa). *Radiat Oncol* (2017) 12(1):107. doi: 10.1186/s13014-017-0844-6
31. Hanahan D, Weinberg RA. Hallmarks of Cancer: The Next Generation. *Cell* (2011) 144(5):646–74. doi: 10.1016/j.cell.2011.02.013
32. Brisson L, Bański P, Sboarina M, Dethier C, Danhier P, Fontenille MJ, et al. Lactate Dehydrogenase B Controls Lysosome Activity and Autophagy in Cancer. *Cancer Cell* (2016) 30(3):418–31. doi: 10.1016/j.ccell.2016.08.005
33. Ding J, Karp JE, Emadi A. Elevated Lactate Dehydrogenase (LDH) Can Be a Marker of Immune Suppression in Cancer: Interplay Between Hematologic and Solid Neoplastic Clones and Their Microenvironments. *Cancer Biomarkers section A Dis Markers* (2017) 19(4):353–63. doi: 10.3233/cbm-160336
34. Yamamoto M, Kawabe T, Sato Y, Higuchi Y, Nariai T, Barfod BE, et al. A Case-Matched Study of Stereotactic Radiosurgery for Patients With Multiple Brain Metastases: Comparing Treatment Results for 1-4 Vs ≥ 5 Tumors: Clinical Article. *J Neurosurg* (2013) 118(6):1258–68. doi: 10.3171/2013.3.jns121900
35. Wu YL, Ahn MJ, Garassino MC, Han JY, Katakami N, Kim HR, et al. CNS Efficacy of Osimertinib in Patients With T790M-Positive Advanced Non-Small-Cell Lung Cancer: Data From a Randomized Phase III Trial (AURA3). *J Clin Oncol Off J Am Soc Clin Oncol* (2018) 36(26):2702–9. doi: 10.1200/jco.2018.77.9363
36. Mok TS, Wu YL, Ahn MJ, Garassino MC, Kim HR, Ramalingam SS, et al. Osimertinib or Platinum-Pemetrexed in EGFR T790M-Positive Lung Cancer. *New Engl J Med* (2017) 376(7):629–40. doi: 10.1056/NEJMoa1612674

Conflict of Interest: The authors declare that the research was conducted in the absence of any commercial or financial relationships that could be construed as a potential conflict of interest.

frontiers in Oncology

ORIGINAL RESEARCH
published: 26 May 2021
doi: 10.3389/fonc.2021.657288

Preoperative Prediction of Meningioma Consistency *via* Machine Learning-Based Radiomics

*Yixuan Zhai, Dixiang Song, Fengdong Yang, Yiming Wang, Xin Jia, Shuxin Wei, Wenbin Mao, Yake Xue and Xinting Wei**

Department of Neurosurgery, The First Affiliated Hospital of Zhengzhou University, Zhengzhou, China

OPEN ACCESS

Edited by:
Brad E. Zacharia, Penn State Milton S. Hershey Medical Center, United States

Reviewed by:
Simon Hanft, Westchester Medical Center, United States
Lekhaj Daggubati, Penn State Milton S. Hershey Medical Center, United States
Sangam Kanekar, Penn State Milton S. Hershey Medical Center, United States

***Correspondence:**
Xinting Wei
weixinting777@126.com

Specialty section:
This article was submitted to Neuro-Oncology and Neurosurgical Oncology, a section of the journal Frontiers in Oncology

Received: *22 January 2021*
Accepted: *12 April 2021*
Published: *26 May 2021*

Citation:
Zhai Y, Song D, Yang F, Wang Y, Jia X, Wei S, Mao W, Xue Y and Wei X (2021) Preoperative Prediction of Meningioma Consistency via Machine Learning-Based Radiomics. Front. Oncol. 11:657288. doi: 10.3389/fonc.2021.657288

Objectives: The aim of this study was to establish and validate a radiomics nomogram for predicting meningiomas consistency, which could facilitate individualized operation schemes-making.

Methods: A total of 172 patients was enrolled in the study (train cohort: 120 cases, test cohort: 52 cases). Tumor consistency was classified as soft or firm according to Zada's consistency grading system. Radiomics features were extracted from multiparametric MRI. Variance selection and LASSO regression were used for feature selection. Then, radiomics models were constructed by five classifiers, and the area under curve (AUC) was used to evaluate the performance of each classifiers. A radiomics nomogram was developed using the best classifier. The performance of this nomogram was assessed by AUC, calibration and discrimination.

Results: A total of 3840 radiomics features were extracted from each patient, of which 3719 radiomics features were stable features. 28 features were selected to construct the radiomics nomogram. Logistic regression classifier had the highest prediction efficacy. Radiomics nomogram was constructed using logistic regression in the train cohort. The nomogram showed a good sensitivity and specificity with AUCs of 0.861 and 0.960 in train and test cohorts, respectively. Moreover, the calibration graph of the nomogram showed a favorable calibration in both train and test cohorts.

Conclusions: The presented radiomics nomogram, as a non-invasive prediction tool, could predict meningiomas consistency preoperatively with favorable accuracy, and facilitated the determination of individualized operation schemes.

Keywords: machine learning, consistency, meningioma, nomogram, radiomics

INTRODUCTION

Meningioma is one of the most common intracranial tumors, with an incidence of 7.86 cases per 100,000 people per year (1). It can arise from any area where arachnoid cap cells are present. Current treatment options for meningioma include observation, surgery and radiosurgery (2). Though, radiosurgery may be a good choice for small tumor (<2 cm) (3), surgical resection is

considered the primary treatment for patients with symptomatic meningiomas (4). However, the operative safe requires a thoroughly preoperative understanding of tumor characteristics and surgical anatomy.

The tumor consistency is one of the most important characteristics that affect surgical difficulty and degree of resection (5). Soft tumors can be removed by means of cutting and suctioning. However, firm tumors are more difficult to be removed, especially skull base meningiomas (6). More surgical instruments, such as ultrasonic aspiration, electrophysiological monitoring, and intraoperative navigation are needed. Thus, it is of vital importance to develop a noninvasive preoperative technique to predict tumor consistency. Previously, tumor consistency was predicted according to the signal intensity of T2 weighted images or Fluid attenuated inversion recovery images, but the accuracy was low (7). Radiomics has been considered as a potent approach for noninvasive high-throughput mining of tumor characteristics, which has been applied in many tumors, such as pituitary adenomas, gliomas (8, 9). Nonetheless, few studies have focused on radiomics signatures to predict meningioma consistency. Consequently, the current study aimed to establish a radiomics model for preoperative prediction of meningiomas' consistency.

METHODS

Patients

From January 2019 to May 2020, a total of 172 patients with meningiomas undergoing open craniotomy at the First Affiliated Hospital of Zhengzhou University were included in this study. The inclusion criteria were as follows: 1) meningioma diagnosis was confirmed by pathological report, 2) medical and imaging records were complete, 3) no history of medical treatment for meningioma. Excluding criteria were as follow: 1) incomplete medical records, 2) poor image quality, 3) preoperative treatment such as radiotherapy. The study was approved by the medical ethics committee of the First Affiliated Hospital of Zhengzhou University.

The patients were divided randomly into train cohort (n=120), which was used for model building, and test cohort (n=52), which was used for model validation. The following patients' data were collected: clinical features (gender, age), conventional imaging features (tumor location, edema surrounding meningioma, CSF space surrounding meningioma), and pathology feature (WHO grade). The general characteristics of patients were displayed in **Table 1**. After surgery, the tumor consistency was classified as soft or firm according to Zada's consistency grading system (10). Soft meningiomas were defined as those amenable to be removed totally or mainly with suction, which corresponding to Grade 1 and Grade 2 of Zada's consistency grading system. Firm meningiomas were defined as those required sharp resection, ultrasonic aspiration or with calcified lesions, which corresponding to Grade 3, Grade 4 ad Grade 5 of Zada's consistency grading system. We reviewed the surgical videos and operative recordings to determine the tumor consistency.

TABLE 1 | General characteristics of patients.

	Train cohort (n=120)			Test cohort (n=52)		
	Soft	**Firm**	***P* value**	**Soft**	**Firm**	***P* value**
Age (mean, years)	52.8	52.4	0.86	53.3	55.5	0.62
Gender						
Male	7	18	0.90	2	10	0.75
Female	23	72		6	34	
Location						
Left	10	36	0.66	3	17	0.90
Right	15	44		3	19	
Midline	5	10		2	8	
Peritumoral edema						
No	22	57		5	27	
CSF space surrounding tumor						
Yes	17	51	1.0	5	29	0.83
No	13	39		3	15	
WHO grade						
WHO I	29	80	0.36	7	39	0.61
WHO II	1	10		1	5	

MR Imaging Acquisition and Preprocessing

All patients underwent head MR imaging scan before surgery. Imaging was conducted on three models of MRI scanners, including Prisma, TrioTim and Verio (Siemens Healthineers, Erlangen, Germany). The MR imaging protocol included T1-weighted contrast-enhanced imaging (T1C), T2-weighted imaging (T2WI), Fluid attenuated inversion recovery imaging (FLAIR), Apparent diffusion coefficient imaging (ADC). The T1C sequence was acquired with the following range of parameters: repetition time (TR)/echo time (TE), 163-250/2.46-2.48msec; slice thickness, 5mm; spacing between slices, 6.50-6.75mm. The T2 sequence was acquired with the following range of parameters: TR/TE, 3900-5220/92-150msec; slice thickness, 5mm; spacing between slices, 6.50-6.75mm. The FLAIR sequence was acquired with the following range of parameters: TR/TE, 5000-8000/79-94msec; slice thickness, 5mm; spacing between slices, 6.50-6.75mm. The ADC sequence was acquired with the following range of parameters: TR/TE, 3000-4600/81-102msec; slice thickness, 5mm; spacing between slices, 6.50-6.75mm.

Preprocessing was performed in 3D-Slicer software (v4.9.0). First, image registration was performed to register T2WI, FLAIR, ADC sequence images to the T1C sequence images for each patient. Next, N4 bias field correction was applied to each sequence images to correct intensity non-uniformities.

Tumor Segmentation and Feature Extraction

The region of interest (ROI) was manually drawn on T1C imaging by two neuroradiologists independently, using 3D-Slicer software. The neuroradiologists were blinded to the clinical data. The extraction of radiomic features was performed by using PyRadiomics package, which was an open-

source python package for the extraction of radiomics features from medical imaging. The detail parameter settings of feature extraction were provided in the **Supplementary Document**. To avoid data heterogeneity bias, all MRI data were normalized (the intensity of image was scaled to 0-100) and resampled to the same resolution (3*3*3mm) before feature extraction. For each imaging sequence, three image types (original, Laplacian of Gaussian (LoG), wavelet) were applied, and six feature classes (shape, first order statistics, gray level cooccurrence matrix (glcm), gray level run length matrix (glrlm), gray level size zone matrix (glszm), gray level dependence matrix (gldm)) were calculated, which resulted in a total of 960 radiomic features (14 shape features, 18 first-order statistics features, 68 texture features, 172 LoG features, and 688 wavelet features). For each patient, a total of four imaging sequences were calculated, which generating 3840 radiomic features. Intraclass correlation coefficients (ICCs) analysis was performed on the two sets of ROIs, which were drawn by the two neuroradiologists. We defined the radiomic features with ICCs > 0.8 as stable features, which would be used in further analysis.

Feature Selection and Establishment of Prediction Model

To avoid overfitting, feature selection was performed before model establishment. Features were selected by a two-stage process based on the radiomic features extracted by PyRadiomcs package. First, variances of each feature between soft and firm cases were calculated by t-test (11). Then, the features whose p-values of t-test were less than 0.05 were further analyzed by the least absolute shrinkage and selection operator (LASSO) regression algorithm. 10-fold cross-validation with a maximum area under the curve (AUC) criterion was performed to find the optimal λ. Finally, the features with non-zero coefficients were used to construct the prediction model, and the corresponding non-zero coefficients were defined as the Rad-score. The radiomics signature for each patient was generated using the linear combination of the values of selected features that were weighted by the Rad-score.

We applied five supervised machine-learning algorithms to establish the prediction model, including Random Forest (RF), K-nearest Neighbor (KNN), Support Vector Machine (SVM), Logistic Regression (LR), Adaboost Classifier (Ada), which generated 5 prediction models.

Predictive Performance of Model

The test cohort was applied to evaluate performance of the model. The performance of both train and test cohorts was evaluated using AUC, sensitivity, specificity, and accuracy. The model with the highest AUC in test cohort was established as the final prediction model. The flowchart of this study is shown in **Figure 1**.

Statistical Analysis

Differences in clinical characteristics between train and test cohort were assessed by Student's t-test or chi-square test, as appropriate, and a two-sided p-value < 0.05 was considered

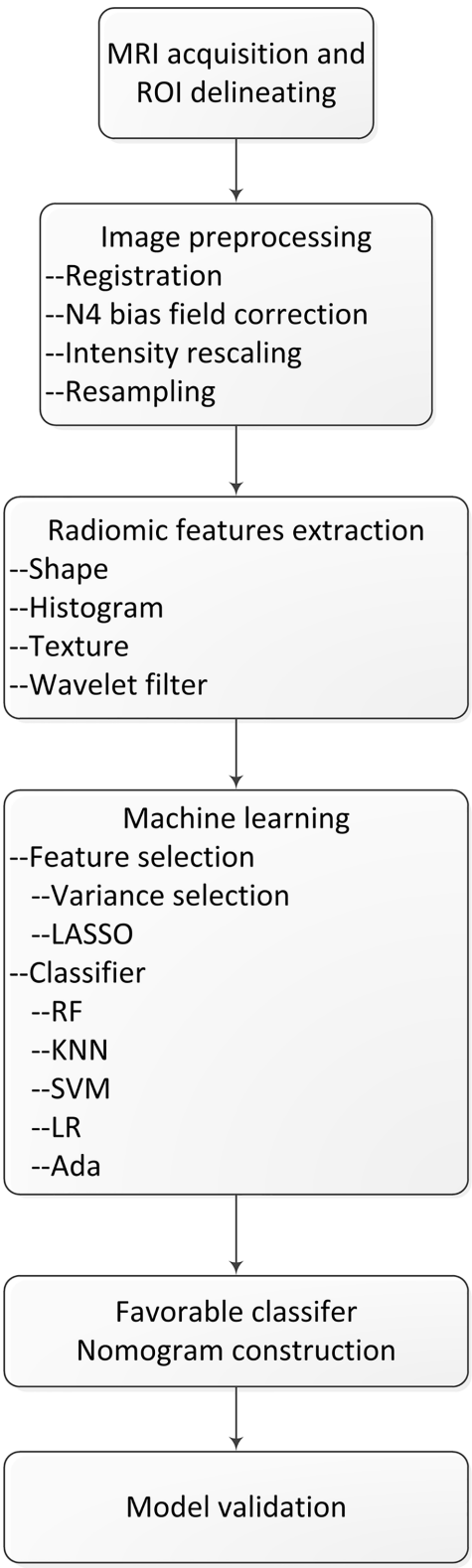

FIGURE 1 | The flowchart of our study.

statistically significant. Statistical analysis was conducted in Python (v3.7.6) and R software (v4.0.0).

RESULTS

Patient Clinical Characteristics

A total of 172 patients were included in the study (120 cases in the train cohort, 52 cases in the test cohort). No significant differences between the soft and firm groups were detected in age, gender, tumor location, peritumoral edema, CSF space surrounding tumor and WHO grade.

Feature Selection and Radiomic Machine-Learning Classifier Selection

In total, 3840 radiomics features were extracted in this study. 3719 radiomics features were stable features after being selected by ICCs. Finally, through variances selection and LASSO regression algorithm, 28 features were selected. The details of the selected features were shown in **Table 2**. The selected radiomics features were statistically different between the two tumor consistencies.

The performances of the five prediction models were shown in **Table 3**. Notably, the LR and Ada models performed well in the validation, with AUCs of 0.83 and 0.82, respectively. The sensitivities of LR and Ada models were 0.91 and 0.89 in the test

TABLE 2 | The details of selected radiomics features.

Class	Feature name	Feature type	Sequence	Soft	Firm	*p*-value
Log filter (sigma=5.0mm)	glszm_GrayLevelNonUniformityNormalized	Texture	CET1	0.3152 ± 1.0513	-0.1098 ± 0.9469	0.0183
LLH wavelet filter	gldm_DependenceVariance	Wavelet	CET1	0.4287 ± 1.4918	-0.1169 ± 0.7826	0.0355
LHL wavelet filter	firstorder_Minimum	Wavelet	CET1	0.3146 ± 0.8763	-0.0993 ± 1.0174	0.0239
LHL wavelet filter	glszm_GrayLevelNonUniformityNormalized	Wavelet	CET1	0.2645 ± 1.0801	-0.1028 ± 0.9171	0.0379
LHH wavelet filter	glcm_MaximumProbability	Wavelet	CET1	0.3129 ± 1.1039	-0.0927 ± 0.9607	0.0277
HLL wavelet filter	firstorder_Entropy	Wavelet	CET1	-0.2845 ± 1.1074	0.0980 ± 0.9413	0.0351
HLL wavelet filter	firstorder_Uniformity	Wavelet	CET1	0.3099 ± 1.1197	-0.1033 ± 0.9389	0.0231
HLL wavelet filter	glszm_LargeAreaLowGrayLevelEmphasis	Wavelet	CET1	0.4034 ± 1.6223	-0.1508 ± 0.5664	0.045
HLH wavelet filter	firstorder_Mean	Wavelet	CET1	-0.3336 ± 1.0352	0.0725 ± 0.9484	0.0237
HHL wavelet filter	glrlm_ShortRunEmphasis	Wavelet	CET1	-0.3436 ± 1.2254	0.0965 ± 0.9164	0.045
HHL wavelet filter	gldm_DependenceVariance	Wavelet	CET1	0.4039 ± 1.5169	-0.1109 ± 0.7745	0.0498
HHH wavelet filter	firstorder_Maximum	Wavelet	CET1	-0.3615 ± 0.6751	0.1149 ± 1.0500	0.0012
Original	glszm_SmallAreaHighGrayLevelEmphasis	Texture	T2WI	0.2909 ± 1.2717	-0.0770 ± 0.9037	0.0459
Log filter (sigma=3.0mm)	firstorder_Mean	Histogram	T2WI	-0.5663 ± 0.9451	0.1659 ± 0.9639	0.0001
LHL wavelet filter	firstorder_Median	Wavelet	T2WI	-0.3615 ± 1.1908	0.0972 ± 0.9249	0.0125
HLL wavelet filter	firstorder_Median	Wavelet	T2WI	-0.3454 ± 1.0061	0.0841 ± 0.9758	0.0185
HLL wavelet filter	firstorder_Skewness	Wavelet	T2WI	0.3982 ± 1.0452	-0.1097 ± 0.9685	0.0056
HLL wavelet filter	glcm_Correlation	Wavelet	T2WI	0.3704 ± 1.0205	-0.1194 ± 0.9641	0.007
LLL wavelet filter	firstorder_10Percentile	Wavelet	T2WI	0.2768 ± 0.8975	-0.0912 ± 1.0122	0.0443
Original	glrlm_LongRunHighGrayLevelEmphasis	Texture	T2flair	0.3360 ± 1.1224	-0.0834 ± 0.9445	0.0218
Original	glszm_HighGrayLevelZoneEmphasis	Texture	T2flair	0.3152 ± 1.2024	-0.0777 ± 0.9196	0.0319
Log filter (sigma=3.0mm)	glcm_ClusterShade	Texture	T2flair	0.3666 ± 1.1785	-0.1018 ± 0.9300	0.0109
LLH wavelet filter	firstorder_Median	Wavelet	T2flair	-0.3452 ± 1.2631	0.1007 ± 0.9009	0.0475
HHH wavelet filter	firstorder_Mean	Wavelet	T2flair	0.2956 ± 0.8445	-0.0713 ± 1.0252	0.045
LHL wavelet filter	firstorder_Skewness	Wavelet	ADC	0.3221 ± 1.0248	-0.0928 ± 0.9849	0.0244
HLL wavelet filter	firstorder_Skewness	Wavelet	ADC	0.3258 ± 1.0802	-0.1050 ± 0.9557	0.0183
HLH wavelet filter	firstorder_Median	Wavelet	ADC	0.2946 ± 0.7405	-0.1275 ± 0.9200	0.0102
HLH wavelet filter	firstorder_Skewness	Wavelet	ADC	-0.2725 ± 1.1742	0.0911 ± 0.9284	0.0467

TABLE 3 | The performances of five prediction models.

Comparisons	Cohorts	RF	KNN	SVM	LR	Ada
AUC	Train	1.0	0.95	1.0	0.89	1.0
	Test	0.56	0.67	0.73	0.83	0.82
Sensitivity	Train	1.0	0.91	1.0	0.87	1.0
	Test	1.0	0.84	0.95	0.91	0.89
Specificity	Train	1.0	0.99	1.0	0.92	1.0
	Test	0.13	0.50	0.50	0.75	0.75
Accuracy	Train	1.0	0.95	1.0	0.89	1.0
	Test	0.87	0.79	0.88	0.88	0.87
F1-score	Train	1.0	0.95	1.0	0.89	1.0
	Test	0.93	0.87	0.93	0.93	0.92

RF, Random Forest; KNN, K-nearest Neighbor; SVM, Support Vector Machine; LR, Logistic Regression; Ada, Adaboost Classifier; AUC, Area Under the Curve.

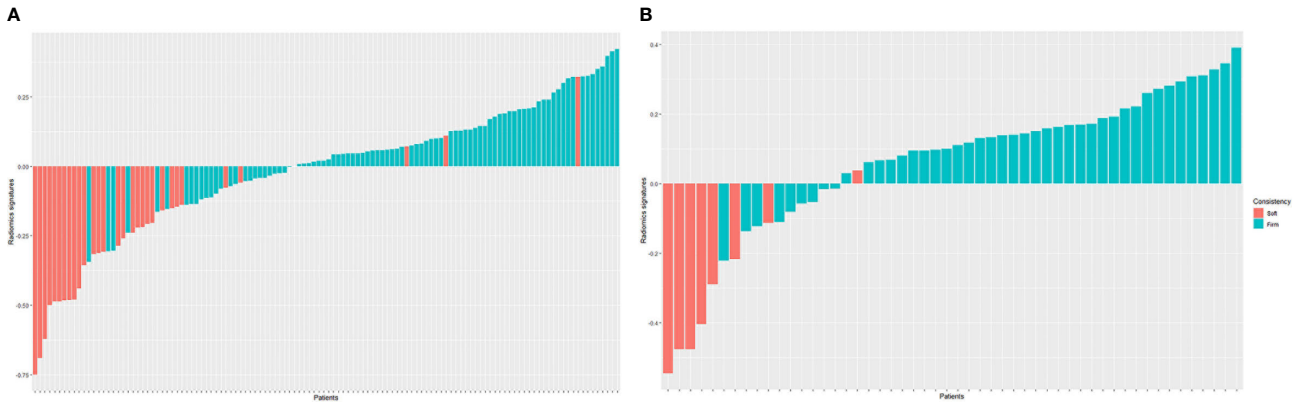

FIGURE 2 | Radiomics signature for each patient in the train cohort **(A)** and test cohort **(B)**. The red bars show the radiomics signature values for the soft meningiomas, and the blue bars show the values for the firm meningiomas.

cohort, respectively, and the accuracies were 0.88 and 0.87 in the test cohort, respectively, the F1-scores were 0.93 and 0.92 in the test cohort, respectively. It revealed that LR model performed best.

Evaluation of Radiomics Signature and Clinical Risk Factors

The radiomics signatures for each patient in train and test cohorts were calculated. The formula of radiomics signatures was presented in **Supplementary Document**. The soft tumors presented lower radiomics signatures than firm tumors (see **Figure 2**). The mean radiomics signature of soft tumor in train cohort was -0.286, which was significantly lower than that of firm tumor (0.075, $p<0.001$). In test cohort, the mean radiomics signatures of soft and firm tumors were -0.311 and 0.122, respectively ($p<0.001$). Radiomics signature and clinical factors were further analyzed using logistic regression to identified the independent predictors of meningioma consistency. The univariate logistic regression showed that only radiomics signature was the significant prediction factor. The logistic regression results were listed in **Table 4**. It showed that only radiomics signature was the independent predictor.

TABLE 4 | The logistic regression results of radiomics signature and clinical risk factors.

	Univariate logistic regression	
	OR (95%CI)	***P* value**
Gender (female vs male)	1.074 (0.712-1.367)	0.851
Age	0.987 (0.960-1.014)	0.343
Peritumoral edema (yes vs no)	0.954 (0.520-1.747)	0.877
Tumor location (right side or middle vs left side)	0.947 (0.599-1.496)	0.816
CSF space surrounding tumor (yes vs no)	1.094 (0.607-1.974)	0.764
Radiomics signature	1407.372 (202.969-13879.683)	<0.001

Radiomics Nomogram Construction and Validation

Based on the logistic regression, a radiomics nomogram was constructed to make it easier to use clinically (see **Figure 3**). According to the radiomics signature, the probability of firm meningioma was obtained. The ROC curve was used to evaluate the sensitivity and specificity of the nomogram (see **Figure 4**). The nomogram showed a good sensitivity and specificity with AUCs of 0.861 and 0.960 in train and test cohorts, respectively. Moreover, the calibration graph of the nomogram showed a favorable calibration in both train and test cohorts (see **Figure 4**). These findings revealed the satisfying ability of the radiomics nomogram to classify meningiomas consistency.

Figure 5 showed the flowchart of prediction. We wrote a python script to facilitate radiomics signature calculation, which was provided in the **Supplementary Document**.

DISCUSSION

Meningiomas are intracranial extra-axial lesion, which are primarily managed by operation. About 40% of meningiomas patients can achieve Simpson I resection, while 35% achieve Simpson II (12). It has been reported that the risk factors of incomplete resection are skull-base location, bone invasion, firm consistency, adhesion to vessels (13). Multiple studies have reported the significance of meningiomas' consistency to determine surgical planning and length of operation time. Especially for meningiomas in skull base area, firm tumor may need more instruments, such as ultrasonic aspirator. Therefore, determination of meningiomas consistency before surgery is important to make the operation plan, avoid the multistage surgical procedure.

There have been several studies that make efforts to predict the consistency of meningiomas. Most of the literatures predict tumor consistency utilizing the conventional MRI techniques. Many studies have reported that hyperintensity on T2WI was associated with soft consistency (14). However, Kashimura et al.

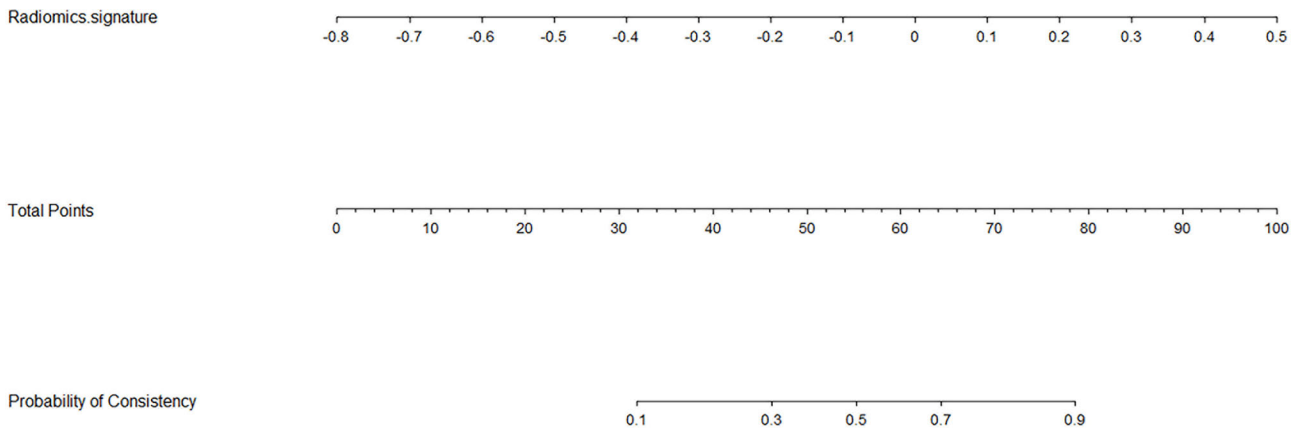

FIGURE 3 | Radiomics nomogram for the meningiomas consistency. As an example, if one patient had the radiomics signature of -0.2, the corresponding total points was about 46, which corresponding to a 30% probability of a firm meningioma. That's to say, using the nomogram, the patient's meningioma consistency was predicted to be soft before surgery.

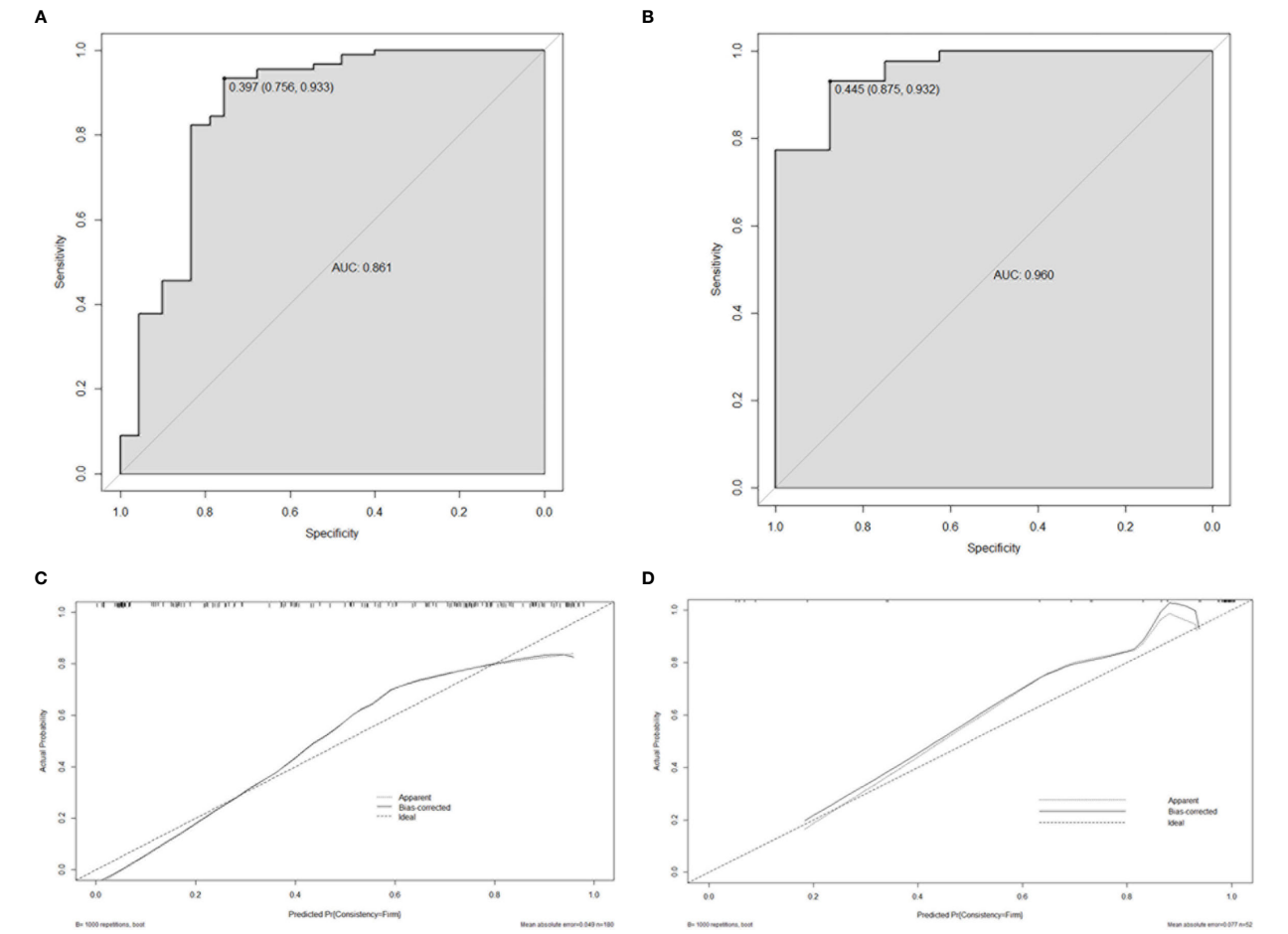

FIGURE 4 | The performance evaluation of the radiomics nomogram. **(A)** the ROC curve in train cohort; **(B)** the ROC curve in test cohort; **(C)** the calibration curve in train cohort; **(D)** the calibration curve in test cohort.

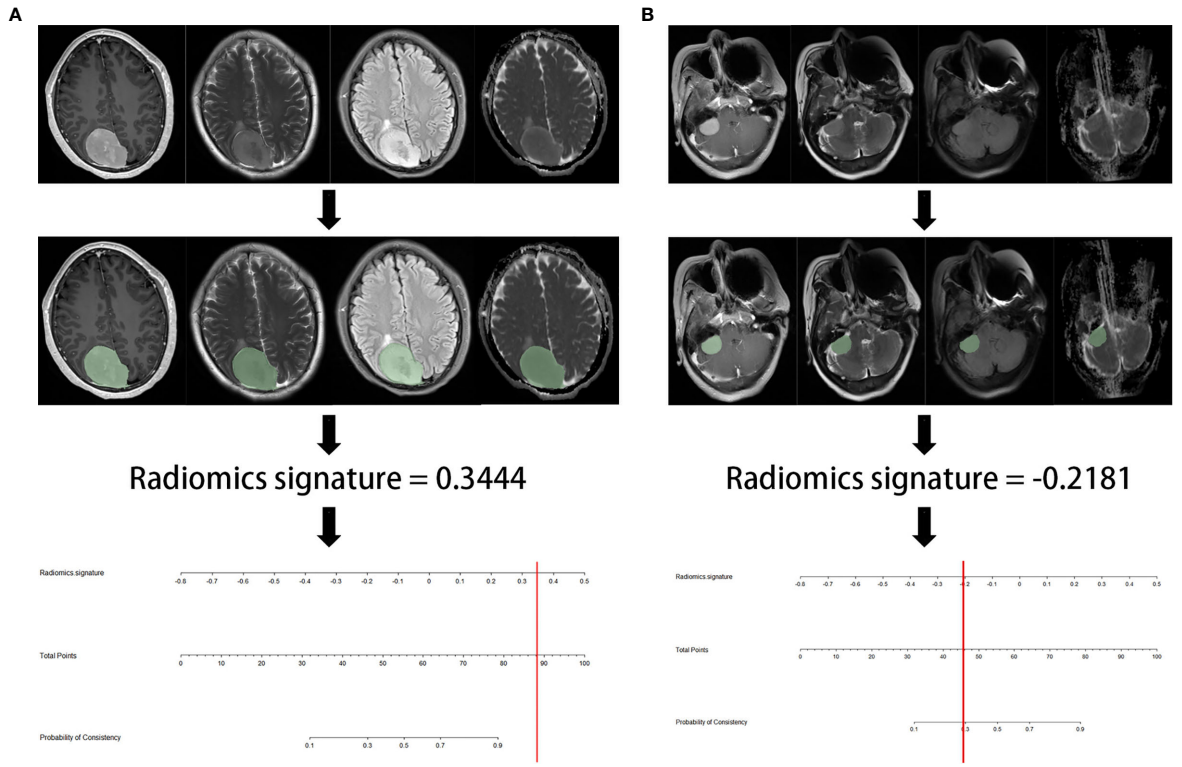

FIGURE 5 | The example flowchart of prediction. **(A)** after ROI delineating, image preprocessing, the value of radiomics signature was 0.3444, which was calculated by the python script including radiomics extraction and model calculation. The result corresponded to >90% probability of a firm consistency. Thus, the meningioma consistency was predicted to be firm, which was confirmed in surgery. **(B)** the radiomics signature was -0.2181, which corresponding to a 30% probability of a firm consistency. Thus, the meningioma consistency was predicted to be soft, which was confirmed in7nbsp;surgery.

reported that there was no association between T2WI intensity and consistency (15). Romani et al. also reported negative results using T1WI, T2WI or FLAIR sequences (16). Both of sensitivity and specificity were low using the conventional MRI prediction method, which providing limited information of consistency before the operation.

Radiomics is a new area of study in which quantitative and high-throughput data are extracted, processed and analyzed to explore their relationships with valuable information. Radiomics technique and machine learning algorithm have been widely used in many tumors' differential diagnosis and consistency prediction before operation (17–20). Yang Zhang et al. developed a radiomics model that could be used in discrimination of lesions located in the anterior skull base (8). In glioblastoma, Xi Zhang reported a radiomics nomogram including 25 selected features, which performing better than clinical risk factors in survival stratification, and the C-index reached up to 0.974 (21).

Only one article that using radiomics features to predict meningiomas consistency was published (22). The author established a model with the Naive Bayes algorithm with an AUC of 0.961. However, the enrolled cases were few, and the model was not validated in the test group, which reduced the reliability. In our study, we have certain advantages. Firstly, a total of 172 patients were enrolled. The large sample size provided reliable results. Secondly, the patients were divided into train and test cohorts. The prediction model was validated in test group for internal validation. The result showed that the AUC in test cohorts was up to 0.960, which meaning that the constructed model can successfully classify soft and firm meningiomas. Thirdly, the model displayed good calibration and discrimination. Fourth, we provided a python script, which could calculate the radiomics signature conveniently. With the help of radiomics nomogram, neurosurgeon can get the consistency prediction result accurately.

This study also had some limitations. First, although we had validated the model in the test cohort, this was not a multicenter study. More prospective datasets are needed for independent verification of the robustness and repeatability of the radiomics nomogram. Second, the patients' MRI imaging were acquired by different scanners, which would increase the data heterogeneity bias. To avoid it, all MRI imaging were subjected to imaging normalization before feature extraction. Finally, although variance selection and LASSO regression methods were highly efficient, they may be less stable when huge number of features

were involved in the model. Other feature selection methods should be investigated in the future work.

In conclusion, our study developed and validated a radiomics nomogram based on the multiparametric MRI imaging. The radiomics nomogram demonstrated a favorable predictive accuracy of meningiomas consistency before surgery, which showing the potential of clinical application.

DATA AVAILABILITY STATEMENT

The raw data supporting the conclusions of this article will be made available by the authors, without undue reservation.

ETHICS STATEMENT

The studies involving human participants were reviewed and approved by Ethics Committee of First Affiliated Hospital of Zhengzhou University. The patients/participants provided their written informed consent to participate in this study.

AUTHOR CONTRIBUTIONS

YZ and XW designed the study. YW, XJ, SW and WM collected clinical and radiomics data. DS, FY and YX pre-processed patients MR imaging and drew the ROI. YZ and DS analyzed the data and developed prediction model. YZ wrote the manuscript. All authors contributed to the article and approved the submitted version.

FUNDING

Joint Construction Project of Medical Science and Technology Planning Project of Henan Province. Grant No.LHGJ20190104.

SUPPLEMENTARY MATERIAL

The Supplementary Material for this article can be found online at: https://www.frontiersin.org/articles/10.3389/fonc.2021.657288/full#supplementary-material

REFERENCES

1. Preusser M, Brastianos PK, Mawrin C. Advances in Meningioma Genetics: Novel Therapeutic Opportunities. *Nat Rev Neurol* (2018) 14:106–15. doi: 10.1038/nrneurol.2017.168
2. Apra C, Peyre M, Kalamarides M. Current Treatment Options for Meningioma. *Expert Rev Neurother* (2018) 18:241–9. doi: 10.1080/14737175.2018.1429920
3. Gupta A, Xu Z, Cohen-Inbar O, Snyder MH, Hobbs LK, Li C, et al. Treatment of Asymptomatic Meningioma With Gamma Knife Radiosurgery: Long-Term Follow-Up With Volumetric Assessment and Clinical Outcome. *Neurosurgery* (2019) 85:E889–99. doi: 10.1093/neuros/nyz126
4. Zeng L, Wang L, Ye F, Chen J, Lei T, Chen J. Clinical Characteristics of Patients With Asymptomatic Intracranial Meningiomas and Results of Their Surgical Management. *Neurosurg Rev* (2015) 38:481–88; discussion 488. doi: 10.1007/s10143-015-0619-1
5. Itamura K, Chang KE, Lucas J, Donoho DA, Giannotta S, Zada G. Prospective Clinical Validation of a Meningioma Consistency Grading Scheme: Association With Surgical Outcomes and Extent of Tumor Resection. *J Neurosurg* (2018) 131(5):1347–682. doi: 10.3171/2018.7.JNS1838
6. Little KM, Friedman AH, Sampson JH, Wanibuchi M, Fukushima T. Surgical Management of Petroclival Meningiomas: Defining Resection Goals Based on Risk of Neurological Morbidity and Tumor Recurrence Rates in 137 Patients. *Neurosurgery* (2005) 56:546–59; discussion 546-559. doi: 10.1227/01.NEU.0000153906.12640.62
7. Karthigeyan M, Dhandapani S, Salunke P, Singh P, Radotra BD, Gupta SK. The Predictive Value of Conventional Magnetic Resonance Imaging Sequences on Operative Findings and Histopathology of Intracranial Meningiomas: A Prospective Study. *Neurol India* (2019) 67:1439–45. doi: 10.4103/0028-3886.273632
8. Zhang Y, Shang L, Chen C, Ma X, Ou X, Wang J, et al. Machine-Learning Classifiers in Discrimination of Lesions Located in the Anterior Skull Base. *Front Oncol* (2020) 10:752. doi: 10.3389/fonc.2020.00752
9. Wang J, Zheng X, Zhang J, Xue H, Wang L, Jing R, et al. An MRI-based Radiomics Signature as a Pretreatment Noninvasive Predictor of Overall Survival and Chemotherapeutic Benefits in Lower-Grade Gliomas. *Eur Radiol* (2021) 31(4):1785–94. doi: 10.1007/s00330-020-07581-3
10. Zada G, Yashar P, Robison A, Winer J, Khalessi A, Mack WJ, et al. A Proposed Grading System for Standardizing Tumor Consistency of Intracranial Meningiomas. *Neurosurg Focus* (2013) 35:E1. doi: 10.3171/2013.8.FOCUS13274
11. Parmar C, Grossmann P, Bussink J, Lambin P, Aerts H. Machine Learning Methods for Quantitative Radiomic Biomarkers. *Sci Rep* (2015) 5:13087. doi: 10.3389/fonc.2015.00272
12. Lemee JM, Corniola MV, Da Broi M, Joswig H, Scheie D, Schaller K, et al. Extent of Resection in Meningioma: Predictive Factors and Clinical Implications. *Sci Rep* (2019) 9:5944. doi: 10.1038/s41598-019-42451-z
13. Shiroishi MS, Cen SY, Tamrazi B, D'Amore F, Lerner A, King KS, et al. Predicting Meningioma Consistency on Preoperative Neuroimaging Studies. *Neurosurg Clin N Am* (2016) 27:145–54. doi: 10.1016/j.nec.2015.11.007
14. Watanabe K, Kakeda S, Yamamoto J, Ide S, Ohnari N, Nishizawa S, et al. Prediction of Hard Meningiomas: Quantitative Evaluation Based on the Magnetic Resonance Signal Intensity. *Acta Radiol* (2016) 57:333–40. doi: 10.1177/0284185115578323
15. Kashimura H, Inoue T, Ogasawara K, Arai H, Otawara Y, Kanbara Y, et al. Prediction of Meningioma Consistency Using Fractional Anisotropy Value Measured by Magnetic Resonance Imaging. *J Neurosurg* (2007) 107:784–7. doi: 10.3171/JNS-07/10/0784
16. Romani R, Tang WJ, Mao Y, Wang DJ, Tang HL, Zhu FP, et al. Diffusion Tensor Magnetic Resonance Imaging for Predicting the Consistency of Intracranial Meningiomas. *Acta Neurochir (Wien)* (2014) 156:1837–45. doi: 10.1007/s00701-014-2149-y
17. Lao J, Chen Y, Li ZC, Li Q, Zhang J, Liu J, et al. A Deep Learning-Based Radiomics Model for Prediction of Survival in Glioblastoma Multiforme. *Sci Rep* (2017) 7:10353. doi: 10.1038/s41598-017-10649-8
18. Han W, Qin L, Bay C, Chen X, Yu KH, Miskin N, et al. Deep Transfer Learning and Radiomics Feature Prediction of Survival of Patients With High-Grade Gliomas. *AJNR Am J Neuroradiol* (2020) 41:40–8. doi: 10.3174/ajnr.A6365
19. Fan Y, Hua M, Mou A, Wu M, Liu X, Bao X, et al. Preoperative Noninvasive Radiomics Approach Predicts Tumor Consistency in Patients With Acromegaly: Development and Multicenter Prospective Validation. *Front Endocrinol (Lausanne)* (2019) 10:403. doi: 10.3389/fendo.2019.00403
20. Li L, Wang K, Ma X, Liu Z, Wang S, Du J, et al. Radiomic Analysis of Multiparametric Magnetic Resonance Imaging for Differentiating Skull Base Chordoma and Chondrosarcoma. *Eur J Radiol* (2019) 118:81–7. doi: 10.1016/j.ejrad.2019.07.006
21. Zhang X, Lu H, Tian Q, Feng N, Yin L, Xu X, et al. A Radiomics Nomogram Based on Multiparametric MRI Might Stratify Glioblastoma Patients According to Survival. *Eur Radiol* (2019) 29:5528–38. doi: 10.1007/s00330-019-06069-z
22. Cepeda S, Arrese I, García-García S, Velasco-Casares M, Escudero-Caro T, Zamora T, et al. Meningioma Consistency can Be Defined by Combining the Radiomic Features of Magnetic Resonance Imaging and Ultrasound

Elastography. A Pilot Study Using Machine Learning Classifiers. *World Neurosurg* (2020) 146:e1147–59. doi: 10.1016/j.wneu.2020.11.113

Conflict of Interest: The authors declare that the research was conducted in the absence of any commercial or financial relationships that could be construed as a potential conflict of interest.

frontiers in Oncology

ORIGINAL RESEARCH
published: 17 November 2021
doi: 10.3389/fonc.2021.772831

Effectiveness and Toxicity of Fractionated Proton Beam Radiotherapy for Cranial Nerve Schwannoma Unsuitable for Stereotactic Radiosurgery

Tanja Eichkorn[1,2]*, *Sebastian Regnery*[1,2], *Thomas Held*[1,2], *Dorothea Kronsteiner*[3], *Juliane Hörner-Rieber*[1,2], *Rami A. El Shafie*[1,2], *Klaus Herfarth*[1,2], *Jürgen Debus*[1,2,4,5,6] *and Laila König*[1,2]

[1] Department of Radiation Oncology, Heidelberg University Hospital, Heidelberg, Germany, [2] National Center for Radiation Oncology (NCRO), Heidelberg Institute for Radiation Oncology (HIRO), Heidelberg, Germany, [3] Institute of Medical Biometry and Informatics, Heidelberg University, Heidelberg, Germany, [4] Clinical Cooperation Unit Radiation Oncology (E050), German Cancer Research Center (dkfz), Heidelberg, Germany, [5] National Center for Tumor diseases (NCT), Heidelberg, Germany, [6] Deutsches Konsortium für Translationale Krebsforschung (DKTK), Partner Site Heidelberg, German Cancer Research Center (dkfz), Heidelberg, Germany

OPEN ACCESS

Edited by:
Alfredo Conti,
University of Bologna, Italy

Reviewed by:
Antonio Pontoriero,
University of Messina, Italy
Scott Soltys,
Stanford University, United States

***Correspondence:**
Tanja Eichkorn
tanja.eichkorn@med.uni-heidelberg.de

Specialty section:
This article was submitted to Neuro-Oncology and Neurosurgical Oncology, a section of the journal Frontiers in Oncology

Received: *08 September 2021*
Accepted: *21 October 2021*
Published: *17 November 2021*

Citation:
Eichkorn T, Regnery S, Held T, Kronsteiner D, Hörner-Rieber J, El Shafie RA, Herfarth K, Debus J and König L (2021) Effectiveness and Toxicity of Fractionated Proton Beam Radiotherapy for Cranial Nerve Schwannoma Unsuitable for Stereotactic Radiosurgery. Front. Oncol. 11:772831. doi: 10.3389/fonc.2021.772831

Purpose: In this benign tumor entity, preservation of cranial nerve function is of special importance. Due to its advantageous physical properties, proton beam radiotherapy (PRT) is a promising approach that spares healthy tissue. Could PRT go along with satisfactory preservation rates for cranial nerve function without compromising tumor control in patients with cranial nerve schwannoma unsuitable for stereotactic radiosurgery?

Methods: We analyzed 45 patients with cranial nerve schwannomas who underwent PRT between 2012 and 2020 at our institution. Response assessment was performed by MRI according to RECIST 1.1, and toxicity was graded following CTCAE 5.0.

Results: The most common schwannoma origin was the vestibulocochlear nerve with 82.2%, followed by the trigeminal nerve with 8.9% and the glossopharyngeal nerve as well as the vagal nerve, both with each 4.4%. At radiotherapy start, 58% of cranial nerve schwannomas were progressive and 95.6% were symptomatic. Patients were treated with a median total dose of 54 Gy RBE in 1.8 Gy RBE per fraction. MRI during the median follow-up period of 42 months (IQR 26–61) revealed stable disease in 93.3% of the patients and partial regression in 6.7%. There was no case of progressive disease. New or worsening cranial nerve dysfunction was found in 20.0% of all patients, but always graded as CTCAE °I-II. In seven cases (16%), radiation-induced contrast enhancements (RICE) were detected after a median time of 14 months (range 2–26 months). RICE were asymptomatic (71%) or transient symptomatic (CTCAE °II; 29%). No CTCAE °III/IV toxicities were observed. Lesions regressed during the follow-up period in three of the seven cases, and no lesion progressed during the follow-up period.

Conclusion: These data demonstrate excellent effectiveness with 100% local control in a median follow-up period of 3.6 years with a promising cranial nerve functional protection rate of 80%. RICE occurred in 16% of the patients after PRT and were not or only mildly symptomatic.

Keywords: acoustic neuroma, vestibular schwannoma, radiation-induced contrast enhancements (RICE), pseudoprogression, radiation necrosis

INTRODUCTION

Schwannomas are usually benign and slowly growing nerve sheet tumors that arise from the Schwann cells lining of peripheral nerves. They are most commonly located in the intradural extramedullary space and therefore affect mainly cranial or spinal nerves (1). Vestibular schwannomas (also known as acoustic neuromas) that commonly arise from the vestibular portion of the eighth cranial nerve account for most schwannomas. The overall incidence is approximately 1 in 100,000 persons per year in Western countries (2). While sporadic schwannomas are rare, they occur frequently in patients with neurofibromatosis. Bilateral vestibular schwannomas in children with neurofibromatosis put them at risk for complete deafness (3–6).

In the past decades, the most effective treatment for progressive cranial nerve schwannomas has been complete surgical resection. While local control rates were excellent, injuries of the affected or adjacent cranial nerves make the treatment of cranial nerve schwannomas a major challenge. A large surgical trial reports in vestibular schwannoma a functional hearing deterioration in up to 60.5% after surgical resection. So, cranial nerve injuries cause a relatively high morbidity compared to the excellent oncologic prognosis (7, 8). Due to the slow progression of schwannomas, the "watch and wait strategy" can be a legitimate treatment option for selected patients (9). Therapy sequelae like hearing impairment and tinnitus, vertigo and gait disturbances, facial nerve palsy, facial pain or hypesthesia, swallowing difficulties, or others also impair the quality of life. Therefore, treatment decision needs to be made carefully, and research on nerve-saving techniques is necessary.

A promising new technique was developed with stereotactic radiosurgery. Even if large prospective data are still lacking, stereotactic radiosurgery (SRS) seems to be superior regarding the risk of cranial nerve damage in schwannomas smaller than 3 cm with excellent local control rates compared to surgical resection and is therefore taken into consideration in the European Association of Neuro-Oncology (EANO) guidelines (9).

But concerns about the induction of malignant transformation of schwannomas or secondary malignancy induction after stereotactic radiosurgery still exist, even if there is no evidence for these concerns in literature, neither for stereotactic radiosurgery nor for particle beam radiotherapy (10–13). Proton beam radiotherapy (PRT) is a promising approach to better spare healthy surrounding tissue and therefore might contribute to the reduction of side effects in patients unsuitable for SRS due to the advanced tumor stage.

The major concern with proton beam radiotherapy is the risk of radiation-induced contrast enhancements (RICE), as known from, e.g., glioma trials (14, 15). RICE are defined by new brain lesions outside the tumor volume related to cerebral irradiation that are usually contrast-enhancing and not caused by the tumor. These RICE are usually transient blood-brain barrier disruptions and rarely real necrosis.

To date, there are only scarce data on PRT for schwannomas. One study investigated efficacy and toxicity rates in 94 patients who underwent fractionated PRT for vestibular schwannoma. These data demonstrated excellent local control rates and a dose-dependent risk for hearing deterioration of 36% to 56% with doses from 50.4 to 54 Gy, while the risk for damage of other cranial nerves was 5% (16). A case series supported the fact that fractionated PRT for vestibular schwannoma is well tolerated and provides good local control (17). A retrospective cohort study investigated proton (!) beam stereotactic radiosurgery and reported a 5-year tumor control rate of 95% and a dose dependency for facial neuropathy (18). No data at all exist on PRT for other schwannomas except for vestibular schwannomas.

This study investigates the effectiveness and toxicity of fractionated proton beam radiotherapy for cranial nerve schwannomas that were unsuitable for SRS. Is excellent tumor control achievable without major sequelae?

PATIENTS AND METHODS

Patient Characteristics

According to its physical properties, in patients with large target volumes (for skull base schwannoma defined by T3-T4 tumors) or tumors in close proximity to the brain stem or other cranial nerves or if patients could not undergo surgery, PRT was chosen, as it is suspected that, in these cases, PRT is more suitable than stereotactic radiosurgery (SRS) and might be more suitable than fractionated photon radiotherapy. Potential physical superiority of protons over photons is well investigated in literature, but potential clinical superiority of fractionated proton radiotherapy over fractionated photon radiotherapy for cranial nerve schwannomas has never been proven. This study shall provide some clinical data on fractionated proton radiotherapy for cranial nerve schwannomas. **Figure 1** demonstrates how decision was made to treat patients with fractionated PRT. We finally included 45 patients with cranial nerve schwannomas who underwent fractionated PRT between 2012 and 2020 at our ion beam therapy center. Patient and treatment data were extracted from a clinical database maintained at our institution and from medical and official records. The first follow-up cMRI was performed 2–3 months after finishing radiotherapy. If no

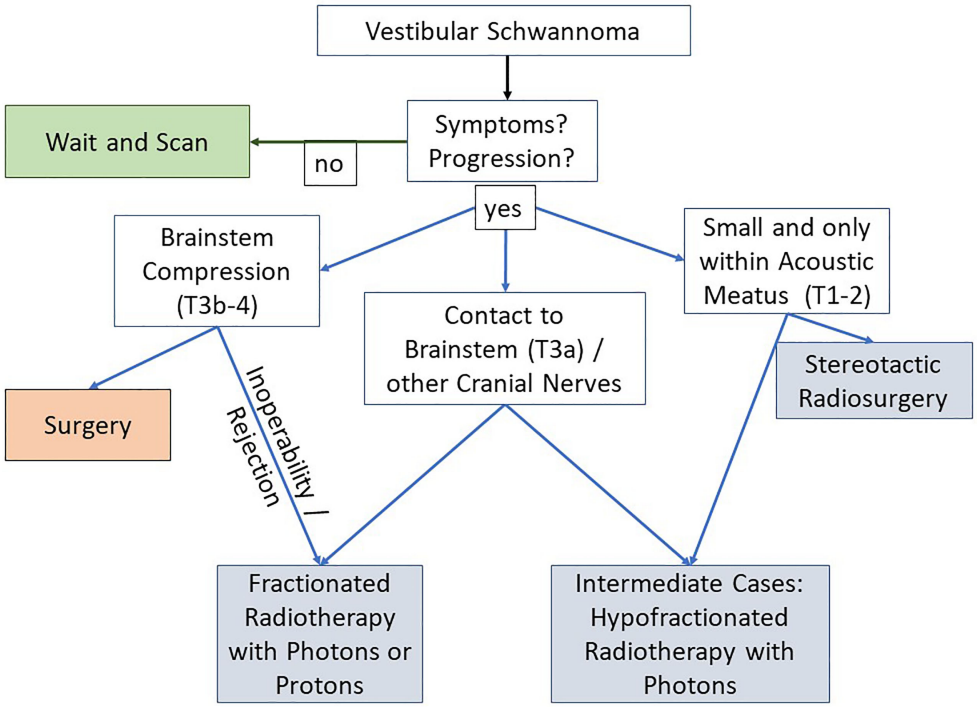

FIGURE 1 | Treatment decision-making in our study cohort exemplarily for vestibular schwannoma. For other cranial nerve neuromas than vestibular schwannoma, similar decision algorithms were used.

abnormalities were found, the following cMRIs were done in time intervals of 6–12 months thereafter. Exploration of RICE risk factors included all available treatment and patient characteristics as listed in the tables.

Planning and Treatment Features

Immobilization was ensured by using individually shaped thermoplastic masks in the head first-supine position. In this positioning, a computed tomography (CT) scan with 3-mm slice thickness as well as a cranial magnetic resonance tomography (cMRI) with contrast were acquired for treatment planning. Gross tumor volume (GTV) comprised the contrast enhanced schwannoma in T1-weightened cMRI. A planning target volume (PTV) margin of 3 mm isotopically was added to account for geometrical uncertainties and physical beam inaccuracies. Treatment planning followed the principle of irradiation dose being as low as reasonably achievable (ALARA) without compromising PTV coverage. Dose prescription to the target volume was performed according to the constraints of ICRU report 50 and 62. Normal tissue constraints according to QUANTEC and Emami et al. (19, 20) were adhered to and sometimes adapted according to the preserved cranial nerve function, e.g., hearing function. Active beam application using raster-scanning technique with a spot size between 8 and 30 mm full width at half maximum (FWHM), with 2–3 mm of overlap in lateral (dx, dy) and longitudinal (dz) directions and synchrotron energy (48–250 MeV), was used, the active change of energy being available in 256 discrete steps, using two to three treatment beams under daily image guidance, orthogonal x-rays mounted on a ceiling robotic arm and with 2D–3D image registration for the robotic couch position correction. Either single-beam optimization (SBO) or multibeam optimization (IMPT) was used. IMPT was aimed for avoiding high-dose gradients per field, e.g., in difficult shaped targets. The final proton dose was scaled with a constant RBE factor of 1.1. Treatment was performed with five to six fractions per week. We took anatomic factors that might lead to dose uncertainties into account and used multiple beams, if needed. Furthermore, in our clinical routine, it is mandatory to regularly perform position verification scans during the treatment period with plan recalculations. So, in case of anatomical changes, e.g., in the petrous bone cavities, we adapted treatment plans. The conformity index (CI) for PTV was calculated according to the RTOG guidelines (21) by division of the CTV covered by the 95% isodose (reference isodose) and the target volume itself. A value close to 1 corresponds to ideal conformity.

Endpoints

Trial endpoints were effectiveness and toxicity of proton beam radiotherapy. Effectiveness was evaluated by "Response Evaluation Criteria in Solid Tumors" (RECIST) version 1.1 and divided into complete or partial response, stable disease, and progressive disease (22, 23). Schwannoma progression was defined as an increase in volume according to RECIST in the

follow-up period without spontaneous regression in the following cranial magnetic resonance imaging (cMRI) to distinguish it from post-treatment edema. Toxicity was graded following the National Cancers Institute's Common Terminology Criteria for Adverse Events (CTCAE) (version 5.0). Cranial nerve functional impairment was assessed by history taking and physical exam. RICE was defined by a new post-treatment contrast enhancement in cMRI outside the GTV during the follow-up period. To face the risk of misinterpretation of RICE as tumor progression or the other way around, all images were reviewed independently by one radiologist and two radiation oncologists. Other toxic effects were assessed based on both medical records and imaging reports.

Statistical Analysis

Descriptive statistics for baseline variables (**Tables 1**, **2**) and for objectives (**Tables 3**–**5**) include means (SD) and/or median (IQR and range, as appropriate) for continuous variables and absolute and relative frequencies for categorical variables. To identify influencing factors on clinical symptom improvement or deterioration in the follow-up period, a logistic regression model was applied using multiple patient and treatment characteristics: age > 55 years, tumor volume ≥ 5ml, technique (IMPT vs. SBO), number of beams, and fractions per week. Since this is a retrospective exploratory data analysis, p-values are of descriptive nature. Statistical analyses are performed with the software R Version 4.0.3.

TABLE 1 | Patient baseline characteristics.

	n = 45 [%]	
Gender		
Female	23	[51.1%]
Male	22	[48.9%]
Age at initial diagnosis (years)		
Mean	51	
Median	51	
Standard deviation	19	
Quartile 1–quartile 3	39–66	
Minimum–maximum	10–82	
Age at radiotherapy (years)		
Median	55	
Minimum–maximum	18–88	
Schwannoma risk factors		
Neurofibromatosis type 2	5	[11.1%]
Cranial nerve		
Trigeminal nerve	4	[8.9%]
Vestibulocochlear nerve	37	[82.2]
Glossopharyngeal nerve	2	[4.4%]
Vagal nerve	2	[4.4%]
Diagnostic methods		
MRI only	28	[62.2%]
DOTATOC-PET-CT	2	[4.4%]
Partial resection/biopsy	14	[31.1%]
Complete resection	3	[6.7%]
Radiotherapy due to recurrence	3	[100%]
Proof of progressive schwannoma before radiotherapy		
Yes	26	[57.8%]
No	19	[42.2%]
Symptomatic schwannoma (at radiotherapy start)		
Yes	43	[95.6%]
No	2	[4.4%]
Tumor size at radiotherapy start (ml)		
Mean	8	
Median	5	
Standard deviation	10	
Quartile 1–quartile 3	3–8	
Minimum–maximum	0.3–60	

RESULTS

Patient and Treatment Characteristics

Median patient age at the beginning of radiotherapy (RT) was 55 years (range: 18–88). Gender was equally distributed. The most common schwannoma origin was the vestibulocochlear nerve with 82.2%, followed by the trigeminal nerve with 8.9% and the

TABLE 2 | Treatment characteristics.

A) Overview	n = 45 [%]	
Primary diagnosis until radiation therapy start (months)		
Median	18	
Minimum–maximum	2–159	
Total dose (Gy RBE)		
Mean	54	
Median	54	
Standard deviation	3	
Quartile 1–quartile 3	54–56	
Minimum–maximum	40–58	
dose per fraction (Gy RBE)		
Mean	1.8	
Median	1.8	
Standard deviation	0.2	
Quartile 1–quartile 3	1.8–1.8	
Minimum - maximum	1.8–2	
Number of fractions		
Mean	29	
Median	30	
Standard deviation	3	
Quartile 1–quartile 3	30–31	
Minimum–maximum	15–32	
Fractions per week		
5 fractions per week	23	[51.1%]
6 fractions per week	22	[48.9%]
Proton beam radiotherapy technique		
IMPT	37	[82.2%]
SBO	8	[17.8%]
Number of beams		
1	2	[4.4%]
2	27	[55.6%]
3	19	[40.0%]
GTV (ml)		
Mean	8	
Median	5	
Standard deviation	10	
Quartile 1–quartile 3	3–8	
Minimum–maximum	0.3–60	
PTV (ml)		
Mean	20	
Median	12	
Standard deviation	22	
Quartile 1–quartile 3	20–23	
Minimum–maximum	4–137	

Dmax, maximum dose; Dmean, mean dose; Gy RBE, gray relative biological effectiveness.

B) Doses for organs at risk (Gy RBE)	Dmax	Dmean
Inner ear		
Mean	49.6	40.4
Median	54	43.8
Quartile 1–quartile 3	51.1–55.4	38–50.3
Minimum–maximum	0–59.4	0–57.3
Adjacent cranial nerves		
Mean	8.6	3.1
Median	2.4	0.4
Quartile 1–quartile 3	0.9–9.3	0.1–1.2
Minimum–maximum	0.3–51.9	0–45.5
Ipsilateral temporal lobe		
Mean	50.3	13.6
Median	53.2	13.6
Quartile 1–quartile 3	50.3–54.8	12.2–16.4
Minimum–maximum	3.7–58.3	0–19.8
Brain stem		
Mean	51.4	12
Median	53.5	10.6
Quartile 1–quartile 3	52–54.6	6.1–14.9
Minimum–maximum	20.3–57.9	0.5–44.9
Ventricular system		
Mean	55.1	6.1
Median	55.1	6.1
Quartile 1–quartile 3	55.1–55.1	6.1–6.1
Minimum–maximum	55.1–55.1	6.1–6.1

Dmax, maximum dose; Dmean, mean dose; Gy RBE, Gray Relative Biological Effectiveness.

TABLE 3 | Treatment effectiveness observation.

	n = 45 [%]	
Time PRT end until first imaging follow-up (weeks)		
Mean	9	
Median	8	
Standard deviation	9	
Quartile 1–quartile 3	6–10	
Minimum–maximum	1–44	
Total follow-up period (months)		
Mean	43	
Median	42	
Standard deviation	25	
Quartile 1–quartile 3	26–61	
Minimum–maximum	3–97	
Response to radiotherapy during follow-up period		
Complete remission	0	[0.0%]
Partial remission	3	[6.7%]
Stable disease	42	[93.3%]
Progressive disease	0	[0.0%]
Progression-free survival		
Yes	45	[100%]
No	0	[0.0%]

glossopharyngeal nerve as well as the vagal nerve, each with 4.4%. A neurofibromatosis type 2 as a risk factor for schwannoma occurrence was found in 11.1% of the patients. Between primary diagnosis and radiotherapy start passed in a median of 18 months (range: 2 months to 12 years). Diagnosis was made mainly by imaging with MRI. In 37.8% of the cases, histology was confirmed by a prior biopsy or resection. In two cases (4.4%), a DOTATOC-PET-CT was needed to exclude meningioma. In 57.8% of the patients, treatment was indicated due to observed progression. About 95.6% of all treated patients complained restrictions in everyday life due to schwannoma symptoms. In median, schwannoma size or gross target volume (GTV) was 5 ml at radiotherapy start ranging from 0.3 to 60 ml. The planning target volume (PTV) was 12 ml in median, ranging from 4 to 137 ml. The median total dose was 54 Gy (range: 40–57.6 Gy) with a median single dose of 1.8 Gy (range 1.8–2 Gy), applied in five to six fractions per week. Two patients were treated with reduced doses due to pre-irradiation in the past. The most commonly used technique was intensity modulated proton therapy (IMPT) with 82.2%, followed by single beam optimization (SBO) with 17.8%. Between one and three beams were used with two beams in 60.0%, three beams in 42.2%, and one beam in 4.4%.

Detailed patient characteristics are presented in **Table 1**; detailed treatment characteristics are presented in **Table 2**.

Efficacy and Toxicity

The follow-up period was 42 months in median (IQR 26–61). In median after 2 months (range: 0.25–11 months), the first follow-up MRI was performed. During the entire follow-up period, 93.3% of the patients showed stable disease, and 6.7% demonstrated partial remission. None of the patients had a schwannoma progression in the observation period. Detailed data on treatment effectiveness observation are presented in **Table 3**.

Before radiotherapy start and during the follow-up period, detailed data on clinical signs and symptoms caused by schwannoma were recorded *via* repeated medical history and physical exam assessment at each follow-up visit. This allows for a longitudinal presentation in the course of time of multiple specific symptoms as presented in **Table 4**. At radiotherapy start, 95.6% reported clinical symptoms due to the schwannoma. With vestibular schwannoma being predominantly observed, most patients complained about hearing impairment (80.0%), followed by vertigo (35.6%) and tinnitus (22.4%). A trigeminal neuralgia was reported by 15.6% of the patients, and 4.4% of the patients suffered from difficulty swallowing. All symptoms were graded analogous to CTCAE grading for better comparability with follow-up findings even if CTCAE grading was not developed to assess pretherapeutic symptoms. After PRT, 60% of the patients had stable symptoms, 4.4% of the patients reported a symptom improvement, and 35.6% of the patients reported any symptom deterioration after PRT, mainly transient fatigue. New or worsening cranial nerve dysfunctions were found in 20.0% of all the patients in the follow-up period, e.g., a worsening in tinnitus, but never relevant for activities of daily life. The reported symptoms described above were mild and graded CTCAE I-II. No CTCAE °III/IV toxicities were observed. Symptoms and toxicities that were not associated to cranial nerves like fatigue, headache, skin toxicity, dysgeusia, and alopecia were mainly observed in the early post-irradiation period and resolved during further follow-up. Explorative analysis *via* logistic regression modeling could not find any substantially influencing factors among all descriptively presented variables on the improvement or deterioration of clinical symptoms.

TABLE 4 | Long-term treatment toxicity assessment.

Clinical symptom	Pre-irradiation				Early post-irradiation				Late post-irradiation				Overall post-irradiation			
	Low grade* (CTCAE I-II)		High grade* (CTCAE ≥III)		Low grade (CTCAE I-II)		High grade (CTCAE ≥III)		Low grade (CTCAE I-II)		High grade (CTCAE ≥III)		Improvement		deterioration	
	n	[%]	n	[%]	n	[%]	n	[%]	n	[%]	n	[%]	n	[%]	n	[%]
Any	43	[95.6%]	0	[0.0%]	45	[100%]	0	[0.0%]	45	[100%]	0	[0.0%]	0	[0.0%]	16	[35.6%]
Cranial nerves																
Olfactory nerve	0	[0.0%]	0	[0.0%]	0	[0.0%]	0	[0.0%]	0	[0.0%]	0	[0.0%]	0	[0.0%]	0	[0.0%]
Optic nerve	0	[0.0%]	0	[0.0%]	0	[0.0%]	0	[0.0%]	0	[0.0%]	0	[0.0%]	0	[0.0%]	0	[0.0%]
Oculomotory nerve	0	[0.0%]	0	[0.0%]	0	[0.0%]	0	[0.0%]	0	[0.0%]	0	[0.0%]	0	[0.0%]	0	[0.0%]
Trochlear nerve	0	[0.0%]	0	[0.0%]	0	[0.0%]	0	[0.0%]	0	[0.0%]	0	[0.0%]	0	[0.0%]	0	[0.0%]
Trigeminal nerve	7	[15.6%]	0	[0.0%]	9	[20.0%]	0	[0.0%]	9	[20.0%]	0	[0.0%]	0	[0.0%]	3	[6.7%]
Abducens nerve	0	[0.0%]	0	[0.0%]	0	[0.0%]	0	[0.0%]	0	[0.0%]	0	[0.0%]	0	[0.0%]	0	[0.0%]
Facial nerve	11	[26.7%]	0	[0.0%]	12	[26.7%]	0	[0.0%]	12	[26.7%]	0	[0.0%]	0	[0.0%]	1	[2.2%]
Vestibulocochlear nerve	37	[82.2%]	0	[0.0%]	37	[82.2%]	0	[0.0%]	37	[82.2%]	0	[0.0%]	2	[4.4%]	5	[11.1%]
Tinnitus	11	[22.4%]	0	[0.0%]	12	[26.7%]	0	[0.0%]	12	[26.7%]	0	[0.0%]	1	[2.2%]	5	[11.1%]
Hearing impairment	36	[80.0%]	0	[0.0%]	36	[80.0%]	0	[0.0%]	36	[80.0%]	0	[0.0%]	0	[0.0%]	0	[0.0%]
Vertigo	16	[35.6%]	0	[0.0%]	16	[35.6%]	0	[0.0%]	16	[35.6%]	0	[0.0%]	2	[4.4%]	3	[6.7%]
Glossopharyngeal nerve	1	[2.2%]	0	[0.0%]	1	[2.2%]	0	[0.0%]	1	[2.2%]	0	[0.0%]	0	[0.0%]	0	[0.0%]
Vagal nerve	1	[2.2%]	0	[0.0%]	1	[2.2%]	0	[0.0%]	1	[2.2%]	0	[0.0%]	0	[0.0%]	0	[0.0%]
Accessory nerve	0	[0.0%]	0	[0.0%]	0	[0.0%]	0	[0.0%]	0	[0.0%]	0	[0.0%]	0	[0.0%]	0	[0.0%]
Hypoglossal nerve	0	[0.0%]	0	[0.0%]	0	[0.0%]	0	[0.0%]	0	[0.0%]	0	[0.0%]	0	[0.0%]	0	[0.0%]
RICE	0	[0.0%]	0	[0.0%]	0	[0.0%]	0	[0.0%]	7	[15.6%]	0	[0.0%]	0	[0.0%]	7	[15.6%]
Others																
Fatigue	0	[0.0%]	0	[0.0%]	11	[24.4%]	0	[0.0%]	3	[6.7%]	0	[0.0%]	0	[0.0%]	11	[24.4%]
Headache	0	[0.0%]	0	[0.0%]	5	[11.1%]	0	[0.0%]	1	[2.2%]	0	[0.0%]	0	[0.0%]	5	[11.1%]
Skin toxicity	0	[0.0%]	0	[0.0%]	1	[2.2%]	0	[0.0%]	0	[0.0%]	0	[0.0%]	0	[0.0%]	1	[2.2%]
Dysgeusia	0	[0.0%]	0	[0.0%]	1	[2.2%]	0	[0.0%]	0	[0.0%]	0	[0.0%]	0	[0.0%]	1	[2.2%]
Alopecia	0	[0.0%]	0	[0.0%]	4	[8.9%]	0	[0.0%]	0	[0.0%]	0	[0.0%]	0	[0.0%]	4	[8.9%]

*Assessment based on medical and physical exam. Early post-irradiation symptoms were assessed in median after 8 (Q1–Q3: 6–10) weeks, and late post-irradiation symptoms were assessed during the total follow-up period (median, Q1–Q3: 42, 26–31 months). RICE, radiation-induced contrast enhancements. *All documented signs and symptoms were graded analogous to CTCAE grading for better comparability. CTCAE, common terminology criteria for adverse events.*

No secondary malignancies were encountered during the follow-up period.

RICE

The follow-up MRIs revealed a contrast enhancement in brain parenchyma after PRT consistent with an RICE in seven cases (15.6%). These lesions were observed after a median of 14 months (range: 2–26 months) after PRT. In two of the seven RICE cases (29%), a deterioration of clinical symptoms was observed; in one case, mild gait disturbances and in the other case a facial paresthesia were reported, which made an outpatinet treatment with a short course of orally administered necessary (both CTCAE °II). Due to sufficient response to corticosteroid treatment, in no case bevacizumab administration as an anti-VEGF antibody was needed. Three of the seven lesions (43%) regressed during the follow-up period, and no lesion showed progression. Further analysis of RICE cases did not reveal considerable differences in the subgroup, in which RICE occurred, compared to the subgroup, in which no RICE was diagnosed. Patients with RICE had been treated with standard therapy of 54–57.6 Gy in 1.8–2.0 Gy RBE per fraction with five to six fractions per week. GTV volume was 2–7 ml. Only one patient underwent previous surgery; none of the patients had neurofibromatosis type 2. CI for PTV was in the median of 0.99 (range 0.98–1.0). Due to lack of power, explorative analysis *via* logistic regression modeling could not find any influencing factors on the development of RICE by comparing the 7 RICE cases to the 38 cases without RICE among the tested variables: age > 55 years, tumor volume ≥5 ml, technique (IMPT vs. SBO), number of beams, and fractions per week. **Table 5** presents a detailed workup of RICE. **Table 5A** demonstrates an overview analysis on all RICE cases, whereas **Table 5B** shows a detailed descriptive analysis of each specific RICE case. **Table 5C** shows the logistic regression model for RICE risk factors. **Figure 1** shows representative images for all seven cases.

DISCUSSION

This study investigates the effectiveness and toxicity of fractionated proton beam radiotherapy for cranial nerve schwannomas.

As expected, most cranial nerve schwannomas affected the vestibulocochlear nerve, and therefore, most patients presenting to our clinic suffered from hearing impairment, tinnitus, or vertigo. Nevertheless, cranial nerve schwannomas originating from the trigeminal nerve, the glossopharyngeal nerve, and the vagal nerve were also found, mainly associated to neurofibromatosis type 2 as supported by literature data (24). Most patients sought for treatment due to clinical symptoms or a documented schwannoma progression under monitoring.

Proton beam radiotherapy for cranial nerve schwannoma was shown to be effective. No schwannoma progression was

observed, and therefore, 100% effectivity can be reported for the follow-up period of 3.5 years in median. These effectivity rates for proton beam radiotherapy are very promising. However, further prolongation of the follow-up period is needed. The only data available on PRT in vestibular schwannoma include 95 patients treated from March 1991 to March 2008 at Loma Linda University Medical Center. Fractionated proton radiotherapy at daily doses of 1.8 Gy and a total dose ranging between 59.6 Gy (RBE) and 50.4 Gy (RBE) was employed, depending on hearing function. Local control rates for the median follow-up time of 64 months were 95–92%, depending on the applied dose. Cranial nerve injuries occurred in two patients. Hearing preservation was maintained in 44–64% of the patients, depending on the applied dose. The overall patient cohort was divided into three groups with graduated dose concepts (16).

For gamma knife, a control rate of 98% after a median follow-up period of 5.8 years was reported (25). For the "watch-and-wait" strategy, a meta-analysis demonstrated in median 43% of schwannoma progressions in a similar follow-up period of 3.2 years (26). For surgery, a median of 9% schwannoma progression was demonstrated in a follow-up of 3.1 years (27) with a considerable rate of surgery-associated cranial nerve damage with chances of hearing preservation between 47% and 88% and even death due to surgery-associated complications (28). Therefore, as stated by the EANO Guideline on the Diagnosis and Treatment of Vestibular Schwannoma, radiotherapy is superior to both the "watch-and-wait" strategy regarding efficacy as well as surgery especially regarding toxicity in small tumors (<3 cm) (9). But both the "watch-and-wait" strategy and surgery are valuable for selected patients. Patients without any symptoms or progression may be suitable for the "watch-and-

TABLE 5 | Detailed analysis of RICE (n=7 [15.6%]).

A) Overall RICE analysis

	n = 7 [16%]	
Time radiotherapy end to first occurrence of RICE (months)		
Mean	14	
Median	14	
Quartile 1–quartile 3	12–16	
Minimum–maximum	2–26	
Symptomatic RICE		
Yes	2 (CTCAE °II)	[28.6%]
No	5	[71.4%]
Treatment needed for RICE		
Steroids only	7	[100%]
Bevacizumab (anti-VEGF antibody)	0	[0%]
Observed regression during follow-up period		
Yes	3	[42.9%]
No	4	[57.1%]
Observed progression during follow-up period		
Yes	0	[0%]
No	7	[100%]

RICE, radiation-induced contrast enhancements.

B) Analysis of specific RICE cases

Case number	1	2	3	4	5	6	7
Gender	Female	Male	Female	Male	Female	Female	Female
Age at radiotherapy (years)	63.9	82.4	67.7	62.8	79.3	77.8	44.3
Latency (months)	17	14.9	2.3	13.8	25.7	10.3	13.3
Treatment	Steroids	Steroids	Steroids	Steroids	Steroids	Steroids	Steroids
Inpatient treatment needed	No	No	No	No	No	No	No
Cranial nerve	Vestibulocochlear nerve	Vestibulocochlear nerve	Vestibulocochlear nerve	Vestibulocochlear nerve	Vestibulocochlear nerve	Vestibulocochlear nerve	Vestibulocochlear nerve
Previous surgery	No	No	No	No	No	No	Yes
Neurofibromatosis type II	No	No	No	No	No	No	No
Any pre-irradiation symptoms	Yes	Yes	Yes	Yes	Yes	Yes	Yes
Pre-irradiation tinnitus	No	No	No	No	No	Yes	Yes
Pre-irradiation hearing impairment	Yes	Yes	Yes	Yes	Yes	Yes	Yes
Pre-irradiation vertigo	No	Yes	No	No	No	Yes	Yes
Any post-irradiation deterioration	No	Yes	No	No	No	Yes	No
Total dose (Gy RBE)	54.0	54.0	54.0	57.6	57.6	54.0	57.6
Dose per fraction (Gy RBE)	1.8	1.8	2.0	1.8	1.8	1.8	1.8
Fractions per week	5	5	6	5	6	6	5
Radiotherapy technique	IMPT	SBO	IMPT	IMPT	IMPT	IMPT	IMPT
Schwannoma size/GTV (ml)	5	5	7	4	5	4	2
Schwannoma maximal diameter (mm)	22	25	26	22	21	24	26
PTV (ml)	10	12	20	9	12	9	5
Maximum dose GTV (Gy RBE)	55.5	55.5	56.1	60.8	56.4	55.9	59.3
Maximum dose brain stem (Gy RBE)	53.2	53.3	54.3	54.7	52.8	52.9	55.5
Number of beams	3	2	2	3	3	3	3
Any pre-irradiation in the past	No	No	No	No	No	No	No

RICE, radiation-induced contrast enhancements.

C) Logistic regression analysis for RICE risk factors

Variable	Estimate (95% CI)	p-value
Age >55 years	-2.41 (5.77 - -0.42)	0.68
Tumor volume ≥5ml	-1.84 (1.24 - 1.48)	0.14
Technique (IMPT vs. SBO)	-0.61 (1.50 - -0.40)	0.69
Number of beams	1.77 (1.17 - 1.51)	0.13
Fractions per week	-0.72 (1.01 - -0.72)	0.47

CI, confidence interval IMPT, intensity-modulated proton therapy; SBO, single beam optimization; RICE, radiation-induced contrast enhancements.

wait" strategy, while very large tumors that have already completely destroyed the nerve and compress the brainstem may be suitable for surgery. For radiotherapy, there are several factors, e.g., dose, fractionation regimes, and treatment techniques, that have to be taken into consideration when deciding about the individually best approach. According to a retrospective comparative analysis of 125 patients in total, hearing preservation rates might be 2.5-fold higher in fractionated radiotherapy than in single fraction stereotactic radiosurgery, but tumor control rates were at least 97% in both groups (29). However, literature demonstrates also data that report similar rates for hearing preservation and local control for both fractionated radiotherapy and single fraction stereotactic radiosurgery, and the dose of single fraction stereotactic radiosurgery was significantly influencing hearing preservation (30). Furthermore, according to literature, it is recommended to use single fraction stereotactic radiosurgery for smaller lesions, while FSRT can be used independently of tumor size and should be preferred in larger tumors (with contact to the brainstem) due to the better adherence to dose constraints with FSRT (30–33). For PRT, fractionated radiotherapy might be less toxic than single fraction stereotactic radiosurgery (16, 18). We cannot directly compare our results to stereotactic radiosurgery as our cohort was defined by unsuitability for stereotactic radiosurgery (T3-T4 tumors). Valid treatment alternatives for our cohort were surgery or fractionated photon radiotherapy. Cranial nerve preservation of the affected cranial nerve in fractionated proton/photon radiotherapy is well known to be superior to surgery. Compared to fractionated photon radiotherapy, fractionated proton radiotherapy spares the adjacent cranial nerves due to steep dose gradients given in proton radiotherapy. This is a dosimetric advantage, and literature is lacking data whether this results in clinically detectable advantages. Since cranial nerve neuromas are mainly located at the skull base often in close proximity to the brain stem or the facial nerve (for acoustic neuroma/vestibular schwannoma), sparing of adjacent structures is critical.

Interestingly, a retrospective analysis found lower tumor control rates in patients with neurofibromatosis type 2 compared to sporadic tumors (29). This was not confirmed by our study using fractionated PRT.

When patients present for radiotherapy, they are usually suffering from schwannoma-associated symptoms that are mainly hearing impairments in vestibular schwannoma. None of our patients reported a new or worsening hearing impairment after PRT despite relevant dose deposition on the inner ear (D_{mean} in median = 43.8 Gy). Nevertheless, data on hearing function are based on medical history and physical exam so a very mild hearing deterioration might be underestimated in this analysis, since audiometry was not performed on a regular basis but only if symptoms were reported. Nevertheless, the used method is appropriate to detect a hearing deterioration that is in any way relevant to the patients' daily life. One-fifth of the patients reported any new or worsening mild clinical symptoms associated to the affected cranial nerve in the follow-up period with a worsening tinnitus being the most common observation. Symptoms like tinnitus or vertigo might represent an irritation of the irradiated cranial nerve. Even if some patients (4.4%) reported an improvement of clinical symptoms, this analysis demonstrates that PRT can irritate or slightly impair the function of the affected cranial nerve leading to a mild deterioration of symptoms even if no loss of cranial nerve function was observed.

To sum up the scarce available data, fractionated proton beam radiotherapy for tumors unsuitable for stereotactic radiosurgery is a promising approach that should be further investigated. For detailed assessment of hearing function using repetitive audiometry, a prospective clinical trial is urgently needed. Such a trial is currently conducted at Boston using fractionated proton radiation therapy for vestibular schwannomas and will close recruitment in a couple of months, so results will be pending for multiple years (ClinicalTrials.gov Identifier: NCT01199978).

A special feature of this study is that RICE has been defined as an endpoint, and it was specifically evaluated for its occurrence, clinical presentation, treatment, and time course. Despite all advantageous properties of proton beam radiotherapy presented above, the rate of 16% for RICE needs to be further focused on. Due to close proximity of the irradiated cranial nerve schwannomas to the brain stem, RICE occurred in the vulnerable healthy brain stem tissue (**Figure 2**). This unfavorable localization was also the reason why RICE treatment was administered liberally, so all of our RICE cases received a short course of corticosteroids. In two (of seven) patients, RICE were mild symptomatic, but corticosteroids relieved symptoms quickly, so none of the patients needed a bevacizumab therapy. Anti-VEGF antibodies like bevacizumab go along with excellent remission rates for RICE and are therefore the treatment of choice in more severe cases of RICE (34, 35). We showed that these lesions occurred after a median of 14 months. In 43%, the lesions regressed during the follow-up period. Due to this observed time course, we recommend a close timeline of follow-up including MRI within the first 2 years. For these 43% of cases, RICE is probably representing a radiation-induced blood-brain barrier disruption and probably not an irreversible radiation necrosis due to its transient nature, as supported by literature (36).

While the applied dose is standard (16), nearly half of our patients received up to six fractions per week, which is due to historical reasons and can therefore be regarded as slight acceleration. We decided at our institution not to proceed the irradiation with six fractions per week for central nervous system tumors as a safety measure. Nevertheless, this was not an influencing factor in the performed exploratory analysis

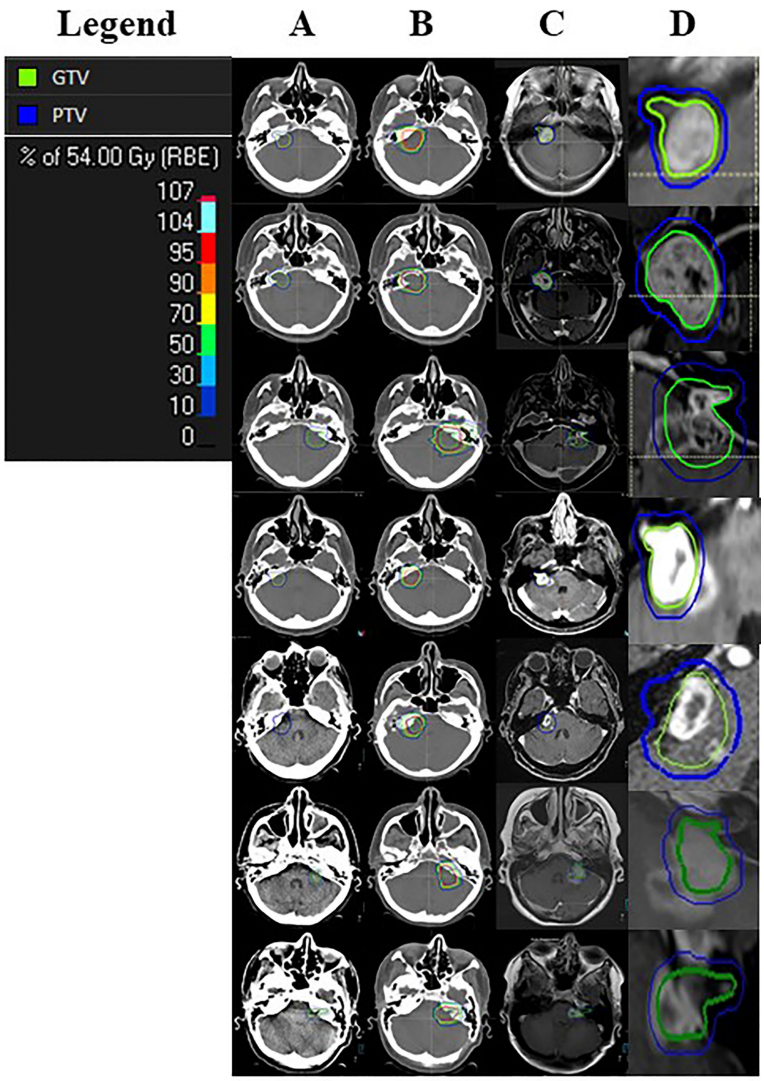

FIGURE 2 | Cases of Radiation-induced Contrast Enhancements (RICE). The image presents all seven cases of RICE observed in our study cohort. Column A presents the planning computer tomography with gross target volume (GTV, green) and planning target volume (PTV, blue) for each patient. Column B demonstrates the treatment plan with isodoses for each patient. Column C presents the follow-up magnetic resonance imaging (MRI) with the observed RICE at the time of its first notice and a projection of the initial GTV and PTV in this MRI with an enlargement of this region (column D).

regarding toxicity, RICE, or response of the treatment, but power was lacking. PTV conformity was sufficient in these cases, so inconformity can be excluded as a potential cause for RICE.

Another hypothesis is that the current technique of dose calculation for proton beam radiotherapy underestimates the real regional biological effectiveness as currently heavily discussed in the proton beam radiotherapy community. Interestingly, an RICE localization exactly behind the peak and therefore exactly distally to the target volume is a typical finding (as also depicted in **Figure 1**). The current method of dose prescription in PRT has known weaknesses. This leads to an uncertainty in dose calculation and therefore to underdosed and overdosed areas. Possibly, also an intrinsic difference in radiosensitivity of different brain tissue types might play a role and makes adaptions in proton beam radiotherapy planning necessary. First approaches for a physical risk model to estimate the probability of the occurrence of RICE for low-grade gliomas can be found in the literature (15). To reduce the risk for RICE without compromising the excellent oncologic outcomes, PRT planning needs to be improved further.

In summary, PRT was demonstrated to be effective and yielded high rates of cranial nerve functional preservation. The comparably low cranial nerve toxicity rates are promising, but the follow-up period needs to be further expanded. Also, a longer follow-up is needed. The analysis of RICE in this context is described for the first time. Even if no clinical relevance of RICE occurrence was demonstrated and corticosteroid response was good, it is above our understanding why some patients develop

RICE and therefore further research is needed. Patients should undergo MRIs on a regular basis after cranial PRT.

CONCLUSION

These data demonstrate excellent effectiveness with 100% local control in a median follow-up period of 3.6 years with a promising cranial nerve functional protection rate of 80%. RICE occurred in 16% of the patients after PRT and were not or only mildly symptomatic but made a short course of dexamethasone necessary.

DATA AVAILABILITY STATEMENT

The raw data supporting the conclusions of this article will be made available by the authors, without undue reservation.

ETHICS STATEMENT

The studies involving human participants were reviewed and approved by Heidelberg University ethics committee, January 2018 (#S-832/2018). Written informed consent for participation was not required for this study in accordance with the national legislation and the institutional requirements.

AUTHOR CONTRIBUTIONS

TE, LK, KH, and JD planned and supervised this analysis. TE performed data extraction and review. TE, RES, and DK performed all statistical analysis. TE reviewed data analysis and drafted the manuscript. All authors contributed patient data and participated in reviewing and improving analysis and manuscript. All authors read and approved the final manuscript.

FUNDING

We acknowledge financial support by Deutsche Forschungsgemeinschaft within the funding program for Open Access Publishing, by the Baden-Württemberg Ministry of Science, Research and the Arts and by Ruprecht-Karls-Universität Heidelberg. TE received funding by Ruprecht-Karls Universität Heidelberg, Herbert Kienzle Foundation, and Else Kröner-Fresenius Foundation.

REFERENCES

1. Klekamp J, Samii M. Surgery of Spinal Nerve Sheath Tumors With Special Reference to Neurofibromatosis. *Neurosurgery* (1998) 42(2):279–89discussion 89–90. doi: 10.1097/00006123-199802000-00042
2. Fisher JL, Pettersson D, Palmisano S, Schwartzbaum JA, Edwards CG, Mathiesen T, et al. Loud Noise Exposure and Acoustic Neuroma. *Am J Epidemiol* (2014) 180(1):58–67. doi: 10.1093/aje/kwu081
3. Parry DM, Eldridge R, Kaiser-Kupfer MI, Bouzas EA, Pikus A, Patronas N. Neurofibromatosis 2 (NF2): Clinical Characteristics of 63 Affected Individuals and Clinical Evidence for Heterogeneity. *Am J Med Genet* (1994) 52(4):450–61. doi: 10.1002/ajmg.1320520411
4. Mautner VF, Lindenau M, Baser ME, Hazim W, Tatagiba M, Haase W, et al. The Neuroimaging and Clinical Spectrum of Neurofibromatosis 2. *Neurosurgery* (1996) 38(5):880–5discussion 5–6. doi: 10.1097/00006123-199605000-00004
5. Maertens O, Brems H, Vandesompele J, De Raedt T, Heyns I, Rosenbaum T, et al. Comprehensive NF1 Screening on Cultured Schwann Cells From Neurofibromas. *Hum Mutat* (2006) 27(10):1030–40. doi: 10.1002/humu.20389
6. Brosseau JP, Pichard DC, Legius EH, Wolkenstein P, Lavker RM, Blakeley JO, et al. The Biology of Cutaneous Neurofibromas: Consensus Recommendations for Setting Research Priorities. *Neurology* (2018) 91(2 Suppl 1):S14–s20. doi: 10.1212/WNL.0000000000005788
7. Gormley WB, Sekhar LN, Wright DC, Kamerer D, Schessel D. Acoustic Neuromas: Results of Current Surgical Management. *Neurosurgery* (1997) 41 (1):50–8; discussion 8-60. doi: 10.1097/00006123-199707000-00012
8. Samii M, Matthies C. Management of 1000 Vestibular Schwannomas (Acoustic Neuromas): Hearing Function in 1000 Tumor Resections. *Neurosurgery* (1997) 40(2):248–60; discussion 60-2. doi: 10.1097/00006123-199702000-00005
9. Goldbrunner R, Weller M, Regis J, Lund-Johansen M, Stavrinou P, Reuss D, et al. EANO Guideline on the Diagnosis and Treatment of Vestibular Schwannoma. *Neuro-Oncology* (2020) 22(1):31–45. doi: 10.1093/neuonc/noz153
10. Lesueur P, Calugaru V, Nauraye C, Stefan D, Cao K, Emery E, et al. Proton Therapy for Treatment of Intracranial Benign Tumors in Adults: A Systematic Review. *Cancer Treat Rev* (2019) 72:56–64. doi: 10.1016/j.ctrv.2018.11.004
11. Hall EJ. Intensity-Modulated Radiation Therapy, Protons, and the Risk of Second Cancers. *Int J Radiat Oncol Biol Phys* (2006) 65(1):1–7. doi: 10.1016/j.ijrobp.2006.01.027
12. Sakthivel V, Ganesh KM, McKenzie C, Boopathy R, Selvaraj J. Second Malignant Neoplasm Risk After Craniospinal Irradiation in X-Ray-Based Techniques Compared to Proton Therapy. *Australas Phys Eng Sci Med* (2019) 42(1):201–9. doi: 10.1007/s13246-019-00731-y
13. König L, Haering P, Lang C, Splinter M, von Nettelbladt B, Weykamp F, et al. Secondary Malignancy Risk Following Proton vs. X-Ray Treatment of Mediastinal Malignant Lymphoma: A Comparative Modeling Study of Thoracic Organ-Specific Cancer Risk. *Front Oncol* (2020) 10:989. doi: 10.3389/fonc.2020.00989
14. Bronk JK, Guha-Thakurta N, Allen PK, Mahajan A, Grosshans DR, McGovern SL. Analysis of Pseudoprogression After Proton or Photon Therapy of 99 Patients With Low Grade and Anaplastic Glioma. *Clin Transl Radiat Oncol* (2018) 9:30–4. doi: 10.1016/j.ctro.2018.01.002
15. Bahn E, Bauer J, Harrabi S, Herfarth K, Debus J, Alber M. Late Contrast Enhancing Brain Lesions in Proton-Treated Patients With Low-Grade Glioma: Clinical Evidence for Increased Periventricular Sensitivity and Variable RBE. *Int J Radiat Oncol Biol Phys* (2020) 107(3):571–8. doi: 10.1016/j.ijrobp.2020.03.013
16. Barnes CJ, Bush DA, Grove RI, Loredo LN, Slater JD. Fractionated Proton Beam Therapy for Acoustic Neuromas: Tumor Control and Hearing Preservation. *Int J Particle Ther* (2018) 4(4):28–36. doi: 10.14338/IJPT-14-00014.1
17. Zhu S, Rotondo R, Mendenhall WM, Dagan R, Lewis D, Huh S, et al. Long-Term Outcomes of Fractionated Stereotactic Proton Therapy for Vestibular Schwannoma: A Case Series. *Int J Particle Ther* (2018) 4(4):37–46. doi: 10.14338/IJPT-17-00032.1
18. Weber DC, Chan AW, Bussiere MR, GRt H, Ancukiewicz M, Barker FG2nd, et al. Proton Beam Radiosurgery for Vestibular Schwannoma: Tumor Control and Cranial Nerve Toxicity. *Neurosurgery* (2003) 53(3):577–86; discussion 86-8. doi: 10.1227/01.NEU.0000079369.59219.C0
19. Emami B, Lyman J, Brown A, Coia L, Goitein M, Munzenrider JE, et al. Tolerance of Normal Tissue to Therapeutic Irradiation. *Int J Radiat oncol biol Phys* (1991) 21(1):109–22. doi: 10.1016/0360-3016(91)90171-Y

20. Marks LB, Yorke ED, Jackson A, Ten Haken RK, Constine LS, Eisbruch A, et al. Use of Normal Tissue Complication Probability Models in the Clinic. *Int J Radiat Oncol Biol Phys* (2010) 76(3 Suppl):S10–9. doi: 10.1016/j.ijrobp.2009.07.1754
21. Shaw E, Kline R, Gillin M, Souhami L, Hirschfeld A, Dinapoli R, et al. Radiation Therapy Oncology Group: Radiosurgery Quality Assurance Guidelines. *Int J Radiat Oncol Biol Phys* (1993) 27(5):1231–9. doi: 10.1016/0360-3016(93)90548-A
22. Schwartz LH, Litière S, de Vries E, Ford R, Gwyther S, Mandrekar S, et al. RECIST 1.1-Update and Clarification: From the RECIST Committee. *Eur J Cancer (Oxford England: 1990)* (2016) 62:132–7. doi: 10.1016/j.ejca.2016.03.081
23. Schwartz LH, Seymour L, Litière S, Ford R, Gwyther S, Mandrekar S, et al. RECIST 1.1 - Standardisation and Disease-Specific Adaptations: Perspectives From the RECIST Working Group. *Eur J Cancer (Oxford England: 1990)* (2016) 62:138–45. doi: 10.1016/j.ejca.2016.03.082
24. Fisher LM, Doherty JK, Lev MH, Slattery WH3rd. Distribution of Nonvestibular Cranial Nerve Schwannomas in Neurofibromatosis 2. *Otol neurotol: Off Publ Am Otol Society Am Neurotol Soc [and] Eur Acad Otol Neurotol* (2007) 28(8):1083–90. doi: 10.1097/MAO.0b013e31815a8411
25. Tucker DW, Gogia AS, Donoho DA, Yim B, Yu C, Fredrickson VL, et al. Long-Term Tumor Control Rates Following Gamma Knife Radiosurgery for Acoustic Neuroma. *World Neurosurgery* (2019) 122:366–71. doi: 10.1016/j.wneu.2018.11.009
26. Smouha EE, Yoo M, Mohr K, Davis RP. Conservative Management of Acoustic Neuroma: A Meta-Analysis and Proposed Treatment Algorithm. *Laryngoscope* (2005) 115(3):450–4. doi: 10.1097/00005537-200503000-00011
27. Sughrue ME, Kaur R, Rutkowski MJ, Kane AJ, Kaur G, Yang I, et al. Extent of Resection and the Long-Term Durability of Vestibular Schwannoma Surgery. *J Neurosurg* (2011) 114(5):1218–23. doi: 10.3171/2010.11.JNS10257
28. Samii M, Matthies C. Management of 1000 Vestibular Schwannomas (Acoustic Neuromas): The Facial Nerve–Preservation and Restitution of Function. *Neurosurgery* (1997) 40(4):684–94; discussion 94-5. doi: 10.1097/00006123-199704000-00006
29. Andrews DW, Suarez O, Goldman HW, Downes MB, Bednarz G, Corn BW, et al. Stereotactic Radiosurgery and Fractionated Stereotactic Radiotherapy for the Treatment of Acoustic Schwannomas: Comparative Observations of 125 Patients Treated at One Institution. *Int J Radiat Oncol Biol Phys* (2001) 50(5):1265–78. doi: 10.1016/S0360-3016(01)01559-0
30. Combs SE, Welzel T, Schulz-Ertner D, Huber PE, Debus J. Differences in Clinical Results After LINAC-Based Single-Dose Radiosurgery Versus Fractionated Stereotactic Radiotherapy for Patients With Vestibular Schwannomas. *Int J Radiat Oncol Biol Phys* (2010) 76(1):193–200. doi: 10.1016/j.ijrobp.2009.01.064
31. Combs SE, Engelhard C, Kopp C, Wiedenmann N, Schramm O, Prokic V, et al. Long-Term Outcome After Highly Advanced Single-Dose or Fractionated Radiotherapy in Patients With Vestibular Schwannomas - Pooled Results From 3 Large German Centers. *Radiotherapy Oncol* (2015) 114(3):378–83. doi: 10.1016/j.radonc.2015.01.011
32. Kessel KA, Fischer H, Vogel MM, Oechsner M, Bier H, Meyer B, et al. Fractionated vs. Single-Fraction Stereotactic Radiotherapy in Patients With Vestibular Schwannoma: Hearing Preservation and Patients' Self-Reported Outcome Based on an Established Questionnaire. *Strahlentherapie und Onkologie: Organ der Deutschen Rontgengesellschaft [et al]* (2017) 193(3):192–9. doi: 10.1007/s00066-016-1070-0
33. Wagner J, Welzel T, Habermehl D, Debus J, Combs SE. Radiotherapy in Patients With Vestibular Schwannoma and Neurofibromatosis Type 2: Clinical Results and Review of the Literature. *Tumori* (2014) 100(2):189–94. doi: 10.1177/030089161410000212
34. Gonzalez J, Kumar AJ, Conrad CA, Levin VA. Effect of Bevacizumab on Radiation Necrosis of the Brain. *Int J Radiat Oncol Biol Phys* (2007) 67(2):323–6. doi: 10.1016/j.ijrobp.2006.10.010
35. Zhuang H, Shi S, Yuan Z, Chang JY. Bevacizumab Treatment for Radiation Brain Necrosis: Mechanism, Efficacy and Issues. *Mol Cancer* (2019) 18(1):21. doi: 10.1186/s12943-019-0950-1
36. Rubin P, Gash DM, Hansen JT, Nelson DF, Williams JP. Disruption of the Blood-Brain Barrier as the Primary Effect of CNS Irradiation. *Radiotherapy Oncol* (1994) 31(1):51–60. doi: 10.1016/0167-8140(94)90413-8

Conflict of Interest: TE reports grants from Ruprecht-Karls Universität Heidelberg, Herbert Kienzle Foundation, and Else Kröner-Fresenius Foundation and received travel reimbursement from Bristol-Myers Squibb outside the submitted work. JH-R received speaker fees and travel reimbursement from ViewRay Inc, as well as travel reimbursement and grants from IntraOP Medical and Elekta Instrument AB outside the submitted work. RS reports grants from Ruprecht-Karls Universität Heidelberg, during the conduct of the study; personal fees from Accuray Inc., personal fees from AstraZeneca GmbH, personal fees from Bristol Myers Squibb GmbH & Co., personal fees from Novocure GmbH, personal fees from Merck KGaA, personal fees from Takeda GmbH, and grants from Accuray Inc., outside the submitted work. JD reports grants from the Clinical Research Institute (CRI), grants from View Ray Incl., grants from Accuray International, grants from Accuray Incorporated, grants from RaySearch Laboratories AB, grants from Vision RT limited, grants from Merck Serono GmbH, grants from Astellas Pharma GmbH, grants from Astra Zeneca GmbH, grants from Siemens Healthcare GmbH, grants from Solution Akademie GmbH, grants from Eromed PLC Surrey Research Park, grants from Quintiles GmbH, grants from Pharmaceutical Research Associates GmbH, grants from Boehringer Ingelheim Pharma GmbH Co, grants from PTW-Frieburg Dr. Pychlau GmbH, grants from Nanobiotix A.a., grants from IntraOP Medical, outside the submitted work. LK reports grants from Ruprecht-Karls Universität Heidelberg, personal fees from Accuray Inc., and Novocure GmbH outside the submitted work.

The remaining authors declare that the research was conducted in the absence of any commercial or financial relationships that could be construed as a potential conflict of interest.

Publisher's Note: All claims expressed in this article are solely those of the authors and do not necessarily represent those of their affiliated organizations, or those of the publisher, the editors and the reviewers. Any product that may be evaluated in this article, or claim that may be made by its manufacturer, is not guaranteed or endorsed by the publisher.

frontiers in Oncology

ORIGINAL RESEARCH
published: 25 February 2022
doi: 10.3389/fonc.2022.757686

A Radiosensitivity Prediction Model Developed Based on Weighted Correlation Network Analysis of Hypoxia Genes for Lower-Grade Glioma

Zixuan Du[1,2†], Hanshan Liu[3†], Lu Bai[1,2], Derui Yan[1], Huijun Li[1], Sun Peng[4], JianPing Cao[5], Song-Bai Liu[2] and Zaixiang Tang[1*]*

[1] Department of Biostatistics and Jiangsu Key Laboratory of Preventive and Translational Medicine for Geriatric Diseases, School of Public Health, Medical College of Soochow University, Suzhou, China, [2] Suzhou Key Laboratory of Medical Biotechnology, Suzhou Vocational Health College, Suzhou, China, [3] Department of Medical Oncology, Jiangsu Provincial Corps Hospital, Chinese People's Armed Police Forces, Yangzhou City, China, [4] Department of Otolaryngology, The First Affiliated Hospital of Soochow University, Suzhou, China, [5] School of Radiation Medicine and Protection and Collaborative Innovation Center of Radiation Medicine of Jiangsu Higher Education Institutions, Soochow University, Suzhou, China

OPEN ACCESS

Edited by:
Alfredo Conti, University of Bologna, Italy

Reviewed by:
Xingjie Hao, Huazhong University of Science and Technology, China
Maria Caffo, University of Messina, Italy

***Correspondence:**
Zaixiang Tang
tangzx@suda.edu.cn
Song-Bai Liu
liusongbai@126.com

[†]These authors have contributed equally to this work

Specialty section:
This article was submitted to Neuro-Oncology and Neurosurgical Oncology, a section of the journal Frontiers in Oncology

Received: *12 August 2021*
Accepted: *31 January 2022*
Published: *25 February 2022*

Citation:
Du Z, Liu H, Bai L, Yan D, Li H, Peng S, Cao J, Liu S-B and Tang Z (2022) A Radiosensitivity Prediction Model Developed Based on Weighted Correlation Network Analysis of Hypoxia Genes for Lower-Grade Glioma. Front. Oncol. 12:757686. doi: 10.3389/fonc.2022.757686

Background and Purpose: Hypoxia is one of the basic characteristics of the physical microenvironment of solid tumors. The relationship between radiotherapy and hypoxia is complex. However, there is no radiosensitivity prediction model based on hypoxia genes. We attempted to construct a radiosensitivity prediction model developed based on hypoxia genes for lower-grade glioma (LGG) by using weighted correlation network analysis (WGCNA) and least absolute shrinkage and selection operator (Lasso).

Methods: In this research, radiotherapy-related module genes were selected after WGCNA. Then, Lasso was performed to select genes in patients who received radiotherapy. Finally, 12 genes (*AGK*, *ETV4*, *PARD6A*, *PTP4A2*, *RIOK3*, *SIGMAR1*, *SLC34A2*, *SMURF1*, *STK33*, *TCEAL1*, *TFPI*, and *UROS*) were included in the model. A radiosensitivity-related risk score model was established based on the overall rate of The Cancer Genome Atlas (TCGA) dataset in patients who received radiotherapy. The model was validated in TCGA dataset and two Chinese Glioma Genome Atlas (CGGA) datasets. A novel nomogram was developed to predict the overall survival of LGG patients.

Results: We developed and verified a radiosensitivity-related risk score model based on hypoxia genes. The radiosensitivity-related risk score served as an independent prognostic indicator. This radiosensitivity-related risk score model has prognostic prediction ability. Moreover, a nomogram integrating risk score with age and tumor grade was established to perform better for predicting 1-, 3-, and 5-year survival rates.

Conclusions: We developed and validated a radiosensitivity prediction model that can be used by clinicians and researchers to predict patient survival rates and achieve personalized treatment of LGG.

Keywords: lower-grade glioma, radiosensitivity prediction model, radiosensitivity, Lasso, WGCNA

INTRODUCTION

Lower-grade glioma (LGG) consists of diffuse low-grade and intermediate-grade gliomas (World Health Organization grades II and III) (1). For the first time, in the WHO 2016 classification of gliomas, gliomas were defined based on the presence/absence of isocitrate dehydrogenase (IDH) mutation and 1p/19q codeletion (2). This is a transition from histological classification to molecular classification, and it provides strong support for the individualized treatment of LGG patients.

Treatments for LGG usually include surgery, chemotherapy, immunotherapy, and radiotherapy. One study showed that radiotherapy can increase progression-free survival (PFS) and improve the overall survival (OS) of LGG patients (3). A nationwide analysis of LGG patients found that radiotherapy was associated with improved survival outcomes (4). However, due to individual differences, some patients showed radiation toxicity after receiving radiotherapy. The radiosensitivity of tumors is the key factor in determining the curative effect of radiotherapy. The purpose of predicting the radiosensitivity of patients is to identify the population sensitive to radiotherapy and maximize the treatment benefit of radiotherapy. Thus, it is imperative to exploit new treatments closely related to radiotherapy for LGG to improve the prognosis.

The occurrence and development of tumors are related to the excessive proliferation and reduced apoptosis of tumor cells. The hypoxic microenvironment promoted the growth, infiltration, and metastasis of tumor cells. Hypoxia is one of the basic characteristics of the physical microenvironment of solid tumors and can influence immune cell functions (5). Tumor hypoxia and the resulting energy metabolism of tumor cells are important features of cancer and also the driving force and basis of cancer metastasis. Hypoxic conditions are considered to be a feasible approach for targeted immunotherapy (6).

The relationship between radiotherapy and hypoxia is complex. Radiotherapy is the targeted administration of X-rays to destroy cancer cells and tumor tissue. It targets rapidly proliferating tumor cells by inducing oxidative stress through increased reactive oxygen species (ROS) (7). Hypoxia condition is the main factor of tumor radiation resistance (8). Tumor cells in hypoxic conditions thus attain aggressive phenotypes and become resistant to chemo- and radiotherapies resulting in higher mortality (9). In addition to the well-known protective effect of hypoxia on the radiological responses of cells and tissues, hypoxic conditions can also lead to altered gene expression patterns, resulting in more or less genomic alterations in different cell populations (10).

Lin et al. developed a hypoxia signature to evaluate and predict prognosis in glioma, and this model reflected overall immune response intensity in the glioma microenvironment (11). Wang et al. developed a risk signature with five genes that could serve as an independent factor for predicting the prognosis of patients with glioblastoma (GBM) (12). Xiao et al. explored a three-gene signature as a candidate prognostic biomarker for LGG (13). Likewise, Li et al. developed a radiosensitive gene signature by using coexpression and ceRNA network analysis to select genes (14). However, a model for predicting the benefit of radiotherapy based on hypoxia-related genes by using weighted correlation network analysis (WGCNA) in LGGs has not been established.

In this study, WGCNA was used to screen the most relevant radiotherapy module. This study aims to develop a radiotherapy signature related to hypoxia-related genes to provide survival and radiotherapy response prediction for LGG patients.

MATERIALS AND METHODS

Data Sources

LGG patients with clinical and gene expression files were downloaded from a public database The Cancer Genome Atlas (TCGA; http://cancergenome.nih.gov/) by using the R package TCGA-Assembler (15). LGG patients with survival information were procured from the UCSC Cancer Genomics Browser (https://xenabrowser.net/datapages/) (16). We used OS and PFS as endpoints and removed those without radiotherapy information (n = 29) and survival information (n = 3). Hypoxia-related genes were extracted from GeneCards (https://www.genecards.org/). Genes with a common symbol name in TCGA were selected. The flowchart is summarized in **Figure 1**. Finally, we obtained 466 patients with 5,403 hypoxia-related genes for analysis. Gene expression and clinical profiles of 443 LGG patients (CGGA693 dataset) (17, 18) and 182 LGG patients (CGGA325 dataset) (19, 20) were downloaded as external validation datasets from the Chinese Glioma Genome Atlas (CGGA) dataset (http://www.cgga.org.cn/). The RNA-seq transcriptome data were estimated as log2(x + 1) transformed. The cleaned clinical data are summarized in **Supplementary Tables 1**, **2**.

Weighted Correlation Network Analysis

WGCNA can identify highly related genes in thousands of genes and cluster them into modules and then was used to establish the relationship between phenotypic traits and gene expression data. By calculating the correlation degree between the gene module and the external clinicopathological information, we can obtain the module genes highly related to the clinicopathological information and obtain the hub genes. WGCNA can be implemented by R package WGCNA (21).

In our study, WGCNA was performed to discover radiotherapy-related genes. We analyzed hypoxia-related genes and clinical data, including OS status, PFS status, age, grade, radiotherapy, and treatment response. First, hierarchical clustering analysis was utilized to exclude the outliers. Subsequently, the "pickSoftThreshold" function was performed to estimate the value of the powers. The R-squared criterion was set to 0.9. Pearson's correlation matrices were used for all pairs of genes, and the weighted adjacency matrix was constructed using the power function. After the power was selected, the adjacency matrix was converted to a topological overlap matrix (TOM). Genes with similar expression profiles were classified into gene modules, and hierarchical clustering was performed by the class average method based on TOM. The minimum gene size in each module was set as 30. To further analyze the modules, the

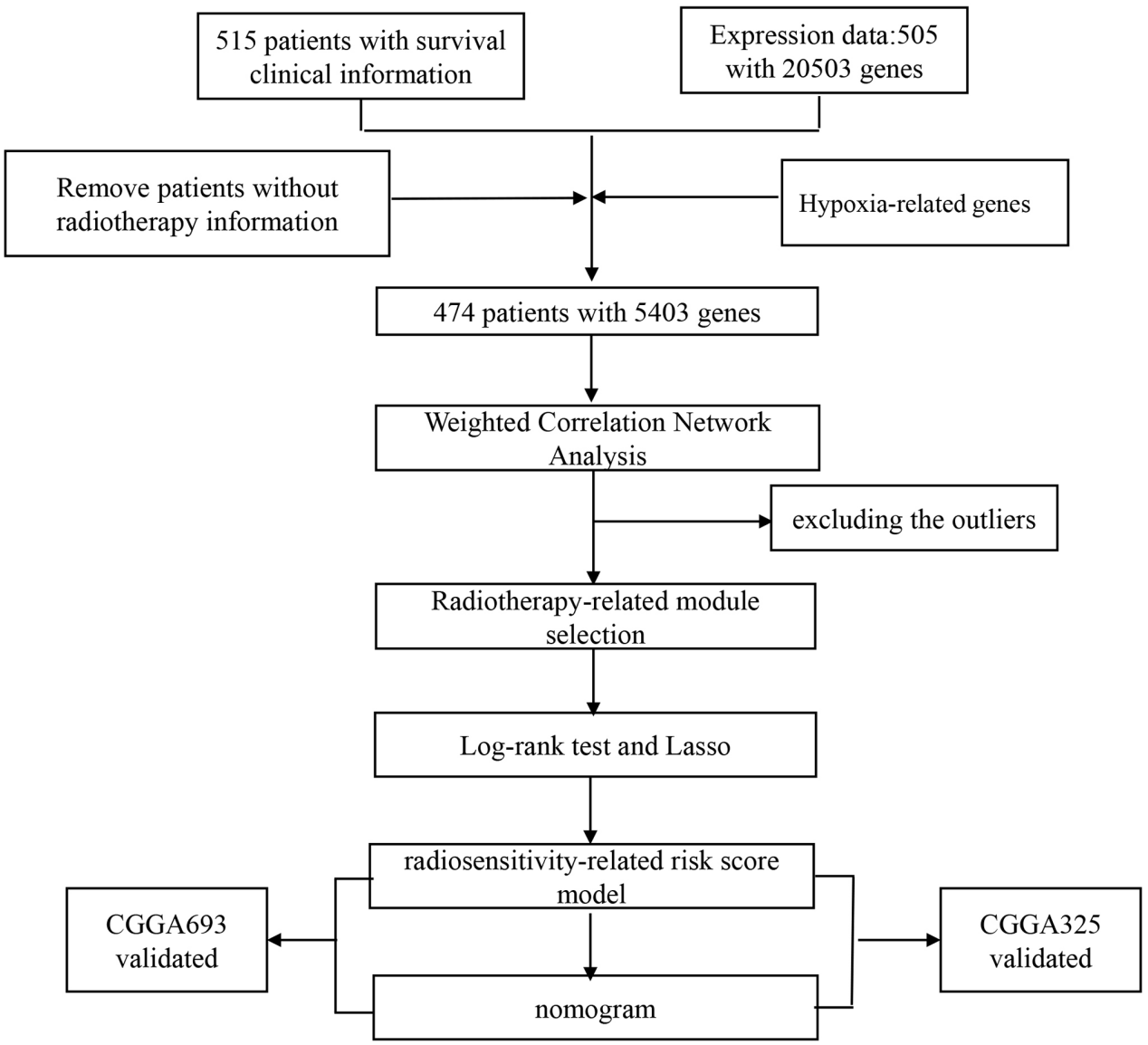

FIGURE 1 | The flowchart of study design, patient selection, and gene selection.

dissimilarity of module eigengenes was calculated, and some modules were merged. The merged cutoff threshold was set to 0.2, which meant that modules with a similarity higher than 0.8 were merged into one module. Then, the correlations between modules and clinical factors of LGG were investigated by using Pearson's correlation test. Finally, the genes of the most significant radiotherapy-related module were chosen for subsequent analysis.

Functional Enrichment Analysis

To obtain the function of genes in the radiotherapy-related module, we performed the Gene Ontology (GO) and Kyoto Encyclopedia of Genes and Genomes (KEGG) analyses by using the R clusterprofiler (22). The GO analysis included biological processes (BPs), cellular component (CC), and molecular function (MF).

Definition of Radiosensitivity and Radiosensitivity Prediction Model

In our study, radiosensitivity for the patients was defined in terms of survival benefit (**Supplementary Figure 1**). 1) In patients who received radiotherapy, patients in group A had a better survival rate than the patients in group B. Then patients in group A could be defined as radiosensitive patients (RS group). 2) In patients who did not receive radiotherapy, the survival rate of group A (RS group) was not better (equal or worse) than that of the other group.

The radiosensitivity prediction model was constructed in the patients who had received radiotherapy. Patients who received

radiotherapy provided more information related to radiosensitivity. We defined a radiosensitivity prediction model for the patients satisfying both of the following criteria: the constructed radiation sensitivity correlation model constructed can be used to divide the population into a high-risk group and a low-risk group. 1) In the radiotherapy patients, the survival rate of the low-risk group was higher than that of the high-risk group. 2) There was no significant difference in survival between the high- and low-risk groups in the group that did not receive radiation therapy. The low-risk group was defined as the RS group, and the high-risk group was defined as the radioresistant (RR) group. Therefore, the radiosensitivity model can select the patients with better benefit from radiotherapy, while the results in the population without radiotherapy can better show that the model is related to radiosensitivity.

Radiosensitivity-Related Risk Score Construction

A log-rank test was applied to assess the relationship between the expression of genes in radiotherapy-related modules and the OS of radiotherapy patients in TCGA. Whole LGG patients were divided into the high- and low-expression level groups using the median gene expression level as a cutoff point. The RNAs with log–rank $p < 0.05$ in the radiotherapy patients and log-rank $p > 0.05$ in the non-radiotherapy patients were identified as radiosensitivity–related RNAs. Then, the least absolute shrinkage and selection operator (Lasso) regression was performed to narrow the range of genes in patients who received radiotherapy. The radiosensitivity-related risk score was computed as follows:

$$Radiosensitivity - related\ risk\ score = \Sigma(\beta RNAn \times exprRNAn)$$

Radiosensitivity-Related Risk Score Validation

The LGG patients were divided into the high- and low-risk groups with the median radiosensitivity-related risk score as the cutoff. The Kaplan–Meier method was used to plot survival curves. Time-dependent receiver operating characteristic (ROC) curve analysis was used to evaluate the prognostic value. The radiosensitivity-related risk score was validated in TCGA and two CGGA datasets.

The Radiosensitivity-Related Risk Score Is an Independent Prognostic Indicator

Univariate and multivariate Cox proportional hazard regression analyses were used to examine whether the radiosensitivity-related risk score was an independent prognostic factor. The forest plot was plotted to show the hazard ratio (HR) and 95% CIs.

Development and Validation of the Nomogram

To evaluate the 1-, 3-, and 5-year survival probability for patients with LGG, a nomogram model including all independent prognostic factors was built for LGG patients in TCGA. The nomogram model was validated with the PFS of TCGA and two CGGA datasets.

Analysis Method

All statistical analyses were performed using R software (4.0.2). WGCNA was performed by using the "WGCNA" R package. Lasso analysis was conducted by using the "glmnet" R package. A bilateral p-value <0.05 was considered statistically significant.

RESULTS

Weighted Coexpression Network Construction and Identification of Radiotherapy-Related Modules

WGCNA was performed in TCGA-LGG dataset to determine the coexpression network most highly associated with the radiotherapy modules. The hclust function was used to determine if there were any outliers (**Supplementary Figure 2**). A total of 466 samples were in the clusters after removing 8 outliers in the samples based on the average linkage method. When the soft threshold power value was $\beta = 7$ and the scale $R^2 = 0.84$, the average connectivity of the RNA group was high, and the connectivity between genes conformed to the scale-free network distribution (**Figures 2A, B**). The scale-free topological fitting index R-square was calculated to reach 0.84 (**Figures 2C, D**). Next, the TOM was constructed (**Figure 3A**), and a topological overlapping heatmap was depicted of the TOM including the top 400 genes (**Figure 3B**). A total of 13 modules were identified from the RNA coexpression network after merging modules with a similarity higher than 0.8. The relationships between gene modules and clinical traits are shown in a heatmap (**Figure 4A**). Thus, the black module was considered to have the highest correlation with radiotherapy ($r = 0.69$, $p < 0.001$) and was considered a "radiotherapy-related module" (**Figure 4B**).

Functional Analysis of Genes Radiotherapy-Related Module

GO analysis was performed to analyze the function of the radiotherapy-related module (**Figure 4C**). We discovered that the radiotherapy-related module was functionally associated with responding to oxygen levels, responding to decreased oxygen levels, and responding to hypoxia, cardiac chamber morphogenesis, cardiac chamber development, regulation of mRNA stability, and regulation of RNA stability. CCs include the transcription repressor complex, nuclear speck, transcription regulation complex, and methyltransferase complex.

Construction of Radiosensitivity-Related Signature

We selected modules related to radiotherapy for further analysis. A total of 231 genes were subjected to the log-rank test in radiotherapy patients and non-radiotherapy patients. Thirty-six radiosensitivity –related genes were identified in the univariate analysis. Subsequently, the Lasso Cox regression model was used to identify the most robust markers for prognosis (**Figures 5A, B**).

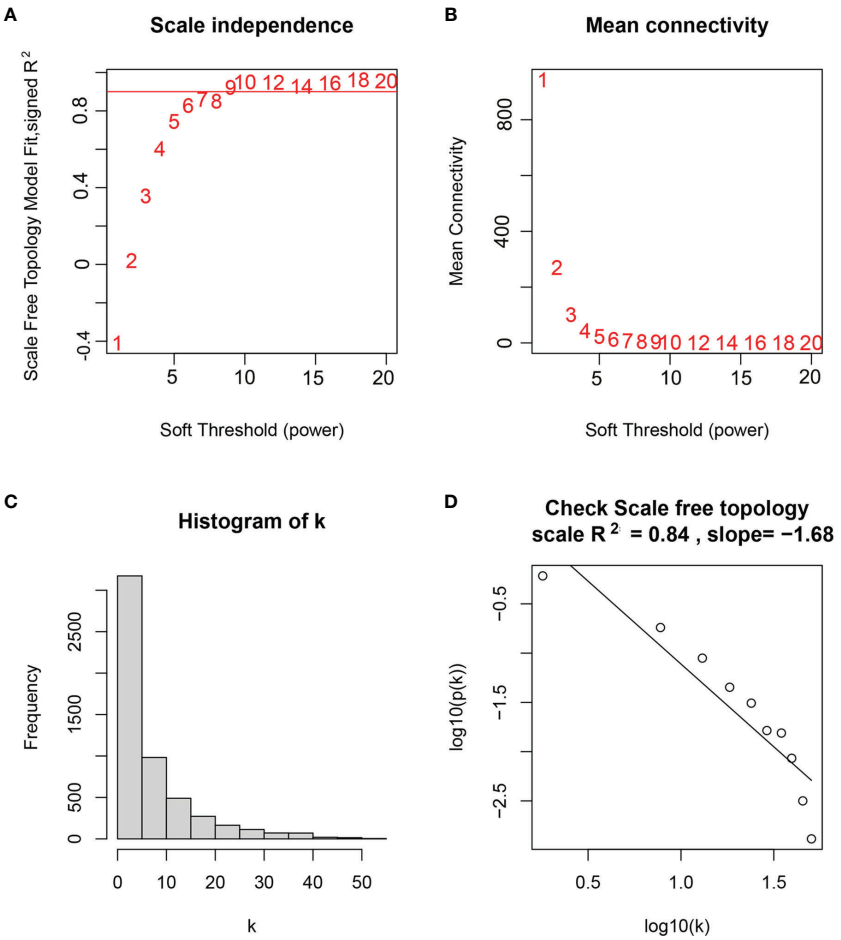

FIGURE 2 | Selection of weighted value β. **(A)** Determine the weighted value β that satisfies the law of scale-free networks. **(B)** Determine the soft threshold based on the network connectivity. **(C)** β = 7, the connection degree of each node in the network histogram distribution. **(D)** The scale-free topology test.

Finally, 12 genes (*AGK*, *ETV4*, *PARD6A*, *PTP4A2*, *RIOK3*, *SIGMAR1*, *SLC34A2*, *SMURF1*, *STK33*, *TCEAL1*, *TFPI*, and *UROS*) were included in the model. The radiosensitivity-related risk scores were calculated based on the linear combination of the expression levels of genes multiplied by the corresponding Lasso coefficients. The radiosensitivity-related risk score was as follows: radiosensitivity-related risk score = 0.16864 * *AGK* + 0.14242 * *ETV4* – 0.14386 * *PARD6A* + 0.00584 * *PTP4A2* – 0.09746 * *RIOK3* – 0.23212 * *SIGMAR1* + 0.07849 * *SLC34A2* + 0.18813 * *SMURF1* + 0.04491 * *STK33* – 0.4922 * *TCEAL1* + 0.01536 * *TFPI* – 0.4694 * *UROS*.

Then, the patients with LGG in TCGA dataset were divided into the high-risk (n = 233) or low-risk groups (n = 233) according to the median risk score. The Kaplan–Meier analysis revealed that OS time was significantly increased in the low-risk group compared with the high-risk group in patients who received radiotherapy ($p < 0.001$, **Figure 5C**). There was no difference in OS between the high-risk group and low-risk group in patients who did not receive radiotherapy ($p = 0.54$, **Figure 5D**). The low-risk group was defined as an RS group, and the high-risk group was defined as an RR group. The risk score distribution of each patient in TCGA is shown in **Figure 5E**.

Then, ROC analysis was used to evaluate the predictive efficiency of the radiosensitivity-related risk score model in the 1-, 3-, and 5-year survival rates (1-year area under the curve (AUC): 0.935 (0.904–0.967); 3-year AUC: 0.856 (0.778–0.933); 5-year AUC: 0.787 (0.704–0.87), **Figure 5F**).

Validation of Radiosensitivity Model in Validation Sets

A radiosensitivity model was validated in TCGA with PFS as the endpoint. The Kaplan–Meier plots indicated that patients in the RR group exhibited worse PFS than patients in the RS group in patients who received radiotherapy ($p < 0.001$, **Figure 6B**). Time-dependent ROC analysis results showed that the AUCs of the radiosensitivity model were 0.74, 0.676, and 0.732 at survival times of 1, 3, and 5 years, respectively (**Figure 6C**). Plots of risk score distribution are shown in **Figures 6A, D, G**.

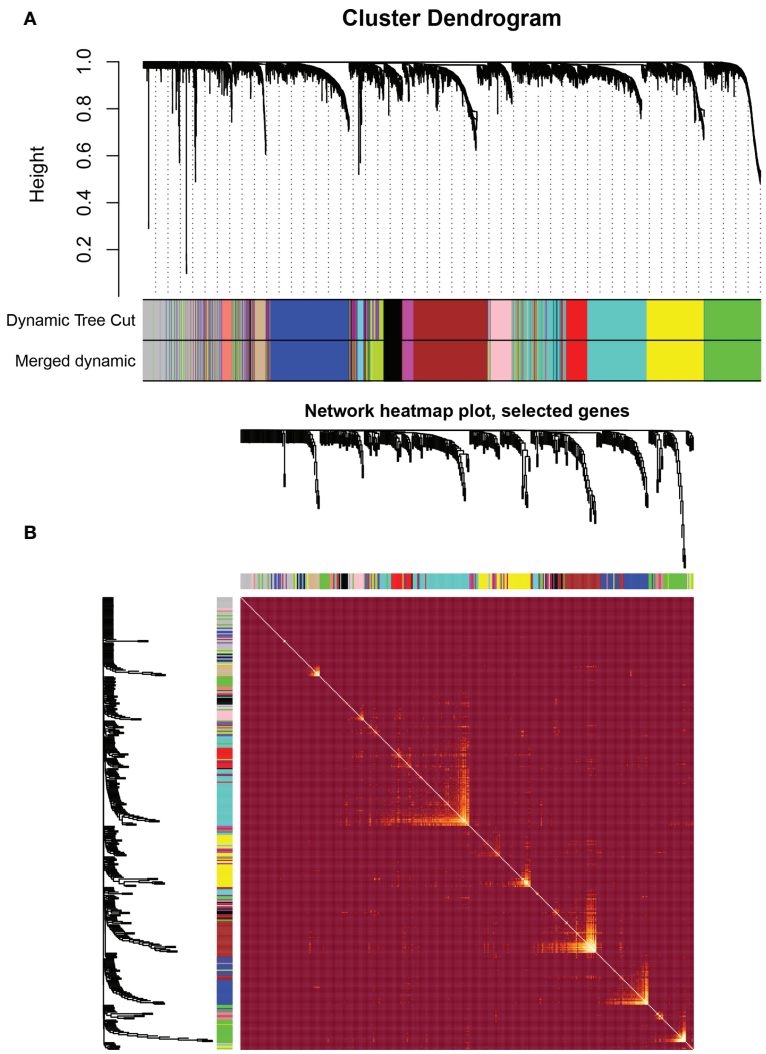

FIGURE 3 | Weighted correlation network analysis. **(A)** Clustering dendrogram of genes based on topological overlapping. **(B)** Network heatmap of the whole genes.

Patients in the CGGA693 and CGGA325 datasets were divided into the RS group and RR group based on the median risk score in each dataset. The Kaplan–Meier analysis showed that patients in the RS group had a more favorable outcome than patients in the RR group in patients who received radiotherapy (CGGA693, $p < 0.001$; CGGA325, $p < 0.001$; **Figures 6E, H**). These results indicated the accuracy of the radiosensitivity-related signature in predicting the outcomes of LGG patients. ROC curves were used to evaluate the predictive accuracy for 1-, 3-, and 5-year survival. AUC values revealed the high predictive value of the radiosensitivity-related risk score for LGG patients (CGGA693: 1-year AUC: 0.636 (0.527–0.746); 3-year AUC: 0.655 (0.587–0.732); 5-year AUC: 0.643 (0.572–0.713); CGGA325: 1-year AUC: 0.696 (0.567–0.862); 3-year AUC: 0.745 (0.644–0.845); 5-year AUC: 0.731 (0.639–0.823), **Figures 6F, I**).

The Radiosensitivity-Related Risk Score Is an Independent Prognostic Factor

Then, univariate and multivariable Cox regression analyses were conducted to evaluate whether the radiosensitivity-related risk score is an independent prognostic factor for LGG. The results indicated that factors such as risk score and grade were significantly correlated with patient survival in both TCGA dataset and two CGGA datasets. Age (HR: 1.054, 95% CI: 1.038–1.071, $p < 0.001$), tumor grade (HR: 2.715, 95% CI: 1.736–4.247, $p < 0.001$), and risk score (HR: 2.712, 95% CI: 1.763–4.171, $p < 0.001$) were significantly associated with OS. The univariate analysis indicated that a high-risk score was significantly correlated with poor OS. The multivariate Cox regression results showed that the radiosensitivity-related risk score was an independent prognostic factor for LGG patients after adjusting for clinical factors such as age, sex, tumor grade, race, and IDH1. When OS was used as an endpoint, the HR was

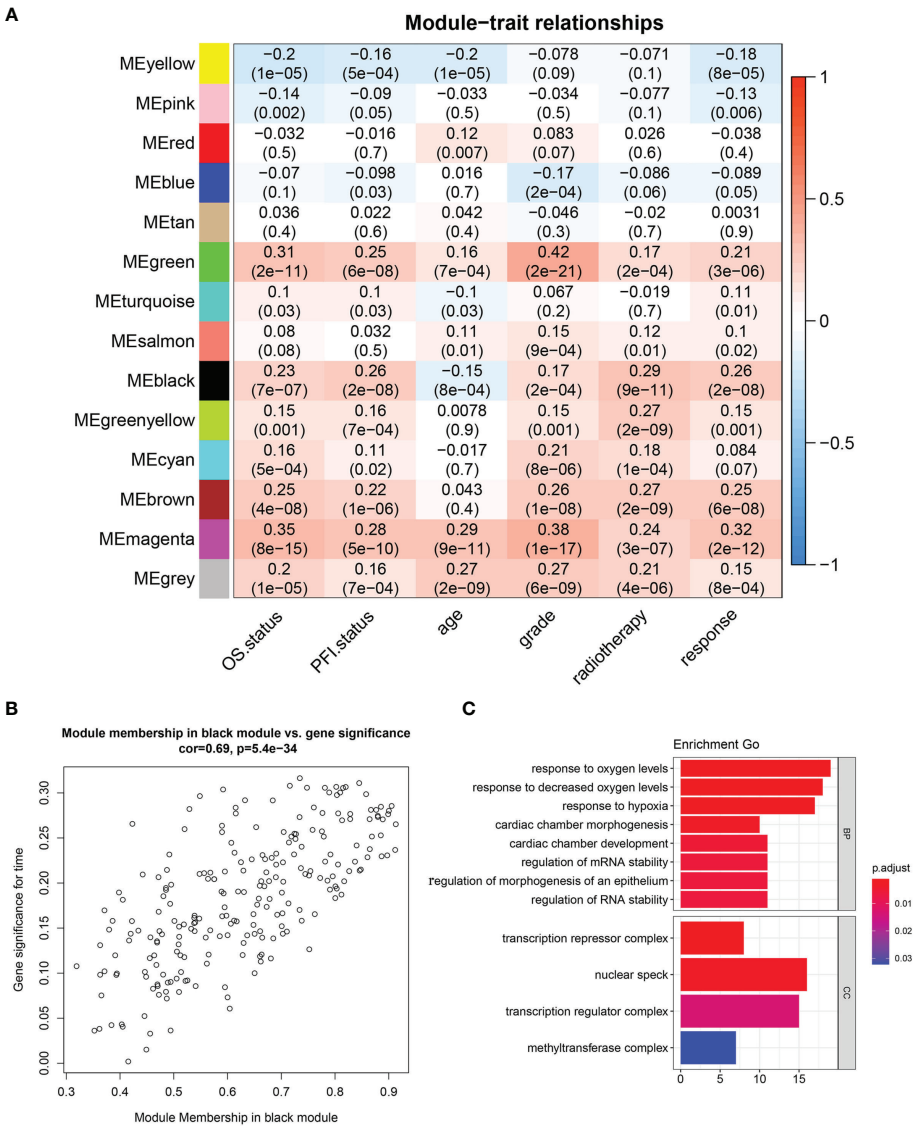

FIGURE 4 | Identification of significant modules. **(A)** Module trait relationship heatmap. **(B)** Scatterplot of gene significance for radiotherapy (y-axis) vs. module membership (x-axis) in the black module. **(C)** GO enrichment analysis of genes in radiotherapy module. BP, biological process; MF, molecular function; CC, cellular component; GO, Gene Ontology.

2.029 (95% CI: 1.407–3.448, p < 0.001, **Figure 7A**). When PFS was used as an endpoint, the HR was 2.170 (HR: 2.170, 95% CI: 1.526–3.086, p < 0.001, **Figure 7B**). In CGGA datasets, we adjusted for clinical factors such as age, sex, tumor grade, race, IDH2, and X1p19q2, and the multivariate Cox regression results also demonstrated that the radiosensitivity-related risk score was an independent prognostic factor for LGG (CGGA693: HR: 1.730, 95% CI: 1.215–2.463, p = 0.003; **Figure 7C**). Unfortunately, the multivariate Cox regression result was not significant in the CGGA325 dataset (CGGA325: HR: 1.609, 95% CI: 0.902–2.871, p = 0.112; **Figure 7D**). We consider that there are too few patients in the CGGA325 database.

Construction and Validation of Nomogram

Age, tumor grade, and risk score were listed as candidate indicators for nomogram construction. Then, an optimal nomogram was established combining age, tumor grade, and risk score to predict a certain clinical outcome (**Figure 8A**). **Figure 8B** shows that AUCs of the nomogram for 1-, 3-, and 5-year OS were 0.947 (0.915–0.978), 0.888 (0.83–0.946), and 0.850 (0.779–0.922), respectively, which were better than those of the models with a single risk score model. **Figure 8C** demonstrates that AUCs of the nomogram for 1-, 3-, and 5-year PFS were 0.74 (0.665–0.815), 0.676 (0.601–0.750), and 0.732 (0.638–0.826), respectively. We also used two CGGA datasets to verify a nomogram model. **Figure 8D** demonstrates that the AUCs of

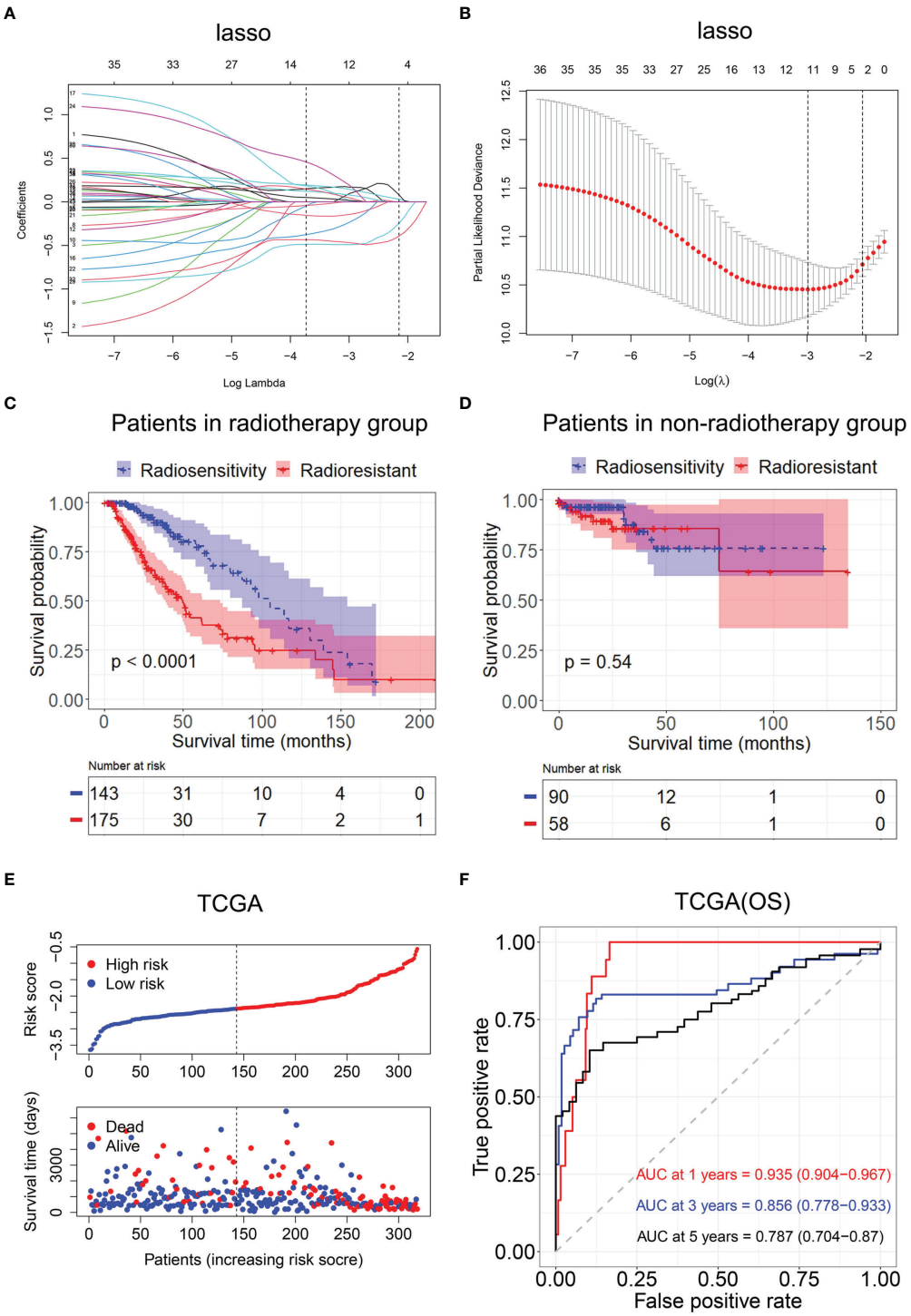

FIGURE 5 | Construction of the radiosensitivity-related risk score model. **(A)** The solution paths of the Lasso. **(B)** The partial log-likelihood profiles of the Lasso. **(C)** Kaplan–Meier curves for the RS group and RR group in patients with radiotherapy and patients who did not receive radiotherapy. RR, radioresistant group; RS, radiosensitive group. **(D)** Kaplan–Meier curves for the RS group and RR group in patients who did not receive radiotherapy. RR, radioresistant group; RS, radiosensitive group. **(E)** Risk score distribution of each patient in TCGA (OS). **(F)** Time-dependent ROC curve analysis of the radiosensitivity-related risk score in TCGA (OS). OS, overall survival; TCGA, The Cancer Genome Atlas; ROC, receiver operating characteristic.

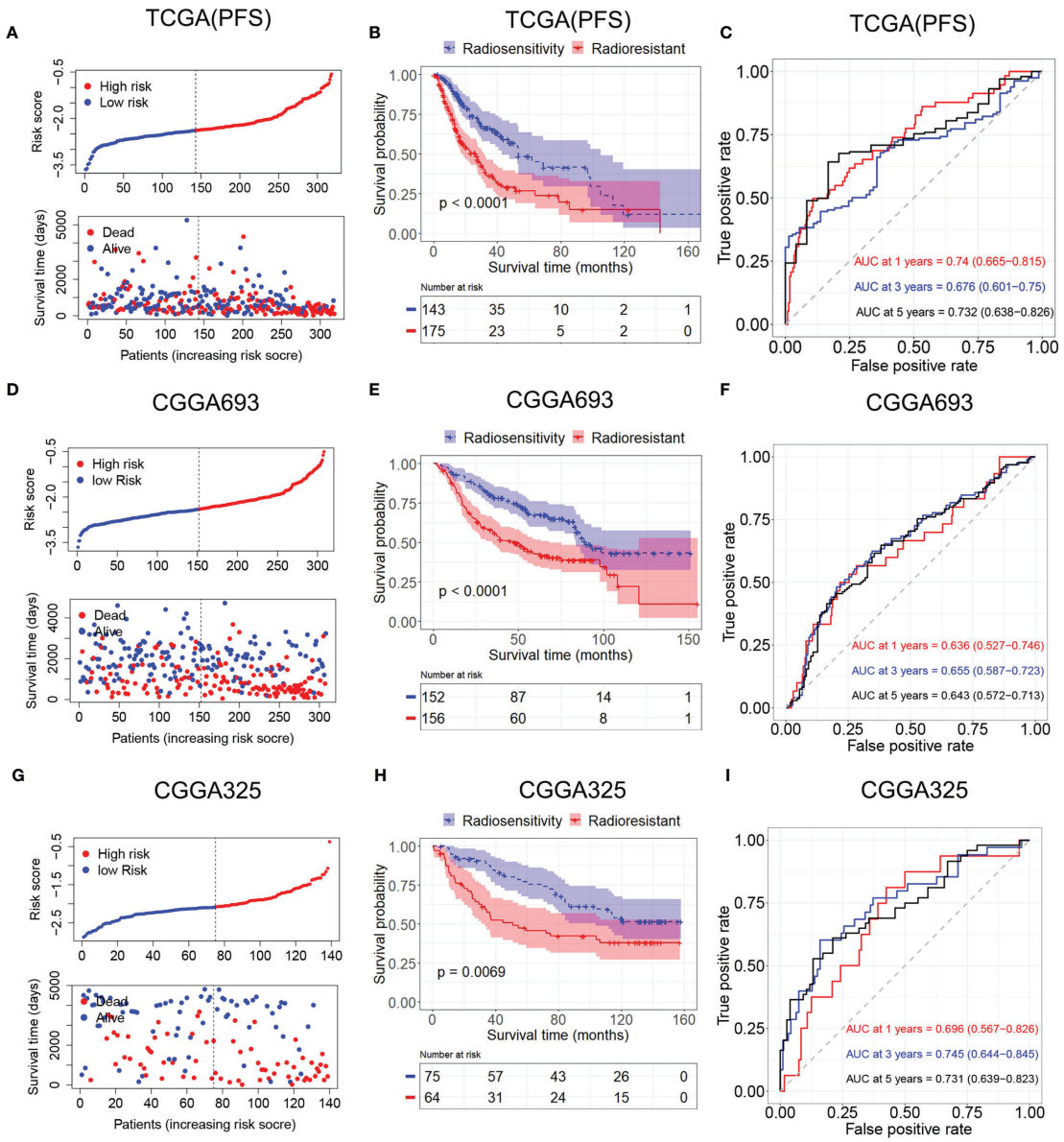

FIGURE 6 | Validation of the radiosensitivity-related risk score model. **(A)** Risk score distribution of each patient in TCGA (PFS). **(B)** Kaplan–Meier curves for the RS group and RR group in patients with radiotherapy from TCGA (PFS). **(C)** Time-dependent ROC curve analysis of the radiosensitivity-related risk score in TCGA (PFS). **(D)** Risk score distribution of each patient in the CGGA693. **(E)** Kaplan–Meier curves for the RS group and RR group in patients with radiotherapy from CGGA693. **(F)** Time-dependent ROC curve analysis of the radiosensitivity-related risk score in the CGGA693. **(G)** Risk score distribution of each patient in the CGGA325. **(H)** Kaplan–Meier curves for the RS group and RR group in patients with radiotherapy from CGGA325. **(I)** Time-dependent ROC curve analysis of the radiosensitivity-related risk score in the CGGA325. TCGA, The Cancer Genome Atlas; PFS, progression-free survival; RS, radiosensitive; RR, radioresistant; ROC, receiver operating characteristic.

nomogram at 1, 3, and 5 years were 0.64 (95% CI: 0.542–0.739), 0.669 (95% CI: 0.602–0.736), and 0.64 (95% CI: 0.569–0.711), respectively, for CGGA693. **Figure 8E** demonstrates that the AUCs of nomogram at 1, 3, and 5 years were 0.740 (95% CI: 0.608–0.872), 0.787 (95% CI: 0.694–0.88), and 0.79 (95% CI: 0.707–0.872), respectively, for CGGA325. The nomogram model for the prognostic model displayed superior predictive performance as compared with the risk score in the CGGA325.

DISCUSSION

LGG is one of the leading causes of cancer-related death worldwide. The treatments of LGG include surgery, chemotherapy, and radiotherapy. Radiotherapy may not be appropriate for all patients due to its toxicity. Thus, it is important to develop risk scores based on genetic and clinical characteristics to help determine which patients would benefit the most from radiation therapy.

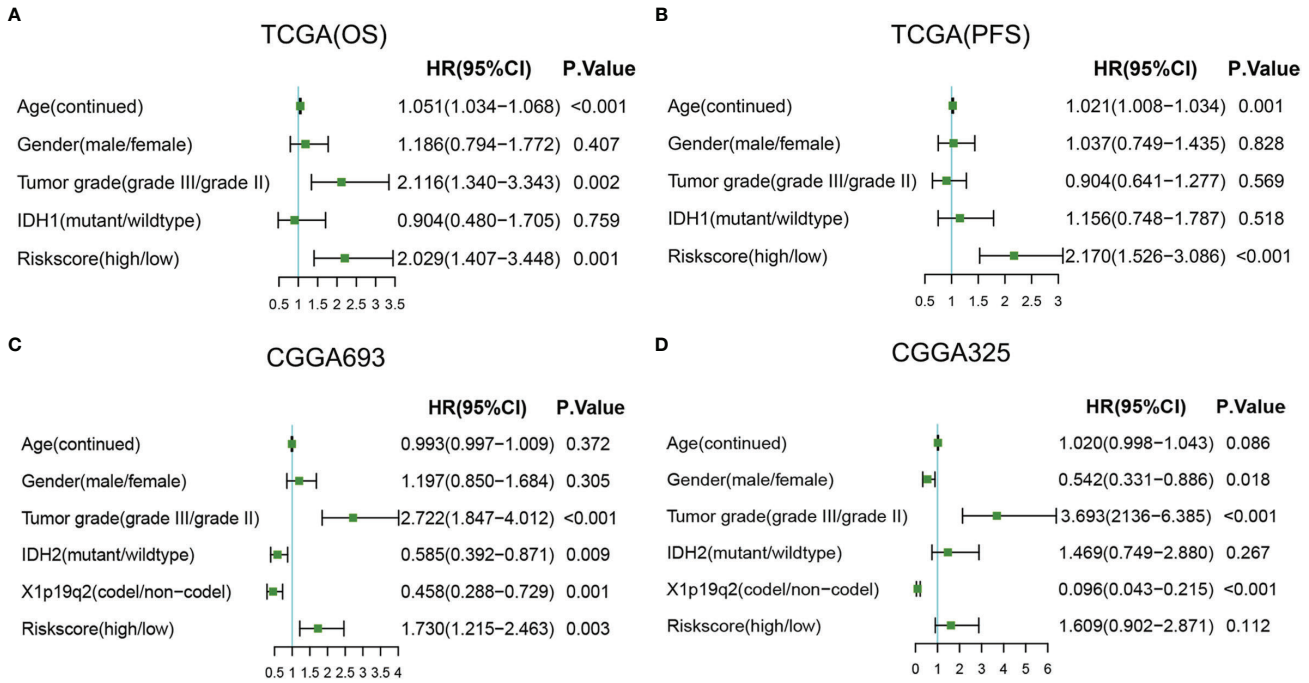

FIGURE 7 | Forest plots of multivariate Cox regression. **(A)** Forest plots of multivariate Cox regression in TCGA (OS). **(B)** Forest plots of multivariate Cox regression in TCGA (PFS). **(C)** Forest plots of multivariate Cox regression in CGGA693. **(D)** Forest plots of multivariate Cox regression in CGGA325. A, astrocytoma; OA, oligoastrocytoma; O, oligodendroglioma; TCGA, The Cancer Genome Atlas; OS, overall survival; PFS, progression-free survival.

Hypoxia is a marker of the tumor microenvironment and plays an important role in tumor occurrence, development, metastasis, and metabolism (23). The relationship between hypoxia and radiotherapy is complex. ROS are essential for destroying tumor cells by ionizing radiation. Under hypoxia, oxygen reduction interferes with ROS produced by ionizing radiation, and tumor cells have developed various mechanisms for evading apoptosis mediated by HIF-1 (24). Tumor hypoxia is a serious problem for radiotherapy because radiosensitivity is gradually limited when partial oxygen pressure in the tumor is low (25).

In this study, 6,327 hypoxia-related genes were downloaded from the GeneCards website. We identified genes of the radiotherapy-related model by WGCNA. Further log-rank tests and Lasso Cox regression analyses were performed to identify 12 genes in patients who received radiotherapy. A radiosensitivity-related risk score model was established based on the OS of TCGA dataset in patients who received radiotherapy. Then, this model was validated based on the PFS of TCGA dataset and two CGGA datasets. This radiosensitivity-related risk score model has prognostic prediction ability and is an independent prognostic indicator in LGG.

Of the 12 model genes, *PARD6A*, *RIOK3*, *SIGMAR1*, *TCEAL1*, and *UROS* expression levels were positively correlated with favorable outcomes, whereas *AGK*, *ETV4*, *PTP4A2*, *SLC34A2*, *SMURF1*, *STK33*, *RCN1*, *SPP1*, *RPN2*, and *ATP2A2* expression levels were associated with adverse outcomes. *AGK* (acylglycerol kinase) is a lipid kinase. The *AGK-PTEN* axis is a key pathway that coordinates the glycolysis and the function of CD8+ T cells (26). There have been many research findings that *AGK* is overexpressed in many cancers, such as gastric cancer (27) and cervical squamous cell cancer (28). In glioma, the expression level of *AGK* was identified as an independent prognostic factor and associated with the poor prognosis (29). *ETV4* (ETS Translocation Variant 4) is one of an *ETS* family transcription factor and is aberrantly expressed in a variety of human tumors such as prostate cancer (30) and non-small cell lung cancer (31). *ETV4* plays a wide role in the regulation of hypoxic genes (32). The *RAS-RAF-MEK-ERK* (MAPK) signaling pathway and *PI3K/Akt* signaling can activate *ETV4* expression in cancer (33). *PTP4A2* (protein tyrosine phosphatase 4A2) is associated with the overall and disease-free survival of breast cancer (34). Du et al. found that high *PTP4A2* expression is associated with ROS-induced cell death, which may contribute to cancer patient survival and response to radiotherapy (35). *RIOK3* expression is increased during hypoxic exposure and increases cell migration and invasion in cancer (36). High *RIOK3* levels in gliomas contribute to proliferation, migration, and invasion of glioma cells (37). *SLC34A2* (solute carrier family 34 member A2) is a member of the *SLC34* family and is usually overexpressed in glioma tissues and cell lines. *SLC34A2* knockdown exhibited suppressive effects on cell proliferation and migration/invasion (38). *SMURF1* is involved in the regulation of cellular processes, including autophagy, growth, and cell migration. Chang et al. proved that *SMURF1* was associated with glioma cell migration (39). *STK33* (serine/threonine kinase 33) is a serine/threonine kinase and plays an important role in cancer cell proliferation (40). *TFPI* (tissue factor pathway inhibitor) has been

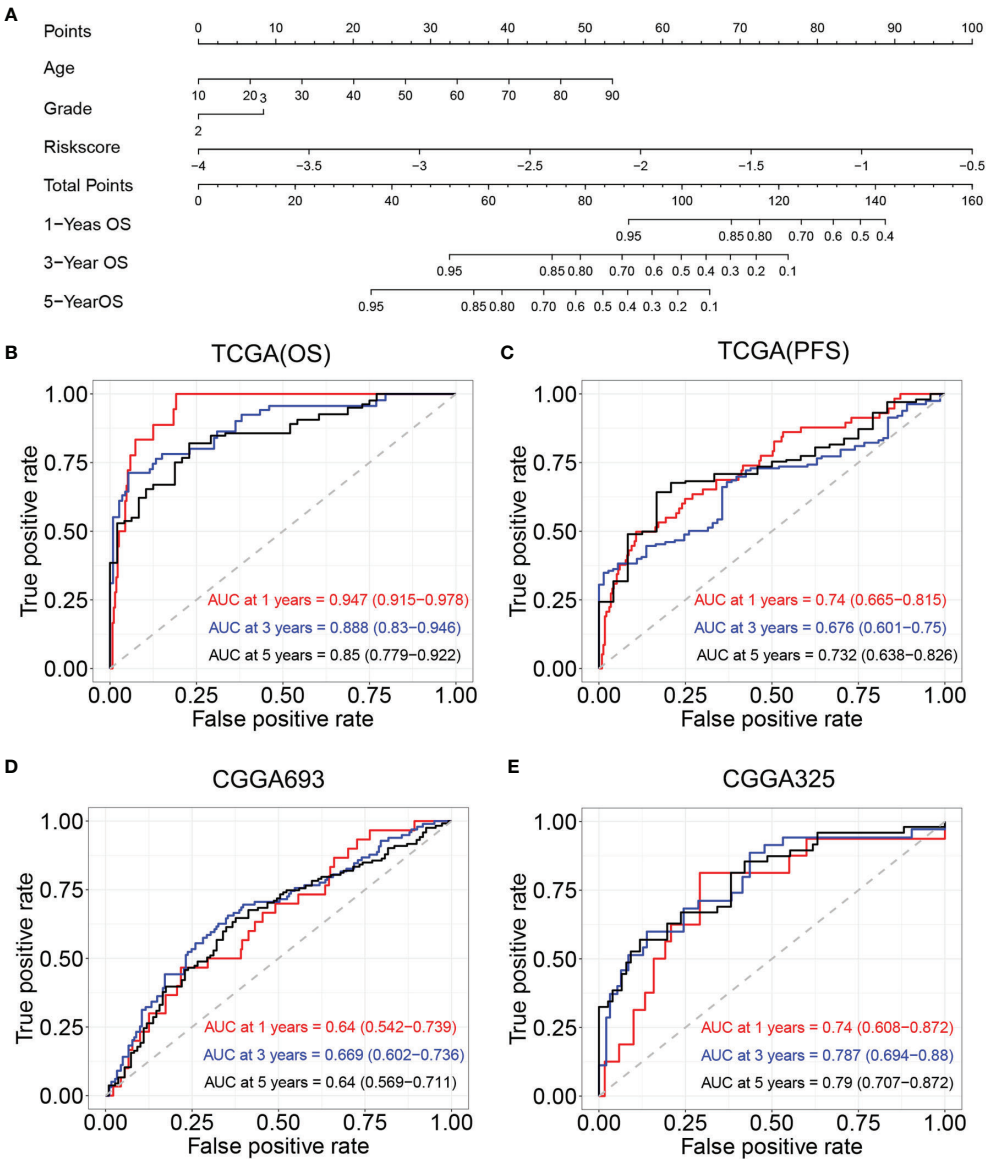

FIGURE 8 | Construction and validation of nomogram model. **(A)** Nomogram model for predicting the probability of 1-, 3-, and 5-year OS in LGGs. **(B)** Time-dependent ROC curve analyses of the nomogram model in TCGA (OS). **(C)** Time-dependent ROC curve analyses of the nomogram model in TCGA (PFS). **(D)** Time-dependent ROC curve analyses of the nomogram model in the CGGA693. **(E)** Time-dependent ROC curve analyses of the nomogram model in the CGGA325. OS, overall survival; LGGs, lower-grade gliomas; ROC, receiver operating characteristic; TCGA, The Cancer Genome Atlas; PFS, progression-free survival.

associated with radiosensitivity or radiosensitivity in previous studies (41). However, we were unable to find a report about the relationship between LGG and *PARD6A* (partitioning defective 6 homolog alpha), *SIGMAR1* (sigma non-opioid intracellular receptor 1), *TCEAL1* (transcription elongation factor A-like 1) and *UROS* (uroporphyrinogen synthase) genes.

A novel nomogram model integrating risk score with age and tumor grade was developed to predict the OS of LGG patients. We also validated the nomogram model in two CGGA datasets. According to the radiosensitivity-related risk score and nomogram, clinicians can be able to identify a group of patients who can benefit better from radiotherapy and then can predict the 1-, 3-, and 5-year OS of LGG. Nomograms could provide probabilistic predictions for individual patients. In our study, we constructed a nomogram that can predict the OS in LGG patients. The survival rates in CGGA datasets indicate that the nomogram had a good predictive performance. At the same time, the nomogram model that integrated risk score with age and tumor grade had better predictive performance than the model constructed by a radiosensitivity-related risk score factor.

Much work thus far has focused on the relationship between hypoxia and radiotherapy in tumors. Hypoxia is an important characteristic of the tumor microenvironment, and it is closely related to the occurrence and development of tumors.

Several hypoxia genes have been used to develop gene expression signatures for evaluating tumor prognosis. Liu et al. identified low hypoxia status and high immune status as factors for gastric cancer patients' OS and developed a hypoxia-immune-based gene signature (42). A hypoxia risk model was developed in TCGA and validated in CGGA to reflect overall immune response intensity in the glioma microenvironment (11). The hypoxia-related signature was also developed and validated in breast cancer (43) and lung adenocarcinoma (44). To our knowledge, this is the first study to construct a model to predict radiotherapy sensitivity from hypoxia genes from the perspective of radiotherapy.

Our study provides new insights into the individualized treatment for LGG. The main strength of this study is that the WGCNA method was used to construct a radiosensitivity-related model in LGG patients. WGCNA can use all genes to identify the gene set of interest, and it can be associated with the sample phenotype. At the same time, WGCNA can also be applied to small samples (21). Considering the importance of hypoxia genes in the tumor microenvironment, we selected hypoxia genes to be included in the study. We focused on radiotherapy, so we used WGCNA to select the gene module most related to radiotherapy. Then Lasso Cox was used to select genes. Finally, a radiosensitivity-related model based on hypoxia genes was developed in TCGA dataset and validated in CGGA datasets. The radiosensitivity-related model can identify LGG patients most likely to benefit from radiotherapy. However, a limitation of our study is that this was a retrospective study, and the models should be further confirmed by prospective studies. From the perspective of clinical treatment, the risk score we constructed can select the people who benefit from radiotherapy, so as to improve the effect of radiotherapy. On the other hand, we can develop a test kit according to the risk score for clinical application.

In conclusion, the radiosensitivity-related score was demonstrated to be an independent prognostic factor for LGG patients. Patients with LGG can be divided into the RS and RR groups by radiosensitivity-related score. The patients in the RS group were more likely to benefit from radiotherapy. This model can be used by clinicians and researchers to predict patient survival rates and achieve personalized treatment of LGG.

DATA AVAILABILITY STATEMENT

Publicly available datasets were analyzed in this study. We obtained the patients with LGG datasets from TCGA (http://cancergenome.nih.gov/) and CGGA (http://www.cgga.org.cn/).

AUTHOR CONTRIBUTIONS

Study conception and design: ZD, HSL, SL, and ZT. Data collection and cleaning: ZD, DY, LB, and SL. Real data analysis and interpretation: ZD, HJL, SP, SL, and JC. Drafting of the manuscript: ZD, HSL, HJL, DY, JC, and ZT. All authors listed have made a substantial, direct, and intellectual contribution to the work and approved it for publication.

FUNDING

This work was supported in part by the National Natural Science Foundation of China (81773541), funded by the Priority Academic Program Development of Jiangsu Higher Education Institutions at Soochow University, the State Key Laboratory of Radiation Medicine and Protection (GZK1201919) to ZT, National Natural Science Foundation of China (81872552, U1967220) to JC. This work was also supported by the Jiangsu higher education institution innovative research team for science and technology (2021), Key technology program of Suzhou people's livelihood technology projects (Grant No. SKY2021029), Key programs of the Suzhou Vocational Health College (Grant No. szwzy202102), and Qing-Lan Project of Jiangsu Province in China (2021).

SUPPLEMENTARY MATERIAL

The Supplementary Material for this article can be found online at: https://www.frontiersin.org/articles/10.3389/fonc.2022.757686/full#supplementary-material

Supplementary Figure 1 | The definition of radiosensitivity and radioresistant. **(A)** Definition of radiosensitivity. **(B)** Definition of non-radiosensitivity. RR, radioresistant; NRT, non-radiotherapy; RS, radiosensitivity; RT, radiotherapy.

Supplementary Figure 2 | The clustering tree of samples. **(A)** The clustering tree of outliers is not removed. **(B)** The clustering tree of samples without outliers.

Supplementary Figure 3 | Forest plots of univariate Cox regression. **(A)** Forest plots of univariate Cox regression in TCGA (OS). **(B)** Forest plots of univariate Cox regression in TCGA (PFS). **(C)** Forest plots of univariate Cox regression in CGGA693. **(D)** Forest plots of univariate Cox regression in CGGA325. A, Astrocytoma; OA, Oligoastrocytoma; O, Oligodendroglioma.

REFERENCES

1. Cancer Genome Atlas Research Netwrok, Brat DJ, Verhaak RG, Aldape KD, Yung WK, Salama SR, et al. Comprehensive, Integrative Genomic Analysis of Diffuse Lower-Grade Gliomas. *N Engl J Med* (2015) 372(26):2481–98. doi: 10.1056/NEJMoa1402121
2. Wesseling P, Capper D. WHO 2016 Classification of Gliomas. *Neuropathol Appl Neurobiol* (2018) 44(2):139–50. doi: 10.1111/nan.12432
3. Wang TJC, Mehta MP. Low-Grade Glioma Radiotherapy Treatment and Trials. *Neurosurg Clin N Am* (2019) 30(1):111–8. doi: 10.1016/j.nec.2018.08.008
4. Nunna RS, Khalid S, Ryoo JS, Sethi A, Byrne RW, Mehta AI. Radiotherapy in Adult Low-Grade Glioma: Nationwide Trends in Treatment and Outcomes. *Clin Transl Oncol* (2021) 23(3):628–37. doi: 10.1007/s12094-020-02458-9
5. Augustin RC, Delgoffe GM, Najjar YG. Characteristics of the Tumor Microenvironment That Influence Immune Cell Functions: Hypoxia, Oxidative Stress, Metabolic Alterations. *Cancers (Basel)* (2020) 12(12):3802. doi: 10.3390/cancers12123802
6. Vito A, El-Sayes N, Mossman K. Hypoxia-Driven Immune Escape in the Tumor Microenvironment. *Cells* (2020) 9(4):992. doi: 10.3390/cells9040992
7. Shen H, Cook K, Gee HE, Hau E. Hypoxia, Metabolism, and the Circadian Clock: New Links to Overcome Radiation Resistance in High-Grade Gliomas. *J Exp Clin Cancer Res* (2020) 39(1):129. doi: 10.1186/s13046-020-01639-2
8. Horsman MR, Overgaard J. The Impact of Hypoxia and Its Modification of the Outcome of Radiotherapy. *J Radiat Res* (2016) 57(Suppl 1):i90–i8. doi: 10.1093/jrr/rrw007

9. Roy S, Kumaravel S, Sharma A, Duran CL, Bayless KJ, Chakraborty S. Hypoxic Tumor Microenvironment: Implications for Cancer Therapy. *Exp Biol Med (Maywood)* (2020) 245(13):1073–86. doi: 10.1177/1535370220934038
10. Hill RP, Bristow RG, Fyles A, Koritzinsky M, Milosevic M, Wouters BG. Hypoxia and Predicting Radiation Response. *Semin Radiat Oncol* (2015) 25 (4):260–72. doi: 10.1016/j.semradonc.2015.05.004
11. Lin W, Wu S, Chen X, Ye Y, Weng Y, Pan Y, et al. Characterization of Hypoxia Signature to Evaluate the Tumor Immune Microenvironment and Predict Prognosis in Glioma Groups. *Front Oncol* (2020) 10:796. doi: 10.3389/fonc.2020.00796
12. Wang Y, Liu X, Guan G, Zhao W, Zhuang M. A Risk Classification System With Five-Gene for Survival Prediction of Glioblastoma Patients. *Front Neurol* (2019) 10:745. doi: 10.3389/fneur.2019.00745
13. Xiao K, Liu Q, Peng G, Su J, Qin CY, Wang XY. Identification and Validation of a Three-Gene Signature as a Candidate Prognostic Biomarker for Lower Grade Glioma. *PeerJ* (2020) 8:e8312. doi: 10.7717/peerj.8312
14. Li Z, Cai S, Li H, Gu J, Tian Y, Cao J. Developing a lncRNA Signature to Predict the Radiotherapy Response of Lower-Grade Gliomas Using Co-Expression and ceRNA Network Analysis. *Front Oncol* (2021) 11:622880. doi: 10.3389/fonc.2021.622880
15. Zhu Y, Qiu P, Ji Y. TCGA-Assembler: Open-Source Software for Retrieving and Processing TCGA Data. *Nat Methods* (2014) 11(6):599–600. doi: 10.1038/nmeth.2956
16. Kuhn RM, Haussler D, Kent WJ. The UCSC Genome Browser and Associated Tools. *Brief Bioinform* (2013) 14(2):144–61. doi: 10.1093/bib/bbs038
17. Wang Y, Qian T, You G, Peng X, Chen C, You Y, et al. Localizing Seizure-Susceptible Brain Regions Associated With Low-Grade Gliomas Using Voxel-Based Lesion-Symptom Mapping. *Neuro Oncol* (2015) 17(2):282–8. doi: 10.1093/neuonc/nou130
18. Liu X, Li Y, Qian Z, Sun Z, Xu K, Wang K, et al. A Radiomic Signature as a Non-Invasive Predictor of Progression-Free Survival in Patients With Lower-Grade Gliomas. *NeuroImage Clin* (2018) 20:1070–7. doi: 10.1016/j.nicl.2018.10.014
19. Bao ZS, Chen HM, Yang MY, Zhang CB, Yu K, Ye WL, et al. RNA-Seq of 272 Gliomas Revealed a Novel, Recurrent PTPRZ1-MET Fusion Transcript in Secondary Glioblastomas. *Genome Res* (2014) 24(11):1765–73. doi: 10.1101/gr.165126.113
20. Zhao Z, Meng F, Wang W, Wang Z, Zhang C, Jiang T. Comprehensive RNA-Seq Transcriptomic Profiling in the Malignant Progression of Gliomas. *Sci Data* (2017) 4:170024. doi: 10.1038/sdata.2017.24
21. Langfelder P, Horvath S. WGCNA: An R Package for Weighted Correlation Network Analysis. *BMC Bioinform* (2008) 9:559. doi: 10.1186/1471-2105-9-559
22. Yu G, Wang LG, Han Y, He QY. Clusterprofiler: An R Package for Comparing Biological Themes Among Gene Clusters. *OMICS* (2012) 16(5):284–7. doi: 10.1089/omi.2011.0118
23. Mylonis I, Simos G, Paraskeva E. Hypoxia-Inducible Factors and the Regulation of Lipid Metabolism. *Cells* (2019) 8(3):214. doi: 10.3390/cells8030214
24. Manoochehri Khoshinani H, Afshar S, Najafi R. Hypoxia: A Double-Edged Sword in Cancer Therapy. *Cancer Invest* (2016) 34(10):536–45. doi: 10.1080/07357907.2016.1245317
25. Amberger-Murphy V. Hypoxia Helps Glioma to Fight Therapy. *Curr Cancer Drug Targets* (2009) 9(3):381–90. doi: 10.2174/156800909788166637
26. Hu Z, Qu G, Yu X, Jiang H, Teng XL, Ding L, et al. Acylglycerol Kinase Maintains Metabolic State and Immune Responses of CD8(+) T Cells. *Cell Metab* (2019) 30(2):290–302.e5. doi: 10.1016/j.cmet.2019.05.016
27. Huang S, Cao Y, Guo H, Yao Y, Li L, Chen J, et al. Up-Regulated Acylglycerol Kinase (AGK) Expression Associates With Gastric Cancer Progression Through the Formation of a Novel YAP1-AGK-Positive Loop. *J Cell Mol Med* (2020) 24(19):11133–45. doi: 10.1111/jcmm.15613
28. Sun F, Xiong Y, Zhou XH, Li Q, Xiao L, Long P, et al. Acylglycerol Kinase Is Over-Expressed in Early-Stage Cervical Squamous Cell Cancer and Predicts Poor Prognosis. *Tumour Biol* (2016) 37(5):6729–36. doi: 10.1007/s13277-015-4498-4
29. Liu N, Wang Z, Cheng Y, Zhang P, Wang X, Yang H, et al. Acylglycerol Kinase Functions as an Oncogene and an Unfavorable Prognostic Marker of Human Gliomas. *Hum Pathol* (2016) 58:105–12. doi: 10.1016/j.humpath.2016.07.034
30. Qi M, Liu Z, Shen C, Wang L, Zeng J, Wang C, et al. Overexpression of ETV4 Is Associated With Poor Prognosis in Prostate Cancer: Involvement of uPA/uPAR and MMPs. *Tumour Biol* (2015) 36(5):3565–72. doi: 10.1007/s13277-014-2993-7
31. Wang Y, Ding X, Liu B, Li M, Chang Y, Shen H, et al. ETV4 Overexpression Promotes Progression of Non-Small Cell Lung Cancer by Upregulating PXN and MMP1 Transcriptionally. *Mol Carcinog* (2020) 59(1):73–86. doi: 10.1002/mc.23130
32. Wollenick K, Hu J, Kristiansen G, Schraml P, Rehrauer H, Berchner-Pfannschmidt U, et al. Synthetic Transactivation Screening Reveals ETV4 as Broad Coactivator of Hypoxia-Inducible Factor Signaling. *Nucleic Acids Res* (2012) 40(5):1928–43. doi: 10.1093/nar/gkr978
33. Qi T, Qu Q, Li G, Wang J, Zhu H, Yang Z, et al. Function and Regulation of the PEA3 Subfamily of ETS Transcription Factors in Cancer. *Am J Cancer Res* (2020) 10(10):3083–105.
34. Andres SA, Wittliff JL, Cheng A. Protein Tyrosine Phosphatase 4A2 Expression Predicts Overall and Disease-Free Survival of Human Breast Cancer and Is Associated With Estrogen and Progestin Receptor Status. *Horm Cancer* (2013) 4(4):208–21. doi: 10.1007/s12672-013-0141-2
35. Du X, Zhang Y, Li X, Li Q, Wu C, Chen G, et al. PRL2 Serves as a Negative Regulator in Cell Adaptation to Oxidative Stress. *Cell Biosci* (2019) 9:96. doi: 10.1186/s13578-019-0358-z
36. Singleton DC, Rouhi P, Zois CE, Haider S, Li JL, Kessler BM, et al. Hypoxic Regulation of RIOK3 Is a Major Mechanism for Cancer Cell Invasion and Metastasis. *Oncogene* (2015) 34(36):4713–22. doi: 10.1038/onc.2014.396
37. Zhang T, Ji D, Wang P, Liang D, Jin L, Shi H, et al. The Atypical Protein Kinase RIOK3 Contributes to Glioma Cell Proliferation/Survival, Migration/Invasion and the AKT/mTOR Signaling Pathway. *Cancer Lett* (2018) 415:151–63. doi: 10.1016/j.canlet.2017.12.010
38. Bao Z, Chen L, Guo S. Knockdown of SLC34A2 Inhibits Cell Proliferation, Metastasis, and Elevates Chemosensitivity in Glioma. *J Cell Biochem* (2019) 120(6):10205–14. doi: 10.1002/jcb.28305
39. Chang H, Zhang J, Miao Z, Ding Y, Xu X, Zhao X, et al. Suppression of the Smurf1 Expression Inhibits Tumor Progression in Gliomas. *Cell Mol Neurobiol* (2018) 38(2):421–30. doi: 10.1007/s10571-017-0485-1
40. Zhou B, Xiang J, Zhan C, Liu J, Yan S. STK33 Promotes the Growth and Progression of Human Pancreatic Neuroendocrine Tumour *via* Activation of the PI3K/AKT/mTOR Pathway. *Neuroendocrinology* (2020) 110(3-4):307–20. doi: 10.1159/000501829
41. Hall JS, Iype R, Senra J, Taylor J, Armenoult L, Oguejiofor K, et al. Investigation of Radiosensitivity Gene Signatures in Cancer Cell Lines. *PloS One* (2014) 9(1):e86329. doi: 10.1371/journal.pone.0086329
42. Liu Y, Wu J, Huang W, Weng S, Wang B, Chen Y, et al. Development and Validation of a Hypoxia-Immune-Based Microenvironment Gene Signature for Risk Stratification in Gastric Cancer. *J Transl Med* (2020) 18(1):201. doi: 10.1186/s12967-020-02366-0
43. Mo Z, Yu L, Cao Z, Hu H, Luo S, Zhang S. Identification of a Hypoxia-Associated Signature for Lung Adenocarcinoma. *Front Genet* (2020) 11:647. doi: 10.3389/fgene.2020.00647
44. Wang J, Wang Y, Xing P, Liu Q, Zhang C, Sui Y, et al. Development and Validation of a Hypoxia-Related Prognostic Signature for Breast Cancer. *Oncol Lett* (2020) 20(2):1906–14. doi: 10.3892/ol.2020.11733

Conflict of Interest: The authors declare that the research was conducted in the absence of any commercial or financial relationships that could be construed as a potential conflict of interest.

Publisher's Note: All claims expressed in this article are solely those of the authors and do not necessarily represent those of their affiliated organizations, or those of the publisher, the editors and the reviewers. Any product that may be evaluated in this article, or claim that may be made by its manufacturer, is not guaranteed or endorsed by the publisher.

frontiers | Frontiers in Oncology

ORIGINAL RESEARCH
published: 10 May 2022
doi: 10.3389/fonc.2022.781818

Hippocampal Metastasis Rate Based on Non-Small Lung Cancer TNM Stage and Molecular Markers

Sung Jun Ahn[1†], Hyeokjin Kwon[2†], Jun Won Kim[3], Goeun Park[4], Mina Park[1], Bio Joo[1], Sang Hyun Suh[1], Yoon Soo Chang[5] and Jong-Min Lee[6]*

[1] Department of Radiology, Gangnam Severance Hospital, Yonsei University, College of Medicine, Seoul, South Korea, [2] Department of Electronic Engineering, Hanyang University, Seoul, South Korea, [3] Department of Radiation Oncology, Gangnam Severance Hospital, Yonsei University, College of Medicine, Seoul, South Korea, [4] Biostatistics Collaboration Unit, Yonsei University College of Medicine, Seoul, South Korea, [5] Department of Internal Medicine, Gangnam Severance Hospital, Yonsei University, College of Medicine, Seoul, South Korea, [6] Department of Biomedical Engineering, Hanyang University, Seoul, South Korea

OPEN ACCESS

Edited by:
Alfredo Conti,
University of Bologna, Italy

Reviewed by:
Manjari Pandey,
Geisinger Commonwealth School of Medicine, United States
Antonio Pontoriero,
University of Messina, Italy

***Correspondence:**
Jong-Min Lee
ljm@hanyang.ac.kr

[†]These authors have contributed equally to this work

Specialty section:
This article was submitted to Neuro-Oncology and Neurosurgical Oncology, a section of the journal Frontiers in Oncology

Received: *23 September 2021*
Accepted: *04 April 2022*
Published: *10 May 2022*

Citation:
Ahn SJ, Kwon H, Kim JW, Park G, Park M, Joo B, Suh SH, Chang YS and Lee J-M (2022) Hippocampal Metastasis Rate Based on Non-Small Lung Cancer TNM Stage and Molecular Markers. Front. Oncol. 12:781818. doi: 10.3389/fonc.2022.781818

Hippocampal-avoidance whole-brain radiation therapy (HA-WBRT) is justified because of low hippocampal brain metastases (BM) rate and its prevention of cognitive decline. However, we hypothesize that the risk of developing BM in the hippocampal-avoidance region (HAR) may differ depending on the lung-cancer stage and molecular status. We retrospectively reviewed 123 patients with non-small cell lung cancer (NSCLC) at the initial diagnosis of BM. The number of BMs within the HAR (5 mm expansion) was counted. The cohort was divided into patients with and without BMs in the HAR, and their clinical variables, TNM stage, and epidermal growth factor receptor (EGFR) status were compared. The most influential variable predicting BMs in the HAR was determined using multi-variable logistic regression, classification and regression tree (CART) analyses, and gradient boosting method (GBM). The feasibility of HAR expansion was tested using generalized estimating equation marginal model. Patients with BMs in the HAR were more frequently non-smokers, and more likely to have extra-cranial metastases and EGFR mutations ($p<0.05$). Multi-variable analysis revealed that extra-cranial metastases were independently associated with the presence of BM in the HAR (odds ratio=8.75, $p=0.04$). CART analysis and GBM revealed that the existence of extra-cranial metastasis was the most influential variable predicting BM occurrence in the HAR (variable importance: 23% and relative influence: 37.38). The estmated BM incidence of patients without extra-cranial metastases in th extended HAR (7.5-mm and 10-mm expansion) did not differ significantly from that in the conventional HAR. In conclusion, NSCLC patients with extra-cranial metastases were more likely to have BMs in the HAR than those without extra-cranial metastases.

Keywords: Non-small cell lung cancer, Brain metastasis, Hippocampal-avoidance whole-brain radiation therapy, Epidermal growth factor receptor, lung-cancer stage

INTRODUCTION

The brain is a common site of distant metastasis in patients with non-small cell lung cancer (NSCLC) (1, 2). The overall incidence of brain metastases (BMs) is estimated to be 10-20% at initial presentation, but can increase up to 40% throughout the clinical course (3, 4). Recently, epidermal growth factor receptor (EGFR) gene mutations and anaplastic lymphoma kinase (ALK) rearrangements have been identified as significant risk factors for the development of BMs (5–7). Although molecular targeted therapy against mutated driver oncogene such as EGFR or ALK has improved the survival rates of patients with lung cancer, BMs remain an important cause of morbidity and are associated with progressive neurologic deficits (8, 9).

Whole-brain radiation therapy (WBRT) has been the standard of care for patients with multiple BMs. However, most patients experience cognitive deterioration after WBRT, which raises concerns about its toxicity (10–12). Accumulating evidence suggests that neural stem cells in the hippocampus are exquisitely sensitive to therapeutic doses of cranial radiation, which is believed to be a key mechanism underlying the cognitive decline after WBRT (13–15). Intensity-modulated radiotherapy techniques, developed to avoid the hippocampal neural stem-cell niche during WBRT to prevent these adverse effects, reduce the mean dose to this neural stem-cell compartment by ≥80% (15, 16). An international multi-institutional single-arm phase II trial (RTOG 0933) showed that hippocampal-avoidance WBRT (HA-WBRT) prevented cognitive decline in patients with BMs (17). In this study, the mean relative decline in Hopkins Verbal Learning Test-Revised Delayed Recall at 4 months was 7.0%, significantly lower in comparison with that of historical controls treated with WBRT (30%). A prospective multi-institutional randomized phase III trial (NRG CC001) demonstrated that HA-WBRT plus memantine prevented deterioration in executive function at 4 months (23.3% vs. 40.4%) and learning and memory function at 6 months (11.5% vs. 24.7%), as well as alleviated patient-reported symptoms, with no difference in the intracranial progression-free survival and overall survival compared with those treated with WBRT plus memantine (18). On the basis of a recent phase III study of 150 patients with small cell lung cancer, the HA-PCI arm showed a lower decline in the delayed free recall test after 3 months compared with the standard PCI arm (5.8% vs. 23.5%). However, incidence of BMs, overall survival and quality of life were not significantly different between groups (19). Few proactive studies have indicated extending the radiation protected zone from the hippocampus to the limbic system, which is known to regulate memory and emotions (20, 21).

However, for patients with multiple BMs, HA-WBRT is accompanied by the possibility of BMs occurring in the hippocampus after HA-WBRT, leading to treatment failure. Few studies have estimated the risk of metastases in the hippocampal-avoidance region (HAR). A pioneer study with 371 BMs from several primary cancers supported the use of HA-WBRT owing to a low BM rate in the HAR (8.6% of patients) (22). However, the cohort of this study was limited to patients with ≤10 BMs where stereotactic radiosurgery might be preferred over WBRT. A more recent study with 116 patients with BMs reported a slightly higher risk of BMs (11.2%) in the HAR (23). However, it did not conduct risk stratification for the development of BMs in this region. Information about the incidence of hippocampal BM according to the lung cancer stage or EGFR/ALK mutation status can serve as a good guide for the indication for HA-WBRT. Thus, this study aimed to estimate the incidence of BM in the hippocampus in patients with NSCLC as stratified according to the 8th edition of the American Joint Committee on Cancer (AJCC) staging system and EGFR/ALK mutation status.

MATERIALS AND METHODS

Participants

This retrospective study was approved by our institutional review board, which waived the requirement for informed patient consent. We retrospectively searched the electronic medical records to identify lung cancer patients undergoing brain magnetic resonance imaging (MRI) for evaluation of BMs between April 2017 and October 2020. From 1092 available brain MRIs, we excluded 969 for the following reasons: (1) negative BMs (n=633), (2) history of neurosurgery or brain radiation therapy (n=283), (3) presence of other malignant diseases (n=24), (4) primary small cell lung cancer (n=22) and (5) motion or dental material artifacts on the MRIs (n=7). Finally, 123 NSCLC patients with 123 brain MR images showing BMs were included in this study. BMs were considered to be positive when (1) the clinical-radiologic consensus was compatible with BMs, (2) BM was confirmed at pathology with stereotactic biopsy or metastasectomy, (3) lesions suspected to be BMs increased in size at follow-up MRI or (4) decrease in size with treatment (4). The histopathological diagnoses of lung cancer were obtained using bronchoscopic, percutaneous needle-guided, or surgical biopsies for all patients. To determine the EGFR mutation status, DNA was extracted using a DNeasy isolation kit (Qiagen, Valencia, CA, USA) from FFPE tissues according to the manufacturer's instructions. For the EGFR gene, direct DNA sequencing of exons 18 through 21 or PNAClampTM EGFR Mutation Detection Kit (PANAGENE, Daejeon, Korea) was performed. Each case was classified as positive or negative for a mutation based on comparison with the wild-type sequence. To identify ALK and ROS1 rearrangements, fluorescent *in situ* hybridization was performed using a break-apart ALK or ROS1 probe (Vysis LSI Dual Color, Break Apart Rearrangement Probe; Abbott Molecular, Abbot Park, IL, USA), respectively. ALK or ROS1 rearrangements were scored as positive when more than 15% of tumor cells displayed split signals or isolated signals containing a kinase domain (red for ALK and green for ROS1).

All data were completely anonymized, and all experiments were conducted in accordance with the approved guidelines.

Staging

NSCLC staging was performed according to the 8th edition of AJCC guidelines without considering the BMs (24). The tumor–node–metastasis (TNM) stage at the diagnosis of lung cancer was based on computed tomography (CT) scans of the chest and abdomen, whole-bone scanning, and positron-emission

tomography-CT, which were acquired as a part of initial evaluation for NSCLC. Extra-cranial metastasis at BM occurrence was based on the last CT and PET-CT work-up before the detection of BMs. Extra-cranial metastasis was defined as (1) tumor in the contralateral lung, (2) pleural/pericardial nodule, malignant effusion, or (3) extra-thoracic metastasis other than BMs.

MRI and Preprocessing

Routine MRIs for the evaluation of BMs were acquired using the Siemens 3T Vida (Siemens Healthineers, Erlangen, Germany) or GE 3T Discovery MR750 (GE Healthcare, Milwaukee, WI, USA) scanner. Our brain MRI protocol for the Siemens 3T scanner included the acquisition of T1-weighted three-dimensional (3D) magnetization-prepared rapid acquisition with gradient echo (MPRAGE) imaging. A 3D turbo spin-echo T1-weighted image (SPACE) was acquired after administering gadobutrol 0.2 mmol/kg (Gadovist, Bayer Schering Pharma; Berlin, Germany). The sequence parameters for the 3D T1-weighted MPRAGE were as follows: inversion time (TI)=900 ms, echo time (TE) 3 ms, repetition time (TR)=2300 ms, flip angle=9°, slice thickness=1 mm, field-of-view (FOV)=256 mm, matrix=256×256, slice thickness=1 mm, generalized autocalibrating partial parallel acquisition=2, and time of acquisition=5 min 12 s. The sequence parameters for 3D T1-weighted SPACE were as follows: TE=33 ms, TR=700 ms, slice thickness=0.8 mm, FOV=230 mm, matrix=288×288, slice thickness=0.8 mm, acceleration factor of compressed sensing=9, and time of acquisition=3 min 44 s. A corresponding sequence was used with similar MR parameters for the GE scanner.

MRIs were processed using the FMRIB Software Library (http://www.fmrib.ox.ac.uk/fsl). A neuroradiologist labeled the BMs by manually segmenting the 3D BM volumes on the native 3D T1-weighted SPACE images. The binary labels of the BMs were transformed into the Montreal Neurological Institute (MNI) space by co-registering the 3D T1-weighted MPRAGE images to the gadolinium-enhanced 3D T1-weighted SPACE images using rigid body transformation. The native 3D T1-weighted MPRAGE images were converted to the standard MNI 152 T1-1-mm brain model using an affine transform matrix. The estimated transform matrix was concatenated with a co-registration transform matrix, and the resultant matrix was applied to 3D T1-weighted SPACE images and binary labeled BM images. The voxel for the center of gravity was localized for each BM, and binary BM masks were regenerated as spheres with a 5-mm radius to consider the origin of the BMs more accurately and to standardize their chronological development (25).

An atlas-based graph cuts algorithm was utilized to define the hippocampal region (24). First, a hippocampal atlas was manually drawn on the International Consortium for Brain Mapping 152 template. An artificial neural network classifier was used to classify the gray matter, white matter, and cerebrospinal fluid regions (26). Subsequently, voxel-wise partial volume effects (PVEs) were estimated using the trimmed minimum covariance determinant method and the PVE maps were used as a prior information for the subsequent graph cuts segmentation (27). A hippocampal foreground mask was obtained using the graph cuts method, followed by the implementation of morphological opening to limit the false positives. We empirically applied the 25% threshold level to binarize the above-mentioned atlases by visual inspection for quality checks. The HAR was generated by volumetrically expanding the outline of hippocampal mask by 5 mm to account for systematic setup errors and dose falloff between the clinical target volume for the whole brain and hippocampus (15). Consequently, we generated two additional hippocampal masks by dilating the original hippocampal mask with 7.5-mm and 10-mm margins to investigate the possibility of expanding the HAR. Lastly, we counted the number of BM samples in each hippocampal mask (**Figure 1**).

Statistical Analyses

The study cohort was divided into two groups: those with BMs in the HAR and those without BMs in the HAR. History of smoking, age, sex, T stage, N stage, M stage, TNM stage, extra-cranial metastasis at BM occurrence, histology, and EGFR/ALK/ROS1 mutation status were compared between the two groups. Independent t-tests were used for continuous variables, while the chi-squared test or Fisher's exact test was used for categorical variables. Multi-variable logistic regression analysis with backward selection was also performed to adjust for the smoking history, extra-cranial metastasis at BM occurrence, and EGFR mutation status, which were statistically significant in the univariate analysis for the comparison between the presence and absence of BM in the HAR. A decision tree model distinguishing the presence of BM in the HAR from the absence of BM in the HAR was built using classification and regression tree (CART) analysis. CART analysis selects the best predictor variable for splitting the data into two child nodes with maximal purity. The process is repeated recursively for each child node, until either the minimum size of the terminal node is reached, or no further split improves the purity of the terminal node (28). To provide a more accurate estimate of the responsible variable for BM in the HAR, a popular ensemble learning method, gradient boosting method (GBM) was additionally performed. GBM builds an ensemble of shallow and weak successive trees with each tree learning and improving on the previous (29). The proportion of BM between three HARs (hippocampus plus 5-mm margin, 7.5-mm margin, and 10-mm margin) in patients without extra-cranial metastases were compared using a generalized estimating equation (GEE) marginal model to test the feasibility of HAR expansion (30).

RESULTS

Patient Characteristics

A total of 123 patients with NSCLC with BMs were included in this study. Demographics and clinical characteristics are summarized in **Table 1**. Patients with BMs were more frequently non-smokers (83.33% versus 54.29%, p=0.02), more likely to have extra-cranial metastases (94.44% vs. 66.67%, p=0.03), and more likely to have EGFR mutations (66.67% versus 41.11%, p=0.04) than those

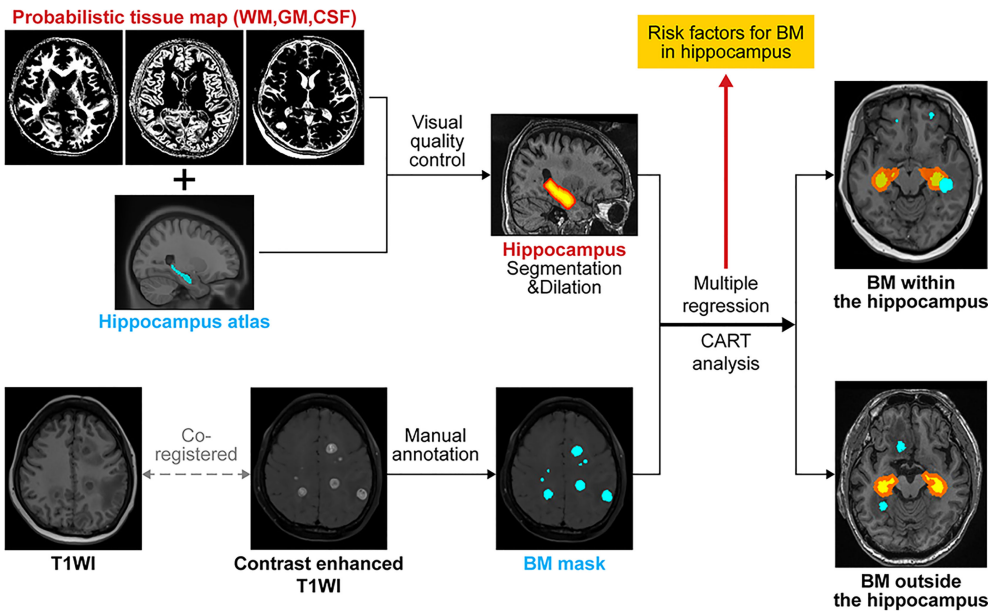

FIGURE 1 | Schematic illustration of the flow of image analysis. BM, brain metastasis; WM, white matter; GM, gray matter; CSF, cerebrospinal fluid; CART, classification and regression tree analysis; T1WI, T1 weighted imaging.

without BMs in the HAR. No significant differences in the age, sex, T stage, N stage, M stage, TNM stage, histology, ALK, and ROS1 status were observed between groups.

Most Influential Variable Predicting BM Occurrence in the HAR

Multivariable analysis did not find any independent predictor for the presence of BM in the HAR (**Table 2**). However, the model using multivariable analysis with backward elimination found that extra-cranial metastasis at BM occurrence was independently associated with the presence of BM in the HAR [odds ratio (OR) =8.75; 95% confidence interval (CI): 1.64, 162.33, p=0.04, **Supplemental Table 1**]. Fifteen patients whose EGFR mutation status was unknown were excluded from the CART analysis. BMs were present in the HAR of 17% (18/108) of patients with NSCLC. The existence of extra-cranial metastasis was the first partitioning predictor in the decision tree model (**Figure 2**). BMs were found in the HAR in 22% (17/76) of patients of NSCLC with extra-cranial metastases, while 3% (1/32) of patients with NSCLC without extra-cranial metastases showed BMs in the HAR. Further branching was based on age of 67 years, followed by duration and sex. BMs were located in the HAR of 31% of patients with NSCLC with extra-cranial metastases and those aged <67 years (13/42), while 12% of patients with NSCLC with extra-cranial metastases and those aged >67 years (4/34) presented with BMs. BMs were observed in the HAR in 41% (9/22) of patients with NSCLC with extra-cranial metastases, age <67 years, and BMs detected during follow-up, while 20% of patients with NSCLC with extra-cranial metastases, age <67 years, and BMs detected at initial screening (4/20) presented with BMs. A total of 57% of female patients with NSCLC with extra-cranial metastases, age <67 years, and BMs detected during follow-up (3/7) demonstrated BMs in the HAR, while 33% of male patients with NSCLC with extra-cranial metastases, age <67 years, and BMs detected during follow-up (5/15) had BMs. The existence of extra-cranial metastasis at BM occurrence showed the highest variable importance score, followed by TNM stage, age, BMs during the course of disease, smoking history, histology, and EGFR mutation (**Table 3**). In addition, in GBM, existence of extra-cranial metastasis demonstrated the highest prediction power for BM occurrence in the HAR, followed by sex, BMs during the course of disease, age, TNM stage, EGFR mutation, smoking history and histology.

Feasibility of Expanding the Hippocampal Avoidance Region

We analyzed whether the number of BMs in the HAR increased when the margin of region was expanded from 5 to 7.5 or 10 mm using a GEE marginal model. This analysis was performed in 36 patients with NSCLC without extra-cranial metastases because this subgroup may be suitable for HA-WBRT. The estimated proportion of the incidence of BM in the HAR was 2.78% with a standard error of 2.75%, which did not differ significantly from that of the expanded regions (hippocampus plus 7.5 mm and hippocampus plus 10 mm, p>0.99, **Supplementary Table 2**).

DISCUSSION

This study tested the hypothesis that the hippocampal metastases rate would differ based on the patient characteristics, clinical

TABLE 1 | Baseline characteristics and staging of patients with BMs from NSCLC.

		Hippocampal avoidance region		
	Total (N=123)	**Absence of BM (N=105)**	**Presence of BM (N=18)**	**p-value**
Smoking history				0.02*
Nonsmoker	72 (58.54)	57 (54.29)	15 (83.33)	
Smoker	51 (41.46)	48 (45.71)	3 (16.67)	
Age (yr)	66.66 ± 10.17	67.11 ± 10.28	64.00 ± 9.27	0.23
Sex				0.12
Male	81 (65.85)	72 (68.57)	9 (50.00)	
Female	42 (34.15)	33 (31.43)	9 (50.00)	
Detection of BM				0.07
At diagnosis of lung cancer	66 (53.66)	60 (57.14)	6 (33.33)	
During the course of disease	57 (46.34)	45 (42.86)	12 (66.67)	
Chemotherapy				0.21
No	87 (70.73)	77 (73.33)	10 (55.56)	
Yes	36 (29.27)	28 (26.67)	8 (44.44)	
T stage				0.61
T1a	1 (0.81)	1 (0.95)	0 (0.00)	
T1b	5 (4.07)	4 (3.81)	1 (5.56)	
T1c	9 (7.32)	7 (6.67)	2 (11.11)	
T2a	20 (16.26)	19 (18.10)	1 (5.56)	
T2b	13 (10.57)	11 (10.48)	2 (11.11)	
T3	20 (16.26)	18 (17.14)	2 (11.11)	
T4	55 (44.72)	45 (42.86)	10 (55.56)	
N stage				0.42
N0	25 (20.33)	24 (22.86)	1 (5.56)	
N1	6 (4.87)	5 (4.76)	1 (5.56)	
N2	38 (30.89)	32 (30.48)	6 (33.33)	
N3	54 (43.90)	44 (41.91)	10 (55.56)	
M stage				0.06
M0	46 (37.39)	43 (40.95)	3 (16.66)	
M1a	8 (6.50)	8 (7.62)	0 (0.0)	
M1b	7 (5.69)	5 (4.76)	2 (11.11)	
M1c	62 (50.41)	49 (46.67)	13 (72.22)	
TNM				0.41
Stage 1	9 (7.32)	8 (7.62)	1 (5.55)	
Stage 2	7 (5.69)	7 (6.67)	0 (0.00)	
Stage 3	29 (23.58)	27 (25.71)	2 (11.11)	
Stage 4	78 (63.41)	63 (60.00)	15 (83.34)	
Extra-cranial metastasis at BM occurrence				0.03*
Absence	36 (29.26)	35 (33.33)	1 (5.56)	
Presence	87 (70.74)	70 (66.67)	17 (94.44)	
Histology				0.22
Adenocarcinoma	98 (79.67)	81 (77.14)	17 (94.44)	
Squamous cell carcinoma	14 (11.38)	14 (13.33)	0 (0.00)	
Large cell carcinoma	11 (8.94)	10 (9.52)	1 (5.56)	
EGFR				0.04*
Wild type	59 (54.63)	53 (58.89)	6 (33.33)	
Mutation	49 (45.37)	37 (41.11)	12 (66.67)	
ALK				0.53
Negative	75 (92.59)	64 (94.12)	11 (84.62)	
Positive	6 (7.41)	4 (5.88)	2 (15.38)	
ROS1				
Negative	52 (100)	9 (100)	61 (100)	
Positive	0 (0.00)	0 (0.00)	0 (0.00)	

NSCLC, non-small cell lung cancer; EGFR, epidermal growth factor receptor; ALK, anaplastic lymphoma kinase; MRI, magnetic resonance imaging; BM, brain metastasis. Asterisk (*) indicates a p-value < 0.05.

stage, and molecular markers. Our results indicated that patients with BMs in the HAR were more likely to have extra-cranial metastases before BM occurrence. The clinical implication of this observation is important because of the possibility that BMs may occur in the hippocampus after the implementation of HA-WBRT in patients with extra-cranial metastases, leading to treatment failure. Thus, different radiation therapy strategies may be necessary depending on the existence of extra-cranial

TABLE 2 | Multiple logistic regression analysis for BM occurrence in the hippocampus plus 5-mm margin region.

	OR (95% CI)	p-value
Smoker	0.34 (0.07-1.31)	0.14
Extra-cranial metastasis at BM occurrence	7.82 (1.44-145.96)	0.05
EGFR mutation	1.68 (0.51-5.84)	0.39

EGFR, epidermal growth factor receptor; BM, brain metastasis.

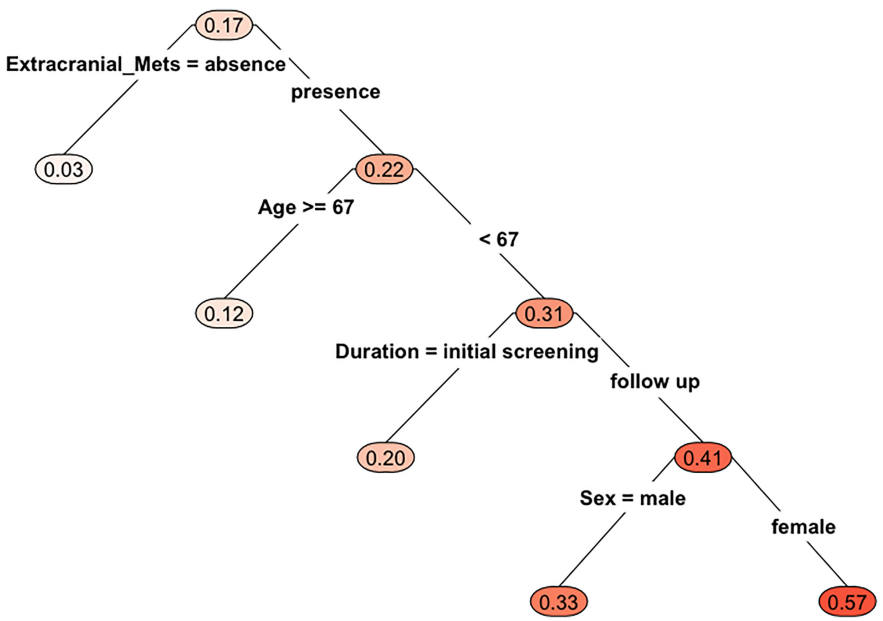

FIGURE 2 | Results of the classification and regression tree analysis (CART). Mets, metastasis.

metastasis in patients with NSCLC. Moreover, our results demonstrated that the hippocampal metastasis rate was low in patients with NSCLC without extra-cranial metastasis and this rate remained low if the avoidance zone was expanded to the hippocampus plus 10-mm region. This observation is also clinically relevant because the application of HA-WBRT to a wider safe zone in patients without extra-cranial metastases may be instrumental in ensuring successful treatment while preventing cognitive decline.

A multi-institutional study with 371 patients with 1133 BMs found BMs within the HAR in 8.6% patients, showing that HA-WBRT may be suitable for controlling BMs (22). However, a more recent single-center analysis demonstrated a relatively high incidence of BMs within the HAR in patients with NSCLC

TABLE 3 | Variables for the prediction of BM incidence in the hippocampal avoidance region using classification and regression tree analysis and gradient boosting.

Cart analysis		Gradient boosting	
Variables	**Importance(%)**	**Variables**	**Relative influence**
Extra-cranial metastasis	25	Extra-cranial metastasis	37.38
TNM stage	22	Sex	31.84
Age	20	BMs during course of disease	14.96
BMs during course of disease	15	Age	12.91
Sex	11	TNM stage	2.39
Smoking history	5	EGFR mutation	0.34
Histology	1	Smoking history	0.14
EGFR mutation	1	Histology	0

BM, brain metastases.

(11.8%, 7/59) (23). In our study, 14% of patients with NSCLC (18/123) had BMs within the HAR. This higher incidence of BMs within the HAR in recent studies can be explained by the prolonged survival of patients with widespread intracranial disease as well as screening with improved MRI techniques, which enhanced the detection of BMs (31). Our results also demonstrated that 83.3% of patients with BMs in HAR (15/18) have extensive BMs (≥10). However, patient stratification by the existence of extra-cranial metastasis revealed significant differences in hippocampal metastasis: 19.5% of patients with extra-cranial metastases (17/87) had BMs in the HAR, while 2.7% of patients without extra-cranial metastases (1/36) had BMs in the HAR. Our multivariate analysis indicated that patients with extra-cranial metastasis are 8.75 times more likely to have BMs in the HAR. CART analysis and GBM also suggested that extra-cranial metastasis was the most influential variable predicting BM occurrence in the HAR. The mechanism underlying this phenomenon is unknown. However, the presence of extra-cranial metastasis has been known as an independent prognostic factor for the survival of patients with BMs (32, 33). In addition, BMs are commonly diagnosed as associated with extra-cranial metastases (34, 35). We may infer that this extra-cranial metastatic burden may increase the risk of BM occurrence in the HAR. Hence, we concluded that HA-WBRT application is safe in patients without extra-cranial metastases; however, caution must be exercised while applying HA-WBRT to patients with extra-cranial metastases; alternatively, a different treatment strategy must be adopted. Recently, stereotactic radiosurgery (SRS) has been preferred over WBRT for limited BMs because its efficacy is non-inferior with greater preservation of neurocognitive functioning, now being applied up to 10 BMs (36, 37). Few trials have investigated the treatment of > 10 BMs with SRS alone (38, 39). Based on our results, whether presence of extra-cranial metastases may increase the risk of treatment failure or not should be considered in these trials.

According to our CART analysis, apart from extra-cranial metastases, age, BMs during course of disease, and sex were important risk factors for BM occurrence in the hippocampus. Our study demonstrated that younger patients (age <67 years) had a higher hippocampal metastasis rate than that of their older counterparts (age ≥67 years). Generally, age is a risk factor for the development BM in NSCLC. Age <60-70 years was associated with the risk of BMs (40–43). We may assume that the cerebrovascular environment in younger patients differ from that in older patients, in addition to better outcomes with a longer survival in the former, leading to higher BM prevalence. Based on the same rationale, younger patients are likely to develop BMs in the hippocampus. The reason for the greater predominance of hippocampal BMs in women during the course of the disease than that at the initial diagnosis of lung cancer is unclear. Further studies are necessary to validate this observation.

Numerous studies have reported that patients with EGFR mutations have a nearly two-fold higher risk of BMs than those without EGFR mutation (44–47). Our univariate analysis revealed that the proportion of EGFR mutation was higher in patients with BMs in the HAR (12/18, 66.67%) than in patients without BMs in the HAR (37/105, 35.24%). The mechanism underlying this phenomenon may be associated with epithelial-mesenchymal transition, which may result in the increased motility and invasiveness of tumor cells (48, 49). However, according to our multivariate analysis, EGFR mutations were not an independent risk factor for BM occurrence in the HAR. ALK-rearrangement tumors exhibit aggressive behavior, including extra-thoracic metastases (50, 51), and have a higher risk of BMs. The cumulative incidence of BMs after diagnosis reaches 58% at 3 years (52, 53). Compared with ALK rearrangement, ROS1 rearrangement is associated with lower rates of extra-thoracic metastases and fewer BMs, but it may still increase the likelihood of BMs (54, 55). Our results demonstrated a higher but not significant proportion of ALK rearrangement (2/13, 15.38%) in patients with BM in the HAR than in patients without (4/68, 5.88%), and no significant difference in the incidence of ROS1 rearrangement between groups (0/61, 0% vs. 0/9, 0%). However, these results should be carefully interpreted because of fairly low incidence in our study.

Several studies have reported the incidence of progressive leukoencephalopathy following cranial radiation (56–58). WBRT injures the small cerebral vasculature and neuropil, resulting in oligodendrocyte death and demyelination (59, 60). Accumulating evidence suggests that diseases of the white matter are associated with neurocognitive dysfunction (61, 62). Injury to the parahippocampal white matter may contribute to memory decline as much as injury to the hippocampus itself (63). Thus, protecting the hippocampus as well as parahippocampal white matter from the radiation dose may prevent the development of neurocognitive dysfunction. Given the lower hippocampal metastasis rate in patients without extra-cranial metastasis, we investigated whether extending the radiation-safe zone was a safe practice. Our results demonstrated that the occurrence of BM in the hippocampus plus 10-mm region did not differ significantly from that in the hippocampus plus 5-mm region. Our results may be applied in planning radiation strategies with a greater safety margin.

Our study had a few limitations. First, the hippocampal metastases rate in our sample was measured before radiation therapy to BMs because the number of available patients who underwent follow-up MRI after HA-WBRT was small (n=26, **Supplemental Table 3**). Other patients were lost to follow-up after being diagnosed with BMs, were treated with SRS, or underwent surgery or conventional WBRT. Thus, as the BM occurrence rate in the HAR after HA-WBRT might differ from our results. Second, we did not assess the effect of targeted therapy for BM occurrence in the HAR. Increasing evidence now suggests that tyrosine kinase inhibitors (TKIs) improves progression-free survival in patients with metastatic NSCLC harboring EGFR mutations or ALK rearrangement (7, 64). Moreover, next-generation TKIs show a superior activity in treating BMs (65, 66). Third, the number of patients with BM

in HAR is relatively small (n=18). To draw a solid conclusion, further validation in a prospective study with a larger cohort is warranted.

CONCLUSION

In conclusion, our study demonstrated that the incidence of BM in the HAR was significantly higher in patients with extra-cranial metastases than in patients without extra-cranial metastases. Age, time interval to BM development, sex, and EGFR mutation status may also affect BM rates in the hippocampal avoidance region. Extending the safety zone from 5 mm to 10 mm in HA-WBRT has little effect on BM incidence in the HAR in patients without extra-cranial metastasis. This study supports the adoption of personalized radiation planning for patients with NSCLC and BMs. These results will allow clinicians to maximize the effectiveness of radiation therapy while minimizing cognitive decline.

DATA AVAILABILITY STATEMENT

The original contributions presented in the study are included in the article/**Supplementary Material**, further inquiries can be directed to the corresponding author.

ETHICS STATEMENT

The studies involving human participants were reviewed and approved by Gangnam severance hospital institutional review board. Written informed consent for participation was not required for this study in accordance with the national legislation and the institutional requirements.

AUTHOR CONTRIBUTIONS

All authors have significantly contributed to the manuscript. Study conception and design, SA and J-ML. Material preparation and data collection, JK and YC. Data analysis, HK and GP. Result interpretation, BJ, MP, and SS. Writing and revision of the manuscript, all authors.

FUNDING

This work was supported by Institute of Information & communications Technology Planning & Evaluation (IITP) grant funded by the Korea government (MSIT) [No.2020-0-01373, Artificial Intelligence Graduate School Program(Hanyang University)] to JML and by a National Research Foundation of Korea (NRF) grant funded by the Korea government (MSIT) (No. 2020R1F1A1056512) and grant from the Central Medical Service (CMS) Research Fund to SA.

SUPPLEMENTARY MATERIAL

The Supplementary Material for this article can be found online at: https://www.frontiersin.org/articles/10.3389/fonc.2022.781818/full#supplementary-material

REFERENCES

1. Sanchez de Cos J, Sojo Gonzalez MA, Montero MV, Perez Calvo MC, Vicente MJ, Valle MH. Non-Small Cell Lung Cancer and Silent Brain Metastasis. Survival and Prognostic Factors. *Lung Cancer* (2009) 63(1):140–5. doi: 10.1016/j.lungcan.2008.04.013
2. Lee H, Jeong SH, Jeong BH, Park HY, Lee KJ, Um SW, et al. Incidence of Brain Metastasis at the Initial Diagnosis of Lung Squamous Cell Carcinoma on the Basis of Stage, Excluding Brain Metastasis. *J Thorac Oncol* (2016) 11 (3):426–31. doi: 10.1016/j.jtho.2015.11.007
3. Cagney DN, Martin AM, Catalano PJ, Redig AJ, Lin NU, Lee EQ, et al. Incidence and Prognosis of Patients With Brain Metastases at Diagnosis of Systemic Malignancy: A Population-Based Study. *Neuro Oncol* (2017) 19 (11):1511–21. doi: 10.1093/neuonc/nox077
4. Kim M, Suh CH, Lee SM, Kim HC, Aizer AA, Yanagihara TK, et al. Diagnostic Yield of Staging Brain MRI in Patients With Newly Diagnosed Non-Small Cell Lung Cancer. *Radiology* (2020) 297(2):419–27. doi: 10.1148/radiol.2020201194
5. Wang H, Wang Z, Zhang G, Zhang M, Zhang X, Li H, et al. Driver Genes as Predictive Indicators of Brain Metastasis in Patients With Advanced NSCLC: EGFR, ALK, and RET Gene Mutations. *Cancer Med* (2020) 9(2):487–95. doi: 10.1002/cam4.2706
6. Balasubramanian SK, Sharma M, Venur VA, Schmitt P, Kotecha R, Chao ST, et al. Impact of EGFR Mutation and ALK Rearrangement on the Outcomes of Non-Small Cell Lung Cancer Patients With Brain Metastasis. *Neuro Oncol* (2020) 22(2):267–77. doi: 10.1093/neuonc/noz155
7. Johung KL, Yeh N, Desai NB, Williams TM, Lautenschlaeger T, Arvold ND, et al. Extended Survival and Prognostic Factors for Patients With ALK-Rearranged Non-Small-Cell Lung Cancer and Brain Metastasis. *J Clin Oncol* (2016) 34(2):123–9. doi: 10.1200/JCO.2015.62.0138
8. Klos KJ, O'Neill BP. Brain Metastases. *Neurologist* (2004) 10(1):31–46. doi: 10.1097/01.nrl.0000106922.83090.71
9. Peters S, Bexelius C, Munk V, Leighl N. The Impact of Brain Metastasis on Quality of Life, Resource Utilization and Survival in Patients With Non-Small-Cell Lung Cancer. *Cancer Treat Rev* (2016) 45:139–62. doi: 10.1016/j.ctrv.2016.03.009
10. Chang EL, Wefel JS, Hess KR, Allen PK, Lang FF, Kornguth DG, et al. Neurocognition in Patients With Brain Metastases Treated With Radiosurgery or Radiosurgery Plus Whole-Brain Irradiation: A Randomised Controlled Trial. *Lancet Oncol* (2009) 10(11):1037–44. doi: 10.1016/S1470-2045(09)70263-3
11. Greene-Schloesser D, Moore E, Robbins ME. Molecular Pathways: Radiation-Induced Cognitive Impairment. *Clin Cancer Res* (2013) 19(9):2294–300. doi: 10.1158/1078-0432.CCR-11-2903
12. Vigliani MC, Duyckaerts C, Hauw JJ, Poisson M, Magdelenat H, Delattre JY. Dementia Following Treatment of Brain Tumors With Radiotherapy Administered Alone or in Combination With Nitrosourea-Based Chemotherapy: A Clinical and Pathological Study. *J Neurooncol* (1999) 41 (2):137–49. doi: 10.1023/a:1006183730847
13. Monje ML, Mizumatsu S, Fike JR, Palmer TD. Irradiation Induces Neural Precursor-Cell Dysfunction. *Nat Med* (2002) 8(9):955–62. doi: 10.1038/nm749
14. Raber J, Rola R, LeFevour A, Morhardt D, Curley J, Mizumatsu S, et al. Radiation-Induced Cognitive Impairments Are Associated With Changes in Indicators of Hippocampal Neurogenesis. *Radiat Res* (2004) 162(1):39–47. doi: 10.1667/rr3206

15. Gondi V, Tolakanahalli R, Mehta MP, Tewatia D, Rowley H, Kuo JS, et al. Hippocampal-Sparing Whole-Brain Radiotherapy: A "How-to" Technique Using Helical Tomotherapy and Linear Accelerator-Based Intensity-Modulated Radiotherapy. *Int J Radiat Oncol Biol Phys* (2010) 78(4):1244–52. doi: 10.1016/j.ijrobp.2010.01.039
16. Hsu F, Carolan H, Nichol A, Cao F, Nuraney N, Lee R, et al. Whole Brain Radiotherapy With Hippocampal Avoidance and Simultaneous Integrated Boost for 1-3 Brain Metastases: A Feasibility Study Using Volumetric Modulated Arc Therapy. *Int J Radiat Oncol Biol Phys* (2010) 76(5):1480–5. doi: 10.1016/j.ijrobp.2009.03.032
17. Gondi V, Pugh SL, Tome WA, Caine C, Corn B, Kanner A, et al. Preservation of Memory With Conformal Avoidance of the Hippocampal Neural Stem-Cell Compartment During Whole-Brain Radiotherapy for Brain Metastases (RTOG 0933): A Phase II Multi-Institutional Trial. *J Clin Oncol* (2014) 32 (34):3810–6. doi: 10.1200/JCO.2014.57.2909
18. Brown PD, Gondi V, Pugh S, Tome WA, Wefel JS, Armstrong TS, et al. Hippocampal Avoidance During Whole-Brain Radiotherapy Plus Memantine for Patients With Brain Metastases: Phase III Trial NRG Oncology Cc001. *J Clin Oncol* (2020) 38(10):1019–29. doi: 10.1200/JCO.19.02767
19. Rodriguez de Dios N, Counago F, Murcia-Mejia M, Rico-Oses M, Calvo-Crespo P, Samper P, et al. Randomized Phase III Trial of Prophylactic Cranial Irradiation With or Without Hippocampal Avoidance for Small-Cell Lung Cancer (PREMER): A GICOR-GOECP-SEOR Study. *J Clin Oncol* (2021) 39 (28):3118–27. doi: 10.1200/JCO.21.00639
20. Marsh JC, Herskovic AM, Gielda BT, Hughes FF, Hoeppner T, Turian J, et al. Intracranial Metastatic Disease Spares the Limbic Circuit: A Review of 697 Metastatic Lesions in 107 Patients. *Int J Radiat Oncol Biol Phys* (2010) 76 (2):504–12. doi: 10.1016/j.ijrobp.2009.02.038
21. Marsh JC, Gielda BT, Herskovic AM, Wendt JA, Turian JV. Sparing of the Hippocampus and Limbic Circuit During Whole Brain Radiation Therapy: A Dosimetric Study Using Helical Tomotherapy. *J Med Imaging Radiat Oncol* (2010) 54(4):375–82. doi: 10.1111/j.1754-9485.2010.02184.x
22. Gondi V, Tome WA, Marsh J, Struck A, Ghia A, Turian JV, et al. Estimated Risk of Perihippocampal Disease Progression After Hippocampal Avoidance During Whole-Brain Radiotherapy: Safety Profile for RTOG 0933. *Radiother Oncol* (2010) 95(3):327–31. doi: 10.1016/j.radonc.2010.02.030
23. Sun Q, Li M, Wang G, Xu H, He Z, Zhou Y, et al. Distribution of Metastasis in the Brain in Relation to the Hippocampus: A Retrospective Single-Center Analysis of 565 Metastases in 116 Patients. *Cancer Imaging* (2019) 19(1):2. doi: 10.1186/s40644-019-0188-6
24. Amin MB, Edge SB. *AJCC Cancer Staging Manual*. New York: Springer (2017).
25. Kwon H, Kim JW, Park M, Kim JW, Kim M, Suh SH, et al. Brain Metastases From Lung Adenocarcinoma May Preferentially Involve the Distal Middle Cerebral Artery Territory and Cerebellum. *Front Oncol* (2020) 10:1664. doi: 10.3389/fonc.2020.01664
26. Zijdenbos AP, Forghani R, Evans AC. Automatic "Pipeline" Analysis of 3-D MRI Data for Clinical Trials: Application to Multiple Sclerosis. *IEEE Trans Med Imaging* (2002) 21(10):1280–91. doi: 10.1109/TMI.2002.806283
27. Tohka J, Zijdenbos A, Evans A. Fast and Robust Parameter Estimation for Statistical Partial Volume Models in Brain MRI. *Neuroimage* (2004) 23(1):84–97. doi: 10.1016/j.neuroimage.2004.05.007
28. Lewis RJ. (2000). An Introduction to Classification and Regression Tree (CART) Analysis, in: *Annual Meeting of the society for Academic Emergency Medicine*, San Francisco, California.
29. Natekin A, Knoll A. Gradient Boosting Machines, a Tutorial. *Front Neurorobot* (2013) 7:21. doi: 10.3389/fnbot.2013.00021
30. Diggle P, Diggle PJ, Heagerty P, Liang K-Y, Heagerty PJ, Zeger S. *Analysis of Longitudinal Data*. Oxford: Oxford University Press (2002).
31. Tong E, McCullagh KL, Iv M. Advanced Imaging of Brain Metastases: From Augmenting Visualization and Improving Diagnosis to Evaluating Treatment Response. *Front Neurol* (2020) 11:270. doi: 10.3389/fneur.2020.00270
32. Bartolucci R, Wei J, Sanchez JJ, Perez-Roca L, Chaib I, Puma F, et al. XPG mRNA Expression Levels Modulate Prognosis in Resected Non-Small-Cell Lung Cancer in Conjunction With BRCA1 and ERCC1 Expression. *Clin Lung Cancer* (2009) 10(1):47–52. doi: 10.3816/CLC.2009.n.007
33. Sperduto PW, Yang TJ, Beal K, Pan H, Brown PD, Bangdiwala A, et al. Estimating Survival in Patients With Lung Cancer and Brain Metastases: An Update of the Graded Prognostic Assessment for Lung Cancer Using Molecular Markers (Lung-molGPA). *JAMA Oncol* (2017) 3(6):827–31. doi: 10.1001/jamaoncol.2016.3834
34. Nieder C, Spanne O, Mehta MP, Grosu AL, Geinitz H. Presentation, Patterns of Care, and Survival in Patients With Brain Metastases: What has Changed in the Last 20 Years? *Cancer* (2011) 117(11):2505–12. doi: 10.1002/cncr.25707
35. Vuong DA, Rades D, Vo SQ, Busse R. Extracranial Metastatic Patterns on Occurrence of Brain Metastases. *J Neurooncol* (2011) 105(1):83–90. doi: 10.1007/s11060-011-0563-z
36. Brown PD, Jaeckle K, Ballman KV, Farace E, Cerhan JH, Anderson SK, et al. Effect of Radiosurgery Alone vs Radiosurgery With Whole Brain Radiation Therapy on Cognitive Function in Patients With 1 to 3 Brain Metastases: A Randomized Clinical Trial. *JAMA* (2016) 316(4):401–9. doi: 10.1001/jama.2016.9839
37. Yamamoto M, Serizawa T, Shuto T, Akabane A, Higuchi Y, Kawagishi J, et al. Stereotactic Radiosurgery for Patients With Multiple Brain Metastases (JLGK0901): A Multi-Institutional Prospective Observational Study. *Lancet Oncol* (2014) 15(4):387–95. doi: 10.1016/S1470-2045(14)70061-0
38. Kim CH, Im YS, Nam DH, Park K, Kim JH, Lee JI. Gamma Knife Radiosurgery for Ten or More Brain Metastases. *J Korean Neurosurg Soc* (2008) 44(6):358–63. doi: 10.3340/jkns.2008.44.6.358
39. Rava P, Leonard K, Sioshansi S, Curran B, Wazer DE, Cosgrove GR, et al. Survival Among Patients With 10 or More Brain Metastases Treated With Stereotactic Radiosurgery. *J Neurosurg* (2013) 119(2):457–62. doi: 10.3171/2013.4.JNS121751
40. Ji Z, Bi N, Wang J, Hui Z, Xiao Z, Feng Q, et al. Risk Factors for Brain Metastases in Locally Advanced Non-Small Cell Lung Cancer With Definitive Chest Radiation. *Int J Radiat Oncol Biol Phys* (2014) 89(2):330–7. doi: 10.1016/j.ijrobp.2014.02.025
41. Bajard A, Westeel V, Dubiez A, Jacoulet P, Pernet D, Dalphin JC, et al. Multivariate Analysis of Factors Predictive of Brain Metastases in Localised Non-Small Cell Lung Carcinoma. *Lung Cancer* (2004) 45(3):317–23. doi: 10.1016/j.lungcan.2004.01.025
42. Ceresoli GL, Reni M, Chiesa G, Carretta A, Schipani S, Passoni P, et al. Brain Metastases in Locally Advanced Nonsmall Cell Lung Carcinoma After Multimodality Treatment: Risk Factors Analysis. *Cancer* (2002) 95(3):605–12. doi: 10.1002/cncr.10687
43. Dimitropoulos C, Hillas G, Nikolakopoulou S, Kostara I, Sagris K, Vlastos F, et al. Prophylactic Cranial Irradiation in Non-Small Cell Lung Cancer Patients: Who Might be the Candidates? *Cancer Manag Res* (2011) 3:287–94. doi: 10.2147/CMR.S22717
44. Matsumoto S, Takahashi K, Iwakawa R, Matsuno Y, Nakanishi Y, Kohno T, et al. Frequent EGFR Mutations in Brain Metastases of Lung Adenocarcinoma. *Int J Cancer* (2006) 119(6):1491–4. doi: 10.1002/ijc.21940
45. Shin DY, Lee DH, Kim CH, Koh JS, Lee JC, Baek HJ, et al. Epidermal Growth Factor Receptor Mutations and Brain Metastasis in Patients With Nonadenocarcinoma of the Lung. *J Cancer Res Ther* (2016) 12(1):318–22. doi: 10.4103/0973-1482.154024
46. Bhatt VR, D'Souza SP, Smith LM, Cushman-Vokoun AM, Noronha V, Verma V, et al. Epidermal Growth Factor Receptor Mutational Status and Brain Metastases in Non-Small-Cell Lung Cancer. *J Glob Oncol* (2017) 3(3):208–17. doi: 10.1200/JGO.2016.003392
47. Li Z, Lu J, Zhao Y, Guo H. The Retrospective Analysis of the Frequency of EGFR Mutations and the Efficacy of Gefitinib in NSCLC Patients With Brain Metastasis. *J Clin Oncol* (2011) 29(15_suppl):e18065–e. doi: 10.1200/jco.2011.29.15_suppl.e18065
48. Benedettini E, Sholl LM, Peyton M, Reilly J, Ware C, Davis L, et al. Met Activation in Non-Small Cell Lung Cancer Is Associated With *De Novo* Resistance to EGFR Inhibitors and the Development of Brain Metastasis. *Am J Pathol* (2010) 177(1):415–23. doi: 10.2353/ajpath.2010.090863
49. Buonato JM, Lazzara MJ. ERK1/2 Blockade Prevents Epithelial-Mesenchymal Transition in Lung Cancer Cells and Promotes Their Sensitivity to EGFR Inhibition. *Cancer Res* (2014) 74(1):309–19. doi: 10.1158/0008-5472.CAN-12-4721
50. Paik JH, Choi CM, Kim H, Jang SJ, Choe G, Kim DK, et al. Clinicopathologic Implication of ALK Rearrangement in Surgically Resected Lung Cancer: A Proposal of Diagnostic Algorithm for ALK-Rearranged Adenocarcinoma. *Lung Cancer* (2012) 76(3):403–9. doi: 10.1016/j.lungcan.2011.11.008

51. Kim TJ, Park CK, Yeo CD, Park K, Rhee CK, Kim J, et al. Simultaneous Diagnostic Platform of Genotyping EGFR, KRAS, and ALK in 510 Korean Patients With Non-Small-Cell Lung Cancer Highlights Significantly Higher ALK Rearrangement Rate in Advanced Stage. *J Surg Oncol* (2014) 110(3):245–51. doi: 10.1002/jso.23646
52. Kim DW, Tiseo M, Ahn MJ, Reckamp KL, Hansen KH, Kim SW, et al. Brigatinib in Patients With Crizotinib-Refractory Anaplastic Lymphoma Kinase-Positive Non-Small-Cell Lung Cancer: A Randomized, Multicenter Phase II Trial. *J Clin Oncol* (2017) 35(22):2490–8. doi: 10.1200/JCO.2016.71.5904
53. Rangachari D, Yamaguchi N, VanderLaan PA, Folch E, Mahadevan A, Floyd SR, et al. Brain Metastases in Patients With EGFR-Mutated or ALK-Rearranged Non-Small-Cell Lung Cancers. *Lung Cancer* (2015) 88(1):108–11. doi: 10.1016/j.lungcan.2015.01.020
54. Preusser M, Streubel B, Birner P. ROS1 Translocations and Amplifications in Lung Cancer Brain Metastases. *J Neurooncol* (2014) 118(2):425–6. doi: 10.1007/s11060-014-1446-x
55. Gainor JF, Tseng D, Yoda S, Dagogo-Jack I, Friboulet L, Lin JJ, et al. Patterns of Metastatic Spread and Mechanisms of Resistance to Crizotinib in ROS1-Positive Non-Small-Cell Lung Cancer. *JCO Precis Oncol* (2017) 2017:1–13. doi: 10.1200/PO.17.00063
56. Fujii O, Tsujino K, Soejima T, Yoden E, Ichimiya Y, Sugimura K. White Matter Changes on Magnetic Resonance Imaging Following Whole-Brain Radiotherapy for Brain Metastases. *Radiat Med* (2006) 24(5):345–50. doi: 10.1007/s11604-006-0039-9
57. Conill C, Berenguer J, Vargas M, Lopez-Soriano A, Valduvieco I, Marruecos J, et al. Incidence of Radiation-Induced Leukoencephalopathy After Whole Brain Radiotherapy in Patients With Brain Metastases. *Clin Transl Oncol* (2007) 9(9):590–5. doi: 10.1007/s12094-007-0108-2
58. Szerlip N, Rutter C, Ram N, Yovino S, Kwok Y, Maggio W, et al. Factors Impacting Volumetric White Matter Changes Following Whole Brain Radiation Therapy. *J Neurooncol* (2011) 103(1):111–9. doi: 10.1007/s11060-010-0358-7
59. Hopewell JW. Late Radiation Damage to the Central Nervous System: A Radiobiological Interpretation. *Neuropathol Appl Neurobiol* (1979) 5(5):329–43. doi: 10.1111/j.1365-2990.1979.tb00633.x
60. Panagiotakos G, Alshamy G, Chan B, Abrams R, Greenberg E, Saxena A, et al. Long-Term Impact of Radiation on the Stem Cell and Oligodendrocyte Precursors in the Brain. *PloS One* (2007) 2(7):e588. doi: 10.1371/journal.pone.0000588
61. Carmichael O, Schwarz C, Drucker D, Fletcher E, Harvey D, Beckett L, et al. Longitudinal Changes in White Matter Disease and Cognition in the First Year of the Alzheimer Disease Neuroimaging Initiative. *Arch Neurol* (2010) 67 (11):1370–8. doi: 10.1001/archneurol.2010.284
62. Breteler MM, van Amerongen NM, van Swieten JC, Claus JJ, Grobbee DE, van Gijn J, et al. Cognitive Correlates of Ventricular Enlargement and Cerebral White Matter Lesions on Magnetic Resonance Imaging. The Rotterdam Study. *Stroke* (1994) 25(6):1109–15. doi: 10.1161/01.str.25.6.1109
63. Stoub TR, deToledo-Morrell L, Stebbins GT, Leurgans S, Bennett DA, Shah RC. Hippocampal Disconnection Contributes to Memory Dysfunction in Individuals at Risk for Alzheimer's Disease. *Proc Natl Acad Sci U.S.A.* (2006) 103(26):10041–5. doi: 10.1073/pnas.0603414103
64. Sperduto PW, Yang TJ, Beal K, Pan H, Brown PD, Bangdiwala A, et al. The Effect of Gene Alterations and Tyrosine Kinase Inhibition on Survival and Cause of Death in Patients With Adenocarcinoma of the Lung and Brain Metastases. *Int J Radiat Oncol Biol Phys* (2016) 96(2):406–13. doi: 10.1016/j.ijrobp.2016.06.006
65. Reungwetwattana T, Nakagawa K, Cho BC, Cobo M, Cho EK, Bertolini A, et al. CNS Response to Osimertinib Versus Standard Epidermal Growth Factor Receptor Tyrosine Kinase Inhibitors in Patients With Untreated EGFR-Mutated Advanced Non-Small-Cell Lung Cancer. *J Clin Oncol* (2018) 36(33):3290–97. doi: 10.1200/JCO.2018.78.3118
66. Camidge DR, Kim HR, Ahn MJ, Yang JCH, Han JY, Hochmair MJ, et al. Brigatinib Versus Crizotinib in Advanced ALK Inhibitor-Naive ALK-Positive Non-Small Cell Lung Cancer: Second Interim Analysis of the Phase III ALTA-1l Trial. *J Clin Oncol* (2020) 38(31):3592–603. doi: 10.1200/JCO.20.00505

Conflict of Interest: The authors declare that the research was conducted in the absence of any commercial or financial relationships that could be construed as a potential conflict of interest.

Frontiers in Oncology

Advances knowledge of carcinogenesis and tumor progression for better treatment and management

The third most-cited oncology journal, which highlights research in carcinogenesis and tumor progression, bridging the gap between basic research and applications to imrpove diagnosis, therapeutics and management strategies.

Discover the latest Research Topics

See more →

Frontiers

Avenue du Tribunal-Fédéral 34
1005 Lausanne, Switzerland
frontiersin.org

Contact us

+41 (0)21 510 17 00
frontiersin.org/about/contact